



ASPERA-4



**Venus
Express**

Reference : VE-ASP-TN-060402
Issue : 1 Rev. : 1
Date : 2006-06-17
Volume : - Page: 1

VEX / ASPERA-4 INSTRUMENT MANUAL

	Name and function	Date	Signature
Prepared by:	Stas Barabash (PI)	2006-04-02	
Verified by:			
Approved by:			
Issued by:			



1 INTRODUCTION

The document provides the information on the ASPERA-4 experiment (Analyzer of Space Plasma and Energetic Atoms) on the ESA Venus Express mission necessary for the data archiving.

2 DOCUMENT STRUCTURE AND REFERENCES

The document consists of the reference part and Appendixes. The appendixes contain the documents referred in the reference part. The list of provided documents, references to Appendixes, and respective references are given in Table 1.

Section	Appendix No.	Reference
Team structure	1	VE-ASP-TN-020312, Issue 1.3
ASPERA-4 instrument description	2	N/A
ASPERA-4 scanner	3	N/A
Main Unit TM / TC description	4	VE-ASP-MA-0005, Issue 1.0
NPD raw data structure	5	NPD_description1_0
HK channel conversion factors	6	N/A
ASPERA-4 sensor numbering	7	N/A
ASPERA-4 calibration report	8	VE-ASP-CR-050530, Issue 1.1
IMA TM / TC description	9	ICA-IMA-VIA TC/TM data formats and related software aspects Issue 1.8, 2004-10-28
IMA: conversion to physics units (IMA "bible")	10	Venus Express ASPERA-4 IMA BIBLE V.1.0 January 26, 2006



ASPERA-4



**Venus
Express**

Reference : **VE-ASP-TN-060402**
Issue : **1** Rev. : **1**
Date : **2006-06-17**
Volume : **-** Page: **4**

APPENDIX 1. TEAM STRUCTURE



VEX ASPERA-4 TEAM STRUCTURE

	Name and function	Date	Signature
Prepared by:	Stas Barabash, Pi	2003-03-05	
Verified by:	Herman Andersson, EM		
Approved by:			



CHANGE RECORD

Version	Date	Changed Paragraphs	Remarks
Issue 1, Rev 0	2003-02-12	All	New document
Issue 1, Rev 1	2003-02-27	3	Team responsibilities extended
Issue 1, Rev. 2	2003-03-04	All	Prof Baumjohann och Dr. Zhang added to Co-I list
Issue 1, Rev. 3	2003-03-05	4	A. Muro, A. Milillo, M. Maggi are added to address list



TABLE OF CONTENTS

1. ASPERA-4 PRINCIPLE INVESTIGATOR AND EXPERIMENT MANAGER.....	4
2. ASPERA-4 CO-INVESTIGATORS.....	4
3.ASPERA-4 TEAM RESPONSIBILITIES.....	5
4. ADRESS LIST.....	7
AZAMURA, KAZUSHI.....	7
BARABASH, STANISLAV.....	7
BAUMJOHANN, WOLFGANG.....	7
BOCHSLER, PETER.....	7
C:SON BRANDT, PONTUS.....	7
CERULLI-IRELLI, RICCARDO.....	7
COATES, ANDREW.....	7
CURTIS, CHARLES.....	7
FEDOROV, ANDREI.....	8
FRAHM, RUDY.....	8
GRANDE, MANUEL.....	8
GRIGORIEV, ALEXANDER.....	8
HSIEH, KE CHIANG.....	8
HOLMSTRÖM, MATS.....	8
KALLIO, ESA.....	8
KOSKINEN, HANNU.....	8
KOZYRA, JANET.....	8
KRUPP, NORBERT.....	9
LUHMANN, JANET.....	9
LUNDIN, RICKARD.....	9
MCKENNA-LAWLOR, SUSAN.....	9
MAGGI, MAURIZIO.....	9
MILILLO, ANNA.....	9
MURA, ALESSANDRO.....	9
ORSINI, STEFANO.....	9
ROELOF, EDMOND.....	10
SANDEL, BILL.....	10
SAUVAUD, JEAN-ANDRE.....	10
SHARBER, JAMES.....	10
SZEGO, KAROLY.....	10
WINNINGHAM, DAVID.....	10
WOCH, JOACHIM.....	10
YAMAUCHI, MASATOSHI.....	10
WURZ, PETER.....	11
ZHANG, TIELONG.....	11



1. ASPERA-4 Principle Investigator and Experiment Manager

Principle Investigator:

Stas Barabash
Swedish Institute of Space Physics, Kiruna, Sweden

Co-Principle Investigator:

Jean-Andre Sauvaud
CESR/CNRS, France

Experiment Manager:

Herman Andersson
Swedish Institute of Space Physics, Kiruna, Sweden

2. ASPERA-4 Co-investigators

R. Lundin, M. Holmström, M. Yamauchi, A. Grigoriev
Swedish Institute of Space Physics, Kiruna, Sweden

K. Asamura
Institute of Space and Astronautical Science, Sagamichara, Japan

W. Baumjohann, Tieolong Zhang
Space Research Institute, Graz, Austria,

A. J. Coates
Mullard Space Science Laboratory, University College London, UK

C. C. Curtis, K. C. Hsieh, B. R. Sandel
University of Arizona, Tucson, USA

A. Fedorov
Centre d'Etude Spatiale des Rayonnements, Toulouse, France

M. Grande,
Rutherford Appleton Laboratory, Oxfordshire, UK

H. Koskinen, E. Kallio
Finnish Meteorological Institute, Helsinki, Finland

J. Kozyra
Space Physics Research Laboratory /University of Michigan, Ann Arbor, USA

N. Krupp, J. Woch
Max-Planck-Institut für Aeronomie, Katlenburg-Lindau, Germany

J. Luhmann
Space Science Laboratory /University of California in Berkeley, Berkeley, USA

S. McKenna-Lawlor
Space technology Ltd., National University of Ireland, Ireland

S. Orsini, R. Cerulli-Irelli, A. Mura, A. Milillo, M. Maggi



Instituto di Fisica dello Spazio Interplanetari, Rome, Italy

E. Roelof, P. C:son Brandt
Applied Physics Laboratory/John Hopkins University, Laurel, USA

Karoly Szego
KFKI Research Institute for Particle and Nuclear Physics
Budapest, Hungary.

D. Winningham, R. Frahm, J. Sharber
Southwest Research Institute, San Antonio

P. Wurz, P. Bochsler,
University of Bern, Physikalisches Institut, Switzerland

3.ASPERA-4 team responsibilities

Staff	Group / Country	Responsibility / sensor
S. Barabash (PI), H. Andersson (EM), R. Lundin, M. Yamauchi, M. Holmström, A. Grigoriev	Swedish Institute of Space Physics, Kiruna, Sweden	PI institute Sensors subsystems: NPI - entire sensor NPD – development, integration, tests IMA sensor: mechanics, integration, HV supply IMA DPU – mechanics, sensor interface, s/w MU HV board – design and manufacturing MU DPU – mechanics Scanner – design, manufacturing, tests Instrument level: integration, verification, and tests
J.-A. Sauvaud (Co-PI), A. Fedorov	Centre d'Etude Spatiale des Rayonnements, Toulouse, France	IMA: development and manufacturing of sensors assembly, final integration, verification, and tests MU DC/DC board Scanner electronics NPI: MCP plates Data processing, Data analysis
K. Asamura	The Institute of Space and Astronautical Science	Planet-C cooperation NPI calibrations
W. Baumjohann, Tieolong Zhang	Space Research Institute, Graz, Austria	Coordination with MAG Data analysis
P. Bochsler, P. Wurz	University of Bern, Physikalisches Institut, Switzerland	STOP surfaces NPD MCP support Mechanical manufacturing
P. C:son Brandt E. Roelof	Applied Physics Laboratory/John Hopkins University , Laurel, USA	Data analysis Theory
R. Cerulli-Irelli , A. Mura,	Instituto di Fisica dello Spazio Interplanetari ,	EGSE Mechanical manufacturing



A. Milillo S. Orsini,	Rome, Italy	NPD FEE electronics Theory and data processing
A. Coats	Mullard Space Science Laboratory, Surrey, UK	ELS: calibration and refurbishment
C. C. Curtis, K. C. Hsieh, B. R. Sandel	University of Arizona , Tucson, USA	START surface (spares from MEX)
R. Frahm, J. Sharber, D. Winningham	Southwest Research Institute , San Antonio, USA	Data processing, Data analysis ELS spare (TBC)
M. Grande	Rutherford Appleton Laboratory , Oxfordshire, UK	MCP for NPD
E. Kallio, H. Koskinen,	Finnish Meteorological Institute, Helsinki, Finland	MU DPU board MU HK board IMA DPU board Theory and data analysis
J. Kozyra	Space Physics Research Laboratory /University of Michigan, Ann Arbor, USA	Theory
N. Krupp, J. Woch	Max-Planck-Institut für Aeronomie, Katlenburg-Lindau, Germany	NPD DigTOF electronics Data analysis
J. Luhmann	Space Science Laboratory /University of California in Berkeley, Berkley, USA	Data analysis Theory
S. McKenna-Lawlor	Space technology Ltd., National University of Ireland, Ireland	H/W support Data analysis
Karoly Szego	KFKI Research Institute for Particle and Nuclear Physics, Budapest,Hungary	Contribution to the calibration facility at IRF



ASPERA-4



**Venus
Express**

Reference : **VE-ASP-TN-060402**
Issue : **1** Rev. : **1**
Date : **2006-06-17**
Volume : **-** Page: **5**

APPENDIX 2. ASPERA-4 INSTRUMENT DESCRIPTION

I. THE SCIENCE

A. Scientific objectives for plasma measurements at Venus

Venus, Earth and Mars, the three largest terrestrial planets, have undergone much different thermal and atmospheric evolution. Mars has evolved rapidly. Initially, we now believe, Mars had a strong internally driven magnetic shield over an atmosphere much denser than present, one possibly supporting rain and flowing water on the surface. But the interior cooled rapidly, the dynamo stopped and much of the atmosphere escaped (*Acuña et al.*, 1998; *Schubert et al.*, 2000). Earth in contrast still has its magnetic field, a substantial atmosphere and abundant water. Venus may be the least evolved of the three planets. A thick crust has kept the interior hot but at the same time stifled the heat flow needed to drive convection in the fluid iron core. Thus Venus has no magnetic shield against the solar wind and perhaps never had (*Russell et al.*, 1980). Venus has a very dense atmosphere but very little water. Clearly the Venus atmosphere has evolved greatly since the planet accreted, yet still much atmosphere remains. Possibly the escape mechanism is very selective favouring the escape of water, or perhaps hydrogen, leaving the oxygen to combine with the soil. We do not know because no mission to Venus was instrumented to address this objective. Therefore, the main scientific objective of the ASPERA-4 (Analyzer of Space Plasmas and Energetic Atoms) experiment is to study solar wind induced atmospheric escape. The specific scientific questions to be addressed are:

- How is the Venus atmosphere coupled with the solar wind? How is mass added to and removed from the atmosphere due to this coupling?
- What is the structure of the interaction region?
- The previous question is connected to the issue of "where did the water go?" The early atmosphere must have contained water equivalent to a few metres deep global ocean as follows from the H/D ratio consideration (*Donahue and Hartle*, 1992). Could the solar wind interaction have contributed to the water escape (mainly increasing H escape)? Is the process the same as for the water escape from Mars?
- What is the mass composition of the escaping plasma? To what degree are the outflow processes mass dependent, and can this explain the Venus loss of water and greenhouse effect?

- What is the neutral-plasma interaction on Venus? How does the presence of the neutral gas affect plasma dynamics?
- What are similarities and differences in the solar wind interaction with the other terrestrial planets, Earth and Mars?

None of the previous missions to Venus covered such a wide range of scientific objectives. The other uniqueness of the instrument is that ASPERA-4 is a replica of the ASPERA-3 experiment orbiting Mars on board the ESA Mars Express mission (*Barabash et al.*, 2004). Combination of the observations made by two identical instruments at two non-magnetised planets exhibiting the similar type of the solar wind interaction but differing significantly in terms of interplanetary conditions, atmospheric characteristics, and size and mass opens completely new perspective for comparative magnetospheric studies.

B. Required measurements

In order to study the escape of the present day Venus atmosphere one must measure the incident solar wind flux, and the escaping ions whose thermal and bulk velocities will range from about 10 to 1000 km s⁻¹, depending on the mechanism at work. Since O₂⁺ ions dissociatively recombine forming a hot oxygen corona out to 4000 km altitude, oxygen ions will be picked up in the solar wind as well as accelerated down the wake or tail of Venus on the night side. Charge exchange between the solar wind and the neutral Venus atmosphere should be an important process because of the Venus dense upper atmosphere. Thus energetic neutral atoms (ENA) (*Gunell et al.*, 2005c) and, possibly X-rays (*Holmström et al.*, 2001) will be generated. This opens up the possibility to image the interaction region in order to obtain instantaneous images of the global distribution of the solar wind and planetary plasmas and qualify the instantaneous escape induced by the solar wind. These measurements should be designed to detect both hydrogen and oxygen atoms at velocities near 400 km s⁻¹. Estimates of the ion loss rate are around 10²⁴ ions/s (*Moore et al.*, 1991). Ion and ENA measurements should be supported by the electron measurements to characterise the local plasma conditions and identify the main plasma domains. Therefore, the ASPERA-4 experiment includes four sensors: the Electron Spectrometer (ELS); the Ion Mass Analyzer (IMA); the Neutral Particle Imager (NPI); and the Neutral Particle detector (NPD).

In order to characterise the environment of the picked up ions and understand the mechanism

involved in their acceleration the magnetic field must be measured. The ambient magnetic field encountered will range from about 1 nT to 200 nT and typically range from 10 nT to 30 nT. Since some spacecraft magnetic field will be present, a range of up to 1000 nT is recommended with gradiometer sensors along a modest (0.5 m) boom with monitoring of current levels of critical sources of stray magnetic fields. The magnetometer MAG (Venus Express Magnetometer) is included in the Venus Express payload (*Zhang et al.*, 2005).

C. The Solar Wind - Atmosphere Interaction

Near-Venus space is strikingly different from Earth-space because of the absence of a substantial intrinsic magnetic field of Venus. Without the magnetic cavity of a magnetosphere to shield the upper atmosphere from the on-coming solar wind, Venus is subject to comet-like atmosphere erosion processes and solar-wind-induced current systems that have no terrestrial counterparts. From experience gained in orbit around Venus on the Pioneer Venus Orbiter (PVO), we have developed ideas of how the upper atmosphere and solar wind interact and the consequences for the planet. In particular, we have observed that the scavenging of planetary ions removes heavy constituents such as oxygen, which plays an important role in the atmosphere's hydration and surface oxidation history. A cartoon showing some of the relevant processes can be found in Fig. 1.

The current atmospheric conditions on Venus indicate that water is present in only trace amounts (\sim a few precipitable micrometres), much less than expected if Venus' early atmosphere was Earth-like. In contrast to the Martian water story (*McKay and Stoker*, 1989) it is unlikely to be frozen and buried or sequestered in polar ice caps. Thus the alternative of escape to space in the form of water's constituents is most likely. It is relatively easy to lose light hydrogen, but oxygen loss is problematic. Small amounts can escape via the production of a hot atomic oxygen corona from ionospheric photochemistry (*Nagy et al.*, 1981), but the bulk of the O₂ and O are gravitationally bound. Independent analyses of surface oxidation on the planet indicates that most of the oxygen left over from photo-dissociation over the history of Venus did not become incorporated into the exposed rocks and soil. What could produce such an effective oxygen escape mechanism? Could the processes associated with the solar-wind interaction account for the escape of sufficient quantities of oxygen to have made an Earth-like water budget for Venus \sim 4 Gyr ago?

ASPERA-4 includes four sensors: NPI, NPD, IMA, and ELS each of which contributes, both alone and in combination, to understanding the different consequences of direct solar wind inter-

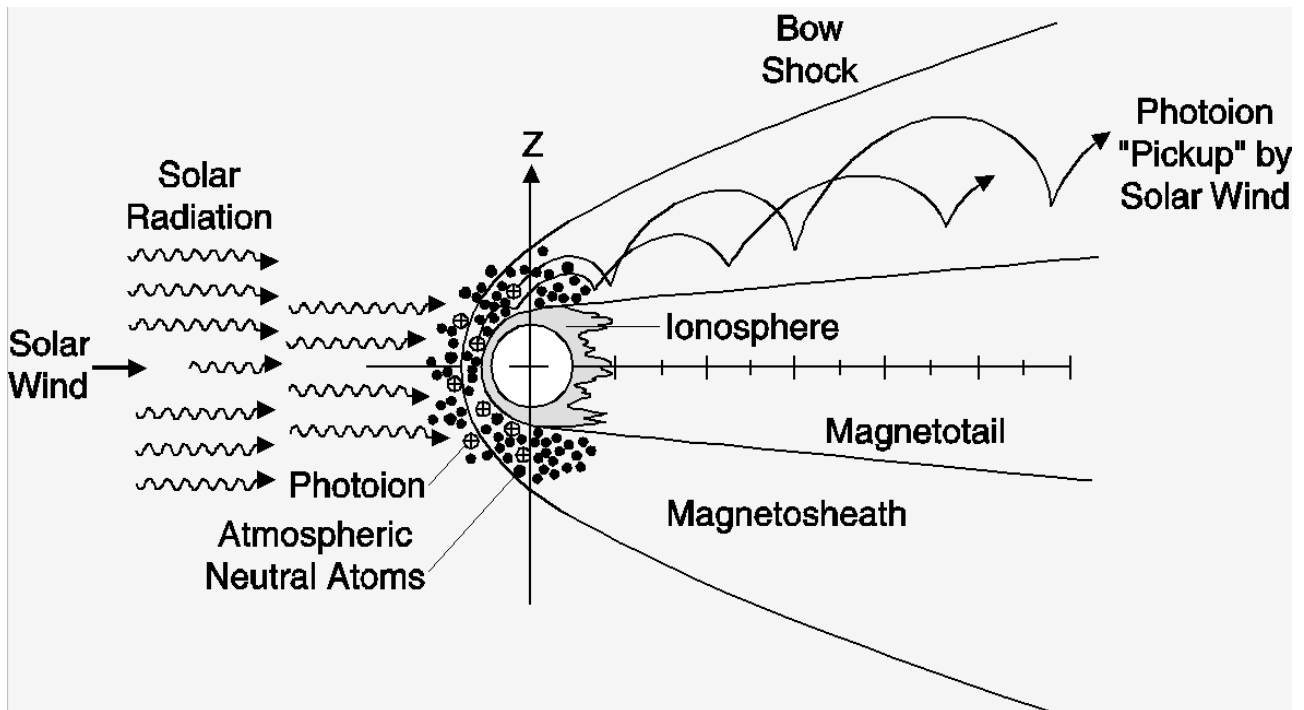


FIG. 1 Cartoon of the Venus solar-wind interaction, highlighting the atmosphere escape processes related to the generation of O^+ pickup ions. Solar radiation ionises the Venus atmosphere producing an ionosphere whose thermal pressure is sufficient to standoff the solar wind flow bounding the ionosphere with an ionopause. The deflection of the supersonic solar wind leads to the formation of a bow shock. The hydrogen and hot oxygen exospheres extend into the shocked solar wind of the magnetosheath where they are photoionised and impact ionised and picked up in cycloidal trajectories gyrating around the magnetic field out of the page here.

action with a planetary atmosphere/ionosphere. Because Venus does not have the complication of the Martian remanent magnetic fields, and has the initial comprehensive reconnaissance provided by PVO, the ASPERA-4 measurements that fill in the knowledge gaps left by PVO will make progress in our understanding far exceeding its own coverage of the Venus solar wind interaction physics. In particular, the IMA puts a definitive composition label on the atmospheric pickup ions produced at Venus and detect them over a much greater (up to 36 keV as opposed to PVO's ~ 8 keV) energy range. The ELS measures both low energy escaping plasma and high energy electrons that contribute to the ion production through electron impact ionisation. The ENAs detected by NPD and NPI provides a measure of solar wind energy deposited in the atmosphere that cannot be estimated from the plasma and field measurements alone, as described below.

A combination of PVO results led to our current picture of atmospheric oxygen escape from

Venus, reproduced in Fig. 1. The UV spectrometer (*Stewart, 1980*) confirmed the existence of an atomic oxygen upper atmosphere extending well into the magnetosheath. This hot O "corona" was shown by *Nagy et al. (1981)* to agree with models of photochemical exospheres produced by dissociative recombination in the O_2^+ ionosphere. Combined magnetometer (*Russell et al., 1980*) and plasma analyser (*Intriligator et al., 1980; Mihalov et al., 1980*) measurements were then used to construct a scenario of both direct O^+ pickup ion escape (*Moore et al., 1990*) and additional sputtering of O from the atmosphere by impacting O^+ pickup ions not on direct escape trajectories (*Luhmann and Kozyra, 1991*). The pickup ions can be created by any ionisation mechanism - photoionisation, solar wind electron impact, or charge exchange with solar wind protons, in all atmospheric regions above the exobase (~ 200 km altitude) penetrated by the solar wind convection electric field. There are also suggestions of other possible ion removal processes in the thermal plasma (below a few eV) energy range at work at the ionopause boundary layer (*Brace et al., 1982*) and in the low altitude wake (*Hartle and Grebowsky, 1990*), distinct from the pickup ion-related mechanisms, which we do not discuss here. In any case, the limited capabilities of the PVO instruments for measuring both solar wind electrons and magnetosheath protons (where the upper atmosphere penetration occurs), as well as solid identification of the pickup ions composition, made it difficult to quantify the details of the escape scenario in Fig. 1. The ASPERA-4 IMA, with the added magnetometer MAG, on Venus Express should finally allow the evaluation of escape rates for oxygen ions as well as other species, their variation with interplanetary conditions, and their implications for related sputtering losses.

Another problem of the solar wind - atmosphere coupling that has not been explored experimentally concerns the energetic consequences for the Venusian atmosphere of the lack of a planetary dipole field of any importance. Kinetic and test-particle models of the Mars-solar wind interaction (*Brecht, 1997; Kallio et al., 1997*) suggest that solar wind absorption by the Martian atmosphere may be an important energy source for the upper atmosphere at that planet. However, at Venus the much smaller relative solar wind proton gyroradii greatly limit the numbers of protons that can reach the exobase which is well below the ionopause (~ 200 km exobase altitude compared to ~ 300 km ionopause altitude. A solar wind proton gyroradius in the inner magnetosheath is typically ~ 10 km). ENA production in the magnetosheath by charge exchange between solar wind protons and the exosphere/thermosphere near the solar wind/ionosphere boundary decouples the energetic neutralised protons from the magnetic field in the sheath, leaving them free to impact the exobase (e.g. *Kallio et al. (1997)*). The ENAs generated as a product of the solar - wind interaction

can thus greatly enhance the deposition of solar wind energy into the upper atmosphere (*Kallio and Barabash, 2000*) and, at the same time, provide a means of “imaging” the solar wind interaction. *Fok et al. (2004)* and *Gunell et al. (2005c)* have modelled the ENA production at Venus using MHD simulations. The NPD will provide tests of the predicted fluxes and composition of the ENAs, while imaging these particles with NPI will show the spots or regions of the most intense ENA precipitation, and give information on their variation with solar wind conditions.

While the energy transfer associated with the ENA precipitation can be important, for the thermal structure of the upper atmosphere, it is the O^+ pickup ion precipitation that causes significant sputtering-induced loss of the atmosphere. *Luhmann and Kozyra (1991)* estimated that O^+ sputtering results in the escape of oxygen atoms from Venus at rates comparable to sputtering losses from the much smaller planet Mars (*Luhmann and Bauer, 1992*). Comparisons of ASPERA-3 results from Mars Express with ASPERA-4 results will provide an invaluable look at the processes and rates by which unmagnetised terrestrial planet atmospheres evolve due to their solar wind interactions.

D. Pickup Ions at Venus

Observations of oxygen pickup ions by the plasma analyser on PVO sparked broad interest in solar wind erosion of unmagnetised planet atmospheres with its first-order picture of the spatial distribution and energies of O^+ pickup ions. These results, collected during PVO’s ~ 14 year, ~ 5000 orbit tour, provide an idea of what is to be expected from IMA measurements on Venus Express.

The PVO Plasma Analyzer (PV OPA) has been described in the literature a number of times (*Intriligator et al., 1980; Mihalov and Barnes, 1982; Moore et al., 1990*). Its key features included its ~ 8 keV/ q energy per charge upper limit for detection and a directional sampling scheme, providing approximately 15° azimuthal and $20^\circ - 30^\circ$ polar angle resolution with respect to the PVO spin axis. The time resolution for a full angle and energy scan was about 9 minutes, which gave only a few samples during each periapsis pass. Thus the best observations of pickup ions were generally obtained during apoapsis at about twelve planetary radii downstream. A sample of a spectrogram constructed from the PV OPA measurements during one orbit in which picked up ions were observed in the wake is shown in Fig. 2. O^+ ions are inferred to be present in the PV OPA energy scans when a second peak is visible at high E/q . The energy and angular coverage

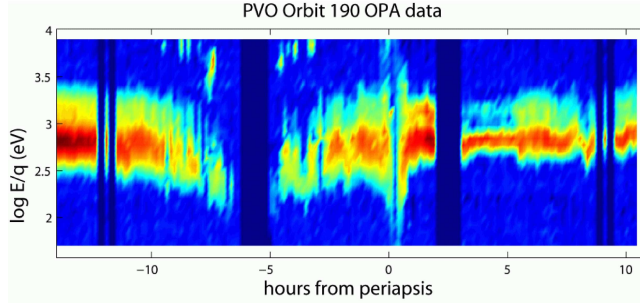


FIG. 2 Sample Energy spectrogram obtained from the PV OPA plasma analyser data. The inferred O^+ is seen as the higher energy peak coexisting with the main proton peak.

limitation implies that a significant amount of the O^+ present was not detected on PVO.

The energies and orbital locations of the oxygen peaks differ from orbit to orbit due to the variability of the solar wind and especially the cross-flow interplanetary magnetic field orientation. The cross-flow interplanetary field orientation creates changing asymmetries in the O^+ spatial distribution due to the large gyroradii of O^+ ions ($\sim 0.5 - 1.0R_p$) relative to the size of the planet and the solar wind interaction region, as illustrated in Fig. 1. Because the direction of the interplanetary magnetic field is usually eastward or westward, the convection electric field $\vec{E} = -\vec{v} \times \vec{B}$ (where \vec{v} is the solar wind plasma velocity and \vec{B} the local magnetic field) produces pickup ion trajectories that are initially either northward or southward as well as anti-sunward. If the ion trajectory does not intersect the exobase at a few hundred kilometres altitude, the trajectory continues down the wake, forming a one-sided ion stream. Thus near the planet terminator and in the near-planet wake, one typically observes O^+ detection locations organised into northern or southern spatial clusters (*Intriligator et al., 1979; Moore et al., 1990*).

The energies at which the inferred O^+ ions were detected on PVO are compared with their accompanying proton peak energies in Fig. 3. Here, a zero proton peak energy identifies those inferred O^+ detections not accompanied by a proton peak in the same spectrum. At 16 times the proton mass, co-moving O^+ ions have 16 times the proton energies. The statistics suggest the detected O^+ peaks are at roughly these energies up to the 8 keV limit of the PVO plasma analyser. O^+ moving at greater than ~ 310 km/s is outside of this range. In the upstream solar wind, outer magnetosheath, and distant wake the solar wind plasma often moves at speeds of 350 to over 600 km/s. IMA on Venus Express will be able to not only detect, but also verify the composition of many of these additional O^+ (and other) pickup ions.

The PVO results suggest the extent to which ASPERA-4 on Venus Express with its energy

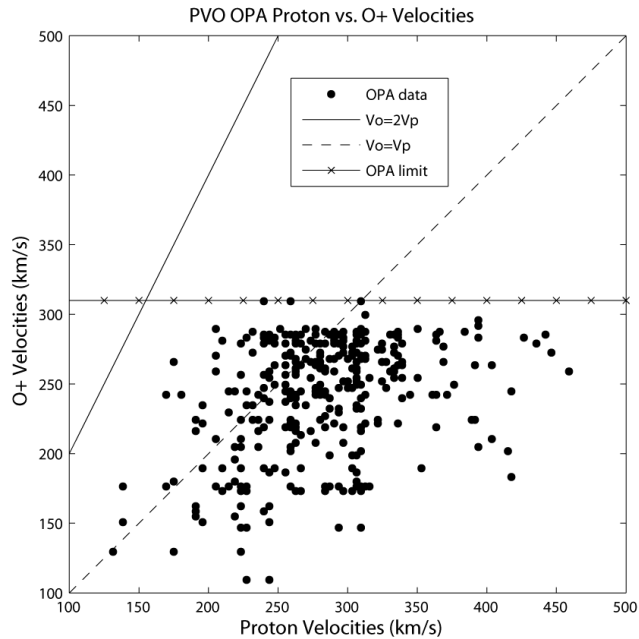


FIG. 3 Relative energies of the detected proton peaks and oxygen peaks in the PV OPA E/Q spectra. A zero proton peak energy implies the presence of only an inferred O^+ peak, based on its proximity to other O^+ peaks or location in the wake proton void. PV OPA has an ~ 8 keV detector E/q limit for O^+ detection.

range of 10 eV to 36 keV, scanning field of view, and ability to separate ion masses, will greatly improve our view of the pickup ion environment around Venus. The currently planned Venus Express orbit is similar to that of PVO, but with periapsis at $\sim 65^\circ$ N Latitude and a periapsis of 250 – 400 km, compared to PVO's 15° N Latitude initial periapsis and nominal ~ 160 km periapsis. The sampling of the pickup ion cloud in an orbit with this geometry, compared to the PVO orbit geometry that produced the spectrogram in Fig. 2, is illustrated in Fig. 4. The Venus Express orbit thus provides a somewhat different perspective, focusing on the magnetosheath, near-terminator, and low altitude wake pickup ion characteristics rather than on the distant pickup ion wake characteristics. This is in fact highly complementary to the PVO orbit geometry sampling which did not allow coverage of the low altitude wake. If the orbit is allowed to evolve so that the sampling region circularises, a broader sampling will be obtained.

E. ENA production at Venus

ENAs are produced in charge exchange collisions between solar wind protons and neutral atoms in the upper part of the atmospheres of the planets. The ASPERA-4 instrument provides ENA

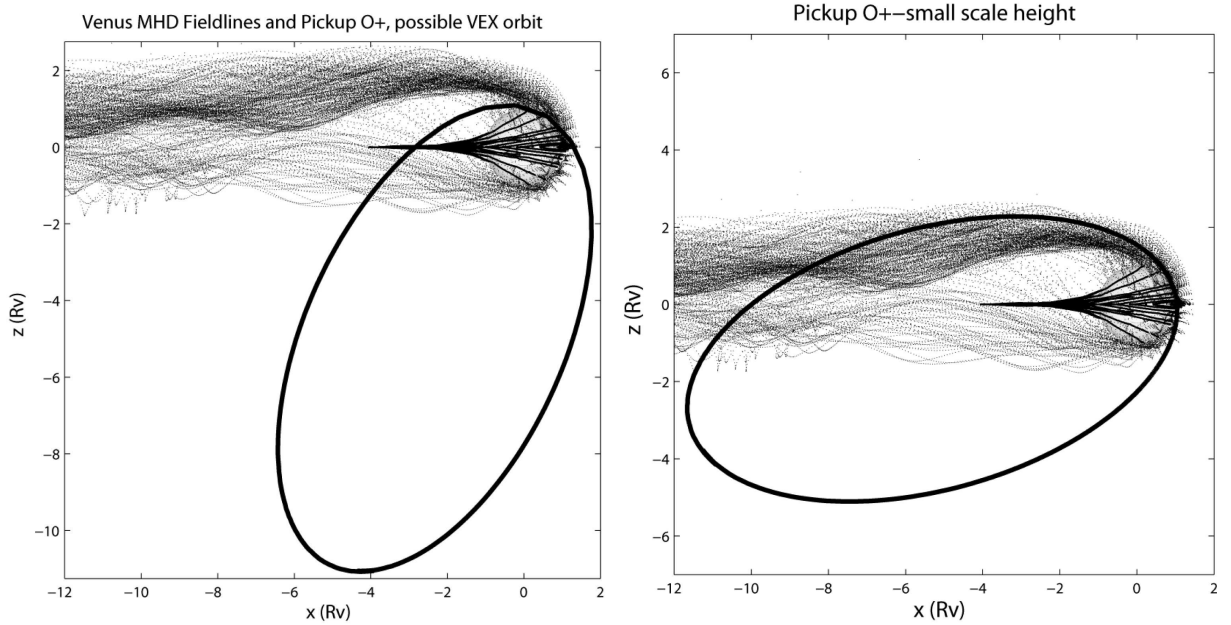


FIG. 4 (a) Illustration of the expected Venus Express orbit with its periapsis at $\sim 65^\circ$ N latitude, relative to O^+ ion test particle trajectories for a particular interplanetary field orientation. The sampling of the pickup ion population is advantageous for near-planet pickup studies. (b) The comparable illustration for a PVO orbit that in contrast sampled the deep ion wake.

images of the Venus-solar wind interaction region. Such images have been simulated through the integration of the ENA production along lines of sight to a virtual ENA instrument (*Fok et al., 2004; Gunell et al., 2005c*). Some of the results from these simulation studies are reviewed here.

Venus Express arrives at Venus during solar minimum conditions. Due to the scarcity of in situ measurements the ionopause altitude at Venus is not well known for solar minimum conditions (*Luhmann, 1992*) It is thought to vary with the solar cycle, but since all in situ measurements were made during solar maximum conditions this variation is still unconfirmed. *Gunell et al. (2005c)* have investigated the ENA emissions as a function of ionopause distance by scaling the ionopause altitude in the plasma model. The ENA flux from the local emission maximum near the planet decreases with increasing ionopause altitude, since with a higher ionopause altitude the protons pass through a region with lower neutral density. This also affects the ENA production and escape rates. The ionopause is thought to be close to the lower end of that range at solar minimum because of the lower ionospheric pressure (*Luhmann, 1992*). The ENA images are then generated by evaluating line of sight integrals in the same way as it has previously been done to simulate ENA images of the Martian environment (*Gunell et al., 2005b; Holmström et al., 2002*). *Gunell et al.*

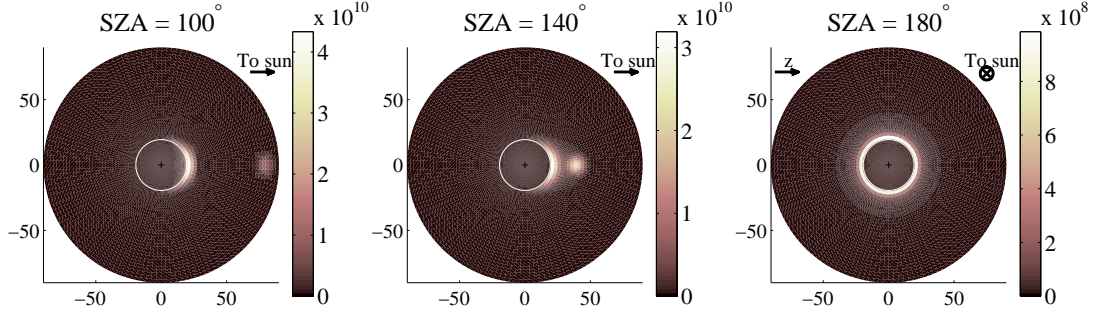


FIG. 5 ENA images of Venus from vantage points $3R_V$ from Venus (planetocentric distance) and solar zenith angles $\theta = 100^\circ$, 140° , and 180° . The ENA flux is shown in units of $\text{sr}^{-1}\text{m}^{-2}\text{s}^{-1}$, and the axes show the polar angle in degrees.

(2005c) have used a semi-analytical MHD model (*Biernat et al.*, 1999, 2000, 2001) to describe the plasma flow around Venus, and a neutral gas density model that is based on published data from measurements. The input parameters were the following: solar wind density $n_{sw} = 1.5 \times 10^7 \text{m}^{-3}$; solar wind speed $v_{sw} = 4.4 \times 10^5 \text{m/s}$; solar wind temperature $T_{sw} = 2 \times 10^5 \text{K}$; and solar wind magnetic field $B_{sw} = 1.2 \times 10^{-8} \text{T}$. Three ENA images from vantage points in the xz -plane at different solar zenith angles are shown in Fig. 5. The vantage points are located three Venus radii from the centre of Venus, and the solar zenith angles are 100° , 140° , and 180° for the three images respectively. The ENA flux is shown in units of $\text{sr}^{-1}\text{m}^{-2}\text{s}^{-1}$. The centre of each image corresponds to the direction looking straight toward the centre of Venus. The white circle shows the location of Venus' surface. For all three images the ionopause altitude is 250 km at the subsolar point. In the images from solar zenith angles 100° and 140° the ENA flux has two local maxima: one on the dayside of Venus and the other in the direction of the sun. The latter maximum is produced upstream of the bow shock by charge exchange collisions between the protons in the unperturbed solar wind and atoms in the exosphere of Venus. At $\theta = 180^\circ$ the Sun is occulted by Venus. Fig. 6 shows the ENA production rate per unit volume in cylindrical coordinates for an ionopause altitude of 400 km in units of $\text{m}^{-3}\text{s}^{-1}$. The total hydrogen ENA production rate integrated over the whole region shown in Fig. 6 is $5.6 \times 10^{24} \text{s}^{-1}$. For an ionopause altitude of 250 km the total production rate is $8.1 \times 10^{24} \text{s}^{-1}$.

The ENA production, escape and precipitation rates were calculated for ionopause altitudes of 250 km and 400 km. These numbers together with the corresponding numbers for Mars are found in table I. For Mars both the numbers obtained by *Holmström et al.* (2002) using an empirical

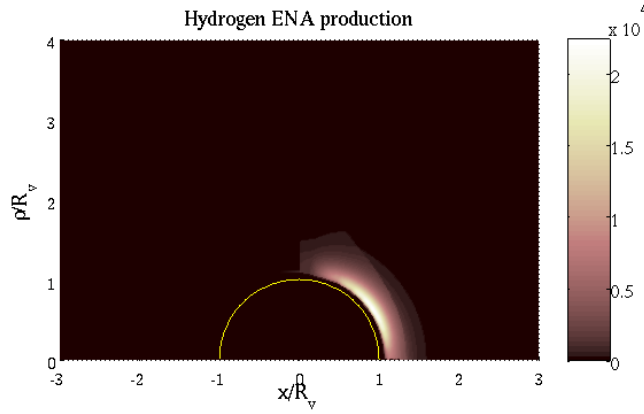


FIG. 6 ENA production rate for an ionopause altitude of 400 km. The cylindrical coordinate $\rho = \sqrt{y^2 + z^2}$ is the distance to the Venus-sun line. The production rate is shown in units of $\text{m}^{-3}\text{s}^{-1}$.

TABLE I A comparison of some aspects of the results from Venus and Mars. Values for Venus are given for ionopause altitudes 250 km and 400 km respectively. Venus' upper atmosphere is approximately the same independent of the solar cycle. The values for Mars from *Holmström et al. (2002)* are all for solar minimum conditions. Values from the MHD simulation of Mars were taken from *Gunell et al. (2005b)*. “Max. flux” refers to the maximum flux in an ENA image of the interaction region downstream of the bow shock. Solar minimum and maximum conditions are denoted by “min” and “max” respectively.

	Venus	Venus	Mars	Mars	unit
	IP 250 km	IP 400 km	Holmström	MHD (Gunell)	
Production rate	$7.8 \cdot 10^{24}$	$5.6 \cdot 10^{24}$	$1.7 \cdot 10^{25}$	$\left\{ \begin{array}{l} 2.4 \cdot 10^{25}, \text{ min} \\ 5.1 \cdot 10^{24}, \text{ max} \end{array} \right.$	s^{-1}
Escape rate	$5.3 \cdot 10^{24}$	$4.0 \cdot 10^{24}$	$1.5 \cdot 10^{25}$		s^{-1}
Precip. rate	$2.2 \cdot 10^{24}$	$1.2 \cdot 10^{24}$	$1.4 \cdot 10^{24}$		s^{-1}
Max. flux	$5.8 \cdot 10^{10}$	$3.8 \cdot 10^{10}$	$3 \cdot 10^{11}$	$1.1 \cdot 10^{11}, \text{ min}$	$\text{sr}^{-1}\text{m}^{-2}\text{s}^{-1}$

plasma flow model and those obtained by *Gunell et al. (2005b)* using an MHD model are reported. The precipitation rate at Venus is higher than at Mars. This is not unexpected because Venus is a larger planet, and the Venusian ENA production region is located closer to Venus than the Martian ENA production region is to Mars, which is seen in Fig. 7. The left panel of Fig. 7 shows an ENA image of Mars (*Gunell et al., 2005b*), that is based on an MHD model for the plasma flow (*Ma et al., 2002*). The right panel of Fig. 7 shows an ENA image of Venus. Both images are

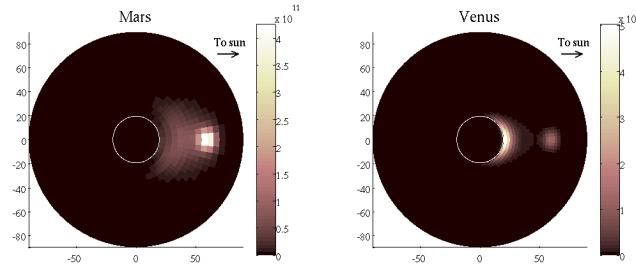


FIG. 7 ENA images from Mars (left) and Venus (right) from vantage points with solar zenith angles of 120° and planetocentric distance three radii of the respective planet. The image of the Martian environment (Gunell *et al.*, 2005b) is based on an MHD model of the plasma flow around Mars.

from vantage points at solar zenith angle 120° and a planetocentric distance of three radii of the respective planet.

The ENA flux and production rates at Venus are lower than at Mars even though the solar wind flux is greater at Venus. The reason for this is that the neutral gas density at relevant heights is lower in Venus' than Mars' exosphere. The neutral density falls off more rapidly with altitude at Venus, because of the larger mass of that planet, which is 7.5 times greater than the mass of Mars. The dominant contribution to the neutral density at high altitudes at Mars during solar minimum conditions is the large hydrogen corona (Krasnopolsky and Gladstone, 1996). The hydrogen density at Mars is greater than that at Venus everywhere above the exobase, and hydrogen is by far the most important species for ENA production at Mars (Holmström *et al.*, 2002).

To show the contributions from different regions, and to illustrate the differences between Venus and Mars, we examine the contributions from different positions along a line of sight. Fig. 8 shows, in the three panels on the left side, from top to bottom, the total neutral gas density, the plasma flux, and the rate of ENA production in the direction toward the vantage point, as functions of distance along the line of sight from the vantage point. The ENA production rate, when integrated along the line of sight, gives the differential ENA flux that is shown in the ENA images. The right panel shows the lines of sight along for which the different quantities are plotted in the left panels. The filled red circle represents Mars and the yellow Venus. The vantage points are at solar zenith angle 100° and a planetocentric distance of three radii of the respective planet. The direction of the lines of sight corresponds to the direction of the pixel with the maximum flux of an ENA image from that vantage point. Because the topology of the plasma flow is different at Venus and Mars the directions of the maximum flux is also different at the two planets. The higher exospheric density at Mars is what makes the ENA flux at Mars greater than at Venus, as is seen

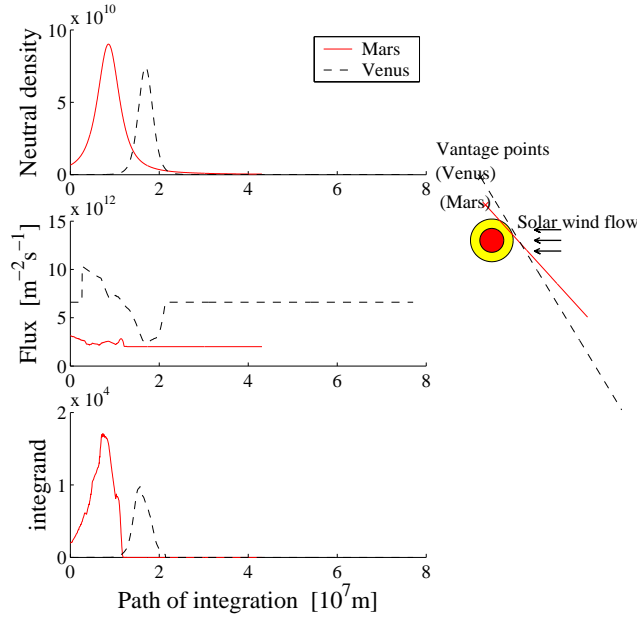


FIG. 8 The three panels on the left side show, from top to bottom, the total neutral gas density, the plasma flux, and the rate of ENA production in the direction toward the vantage point, as functions of distance along the line of sight from the vantage point. Solid and dashed lines represent values at Mars and Venus respectively. The right panel shows the lines of sight along for which the different quantities are plotted in the left panels. The filled red circle represents Mars and the yellow Venus.

in the top left panel. Although the solar wind density is higher at Venus, the flux in the relevant region, i.e., close to the planet, is similar to that at Mars (middle left panel). The bulk speed of the plasma is slowed down near the planet, and the line of sight that yields the highest differential flux is farther away from the planet at Mars than at Venus.

It is interesting to compare the results obtained here with the results of *Fok et al. (2004)*. Although their parameters are not exactly the same as ours they are at least similar. *Fok et al. (2004)* took the effect of space craft motion into account. We do not. Since we are considering ENAs with energies above 50 eV this amounts only to a small correction in our case. Both models yield ENA fluxes of the same order of magnitude, and one can conclude that the two models are in reasonable agreement considering the uncertainties of the models. Real measurements will be required to determine between them, or indeed to say anything conclusively about the accuracy of the models.

II. THE INSTRUMENT

A. Overall configuration

The ASPERA-4 instrument is a replica of ASPERA-3 on board Mars Express mission (*Barabash et al.*, 2004). The experiment is a comprehensive plasma diagnostic package to measure ENAs, electrons, and ions with a wide angular coverage from a three axis stabilised platform. Mechanically ASPERA-4 consists of two units, the Main Unit (MU) and the Ion Mass Analyzer (IMA) (Fig. 9). The Main Unit comprises three sensors: the Neutral Particle Imager (NPI), the Neutral Particle Detector (NPD), the Electron Spectrometer (ELS), and a digital processing unit (DPU), which all are located on a turnable platform. The combination of the 360° sensor field of view (180° for the NPD) and the scans from 0° to 180° give, ideally, the required 4π maximum coverage, but part of the field of view is blocked by the spacecraft body. The real coverage depends on the instrument location on the spacecraft. All electrical interfaces of the instrument with the spacecraft are made through the scanner. Electrically IMA interfaces only MU. The total mass of the instrument is 9.00 kg; the main unit flight model mass without thermal hardware is 6.63 kg; and the mass of the IMA flight model is 2.37 kg without thermal hardware. The maximum power consumption is 18 W. The Main unit envelope is $350 \times 263 \times 288 \text{ mm}^3$ and for the IMA $287 \times 187 \times 165 \text{ mm}^3$.

The ASPERA-4 two ENA sensors complement each other. The NPI is designed to provide measurements with relatively high angular resolution but no mass and energy discrimination while the NPD performs mass and energy analysis of the incoming ENAs, but the angular resolution is crude. This approach also gives the necessary redundancy as well as the independent cross-checking that is necessary for such measurements in a new environment. The charged particle sensors not only provide characterisation of the local plasma environment but also support ENA measurements in terms of charged particles background and inter-calibrations. The ELS is a standard top-hat electrostatic analyser in a very compact design and high energy resolution. The IMA is an improved version of the ion mass spectrographs TICS/Freja, IMIS/Mars-96, IMI/Planet-B (*Norberg et al.*, 1998), and an exact copy of the ICA (Ion Composition Analyzer) instrument that is flying on the Rosetta mission. Since the IMA is not accommodated on the scanner, electrostatic sweeping is used to achieve $\pm 45^\circ$ elevation coverage.

The instrument design, while based on a moduled structure, demonstrates high degree of pack-

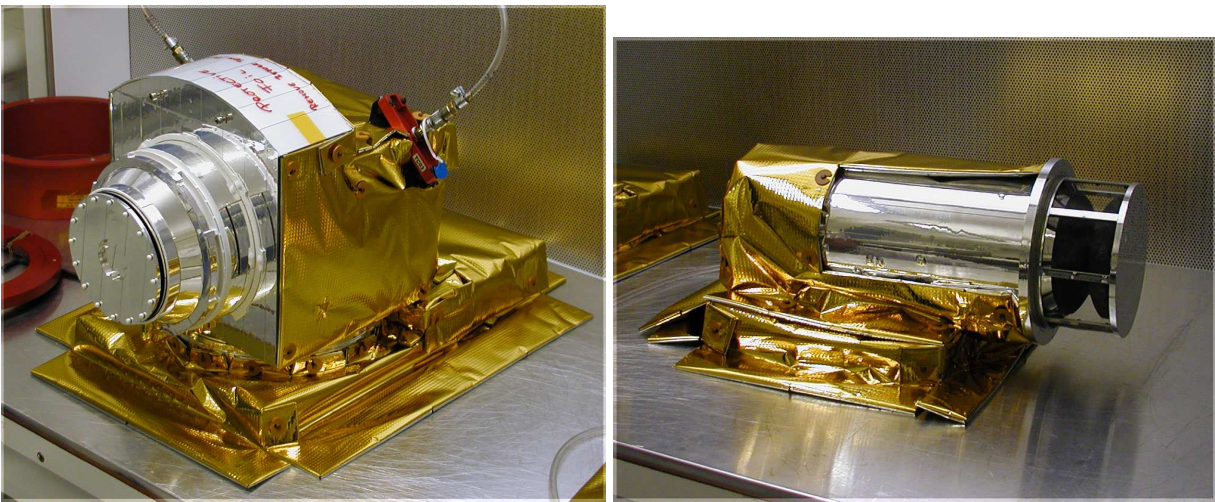
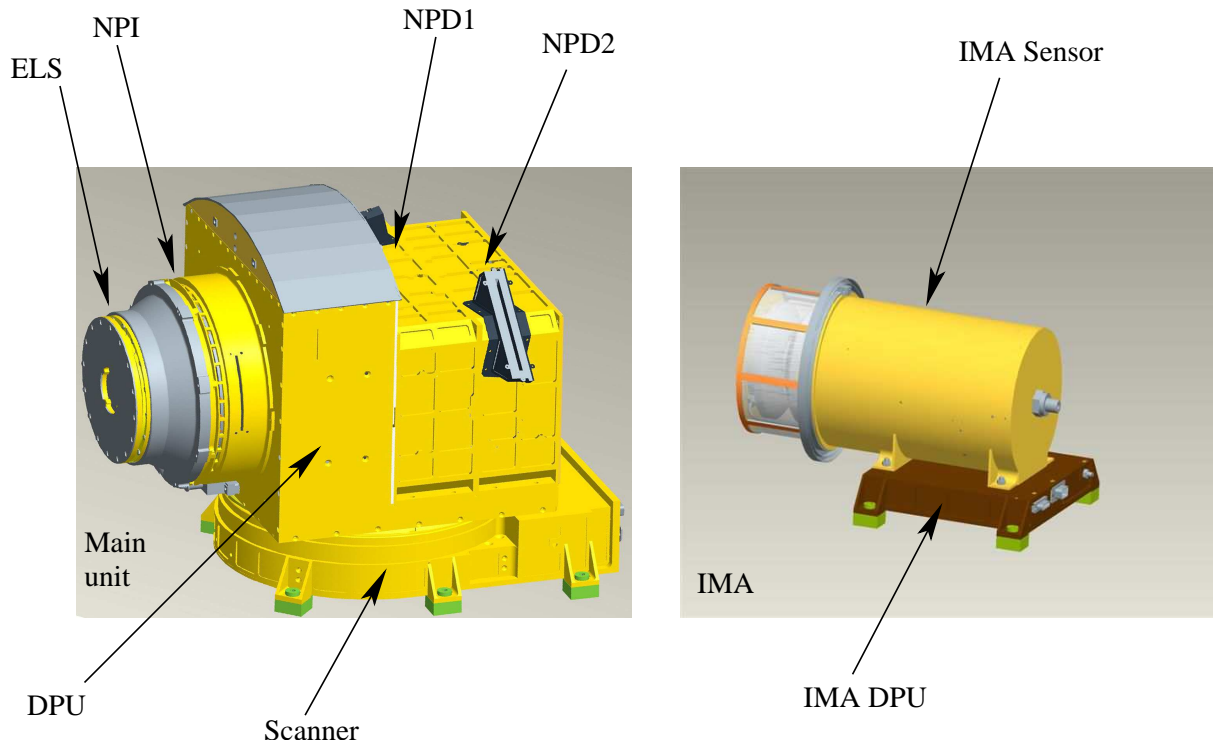


FIG. 9 The ASPERA-4 overall configuration, main unit, and ion mass analyzer

aging and sharing of internal resources. The instrument DC/DC converters are shared between all 5 units including the two identical NPD sensors. The DPU mechanical structure also serves as the carrying support for mounting the NPD sensors and the NPI which in turn is carrying the ELS. The internal walls that separate the DPU, NPI, and the two NPD sensors have been replaced by conductive kapton foils to minimise mass, while maintaining sufficient electromagnetic shielding. Because of the high radiation hardness requirement (30 krad) tantalum point shielding is used.

TABLE II The performance of the NPI, NPD, ELS, and IMA sensors.

Parameter	NPI	NPD	ELS	IMA
Particles to be measured	ENA	ENA	electrons	ions
Energy, keV per charge	$\approx 0.1-60$	0.1-10	0.01-15	0.01-36
Energy resolution, $\Delta E/E$	-	0.8	0.07	0.07
Mass resolution	-	H, O	-	m/q=1,2,4,8,16,32,>40
Intrinsic field of view	$9 \times 344^\circ$	$9 \times 180^\circ$	$10 \times 360^\circ$	$90 \times 360^\circ$
Angular resolution, FWHM	$4.6 \times 11.5^\circ$	$5 \times 30^\circ$	$10 \times 22.5^\circ$	$4.5 \times 22.5^\circ$
G-factor / pixel, $\text{cm}^2 \text{sr}$	$2.7 \cdot 10^{-3}$	$6.2 \cdot 10^{-3}$	$7 \cdot 10^{-5}$	$3.5 \cdot 10^{-4}$
Efficiency, %	≈ 1	0.5-15	incl. in G-factor	incl. in G-factor
Time resolution (full 3D), s	32	32	32	196
Mass, kg	0.7	0.65 each	0.3	2.2

The ELS uses an external metallic conic-shape ring to protect the sensitive electronics. Table II summarises the instrument performance.

B. The Neutral Particle Imager (NPI)

The ASPERA-4 NPI on Venus Express is a spare model of the ASPERA-3 NPI currently flying on board the Mars Express spacecraft which in turn is a replica of the NPI-MCP sensor developed for the ASPERA-C experiment on the Mars-96 mission and successfully flown on the Swedish microsatellite Astrid launched in 1995 (*Barabash, 1995*).

In the NPI the charged particles, electrons and ions, are removed by the electrostatic deflection system, which consists of two disks separated by a 3 mm gap (Fig. 10). The 5 kV potential between the grounded and biased disks results in a strong electric field, which sweeps away all charged particles with energies up to 60 keV. Since the integral ENA flux substantially exceeds the charged particle flux for energies greater than 60 keV, this rejection energy is sufficient for satisfactory performance. The disks also collimate the incoming beam over the azimuth angle. Apart from being ON or OFF, the deflection system can be operated in two other modes, alternative mode and sweeping mode. In the alternative mode, the deflection system is turned on and off for one sampling time. This mode is used for more accurate separation between charged and

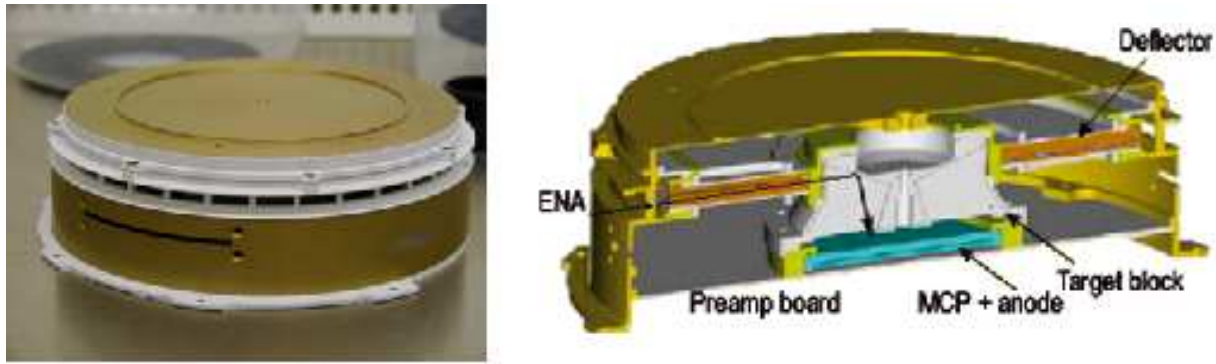


FIG. 10 Photograph and cut-away view of the NPI sensor.

neutral particles entering the system. The deflection system is connected to the high voltage supply via an optocoupler. Regulating the optocoupler reference voltage one can change the deflection voltage performing the sweeping and alternating. In order to reduce the time for discharging of the deflection system disks down to 1 ms, a second parallel optocoupler is used.

The space between the deflection system disks is divided into 32 sectors by plastic (PEEK) spokes forming 32 azimuthal collimators with a field of view of $9^\circ \times 18^\circ$ each. Neutrals passing through the deflection system hit a 32-sided cone target at a grazing angle of incidence of 20° . On impact with the target block the incident neutral can either be reflected, produce secondary particles, or both. The secondaries can be both ions and electrons. A 56 mm diameter PHOTONIS MCP stack in chevron configuration followed by a 32 sector anode detects the particles leaving the target. The signal from the MCP gives the direction of the primary incoming neutral. The MCP operates in ion mode with a negative bias of slightly more than -2.2 kV applied to the front side and thus detects (a) sputtered positive ions of the target material, (b) positive ions resulting from ionising of the primary neutrals, and (c) neutrals reflected from the target surface. In order to improve the angular resolution and collimate the particles leaving the interaction surface, 32 separating walls are attached to the target forming a star-like structure. This configuration allows the entering particles to experience multiple reflections and reach the MCP. NPI covers 4π in one scanner scan (except a fraction blocked by the spacecraft body) and produces an image of the ENA flux distribution in the form of an azimuth \times elevation matrix. The direction vector of 32 elements is read out once every 62.5 ms. Two sectors centred around the spin axis and looking toward the spacecraft body are blocked intentionally to provide monitoring of the MCP assembly dark counts. This space is also used for the ELS sensor harness. The internal views of the NPI sensor is given

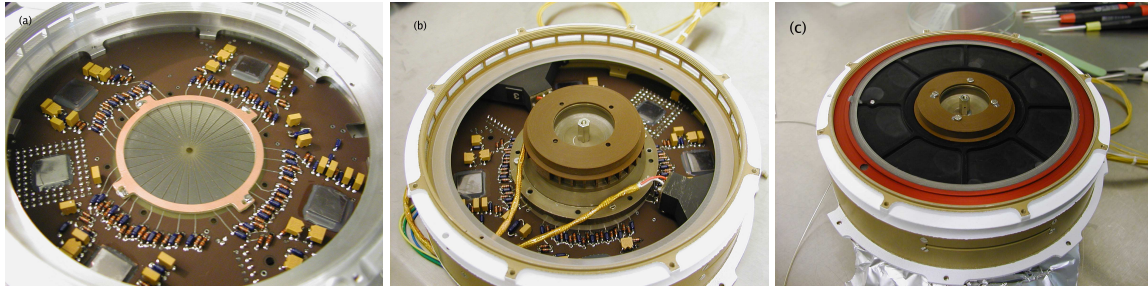


FIG. 11 NPI integration: the sectioned anode (a), target block installed (b), and deflection system mounted (c).

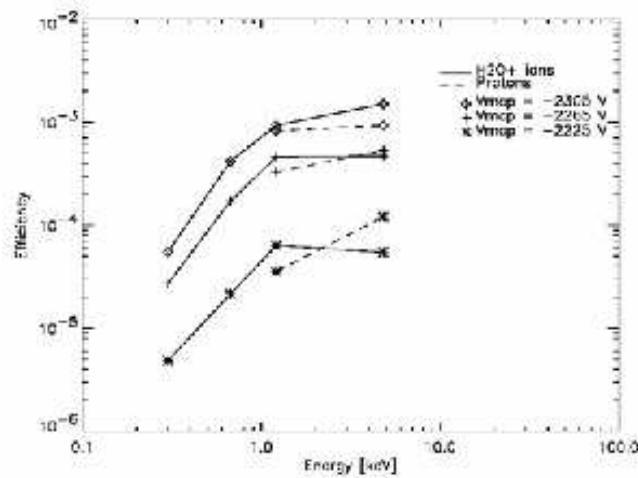


FIG. 12 The efficiency of sector 4 with neighbouring sectors mechanically blocked.

in Fig. 11

A calibration of the NPI sensor was performed to characterise the sensor response. MCP-saturation bias, dark count level, angular response in elevation and azimuth, and efficiency. One sector (number 4) was thoroughly investigated, and a scan with the calibration beam in the central plane of all sectors was used to find the relative response of the other 31 sectors. The calibration was performed using an ion beam as a particle source. This is equivalent to using an ENA beam, since particles “forget” their initial charge state when interacting with the surface of the target block.

Fig. 12 is the efficiency of the NPI measured with H_2O^+ ions and protons in the beam for different MCP bias and energies. The efficiency was measured in sector 4 with the neighbouring sectors mechanically blocked. For the MCP operating bias 2.2 kV the efficiency for solar wind energies (~ 1 keV) is around 5×10^{-4} . Fig. 13 is showing a scan in the central plane of all sectors over a wide parallel beam of 5 keV protons. This measurement was performed to calibrate out the rela-

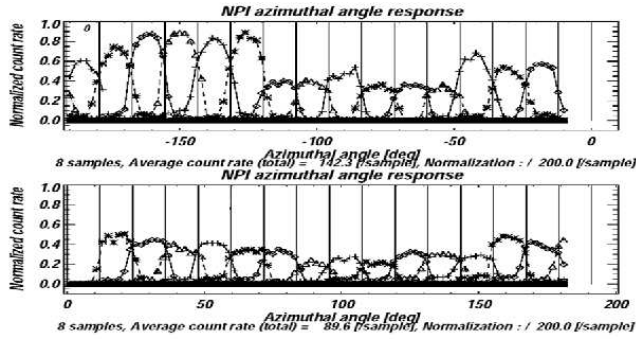


FIG. 13 Scan through the central plane of the sectors.

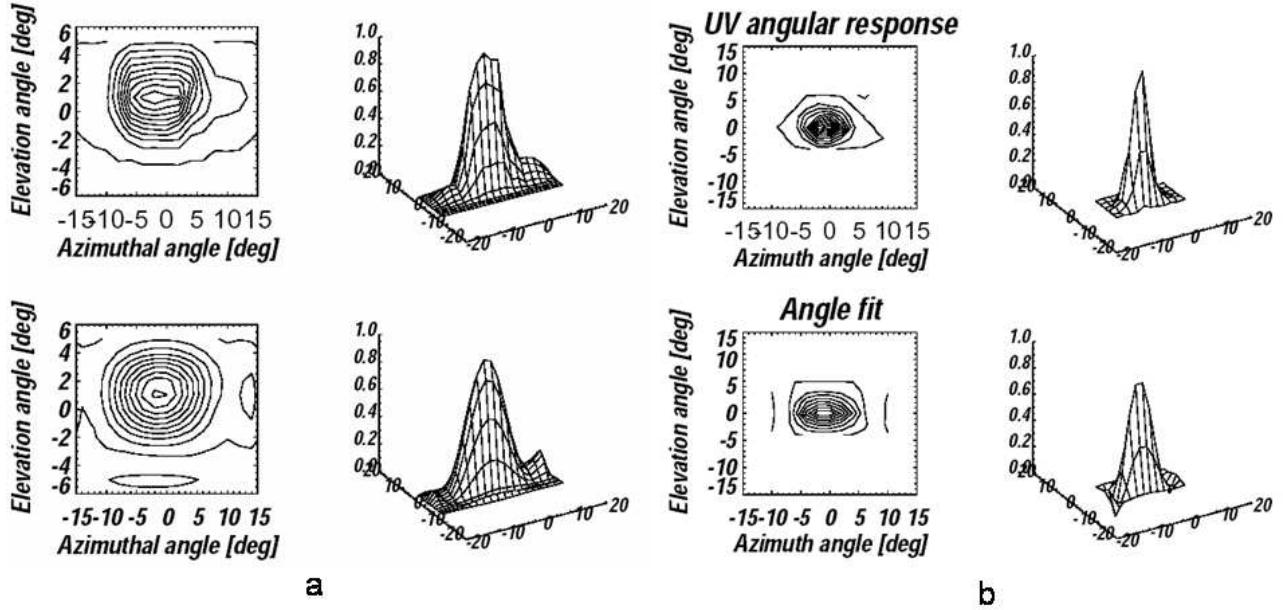


FIG. 14 a) Full angular scan with sector 4 in the particle beam (protons). The lower panels show a polynomial fit. (b) Full angular scan with sector 4 in a UV photon beam (Lyman- α). The lower panels show a polynomial fit.

tive sensitivity of the sectors, which varies significantly. Since the sector angular (polar–azimuth) response function should be included in the ENA image inversion models it was measured and analytical fits were produced. The upper panels of Fig. 14(a) show the measured data and response function and the lower panels show a polynomial fit to the response.

An important issue in the NPI design is the coating of the target block for suppressing UV photon fluxes, which enter the instrument and produce the UV background in the measurements. NPI uses the same coating as in the experiments PIPPI (Prelude in Planetary Particle Imaging) on board Astrid-1 and ASPERA-C on board MARS-96, namely, DAG 213, a resin-based graphite

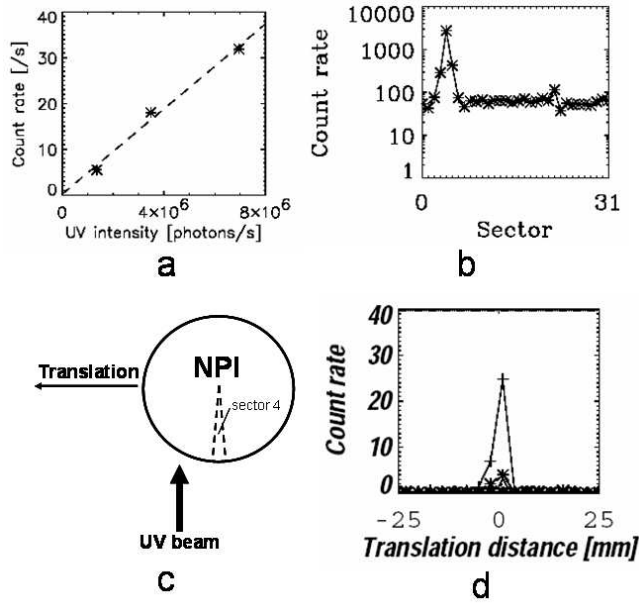


FIG. 15 (a) NPI sensitivity to UV intensity. (b) Total count during angular scan of sector 4 with UV beam. (c) Translation measurement set up. (d) Translation measurement results.

dispersion. This is similar to Aquadag, which is a graphite dispersion in water. The coating demonstrated satisfactory performance in the PIPPI experiment flown in the Earth's magnetosphere (*C:son Brandt et al., 2000*). To determine the target block UV separation the NPI was calibrated against hydrogen Lyman- α photons ($\lambda = 121.6$ nm). The calibration philosophy was similar as that of the particle calibration in that the response of one sector (number 4) was fully characterised then a relative measurement was made for the other sectors.

During calibrations conducted at the University of Arizona the UV-intensity in the beam was continuously monitored by an absolutely calibrated channeltron. The maximum intensity measured was 10^7 photons per second into the aperture of the NPI. The measured count rate was ~ 30 counts per second, which corresponds to a UV suppression efficiency of $10^7/30 \approx 3 \times 10^{-5}$. This is somewhat higher than what was previously reported by *Barabash (1995)*.

The intensity measurement is important to understand the NPI UV response. If we know that the response is more or less linear within certain intensities we can scale the response against what is present in space to determine the photon related background. Due to an unstable beam only three points on this curve were obtained. The NPI count rates for the respective beam intensities are plotted in Fig. 15.

It is important to know what the UV-response is at different incident angles to an NPI aperture. An angular scan could reveal if there are any reflections off of the deflection plates or the spokes in

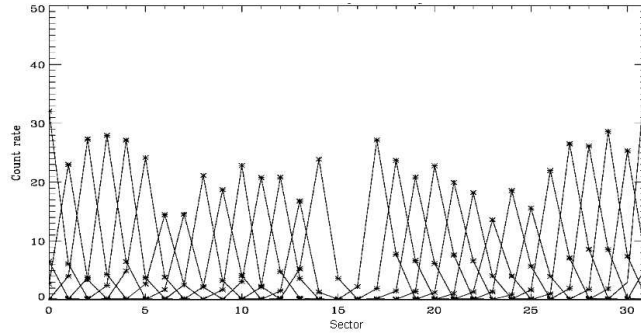


FIG. 16 The relative response of all sectors to the UV photons (Lyman- α). The measurements are taken with the UV beam centred on the aperture of each sector.

the electrostatic deflection system. The angular scan was made with respect to the aperture plane of the NPI (sector 4). We should thus expect not to see any counts in any other sector than number 4. If we do this must be a result of internal reflections since all photons from the beam are directed into the centre of sector 4 for all angles. The result of the angular scan is in Fig. 14(b) and Fig. 15(b) shows the sum of all counts during the angular scan in all sectors. There are visible counts in sectors 3, 4 and 5 at around 10% of that in sector 4. To ensure that there are no reflections from the spokes of sectors other than the centre a translation measurement was made. Sector aperture number 4 was centred in the UV beam direction and the NPI was horizontally translated according to figure Fig. 15(c). The space in the tank limited the translation to less than the full diameter of the NPI. However, reflections from aperture spokes further away than the translation range is highly unlikely as it would require a multitude of reflections to reach the target block. The resulting counts are in Fig. 15(d). It shows that there are not significant counts in any sector other than 4.

The relative response of other sectors was measured with the beam centred in the centre of each sector aperture. The beam intensity-compensated result is in Fig. 16.

Fig. 17 shows an example of NPI data from ASPERA-3 on Mars Express. Simulations of the ENA emissions from the corresponding directions (sectors) are also included. The increase in the count at around 20:10–20:20 UT results from ENA fluxes generated in the Martian magnetosheath when the shocked solar wind protons charge exchange on the exosphere and move further as hydrogen atoms along lines tangential to the solar wind stream lines. From data such as these one can find important parameters. For example, the position of the Induced Magnetosphere Boundary near Mars can be found (*Gunell et al.*, 2005a).

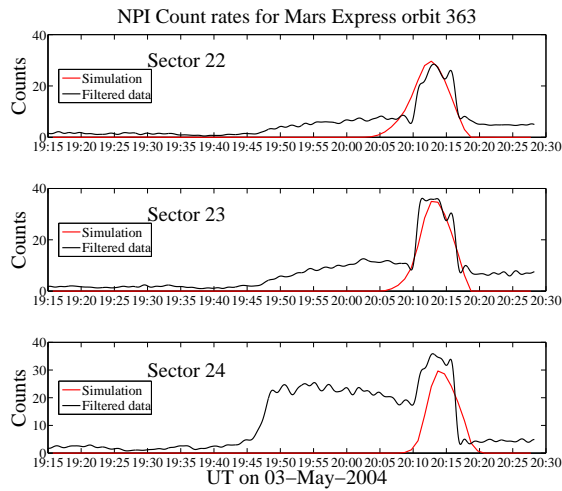


FIG. 17 Simulations (red curves) and filtered data (black curves) from Mars Express orbit 363 and the ASPERA-3 NPI sensor. The highest count rates in sector 23 correspond to a flux of $1.3 \times 10^{11} \text{m}^{-2} \text{sr}^{-1} \text{s}^{-1}$.

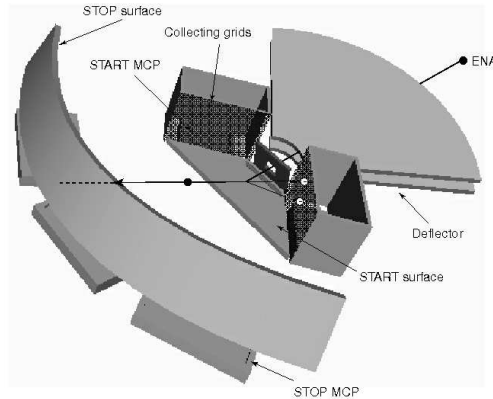


FIG. 18 Three-dimensional view of the NPD principal components.

C. The Neutral Particle Detector (NPD)

The NPD sensor consists of two identical detectors, each of which is a pinhole camera. Fig. 18. provides a conceptual view of one detector.

In each detector the charged particles, electrons and ions, are removed by a deflection system, which consists of two 90° sectors separated by a 4.5 mm gap. In the normal operational mode the 10 kV potential (± 5 kV) applied to the disks and the resulting strong electric field sweeps away all charged particles with energies up to 70 keV. The deflector also collimates the incoming beam in the elevation angle. The collimated ENA beam emerging from the 3.5×4.5 mm pin-hole hits the START surface under a 15° grazing angle causing secondary electron emission. By a system of

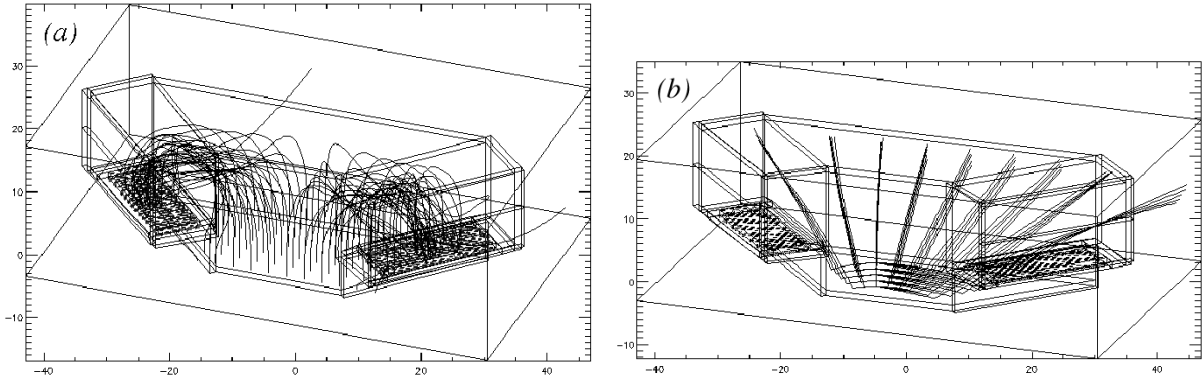


FIG. 19 Ray-tracing of electron (a) and 80 eV ion trajectories (b) in the START assembly optics.

collecting grids, the secondary electrons are transported to one of two MCP assemblies that give the START signal for TOF electronics.

Depending on the azimuth angle, the collection efficiency varies from 80% to 95%. The incident ENAs are reflected from the START surface near-specularly. Since the charge state equilibrium is established during the interaction with the surface, the emerging beam contains both the neutral and ionised (positive and negative) components. To increase the total efficiency, no further separation by the charge is made.

As proven by the ion tracing, there is very little disturbance to the reflected atomic ions leaving the START surface with an energy above 80 eV, introduced by the START electron optics. Fig. 19 shows the results of electron and ion ray-tracing in the START assembly electron optics.

Therefore particles of all charge states, i.e., negative, neutral, and positive, will impact the second surface, the STOP surface, and again produce secondary electrons, which are detected by one of the three MCP assemblies giving the STOP signal. The time of flight over a fixed distance of 8 cm defines the particle velocity. Three STOP MCPs also give crude resolution over azimuth within 90° acceptance angle. Since the secondary electron yield depends on mass for the same velocity, the pulse height distribution analysis of the STOP signals provides the estimation of ENA mass. Each event is stored in the array STOP MCP charge \times time-of-flight \times direction. The array is accumulated over the sampling time $62.5 \mu\text{s}$.

Fig. 20 shows a cross-section of the NPD sensor and its main elements with an ENA trajectory shown in blue. Fig. 21 shows the views of the flight model of the NPD sensor. Each sensor has 90° acceptance angle. Two identical sensors are built in a package installed on the scanning platform proving 180° scan and thus organising 2π coverage. Fig. 22 shows the two flight NPD sensors during installation into the ASPERA-4 instrument with apertures covered by red-tagged covers

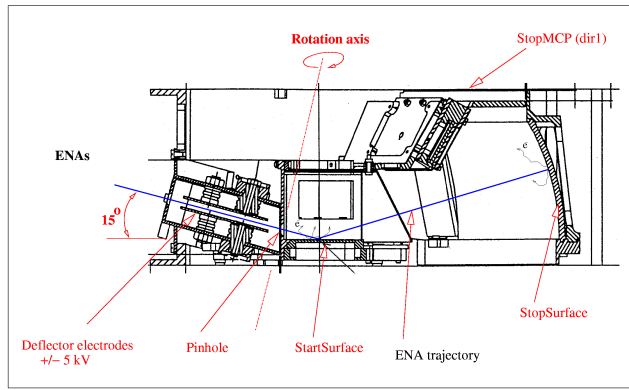


FIG. 20 Cross-view of the NPD sensor.

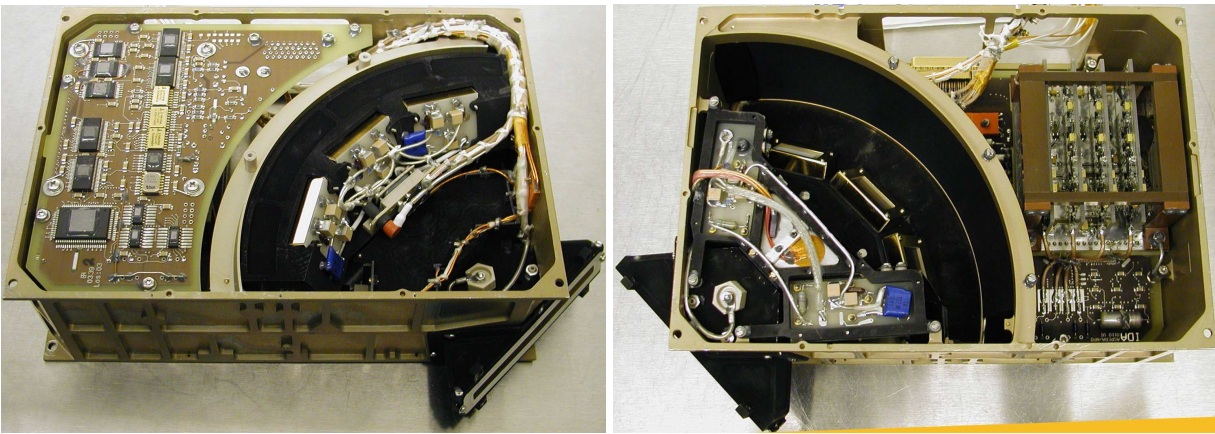


FIG. 21 Top and bottom view of the flight model of the NPD sensor.



FIG. 22 The flight model of the NPD sensor during installation.

with nitrogen purging tubes connected.

The selection of the START and STOP surfaces was the most challenging part of the NPD development. Extensive studies have been performed at University of Bern (*Jans, 2000*) and Brigham Young University (USA) to optimise the performance of the surfaces which must satisfy a number of requirements, namely, high secondary electron yield, high UV absorption even at grazing angles, high particle reflection coefficient (START surface), low angular scattering, and low photoelectron yield. For the START surface we chose a multi-layer coating composed of a thin layer of Cr_2O_3 , covered by a thicker layer of MgF, and topped with a thin layer of WO_2 . The coating is optimised for the absorption of the 121.4 nm line at the 15° incident angle. The reflection coefficient reached was about 30%, a factor of 2 lower than the uncoated surface. The coating is applied on a titanium substrate polished down to 100 Å roughness.

The STOP surface is graphite (roughness around 100 nm) covered by a MgO layer of about 500 nm. This combination has a very high secondary electron yield, low photoelectron yield, and high UV absorption. A lot of efforts have been made to increase the stability of the MgO coating against moisture. It was established that polishing the graphite substantially improves the stability and possible increases in air humidity during storage and pre-launch operations does not present any problems for the surface performance. Therefore, both surfaces are stable and do not require special maintenance.

The NPD calibrations included determining the efficiency, geometrical factor, angular response and energy resolution. The calibration results fully correspond to the specified performance. Since charge-equilibrium establishes over just a few Å at the particle-surface interaction, ion beams can be used for calibrations of ENA sensors. Fig. 23 shows the TOF distributions for a proton beam at different energies (colour coded) in the energy range 0.1 to 5.0 keV. The displacement of the peaks from the exact energy of the incident particles reflects the energy loss of 33%, which is independent on energy. The full width at half maximum (FWHM) is about 80%. Fig. 24 shows the TOF distributions for H_2O^+ ion beams of different energies covering the energy range from 0.3 keV to 10.0 keV. The energy losses are the same as for the proton beams.

Fig. 25 shows calibrated dependence of the measured TOF on the incoming particle energy for protons and H_2O^+ ions. The dashed lines show the theoretical dependence corresponding to the 33% energy loss in the START surface. The water molecules produced in the ion source break up during the impact, but the residual components carry the same initial velocity corrected for the energy loss in the target. Therefore, water can be used to calibrate the response of the instrument

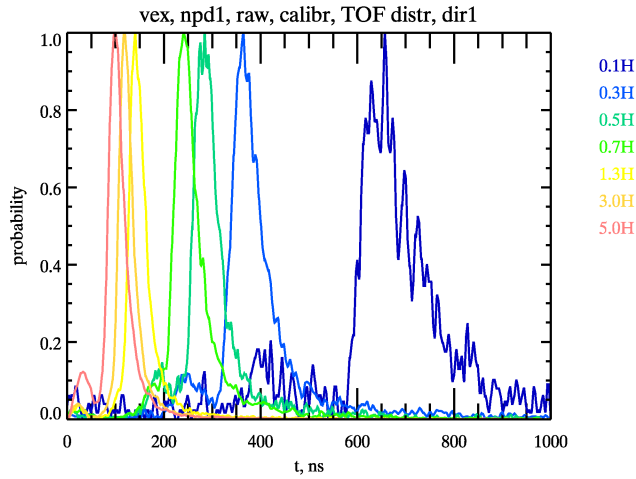


FIG. 23 NPD TOF spectra of proton beams at different energies.

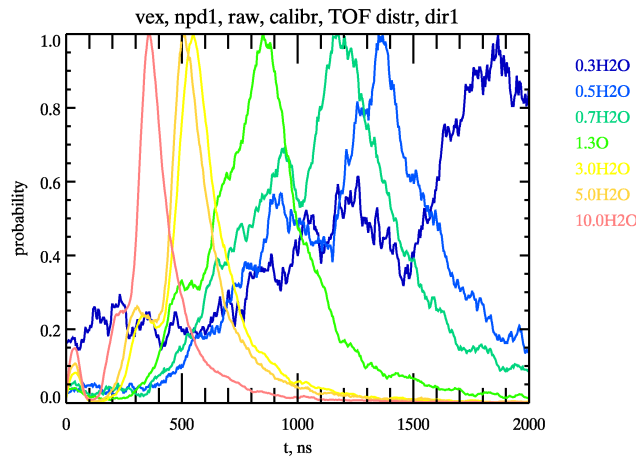


FIG. 24 NPD TOF spectra of H₂O beams at different energies.

to oxygen beams. Since the TOF for oxygen with an energy below 2 keV is longer than the TOF corresponding to slowest protons at around 100 eV TOF measurements alone can be used to identify the particle mass at least in the low energy range.

Fig. 26 shows the NPD angular response over azimuth for a 3 keV proton beam for the three STOP sectors. The red line shows the response of the central sector and the green and the black lines show the side sectors. Fig. 27 shows the sensor angular response over the polar angle. The FWHM over azimuth varies from 52° for the central sector to 35° and 37° for the two side sectors respectively. Over polar angle the FWHM is 4.5° for all directions.

Fig. 28 shows the absolute efficiency of the NPD sensor as a function of energy. The blue line corresponds to the incident proton beam and the red line corresponds to the H₂O⁺ beam.

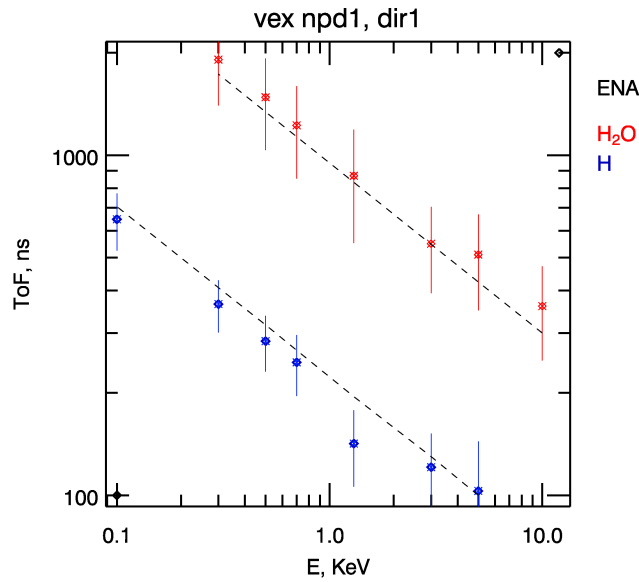


FIG. 25 Time-of-flight measurements for different masses as a function of energy. The dashed lines give the theoretical dependence corresponding to 33% energy loss.

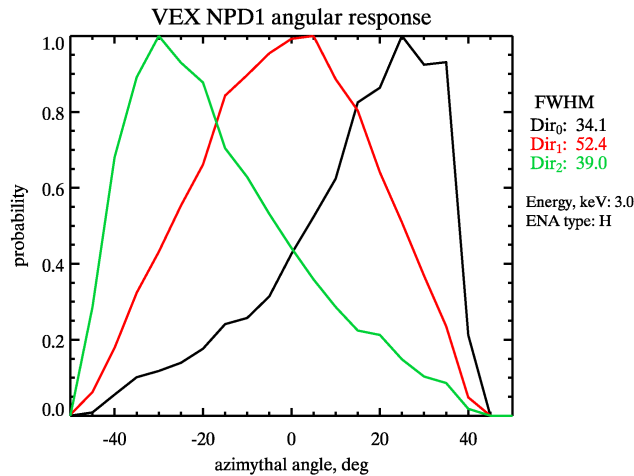


FIG. 26 The angular response of the NPD sensor in the azimuthal direction.

As is seen in Fig. 28 the efficiency is more than 11% for H₂O ENAs at 6 keV. For the H ENA the efficiency reaches 6.5%. Up to a certain energy the efficiency increases with energy, corresponding to an increase of the secondary electron yield. At the energy where the yield reaches unity the efficiency levels out (approximately 3 keV for protons and 6 keV for oxygen). At energies below 1 keV, the efficiency is around few percent.

Fig. 29 shows an example of NPD data from NPD on ASPERA-3 on Mars Express. The six panels correspond to the six directions from the two NPD sensors. For each panel the recorded

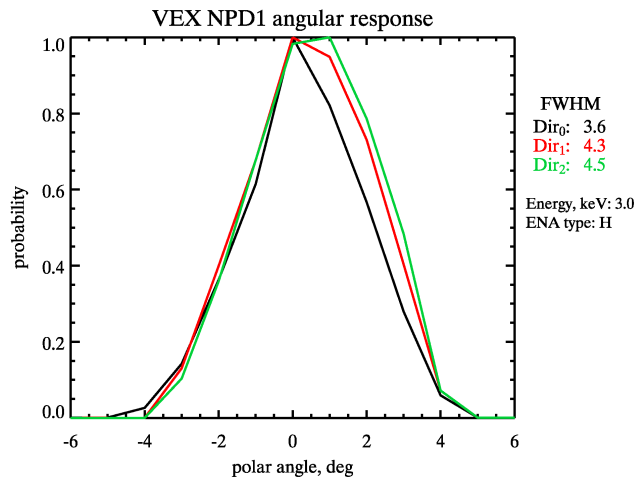


FIG. 27 The angular response of the NPD sensor in the polar direction.

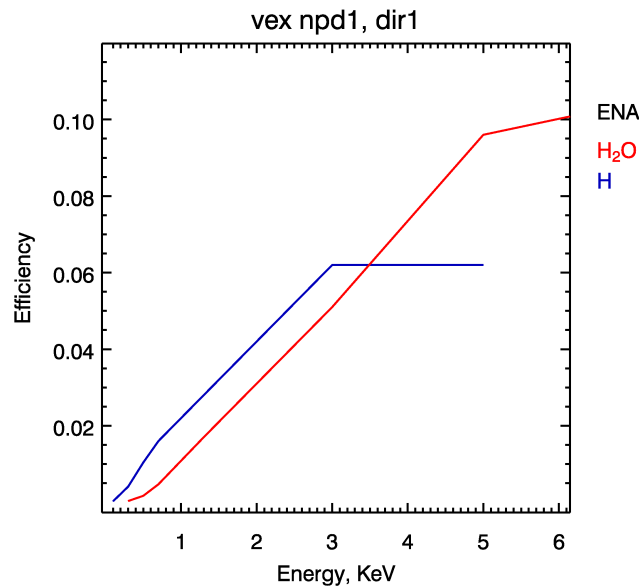


FIG. 28 NPD sensor absolute efficiency

TOF spectrum is shown. NPD1 was looking at the subsolar region of Mars while NPD2 looked at the Martian upper atmosphere. The peaks in panels 1–3 correspond to an intense flux of ENAs emerging from the sub-solar region (*Futaana et al.*, 2005). The origin of this flux is not yet known. It is perhaps similar to ENAs recorded by the NPI (see Fig. 17). The lower peaks visible on panels 4–6 are from ENAs originated from the Martian upper atmosphere. They are the result of backscattering of the solar wind protons precipitating onto the upper atmosphere (*Futaana et al.*, 2005) as predicted by *Kallio and Barabash* (2001). A somewhat similar picture is expected from

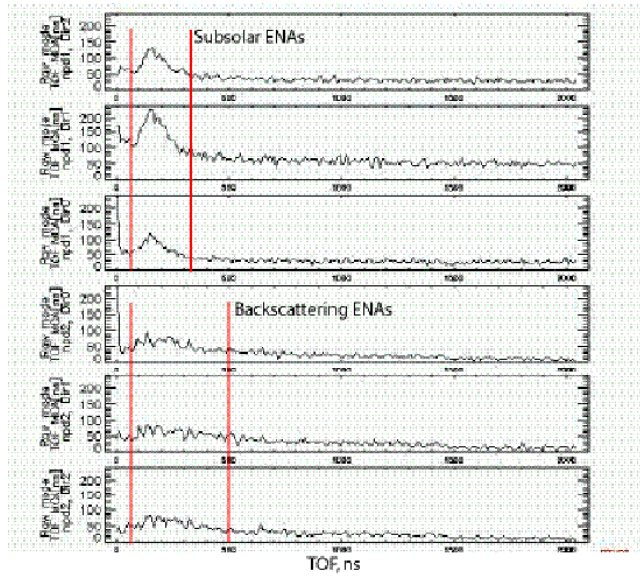


FIG. 29 NPD TOF spectra from Mars Express ASPERA-3 NPD. The six panels correspond to the six viewing directions from the two NPD sensors.

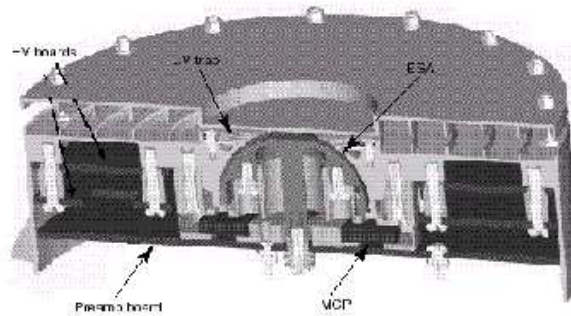


FIG. 30 Cut-away view of the ELS sensor

the NPD on Venus Express ASPERA-4.

D. The Electron Spectrometer (ELS)

The Electron Spectrometer (ELS) sensor represents a new generation of ultra-light, low-power, electron sensor (Fig. 30). It is formed by a 17° spherical top-hat electrostatic analyser and a collimator system with the radii of the inner and outer hemispheres equal to 14.9 mm and 15.9 mm respectively. Particles can enter the aperture at any angle in the plane of incidence. Electrons are then deflected into the spectrometer by applying a positive voltage to the inner hemisphere.

The electrons hit a micro channel plate (MCP) after being filtered in energy by the analyser plates. A spectral measurement is achieved by stepping the plate voltage.

Electrons with energies up to 20 keV/ q are measured, with a maximum time resolution of one energy sweep (consisting of 128 steps) per four seconds. There are 16 anodes behind the MCP, each anode defining a 22.5° sector and each connected to a preamplifier. The ELS sensor is mounted on the ASPERA-4 scanner platform, on top of the NPI sensor, in such a way that the full 4π angular distribution of electrons will be measured during each platform scan. Depending on the mode of operation a sample rotation scan takes 32, 64, or 128 seconds.

The ELS was designed to be solar blind so that it may operate in exposure to direct sunlight. This has been achieved using two UV reducing mechanisms and one secondary electron suppression technique. UV is minimised through the use of a series of light baffles in the ELS collimator and a series of UV light traps at the entrance to the spherical deflection plates. Secondary electrons are reduced by the addition of a special coating, based on a modified Ebanol-C process, which is included through out the deflection surface, light trap, and collimator system (*Johnstone et al.*, 1997).

There are two small differences between the ASPERA-3 (on board Mars Express) and ASPERA-4 ELS units. One is the inclusion of an outer cylindrical 2 mm thick Aluminium shield, which was added to prolong ASPERA-4 ELS operation in the harsher radiation environment of Venus. The other is an offset of the symmetry axes of the ASPERA-4 ELS deflection plates outside the 1% design specification. This happened because the ASPERA-4 ELS, as the refurbished Mars Express flight spare, was actually built earlier than the ASPERA-3 ELS, and therefore did not have the advantage of a critical improvement in the fabrication process that ensured that the stringent 1% requirement was achieved. The misalignment results in differences in instrumental properties as a function of the anode sector position, which will be illustrated in the calibration results discussed below.

The ASPERA-4 Electron Spectrometer (ELS) was calibrated at Mullard Space Science Laboratory, University College, London. The calibration facility (*Johnstone et al.*, 1997), which is based on the technique described by *Marshall et al.* (1986), provides a wide area photoelectron beam at energies ranging from a few eV to 15 keV with variable beam intensities from a few Hz to several MHz. The system is fully automated facilitating calibration scans over the complete range of polar and azimuth angles at several instrument voltage settings both for the analyser as well as the MCP. A flexible data acquisition system was integrated into the automation to provide

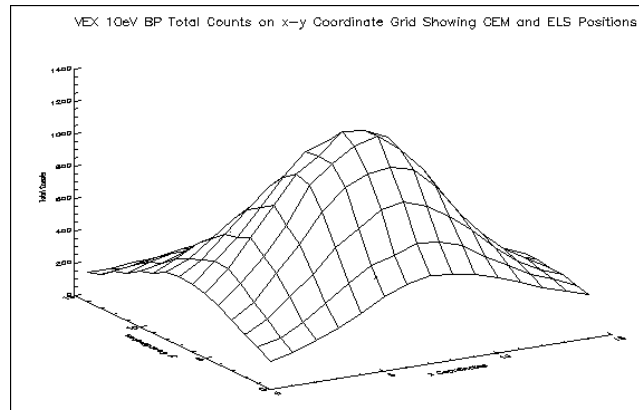


FIG. 31 Profile of 10eV electron beam prior to ELS calibration.

simultaneous measurements from the 16 preamplifier channels, coordinated with the instrument position and voltage settings. Before performing the instrument calibration, a profile of the beam output is recorded at each of the calibration energies by means of a channeltron mounted on an X-Y-table. A typical profile at 10 eV is shown in Fig. 31. During calibrations, the channeltron is mounted as close as possible to the instrument aperture in order to provide a constant reference to the beam intensity. Due to the mechanical imperfections of the instrument mentioned above, the laboratory calibrations were critical for defining the instrument response.

The instrument has two operational voltage ranges for the energy sweeps as described later and hence, tests were carried out at several energies in both ranges to cover $\pm 180^\circ$ in polar and $\pm 3^\circ$ in elevation. Fig. 32 is a typical plot of the voltage-angle scans carried out over the 16 anodes at 30 eV in the lower range. Fig. 33 is a plot of the k-factor across the 16 anodes giving an average value of 11.33. Although this is higher than the design value of 7.5 due to the mechanical imperfections, the variation across the anodes is less than 5%, allowing the instrument response to be made good with the calibrations with small errors. The imperfections result in a lower geometric factor but have the advantage of increasing the maximum energy acceptance of the instrument. The calibrations also establish the MCP operational levels for flight and are found to be 150 V higher for the ASPERA-4 compared to the ASPERA-3 unit. This is possibly due to an MCP with a lower intrinsic gain and/or due to a higher electronics threshold for the readout electronics. Finally, the UV rejection ratio of the analyser was also tested using a Lyman- α UV source (*Alsop et al.*, 1996).

The ELS unit has a self contained, dual range, linear high voltage power supply. The first power supply range is from 0 to about 20 volts (about 150 eV) and has 4096 possible settings. The second power supply range is from 0 to 2800 volts (about 20 keV) and also has 4096 possible

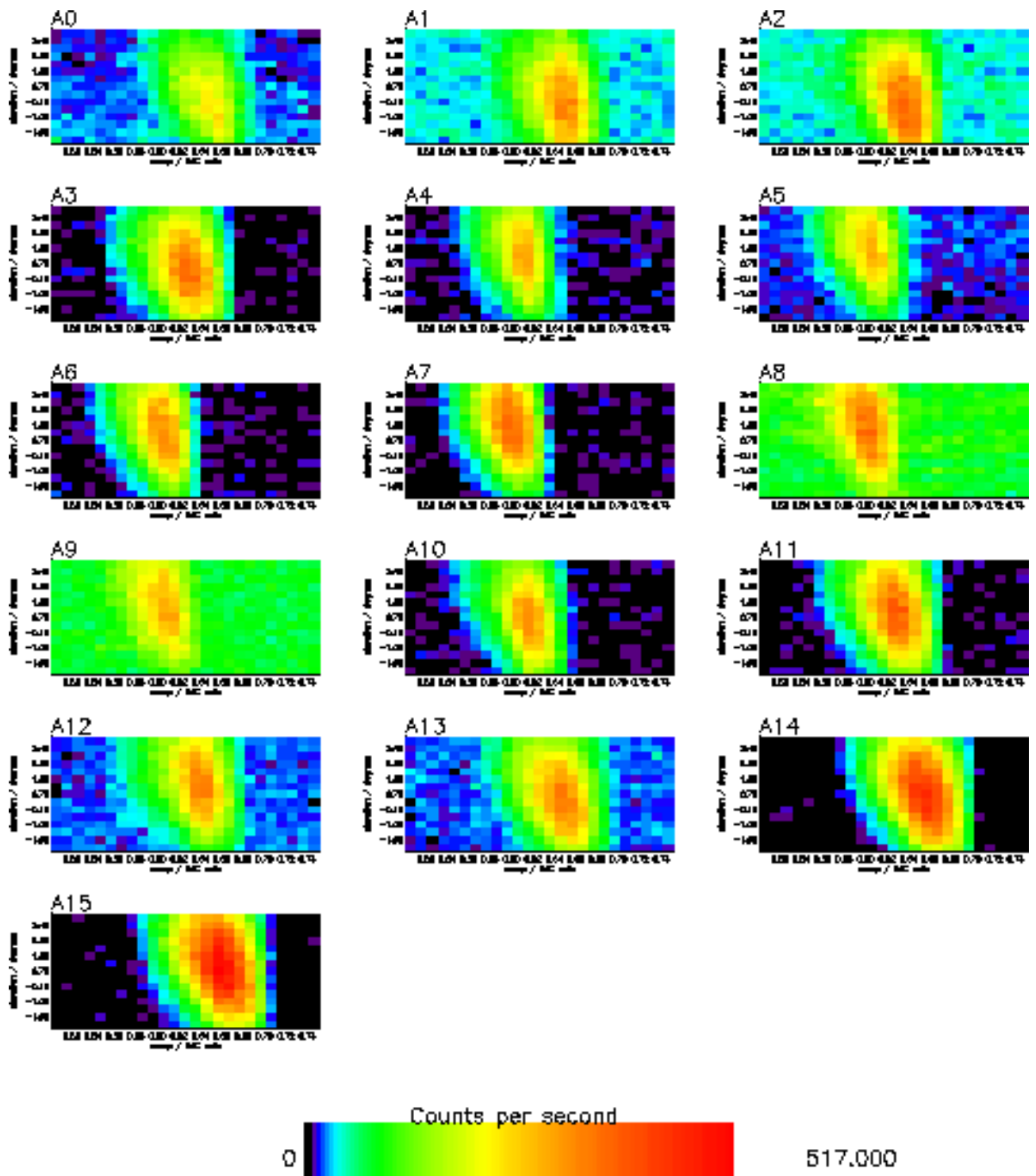


FIG. 32 Spectrograms of elevation angle versus the applied voltage on the inner hemisphere for a 30 eV beam.

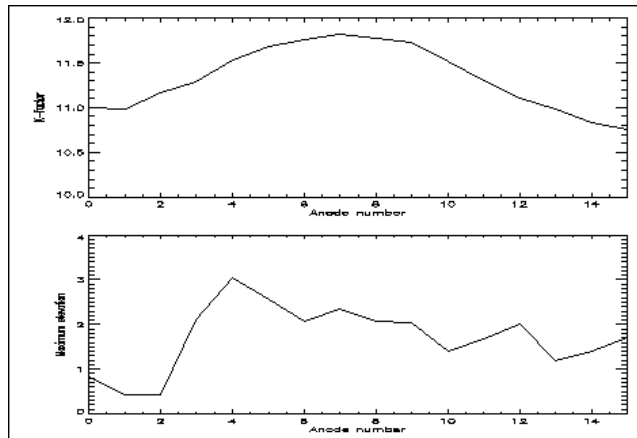


FIG. 33 Plot of the k-factor across the 16 anodes.

settings. The ELS sweep is fully programmable within the constraint of the maximum decay rate of 32 steps/s. On any given step, the deflection plate voltage is held constant during a minimum of 28.125 ms used to accumulate electrons. There is a minimum of 3.125 ms of data latency between energy steps for transition.

In order to obtain high resolution measurements of the energy spectrum, the power supply may be operated in an oversampling mode, which, when combined with the knowledge of the instrumental response function, increases the number of measurement points per energy interval over a reduced energy range. Measurements in this mode are shown in Fig. 34, which shows a clear resolution of the CO₂ photoelectron peaks, characteristic of the Martian atmosphere.

E. The Ion Mass Analyzer (IMA)

The Ion Mass Analyzer (Fig. 35), is an improved version of the ion mass spectrographs TICS (Freja, 1992), IMIS (part of ASPERA-C, Mars-96, 1996), and IMI (Planet-B, 1998) (Norberg *et al.*, 1998). It is an exact copy of the ICA instrument that is on its way to comet 67P/Churyumov-Gerasimenko on board the Rosetta spacecraft.

The principal diagram of the instrument is shown in Fig. 36. Ions enter the analyser through the external grounded grid. Behind the grid there is a deflection system whose purpose is to vary the incident polar angle of particles (shown in Fig. 36 as trajectories 1, 2, and 3). The deflection angle depends on the voltage applied to the deflector electrodes and lies within the $\pm 45^\circ$ from the equatorial plane of the instrument. Fig. 37 shows the instrument polar angle response as a function of the deflector voltage. Then ions pass through the top hat electrostatic analyser which select only

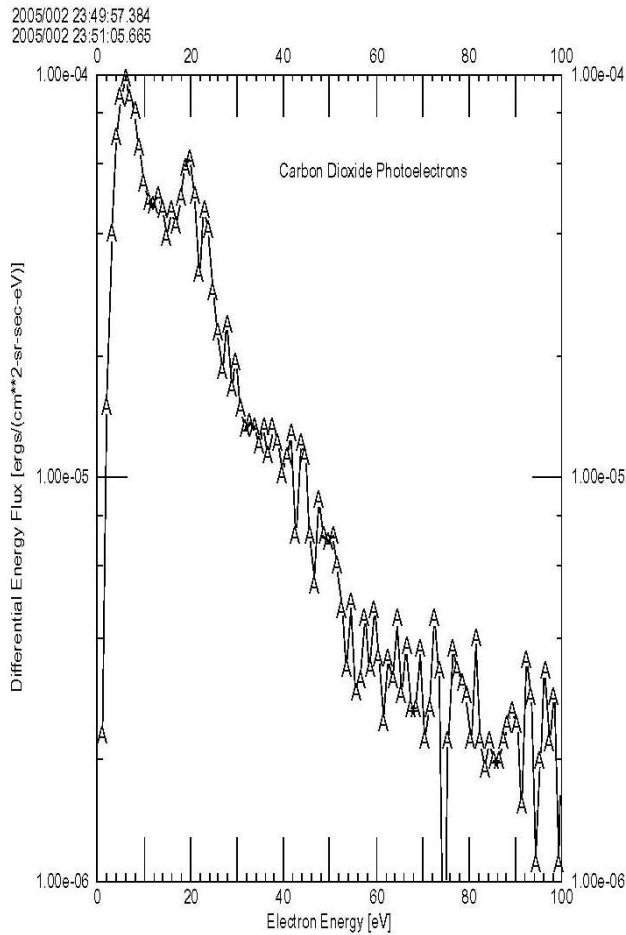


FIG. 34 Photoelectron spectrum from the Mars ionosphere.

the given particle energy according to the interplate voltage. Since the top hat analyser has a full 360° cylindrical symmetry, the azimuthal range (in the plane perpendicular to the symmetry axis) of the instrument is 360° . The parallel incident ion beam is focusing in the vicinity of the exit of the top hat analyser. Thus the particle position at the top hat analyser exit codes its azimuthal angle. Then the ions pass through the magnetic separation section. The cut of this section in the azimuthal plane is shown in the right panel of Fig. 36. The magnets are shown as blue sectors. Sixteen gaps between the magnets correspond to 16 azimuthal sectors of the instrument of 22.5° each. The radial deviation of the ion trajectories at the exit of the magnetic field region corresponds to particle velocity per charge. Since behind electrostatic analyser all particles have the same energy per charge value, ion position codes their masses. The particles are registered by an MCP with a position sensitive anode. The anode resolves 32 bins in the radial position and 16 azimuthal sectors. An example of detector response is shown in Fig. 38.

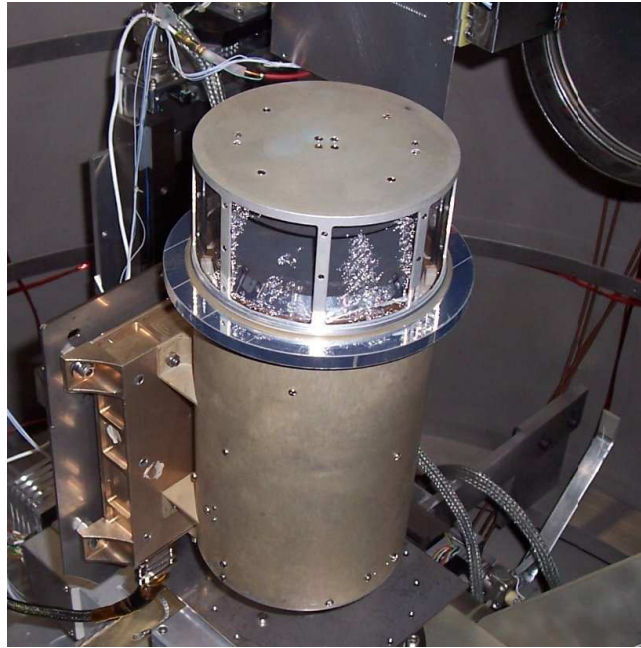


FIG. 35 The IMA sensor in the vacuum chamber.

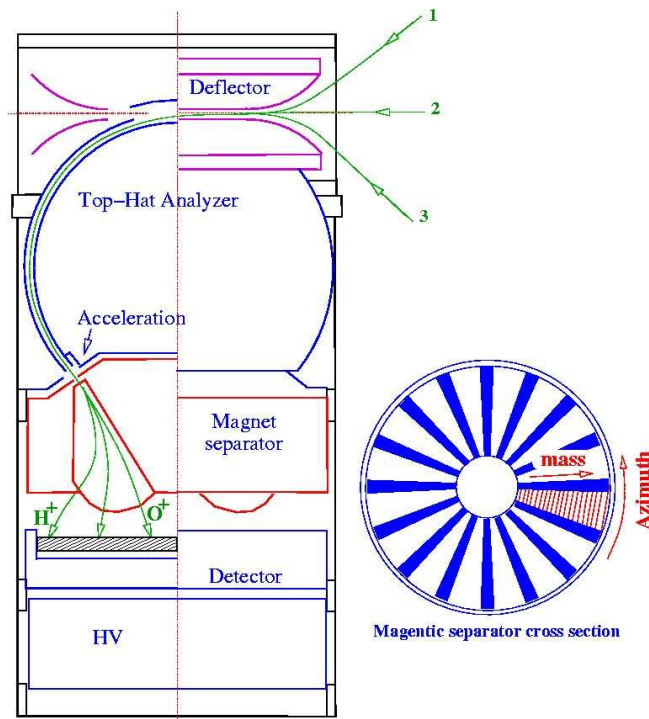


FIG. 36 Cut of the analyser (left) with examples of the ion trajectories, and a cross section of the magnet separator (right).

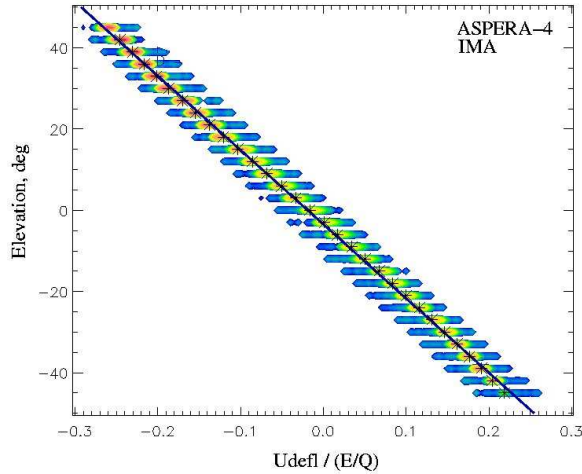


FIG. 37 Colour coded instrument response as a function of polar (elevation) angle and deflector voltage normalised to the ion energy.

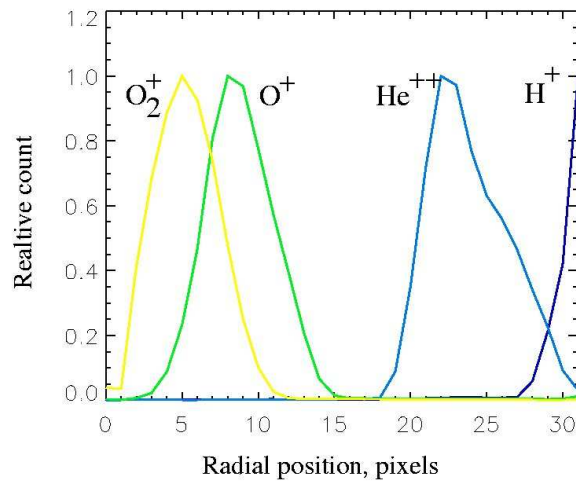


FIG. 38 Radial profiles of a few mass peaks. The particle energy is 1250 eV, and the post acceleration voltage is -2150 V.

To provide the possibility to measure light ions at low energies, ions, such as H^+ which have too small gyro-radius to reach the MCP, can be accelerated between the top hat analyser exit and the magnetic section entrance. Fig. 38 shows the 1 keV particles distribution over the detector surface when the acceleration level is -2150 V. Protons only partially reach the MCP for this post acceleration level. With an acceleration of 3615 V protons hit the detector at least down to an energy of 300 eV. From Fig. 37 one can see that polar angle resolution for constant deflector voltage is about 6° . Fig. 39. shows the azimuthal response of the instrument.

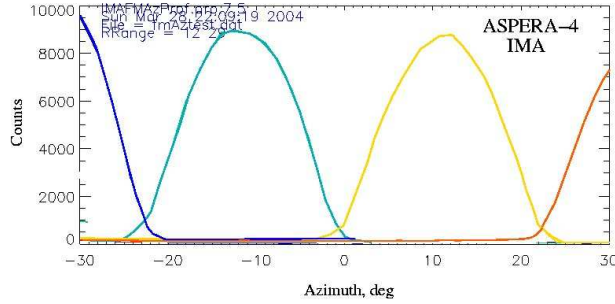


FIG. 39 Azimuthal response for selected sectors.

Logically the IMA instrument consists of the ion optics part shown in Fig. 36, a position sensitive detector,

Besides the ion analyser and position sensitive detector the IMA sensor includes a high voltage unit that provides the sweep voltage for all electrodes and MCP bias, and an IMA DPU. The IMA DPU, which is built around the 16-bit MA31750 processor from Dynex, controls analyser voltages, reads out and accumulates the position information for each detector event, and forms telemetry packets. The hardware operation mode is fixed. The fastest changing parameter is the particle energy. It sweeps from 30 keV down to 10 eV over 96 logarithmically equidistant steps. The exposure time on each energy step is 125 ms. During this time interval 16 radial position spectra (32 points) corresponding to 16 azimuthal sectors are accumulated. After each complete energy sweep the instrument changes the polar angle of the field of view. The polar angle is scanned from -45° up to $+45^\circ$ over 16 steps. The total time to complete a full 3D spectrum is 192 s. This spectrum consists of 32 radial (mass) points \times 16 azimuthal sectors \times 96 energy steps \times 16 polar angles. The data processing includes 3 stages: 1) logarithmic compression of the count values; 2) integration (if necessary) over polar angles, and/or azimuthal angles; and 3) RICE compression of the final spectrum. The processing mode is set by TC or chosen automatically according to the TM rate limitations. The acceleration level is also commandable. Only 3 values of acceleration are available: 0 V, -2150 V, and -3650 V.

Fig. 40. shows an example of a energy-mass matrix of an ion-beam event, and was obtained by the ASPERA-3 IMA on Mars Express. The vertical axis represents the energy per charge in eV and the horizontal axis represents the IMA sensor's mass ring number. The red and blue lines in the figure indicate the calibrated mass band ranges for the different ion species: O_2^+ ; O^+ ; He^{2+} ; and H^+ . Measurements such as these are used to study the ion composition of the plasma that

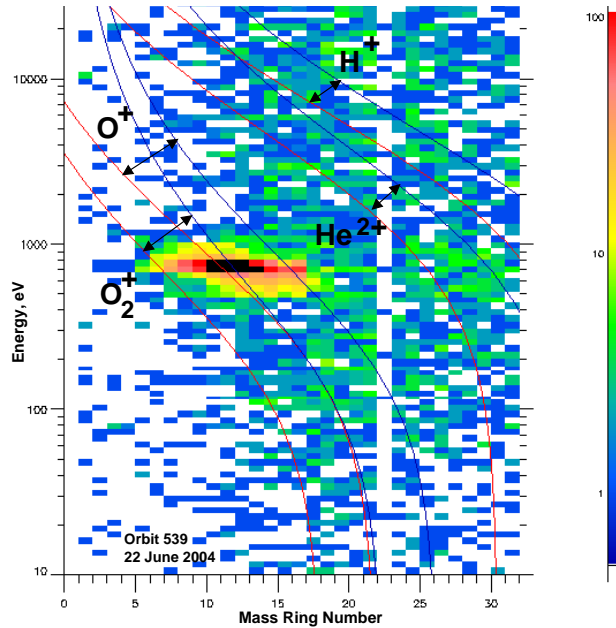


FIG. 40 Energy-mass matrix obtained by the ASPERA-3 IMA during Mars Express orbit no. 539. The vertical axis represents the energy per charge in eV and the horizontal axis the mass ring number. The red and blue lines show the calibrated mass band ranges for O_2^+ , O^+ , He^{2+} , and H^+ .

escapes from Mars (*Carlsson et al.*, 2005).

F. The Digital Processing Unit (DPU)

The ASPERA-4 DPU mechanically includes two boards: the DPU board itself, which is shown in Fig. 41, and a Housekeeping (HK) board, which is shown in Fig. 42. These are connected together with the sensor control electronics and the power supply via a common bus system with 8 address and 16 data lines besides control, analog and power supply lines.

The DPU is built around the 16-bit processor MA31750 from Dynex with 12 MHz system clock frequency and an Actel Field Programmable Gate Array (FPGA) RT54SX32S, which implements memory management, watchdog functions and the serial spacecraft interface protocol. The software runs inside a 128 kByte RAM, organised in 2 banks of two 32kByte static memory chips each. On power-up, a two times 16 kByte bipolar PROM (HARRIS) is activated with a boot loader, which transfers the complete PROM contents into the RAM, changes then the program control to the RAM area and switches the power to the PROMs off via transistor switches to conserve power. It then starts monitoring the telecommand interface for possible boot instructions. This allows the configuration of the instrument in a flexible, but safe manner: If a start configura-

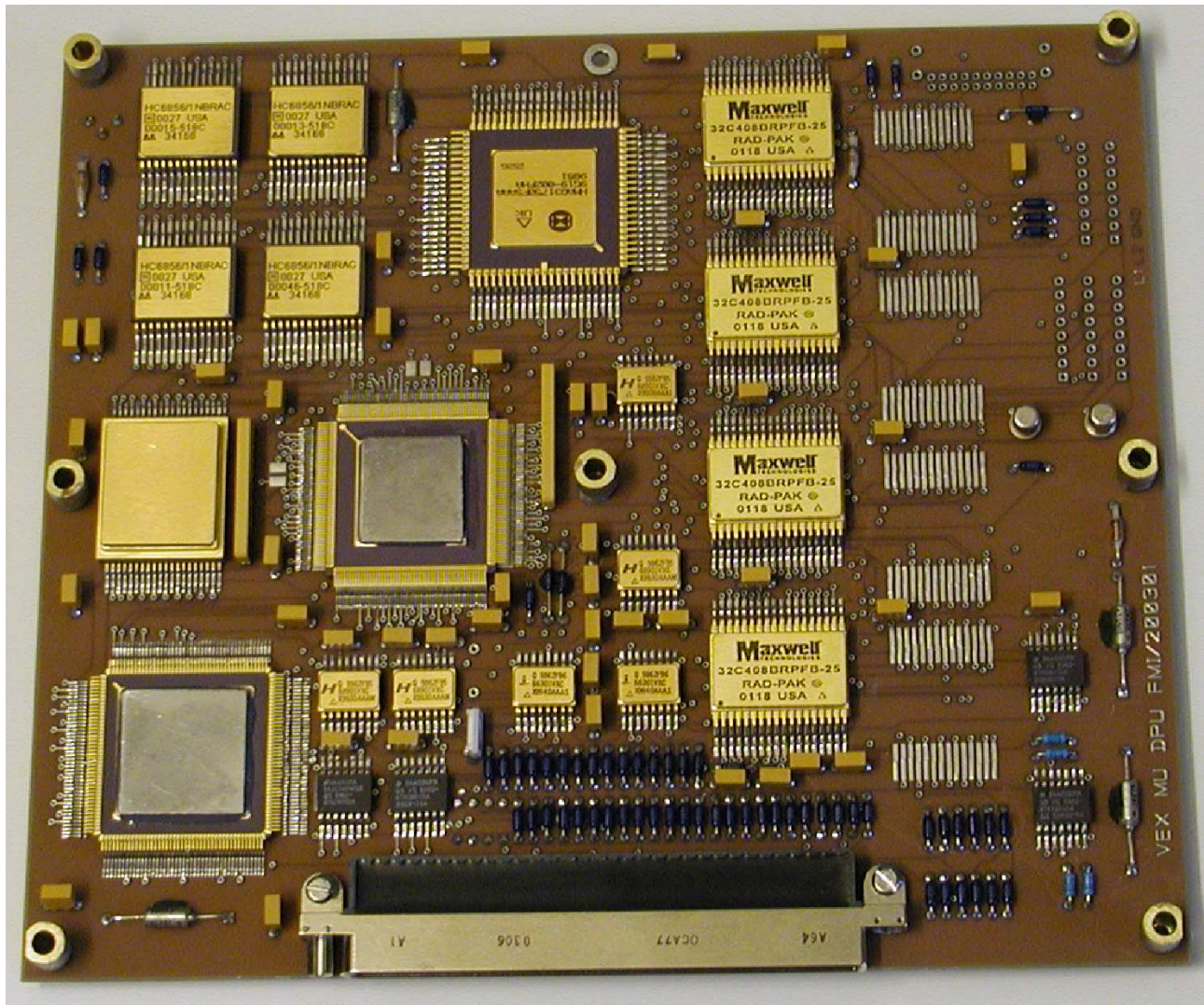


FIG. 41 Main DPU circuit board.

tion is defined via telecommand, the software continues accordingly. Otherwise the default start configuration inside the EEPROM is used. If this is corrupted, the original default configuration from PROM will be used.

A 512 kByte radiation hardened EEPROM (Maxwell) contains additional program code and configuration information, which can be modified from ground. 2 MByte mass memory RAM is used to store measurement data and buffer telemetry packets.

An Actel FPGA RT1280 implements the serial data transfer protocol to the IMA detector with an interface identical to the corresponding hardware used on the Rosetta mission. All interface lines are buffered via special circuits to protect the instrument from external noise effects.

The DPU board is controlled by a 24 MHz crystal which is divided down to 12 MHz and

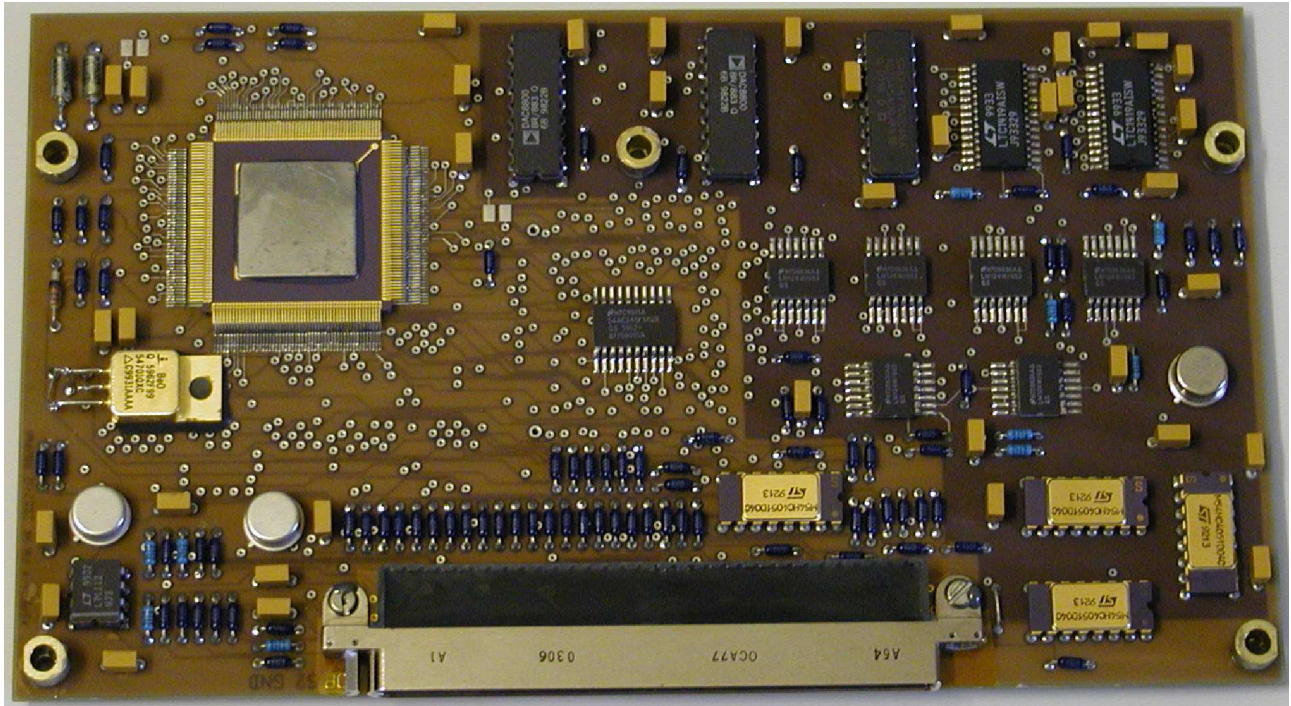


FIG. 42 ASPERA-4 housekeeping board.

buffered inside an FPGA before it is used for FPGA and processor operations and also on the HK board. As the main FPGA needs 2.5 V operations voltage, this is generated by dedicated regulators directly on the DPU and on the HK board. The watchdog circuit inside the FPGA can be enabled by software. Then it has to be reset regularly by software access. Otherwise it issues a hardware reset to the whole DPU board after 16 seconds. Except for a special error message, the behaviour is identical to a boot sequence after power-up. The DPU board controls most detector voltages with direct access to the power supply board.

The HK board is controlled by a separate RT54SX32S FPGA, which maps all input and output functions into standard bus address space. It also implements the needed counters for detector pulses from the NPI and ELS.

Four eight-channel analog multiplexers select one out of 32 analog voltages to be monitored. They are digitalised by one 14-bit Analog-to-Digital-Converter (ADC, LTC1419). Another 14-bit ADC monitors the ELS deflection voltage. Two 8-bit Digital-to-Analog-Converters generate via 8 latching buffers the control voltages for NPD, NPI, ELS and the scanner. Also the sun-sensor electronics is implemented on the HK board

The software is built around a real-time system with scheduler and interrupt handler. All exe-

cutable routines are defined inside a routing table, which resides in EEPROM and can be modified during flight. In this way new or modified software routines can be stored inside a free area of the EEPROM, verified and added to the operating software by including their start address into this routing table. A macro feature of the telecommand handler offers the possibility to generate sequences of standard telecommands automatically according to a pre-defined list, reducing the need for complex telecommand groups to be up-linked over and over again. Besides detector activation and parameter control, compression and averaging of measurement data allow the reduction of the amount of telemetry generated.

G. The Scanner

The scanning platform was originally developed for the ASPERA-C experiment for the Russian Mars-96 project. The modifications that were made for the Mars Express and the Venus Express missions mostly concerned optimisation of the performance during longterm operations and reducing its mass. The ASPERA-4 scanner serves also as a bearing structure for the ELS, NPI, NPD sensors, and the DPU, as well as all electrical interfaces with the spacecraft. The technical data of the scanner system are summarised in table III.

Fig. 43. shows an internal view of the scanner. The large diameter worm wheel (1) to which the sensor assembly is fixed is rotated by a stepper motor (2) via a co-axial worm screw (not visible below the flat cable). The worm wheel is fixed to the structure with a large diameter angular contact ball bearing. During the scanner life time tests, several types of balls, including the ordinary already mounted in the original bearings, were tested. The balls finally used are of ceramic type (Si_3N_4), which was found to be the most suitable. The housing and circular sensor platform are manufactured in a high-strength aluminium alloy. The motor driving electronics (not shown), also located in the scanner, provides the motor control and driving. The position of the movable parts relative the scanner is given by three magnetic sensors, two end-sensors at 0° and 180° (3), and one step counter. Because of the requirements on long-term operations no mechanical contact exist in the sensors. The feed-through cable loop (4) with six cables and 6 connectors, each cable with 26 conductors (a maximum of 156 connections possible) interfacing through D-SUB connectors, provides electrical interface of the whole instrument with the satellite electrical systems.

A worm gear type of mechanism was selected in order to provide self-locking without electrical

TABLE III Mechanical scanner platform technical data.

Technical data	Value	Unit
Maximum angle of rotation	± 100	deg.
Angular movement per step, fs. Mode	0.0190	deg.
Angular movement per step, hs. Mode	0.0095	deg.
Angular position feedback resolution	0.05	deg.
Angular positioning accuracy	0.2	deg.
Operational rotation rate	1.5/3.0/6.0	deg./s
Maximum rotation rate	~ 25.0	deg./s
Power dissipation	0.5–2.0	W
Platform load	3.7	kg
Maximum platform load	~ 12	kg
Dimensions	$60 \times 254 \times 232$	mm
Mass	1.42	kg
Operational lifetime in vacuum	~ 3	years

power, to minimise friction, and to obtain a high gear ratio. The platform is made as a plug-in unit towards the sensor assembly. Great efforts have been spent to reduce mass, volume, power consumption and out-gassing in vacuum as well as to achieve high reliability. On command the platform can be turned to an arbitrary position or perform continuous scanning at any rate of rotation up to the maximum.

The scanner also contains a locking mechanism to avoid possible movements of the platform during vibration. The mechanism contains a wire which ties two small levers locking the worm screw axis. Applying by command a voltage to the wire burns it out and the levers are forced apart by a spring unlocking the axis.

III. THE TEAM

The ASPERA-4 experiment is a large consortium including 16 groups from 11 countries over the entire Europe, USA, and Japan. Table IV shows the primary hardware responsibilities for the different groups.

TABLE IV ASPERA-4 groups and primary hardware responsibilities.

Organisation	Primary hardware contribution
Swedish Institute of Space Physics, Kiruna, Sweden	PI-institute , Instrument provider NPI, NPD, IMA, scanner
Centre d'Etude Spatiale des Rayonnements, Toulouse, France	Co-PI institute , NPI MCPs, IMA anode system, IMA calibrations, IMA development, DC/DC board, scanner driver board, hardware support
Institute of Space and Astronautical Science, Sagamichara, Japan	NPI calibrations and development
University of Bern, Physikalisches Institut, Switzerland	NPD surfaces, NPD mechanics
Instituto di Fisica dello Spazio Interplanetari, Rome, Italy	EGSE, NPI mechanics, NPD electronics
Mullard Space Science Laboratory, UK	ELS calibrations
University of Arizona, Tucson, USA	START surface, NPD UV calibrations
Southwest Research Institute, San Antonio, USA	ELS (MEX spare), data analysis
Rutherford Appleton Laboratory , Oxfordshire, UK	NPD MCPs
Finnish Meteorological Institute, Helsinki, Finland	MU and IMA DPUs, theory
Space Physics Research Laboratory, University, of Michigan, Ann Arbor, Michigan, USA	Theory
Max Planck Institute for Solar System Research, Katlenburg-Lindau, Germany	NPD TOF electronics
Space Science Laboratory, University of California at Berkeley, Berkeley, California, USA	Theory
Space Research Institute, Graz, Austria	Magnetometer team
Space Technology Ireland, National University of Ireland, Maynooth, Co. Kildare, Ireland	Hardware support
Applied Physics Laboratory/John Hopkins University, Laurel, Maryland, USA	Theory

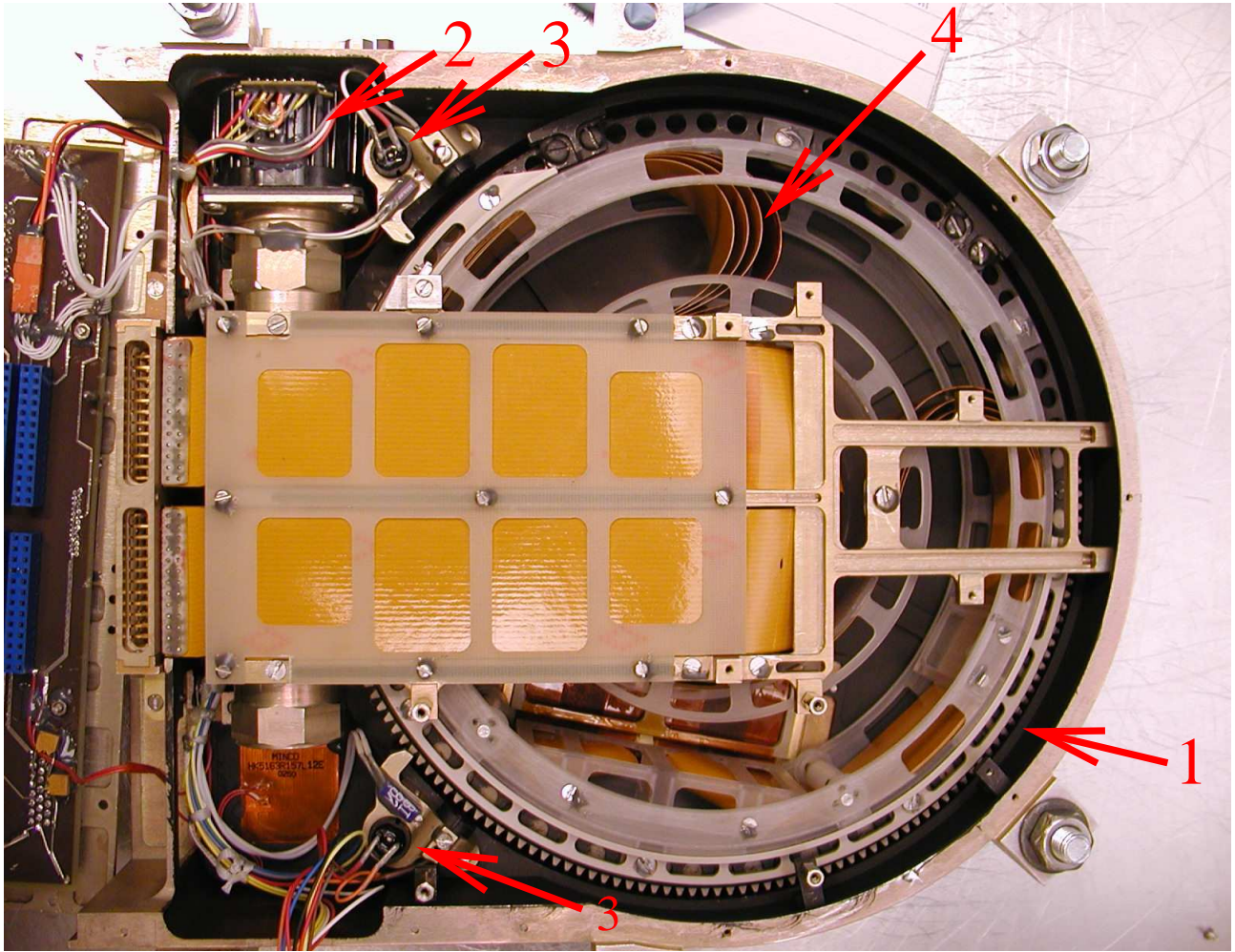


FIG. 43 Internal view of the ASPERA-4 scanner. The numbered items indicate 1) the large diameter worm wheel; 2) a stepper motor; 3) the two end-sensors at scanner position 0° and 180° respectively; and 4) the feed-through cable loop.

IV. ACKNOWLEDGEMENTS

The ASPERA-4 experiment on the European Space Agency (ESA) Venus Express mission is a joint effort between 16 laboratories in 11 countries, all sponsored by their national agencies. We thank all these agencies as well as the various departments/institutes hosting these efforts. The Principle Investigator Institute (Swedish Institute of Space Physics) wishes to acknowledge the Swedish National Space Board for their support. We are indebted to ESA for their courage in embarking on the Venus Express program, the first ESA mission to this planet.

References

- Acuña, M. H., et al., Magnetic field and plasma observations at Mars: Initial results of the Mars Global Surveyor mission, *Science*, 279, 1676, 1998.
- Alsop, C., L. Free, and S. Scott, UV rejection design and performance of the Cluster PEACE 'top-hat' electrostatic analyser, in *AGU Chapman Conference on Measurement Techniques in Space Plasmas*, 1996.
- Barabash, S., Satellite observations of the plasma - neutral coupling near Mars and the earth, *IRF Scientific Report 228*, Swedish Institute of Space Physics, Kiruna, Sweden, 1995.
- Barabash, S., et al., *ASPERA-3: Analyser of Space Plasmas and Energetic Ions for Mars Express*, pp. 121–139, ESA SP-1240: Mars Express: the Scientific Payload, 2004.
- Biernat, H. K., N. V. Erkaev, and C. J. Farrugia, Aspects of MHD flow about Venus, *J. Geophys. Res.*, 104, 12,617–12,626, 1999.
- Biernat, H. K., N. V. Erkaev, and C. J. Farrugia, MHD effects in the Venus magnetosheath, *Adv. Space Res.*, 26, 1587–1591, 2000.
- Biernat, H. K., N. V. Erkaev, and C. J. Farrugia, MHD effects in the Venus magnetosheath including mass loading, *Adv. Space Res.*, 28, 833–839, 2001.
- Brace, L. H., R. F. Theis, and W. R. Hoegy, Plasma clouds above the ionopause of Venus and their implications, *Planetary and Space Science*, 30, 29–37, doi:10.1016/0032-0633(82)90069-1, 1982.
- Brecht, S. H., Solar wind proton deposition into the Martian atmosphere, *J. Geophys. Res.*, 102, 11,287–11,294, doi:10.1029/97JA00561, 1997.
- Carlsson, E., et al., Mass composition of the escaping plasma at Mars, *Icarus*, in press, 2005.
- C:son Brandt, P., S. Barabash, G. R. Wilson, E. C. Roelof, and C. J. Chase, Energetic neutral atom imaging at low (< 10 keV) energies from Astrid: Observations and simulations, *J. of Atmos. and Solar Terrestrial Phys.*, 62, 901–910, 2000.
- Donahue, T. M., and E. Hartle, Solar cycle variations in H⁺ and D⁺ densities in the Venus ionosphere: Implications for escape, *Geophys. Res. Lett.*, 12, 2449–2452, 1992.
- Fok, M.-C., T. E. Moore, M. R. Collier, and T. Tanaka, Neutral atom imaging of solar wind interaction with the Earth and Venus, *J. Geophys. Res.*, 109(A1), A01206, doi:10.1029/2003JA010094, 2004.
- Futaana, Y., et al., First ENA observations at Mars: Subsolar ENA jet, *Icarus*, in press, 2005.
- Gunell, H., K. Brinkfeldt, M. Holmström, et al., Measurements and simulations of energetic neutral atoms produced by charge exchange at Mars, *Icarus*, submitted, 2005a.

- Gunell, H., M. Holmström, S. Barabash, E. Kallio, P. Janhunen, A. F. Nagy, and Y. Ma, Planetary ENA imaging: Effects of different interaction models for Mars, *Planetary and Space Science*, doi:10.1016/j.pss.2005.04.002, in press, 2005b.
- Gunell, H., M. Holmström, H. K. Biernat, and N. V. Erkaev, Planetary ena imaging: Venus and a comparison with mars, *Planetary and Space Science*, 53(4), 433–441, doi:10.1016/j.pss.2004.07.021, 2005c.
- Hartle, R. E., and J. M. Grebowsky, Upward ion flow in ionospheric holes on Venus, *J. Geophys. Res.*, 95, 31–37, 1990.
- Holmström, M., S. Barabash, and E. Kallio, X-ray imaging of the solar wind–Mars interaction, *Geophys. Res. Lett.*, 28(7), 1287–1290, 2001.
- Holmström, M., S. Barabash, and E. Kallio, Energetic neutral atoms at Mars I: Imaging of solar wind protons, *J. Geophys. Res.*, 107(A10), 1277, doi:10.1029/2001JA000325, 2002.
- Intriligator, D. S., H. R. Collard, J. D. Mihalov, R. C. Whitten, and J. H. Wolfe, Electron observations and ion flows from the Pioneer Venus Orbiter plasma analyzer experiment, *Science*, 205, 116–119, 1979.
- Intriligator, D. S., J. H. Wolfe, and J. D. Mihalov, The Pioneer Venus Orbiter plasma analyzer experiment, *IEEE Transactions on Geoscience and Remote Sensing*, 18, 39–43, 1980.
- Jans, S., Ionization of energetic neutral atoms for application in space instrumentation, Master's thesis, Philosophisch-naturwissenschaftlichen Fakultät Universität Bern, 2000.
- Johnstone, A. D., et al., Peace: a Plasma Electron and Current Experiment, *Space Science Reviews*, 79, 351–398, 1997.
- Kallio, E., and S. Barabash, On the elastic and inelastic collisions between precipitating energetic hydrogen atoms and Martian atmospheric neutrals, *J. Geophys. Res.*, 105, 24,973–24,996, doi:10.1029/2000JA900077, 2000.
- Kallio, E., and S. Barabash, Atmospheric effects of precipitating energetic hydrogen atoms on the Martian atmosphere, *J. Geophys. Res.*, 106, 165–178, doi:10.1029/2000JA002003, 2001.
- Kallio, E., J. G. Luhmann, and S. Barabash, Charge exchange near Mars: The solar wind absorption and energetic neutral atom production, *J. Geophys. Res.*, 102, 22,183–22,197, 1997.
- Krasnopolsky, V. A., and G. R. Gladstone, Helium on Mars: EUVE and PHOBOS data and implications for Mars' evolution, *J. Geophys. Res.*, 101(A7), 15,765–15,772, 1996.
- Luhmann, J. G., Comparative studies of the solar wind interaction with weakly magnetized planets, *Adv. Space Res.*, 12(9), 191–203, 1992.
- Luhmann, J. G., and S. J. Bauer, Solar wind effects on atmosphere evolution at Venus and Mars, *Washington*

- DC American Geophysical Union Geophysical Monograph Series*, 66, 417–430, 1992.
- Luhmann, J. G., and J. U. Kozyra, Dayside pickup oxygen ion precipitation at Venus and Mars - Spatial distributions, energy deposition and consequences, *J. Geophys. Res.*, 96(15), 5457–5467, 1991.
- Ma, Y., A. F. Nagy, K. C. Hansen, D. L. DeZeeuw, and T. I. Gombosi, Three-dimensional multispecies MHD studies of the solar wind interaction with Mars in the presence of crustal fields, *J. Geophys. Res.*, 107(A10), 1282, doi:10.1029/2002JA009293, 2002.
- Marshall, F. J., D. A. Hardy, A. Huber, J. Pantazis, J. McGarity, E. Holeman, and J. Winningham, Calibration system for electron detectors in the range from 10 ev to 50 kev, *Rev. Sci. Instrum.*, 57(2), 229–235, 1986.
- McKay, C. P., and C. R. Stoker, The early environment and its evolution on Mars: implications for life, *Rev. Geophys.*, 27, 189, 1989.
- Mihalov, J. D., and A. Barnes, The distant interplanetary wake of Venus - Plasma observations from Pioneer Venus, *J. Geophys. Res.*, 87, 9045–9053, 1982.
- Mihalov, J. D., J. H. Wolfe, and D. S. Intriligator, Pioneer Venus plasma observations of the solar wind-Venus interaction, *J. Geophys. Res.*, 85, 7613–7624, 1980.
- Moore, K. R., D. J. McComas, C. T. Russell, and J. D. Mihalov, A statistical study of ions and magnetic fields in the Venus magnetotail, *J. Geophys. Res.*, 95, 12,005–12,018, 1990.
- Moore, K. R., D. J. McComas, C. T. Russell, S. S. Stahara, and J. R. Spreiter, Gasdynamic modeling of the Venus magnetotail, *J. Geophys. Res.*, 96, 5667–5681, 1991.
- Nagy, A. F., T. E. Cravens, J.-H. Yee, and A. I. F. Stewart, Hot oxygen atoms in the upper atmosphere of Venus, *Geophys. Res. Lett.*, 8, 629–632, 1981.
- Norberg, O., M. Yamauchi, R. Lundin, S. Olsen, H. Borg, S. Barabash, M. Hirahara, T. Mukai, and H. Hayakawa, The ion mass imager on the Planet-B spacecraft, *Earth, Planets, and Space*, 50, 199–205, 1998.
- Russell, C. T., R. C. Elphic, and J. A. Slavin, Limits on the possible intrinsic magnetic field of Venus, *J. Geophys. Res.*, 85, 8319–8332, 1980.
- Schubert, G., C. T. Russell, and W. B. Moore, Timing of the Martian dynamo, *Nature*, 408, 666–667, 2000.
- Stewart, A. I. F., Design and operation of the pioneer venus orbiter ultraviolet spectrometer, *IEEE Transactions on Geoscience and Remote Sensing*, 18, 65–70, 1980.
- Zhang, T., et al., Magnetic field investigation of the Venus plasma environment, *Planetary and Space Science*, submitted, 2005.



ASPERA-4



**Venus
Express**

Reference : **VE-ASP-TN-060402**
Issue : **1** Rev. : **1**
Date : **2006-06-17**
Volume : **-** Page: **6**

APPENDIX 3. ASPERA-4 SCANNER

1 Aspera-4 scanner history

The scanner platform was developed originally for the ASPERA-C experiment for the Russian Mars – 96 project. Some modifications made for Mars Express and Venus express missions mostly concerned optimization of the performance during long term operations and reducing its mass. Aspera-4 scanner is from Aspera-3 scanner further approved with respect to its electronics and mechanical behaviour.

2 Scanner key features

The Aspera-4 scanner key features are shown in table 1.

Technical data	Value	Unit
Maximum angle of rotation	+/-100	[deg.]
Angular movement per step, fs. Mode	0.0190	[deg.]
Angular movement per step, hs. Mode	0.0095	[deg.]
Angular position feedback resolution	0.05	[deg.]
Angular positioning accuracy	0.2	[deg.]
Operational rotation rate	1.5/3.0/6.0	[deg./s]
Maximum rotation rate	~25.0	[deg/s]
Power dissipation	0.5-2.0	[W]
Platform load	3.7	[kg]
Maximum platform load	~12	[kg]
Dimensions	60x254x232	[mm]
Mass	1.42	[kg]
Operational lifetime in vacuum	~3	[years]
Gear ratio	188	-

Table 1 Mechanical scanner platform key features

3 Scanner overview

The Aspera scanner, Aspera-4 scanner shown in figure 1 and 2, constitutes the 0° to 180° rotating platform on which all Aspera sensors (part from IMA) as well as the DPU, high voltage power supply, house keeping and DC/DC boards are situated. The scanner also provides all necessary mechanical and electrical interfaces between the space craft and Aspera (part from IMA).



Figure 1 Aspera-4 scanner

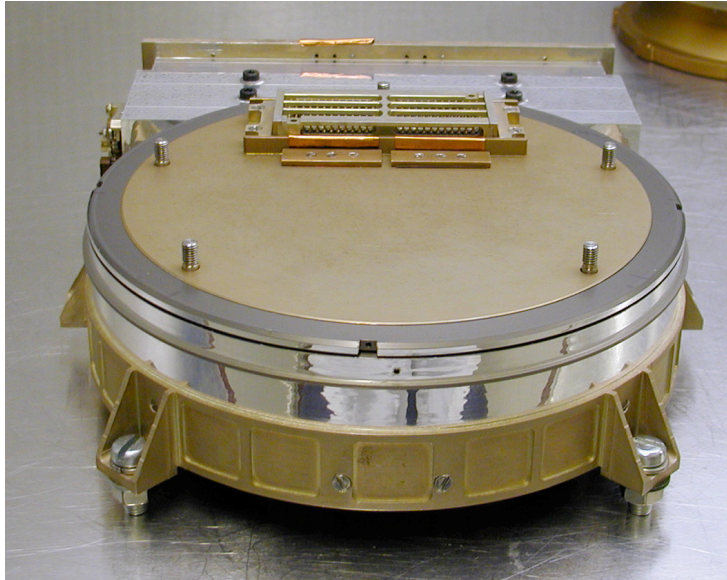


Figure 2 Aspera-4 scanner

Figure 3 shows Aspera-4 scanner with its mechanical and electrical interface with the DPU box that contains almost all necessary electronics as well as all sensors that constitutes Aspera-4 plasma package (part from IMA).

For the rotation feature a worm gear type of mechanism was selected in order to provide self-locking without electrical power, to minimize friction and to obtain a high gear ratio (1:188). The platform is made as a plug-in unit towards the sensor assembly. Great efforts have been spent to reduce mass, volume, power consumption and out-gassing in vacuum as well as to achieve high reliability.

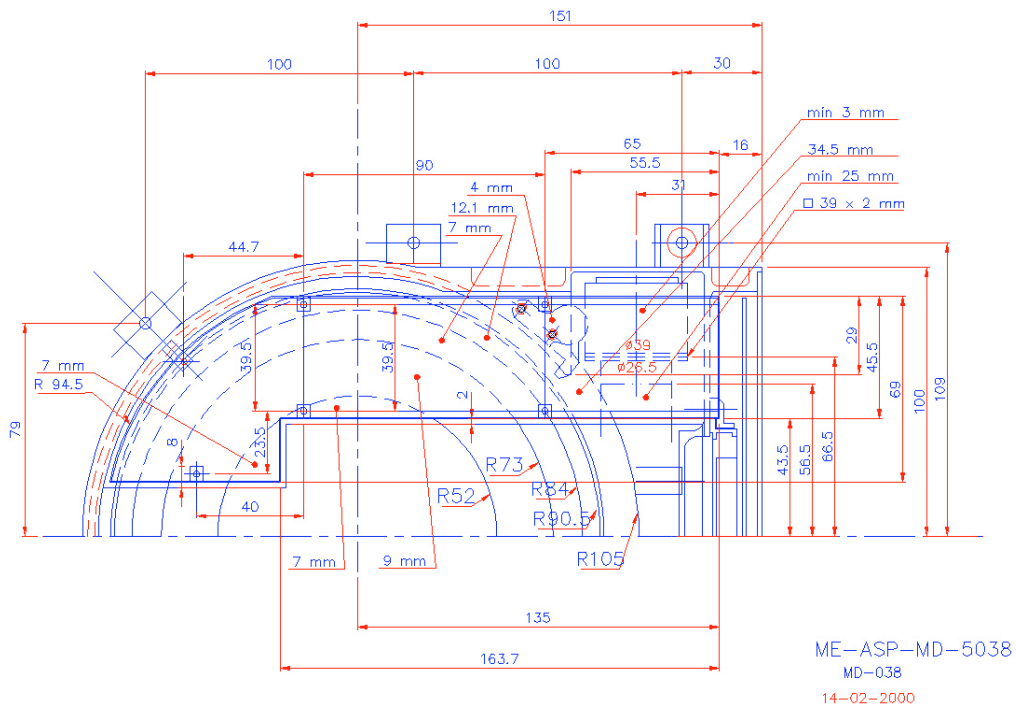


Figure 3 Aspera scanner dimensional overview

3.1 Mechanical overview

Figure 4 shows the scanner internal view. The large diameter worm wheel (1) to which the sensor assembly is fixed is rotated by a stepper motor (2) via a co-axial worm screw (not visible below the flat cable). The worm wheel is fixed to the structure with a large diameter angular contact ball bearing. During the scanner life time tests, several types of balls, including the ordinary already mounted in the original bearings, were tested. The balls finally used are of ceramic type (Si_3N_4), which was found to be the best suited. The housing and circular sensor platform is manufactured in high-strength aluminum alloy. The position of the movable parts relative the scanner is given by three magnetic sensors, two end-sensors at 0° and 180° (3), and one step counter. Because requirements of long-term operations no mechanical contact exist in the sensors. Feed-through cable loop (4) with six cables and 6 connectors, each cable with 26 conductors (a maximum of 156 connections possible) interfacing through D-SUB connectors provides electrical interface of the whole instrument with the satellite electrical systems.

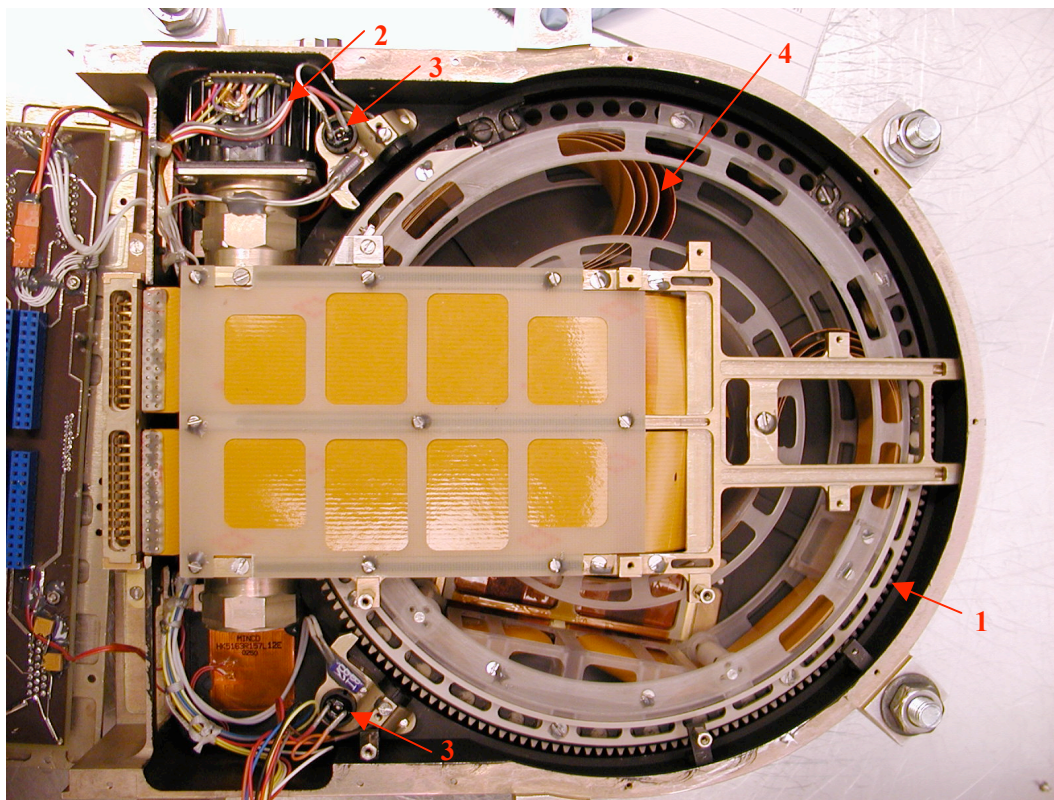


Figure 4. ASPERA – 4 scanner. Internal view. See explanations in text.

3.2 Scanner locking mechanism

The worm gear type of mechanism selected provides a self-locking behaviour without electrical power. However, during launch and other necessary transports, Aspera will encounter heavy mechanical loads; why as a locking mechanism was introduced.

The locking mechanism will avoid unwanted movements of the platform. It contains of a wire which tirs two small levers locking the square shaped worm screw axis. By command, applying a voltage to the ware will burn the wire which forces and the levers apart by a spring, and unlocks the axis, shown in figure 5. Clearly, the release scanner command can only be run once – which in Aspera-4 case is done during commissioning – and in Aspera-3 case in December 2005 (after app. 2 years of orbiting Mars).

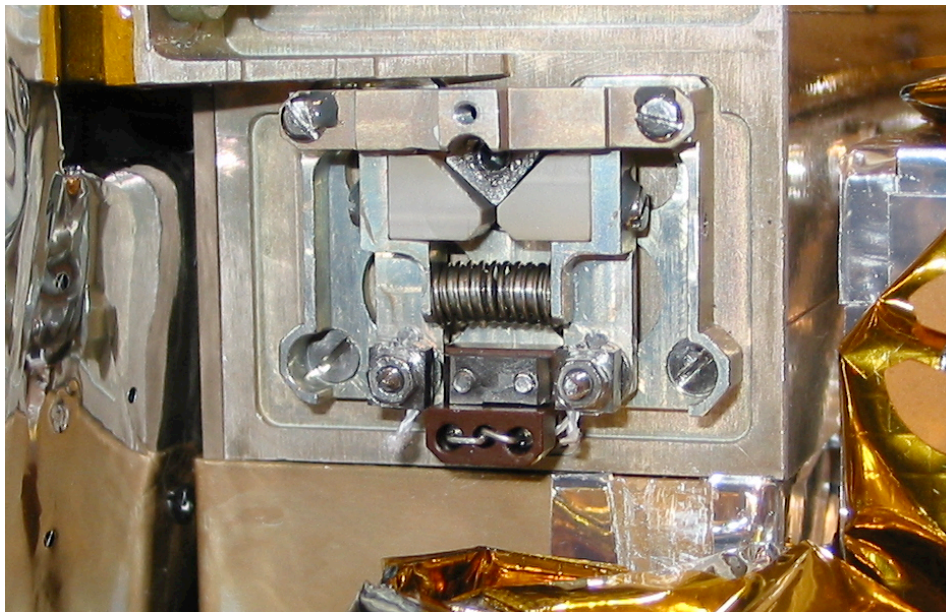


Figure 5 Scanner locking mechanism

3.3 Scanner motor configuration

The stepper motor used is a modified P430 from Escap (Figure 6). The modifications made regards the two ball bearings within the stepper motor holding the motor shaft. The original ball bearings are replaced by type NMB R-1350ZZ bearings surface treated with NoWear Gamma by SKF, Sweden. The balls are mounted at IRF, and are made of Si3N4 (NBD200) by Saint Gobain/Cerbec. The ball diameter is 2.00018 mm, grade 5. The ball holders are designed and manufactured at IRF and are made of Beraloy (Acoflon 100 Mo, 97% PTFE + 3% MoS2). The ball bearings are mounted in the motor with shims for a correct axial displacement. Also, the ball bearings are mounted without any axial tension applied to them in order to release the ball bearings from wear. The motor shaft is isolated from any axial load from the worm screw by a soft split of the motor shaft and worm screw. Also, the rightmost end plate in the picture is reduced in thickness by 0.1 mm by milling in order to increase the axial space in which the magnetic disk rotates.

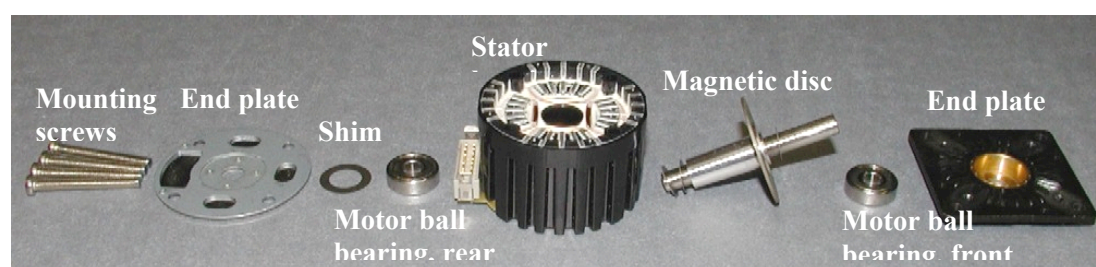


Figure 6. Scanner stepper motor

Key features of the scanner motor are shown in table 2.

Coil dependent parameters		coils in series
		typ
1	Phase resistance	ohm
2	Phase inductance (1 kHz)	mH
3	Nominal phase current (2 ph. on)	A
4	Nominal phase current (1 ph. on)	A
5	Back-EMF amplitude	V/kst/s
Coil independent parameters ¹⁾		
Torque parameters		typ
6	Holding torque (nominal current)	mNm (oz-in)
7	Holding torque (2 x nominal current) ²⁾	mNm (oz-in)
8	Detent torque amplitude and friction	mNm (oz-in)
Thermal parameters		
9	Thermal resistance coil-ambient ³⁾	°C/W
Angular accuracy		
10	Absolute accuracy (2 ph. on full-step mode)	% full-steps
Mechanical parameters		
11	Rotor inertia	kgm ² .10 ⁻⁷
Other parameters		
12	Natural resonance frequency (nominal current)	Hz
13	Electrical time constant	ms
14	Angular acceleration (nominal current)	rad/s ²

Table 2 Scanner motor key features

3.4 Motor drive electronics

The motor driving electronics located in the scanner provides the motor control and driving. The stepper motor is driven by a classical H-bridge drive system with a motor current control system. The location of the board is shown in figure 7.

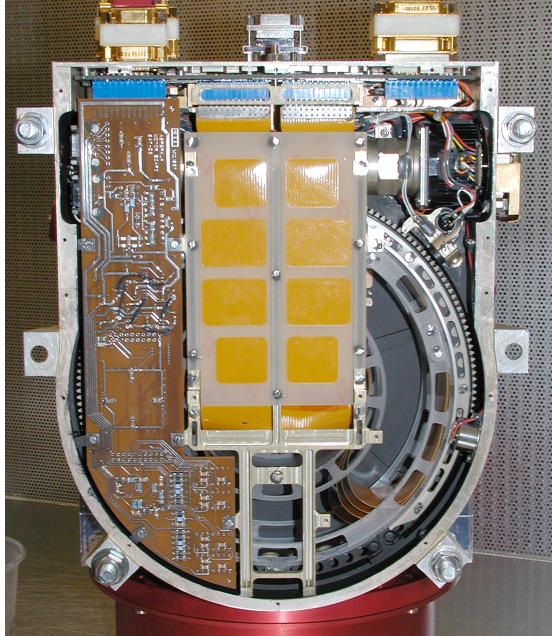


Figure 7 Scanner interior with scanner electronic board

For a smooth stepping of the motor, 16 micro steps per full step and winding is implemented, illustrated in figure 8.

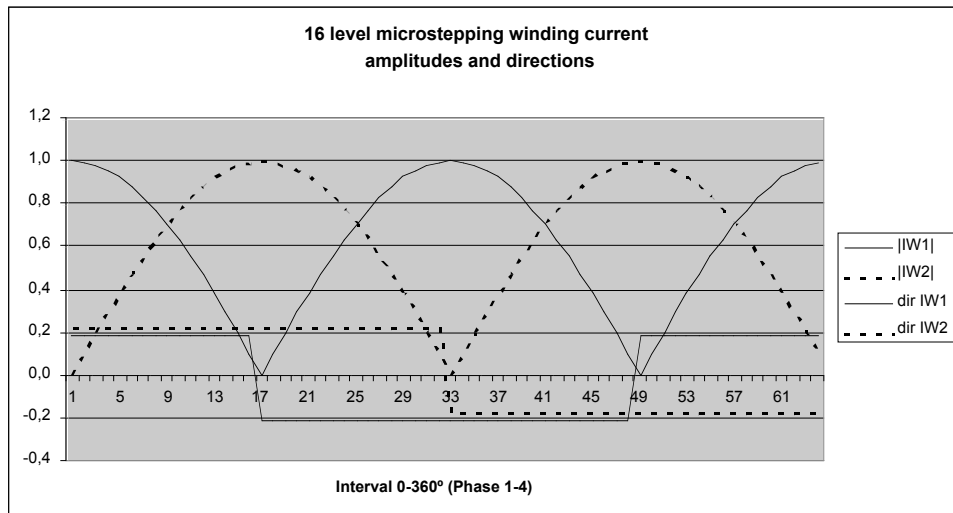


Figure 8 Micro step behaviour

The 16 micro step levels are set by an ACTEL FPGA to a DAC, both situated on the scanner electronics board, and set the current reference value for the motor current control system. Figure 9 shows the same behaviour of the actual reflection voltage of the current and the reference value measured in the current feed back loop.

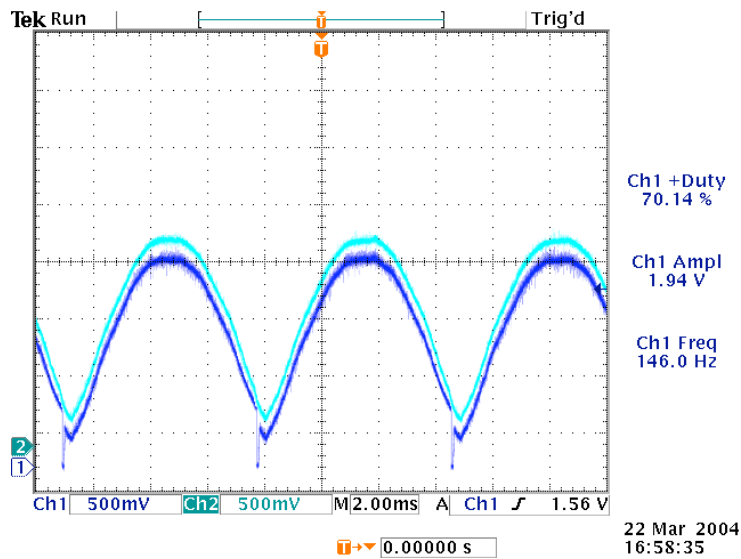


Figure 9 Motor current reflection voltage and current reference voltage

In addition to current control, for minimizing mechanical interaction with its environment the scanner electronics controls the scanner start up sequence in that sense it provides a start up ramp. Given a start up command, the scanner electronics ramps up the scanner speed from zero to full speed in 4 steps, illustrated in figure 10 which is the pulses read out from the wheel pulse generator (see section scanner positioning).

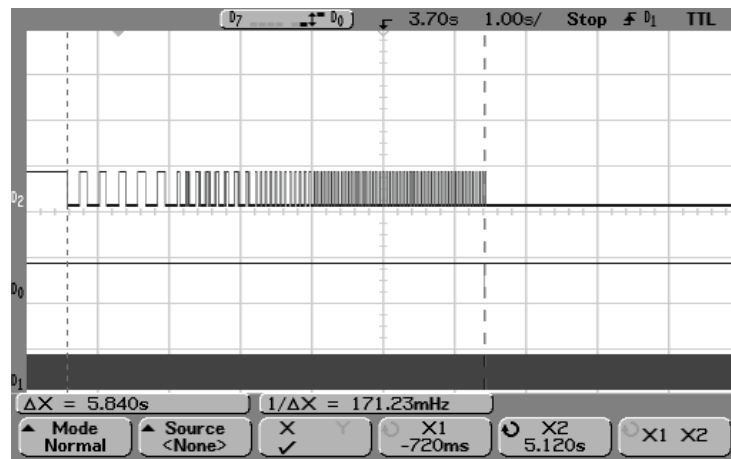


Figure 10 Ramp behaviour

3.5 Motor current settings

In order to increase the torque of the motor, an offset of the current setting can be changed by command. The relation for Aspera-4 between the hexadecimal current reference value and the actual current consumed is shown in figure 11.

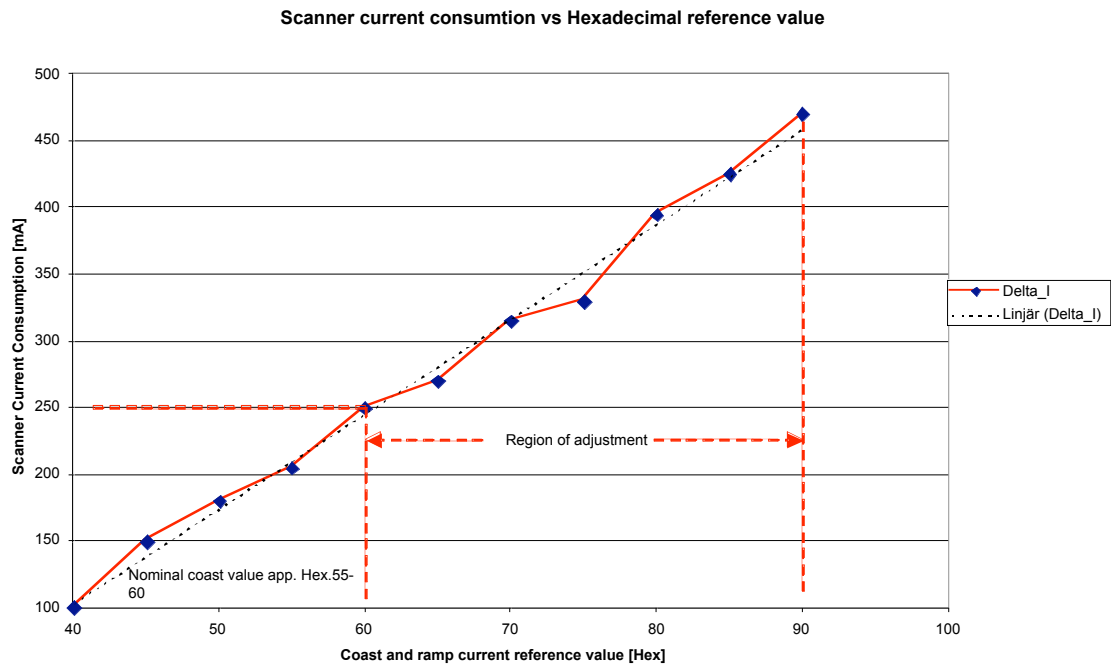


Figure 11 Scanner current setting plot

By command, one can set the coast as well as the ramp current separately, meaning that one can have a higher current (higher torque) during ramp period than during coast period.

3.6 Scanner modes

On command, the platform can be turned to an arbitrary position or perform continuous scanning at any rate of rotation up to the maximum. For all modes, the scanner can be run in speed steps of 128, 64 and 32 seconds/180° turns, called coast speed, which is selected in the command sequence.

3.6.1 Scanner initialization

Scanner will rotate to its home position (CCW) referred to as 0° position, and stay there.

3.6.2 Full scan mode

Continuous back and forth scans between 0° and 180°. Stopped by command.

3.6.3 Stepping mode

Continuous back and forth scans in steps of predefined degrees. Stops a predefined interval between every scan. I.e. one can define the scanner to continuous move 15° - wait for 20 seconds –move 15 further degrees – wait 20 seconds – move – wait - and so on. At end positions the scanner will reverse its direction, and continue. Stopped by command.

3.6.4 Go to position

The scanner will go to a position defined by command, and stay there.

3.7 Scanner positioning

The position determination of the scanner is obtained by counting pulses from the wheel sensor that sits on the motor shaft as it rotates away from one of the two end position sensors. Hence, the end sensors will reset the pulse counter. The position of the scanner is referred to as the direction perpendicular to the centre of the plane of ELS sensor field of view. Hence, in the +x direction in the frame of Aspera-4 coordinate system. The Angular positioning accuracy of the scanner pointing direction is 0.2°. The position can be read out of the house keeping data of Aspera.

3.8 Friction break system

For flawless operation reasons, there is a built in clearance between the gears in the gearbox. The clearance is optimized to a minimum with respect to thermal expansions. The tension introduced by the 6 bended flat cables within the scanner that eventually connects Aspera to the space craft, can cause reduction of mechanical pressure between the gears in the gearbox. The friction system applied in Aspera-4 prevents this to happen. The friction system mainly consists of a peek friction ring, and two flat spring tensioned TiN (Titanium Nitride) coated pads, illustrated in figure 12, 13, and 14. The friction applied is of very small magnitude, and is optimized to prevent the tension of the flat cables to push the gear cogs apart.

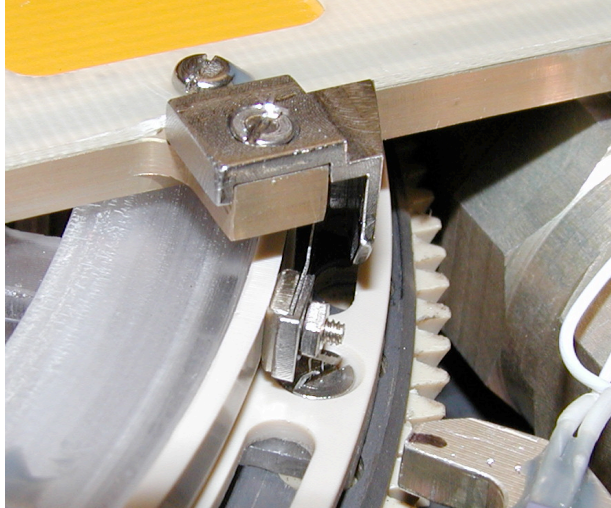


Figure 12 Part of peek ring and friction pads

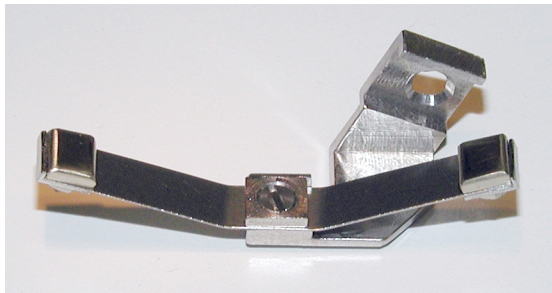


Figure 13 Flat spring tensioned TiN coated pads

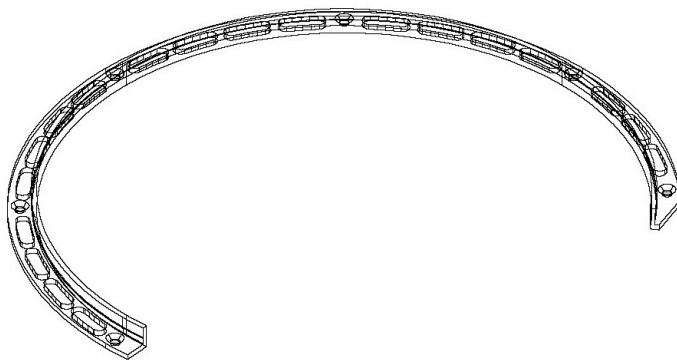


Figure 14 Peek friction ring illustration



ASPERA-4



**Venus
Express**

Reference : **VE-ASP-TN-060402**
Issue : **1** Rev. : **1**
Date : **2006-06-17**
Volume : **-** Page: **7**

APPENDIX 4. MAIN UNIT TM / TC DESCRIPTION



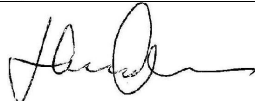
ASPERA-4



**Venus
Express**

Reference : VE-ASP-MA-0005
Issue : 1 Rev. : 0
Date : 2004-05-05
Volume : - Page: 2

Main Unit Software User's Guide

	Name and function	Date	Signature
Prepared by:	Tuukka Säles	2004-05-05	
Verified by:			
Approved by:	Stas Barabash, PI	2004-06-24	
Issued by:	Herman Andersson, EM	2004-06-25	



ASPERA-4



**Venus
Express**

Reference : **VE-ASP-MA-0005**
Issue : **1** Rev. : **0**
Date : **2004-05-05**
Volume : **-** Page: **3**

This page intentionally left blank.



ASPERA-4



**Venus
Express**

Reference : VE-ASP-MA-0005
Issue : 1 Rev. : 0
Date : 2004-05-05
Volume : - Page: 5

This page intentionally left blank.



ASPERA-4



Venus
Express

Reference : VE-ASP-MA-0005
Issue : 1 Rev. : 0
Date : 2004-05-05
Volume : - Page: 6

TABLE OF CONTENTS

ACRONYMS AND DEFINITIONS.....	9
1 GENERAL	11
1.1 Software in general.....	11
1.2 Startup procedure.....	11
1.3 Shutdown procedure.....	11
1.4 On commands.....	11
1.4.1 General	11
1.4.2 On acknowledgments	12
1.4.3 On error conditions.....	12
2 USING IMA	13
2.1 General	13
2.2 IMA Server.....	13
3 TELECOMMANDS.....	14
3.1 General	14
3.2 Field descriptions.....	14
3.3 Telecommand set Part I - commands defined in SGICD	14
3.3.1 TC(3,5) Enable HK Packet generation	14
3.3.2 TC(3,6) Disable HK Packet generation	15
3.3.3 TC(6,2) Load memory using absolute addresses.....	15
3.3.4 TC(6,5) Dump memory using absolute addresses	16
3.3.5 TC(9,1) Accept Time update	16
3.3.6 TC(17,1) Request connection test response.....	17
3.3.7 TC(20,1) Enable Science Report Packet Generation on RTU Link	17
3.3.8 TC(20,2) Disable Science Report Packet Generation on RTU Link	18
3.4 Telecommand set Part II - commands of type 191	19
3.4.1 TC(191,1) Switch ELS +30V on/off	19
3.4.2 TC(191,2) Set ELS Screen Grid Voltage	19
3.4.3 TC(191,3) Set ELS Deflection Voltage.....	20
3.4.4 TC(191,4) Enable ELS High Voltages	20
3.4.5 TC(191,5) Set ELS MCP Bias Voltage	21
3.4.6 TC(191,7) Switch IMA +30V on/off.....	21
3.4.7 TC(191,9) Switch IMA on/off ($\pm 5V$ and $\pm 12V$ on/off).....	22
3.4.8 TC(191,10) Switch NPD Heaters on/off	22
3.4.9 TC(191,11) Switch NPD1 +30V on/off.....	22
3.4.10 TC(191,12) Set NPD1 Bias Voltage.....	23
3.4.11 TC(191,13) Set NPD1 Deflection Voltage	23
3.4.12 TC(191,14) Set NPD1 Start MCP Bias Voltage.....	24
3.4.13 TC(191,15) Set NPD1 Stop MCP Bias Voltage	24
3.4.14 TC(191,16) Switch NPD2 +30V on/off.....	25
3.4.15 TC(191,17) Set NPD2 Bias Voltage.....	25
3.4.16 TC(191,18) Set NPD2 Deflection Voltage	26
3.4.17 TC(191,19) Set NPD2 Start MCP Bias Voltage.....	26
3.4.18 TC(191,21) Switch NPI +30V on/off	27
3.4.19 TC(191,22) Set NPI Bias Voltage	27
3.4.20 TC(191,23) Set NPI Deflection Voltage	28
3.4.21 TC(191,24) Set NPI Deflection Switch	28
3.4.22 TC(191,25) Set Scanner Setup	29
3.4.23 TC(191,26) Set Scanner Voltages	29
3.4.24 TC(191,27) Scanner String Heaters.....	30
3.4.25 TC(191,30) Enable ASPERA-4 Main Unit watch dog.....	30
3.4.26 TC(191,32) NPD1 High Voltage Switch.....	31
3.4.27 TC(191,33) NPD2 High Voltage Switch.....	31
3.4.28 TC(191,34) Set NPD1 Counter Thresholds.....	31
3.4.29 TC(191,35) Set NPD2 Counter Thresholds.....	32



ASPERA-4



Venus
Express

Reference : VE-ASP-MA-0005
Issue : 1 Rev. : 0
Date : 2004-05-05
Volume : - Page: 7

3.4.30	TC(191,255) Confirm Hazardous Command	32
3.5	Telecommand set Part III - commands of type 192.....	33
3.5.1	TC(192,1) Select ELS mode.....	33
3.5.2	TC(192,6) Set NPI Mode	34
3.5.3	TC(192,7) Set NPD Mode.....	34
3.5.4	TC(192,12) Set MU HK Packet Generation Frequency	35
3.5.5	TC(192,13) Set Scanner mode.....	36
3.5.6	TC(192,14) Initialize Scanner	37
3.5.7	TC(192,16) Set High Voltage Shutter Reduced Voltages	37
3.5.8	TC(192,15) Set High Voltage Shutter Mode.....	38
3.5.9	TC(192,20) Run Macro	39
3.5.10	TC(192,21) Terminate Current Macro	39
3.5.11	TC(192,22) Run Single Macro Command.....	40
3.6	Telecommand set Part IV - commands of type 193	41
3.6.1	TC(193,1) Pipe Telecommand	41
3.6.2	TC(193,2) Relax (do nothing)	41
3.6.3	TC(193,3) Generate simulated data.....	41
3.6.4	TC(193,4) Write word to address	42
3.6.5	TC(193,5): Read word from address	42
3.6.6	TC(193,10) Patch EEPROM	42
3.6.7	TC(193,11): Load Module.....	43
3.6.8	TC(193,12) Select Boot Mode.....	43
3.6.9	TC(193,16) Watchdog reset	43
3.7	List of telecommands	45
4	TELEMETRY	47
4.1	General	47
4.2	Telemetry packages	47
4.2.1	TM(1,1) Telecommand Acceptance report - Success.....	47
4.2.2	TM(1,2) Telecommand Acceptance report - Failure	47
4.2.3	TM(1,7) TM Execution acknowledgment report – Success	47
4.2.4	TM(1,8) TM Execution acknowledgment report – Failure	47
4.2.5	TM(3,25) Housekeeping report	48
4.2.6	TM(6,6) Memory dump report packet (as specified in SGICD).....	48
4.2.7	TM(17,2) Connection test report	48
4.2.8	TM(20,3) Science data report	49
4.2.9	TM(193,6) Read word report packet	49
4.2.10	TM(193,128) Piped TC report packet	49
4.3	Telemetry list.....	50
5	EVENT REPORTING	51
5.1	General	51
5.2	Event List.....	51
6	HOUSEKEEPING TELEMETRY	53
6.1	General	53
6.2	HK packet source data field.....	53
6.2.1	Source data field for Main Unit.....	53
7	INSTRUMENT SOFTWARE MODES.....	57
7.1	Instrument modes	57
8	IMA TELEMETRY	58
8.1	Source data field for IMA.....	58
8.2	IMA HK definition	58
8.3	IMA scientific TM modes	60
9	SCIENCE DATA	62
9.1	Science data production modes	62
9.2	Science data packet formats	62
9.3	Science data packet types	62
9.3.1	IMA telemetry packets	63



ASPERA-4



**Venus
Express**

Reference : **VE-ASP-MA-0005**
Issue : **1** Rev. : **0**
Date : **2004-05-05**
Volume : **-** Page: **8**

9.3.2	ELS telemetry packets.....	63
9.3.3	NPD telemetry packets.....	65
9.3.4	NPD Raw data packet.....	65
9.3.5	NPI telemetry packets.....	68
9.3.6	Engineering telemetry packets.....	70



ASPERA-4



**Venus
Express**

Reference : **VE-ASP-MA-0005**
Issue : **1** Rev. : **0**
Date : **2004-05-05**
Volume : **-** Page: **9**

This page intentionally left blank.



ACRONYMS AND DEFINITIONS

EEPROM	Electrically Erasable Programmable Read-Only Memory
HK	Housekeeping
IMA	Ion Mass Analyser
MCP	Microchannel plate
MU	Main Unit
NPD	Neutral Particle Detector
NPI	Neutral Particle Imager
PROM	Programmable Read-Only Memory
S/C	Spacecraft
SGICD	Mars Express Space / Ground Interface Control Document, Issue 2
SW, S/W	Software
TBC	To Be Confirmed
TBD	To Be Defined
TBW	To Be Written
TC	Telecommand
TM	Telemetry



ASPERA-4



**Venus
Express**

Reference : VE-ASP-MA-0005
Issue : 1 Rev. : 0
Date : 2004-05-05
Volume : - Page: 11

This page intentionally left blank.



1 GENERAL

1.1 Software in general

ASPERA-4 Main Unit software is responsible for operating Main Unit according to the telecommands. It will, depending on its mode and received telecommands, produce telemetry. It has also a small server for communications with IMA. This server converts telecommands form spacecraft to form known by IMA. It also converts telemetry sent by IMA to a form known by the spacecraft.

The software is run on a MIL-STD-1750 type microprocessor and is written in C (using POSIX threads) and partly in assembler. Compilers used are m1750-gcc version 1.4.3b2 by XGC Software. Package includes also version gas (gnu assembler) for MIL-STD-1750.

Software described in this Users Guide is the version R-4.8.0, in other words Aspera-4/VenusExpress version of the software.

1.2 Startup procedure

When the experiment boot it will perform a short self-check. If an anomaly is detected (like watchdog reset), the Main Unit will inform the s/c with an event report packet at the end of the boot process. After a short self-check, the s/w will start basic services (TM, limited TC, HK).. At this point an event (with eid=40001) is nominally sent. User must next identify how to proceed by sending command 'select boot mode' to inform s/w from there on to stay at safe mode or to continue with default boot module. If this command is not sent for 17 hours S/W tries to load so called PROM module and executes that. Prom module is module providing MU housekeeping and full IMA services (except memory services of tc type 6). All MU services applicable for safe mode are also available in this mode.

If the default boot module is choosed, s/w can't be loaded from PROMs. It will instead try to load a replacement from a module in EEPROM, starting from address 0x10000 or higher. If the module can't be loaded from EEPROM or ROM, the experiment will enter safe mode (actually stay in safe mode). If **valid** module is found it will be loaded and started. The end status of this process is sent as an event.

If the s/w was loaded successfully, an event report will be generated to show that the experiment has booted properly. Pending error messages from the boot process will be sent.

S/W will verify wether the boot process isrunned due the watchdog reset or power-on. In case of watchdog reset an event is generated (40004).

1.3 Shutdown procedure

There aren't any strict s/w requirements for shutdown. Only after Patch EEPROM command it's recommended to wait long enough to receive an event reporting about successful EEPROM programming. This is to ensure that EEPROM does have valid content.

1.4 On commands

1.4.1 General

One fundamental aspect of the ASPERA-44 Main Unit is the way it uses commands (both telecommands and internal commands). Telecommands can be classified in many ways, but most fundamental is division to direct and indirect telecommands. Direct commands are command with type



255 or under 193. These commands are executed immediately after they have been detected in telecommand input buffer. Indirect commands are forwarded (after verifying command structure) to a specific process, command handler for later execution. Telecommands TC(192,21) and TC(193,11) fall into both categories. If s/w is in safe mode (or some broken state) these commands are used as direct commands. However, in normal situation these are treated as indirect. Indirect commands are handled via a specific `telecommand` table 'Telecommand table' is table that specifies most of the telecommands and most of the restrictions of . It contains also information about functions to be called when an indirect command is found. Due to this table it's relatively easy to change the way some command behave without compiling and reprogramming all of the s/w. It is also important to note that indirect commands, i e commands found only in telecommand table, are not available in safe mode.

Further division is made to classify commands as safe and hazardous. Hazardous commands must be followed immediately by TC(191,255) containing sequence count of hazardous command. Hazardous commands can't be run from macros.

1.4.2 On acknowledgments

The ASPERA-4 MU provides only telecommand acceptance acknowledgment for itself. For IMA, acknowledgments are provided by using execution acknowledgments. When an IMA related telecommand is found, the Main Unit will send an acceptance acknowledgment to the s/w (if acknowledgement is requested in the telecommand headers) and then it forwards the command to IMA. If execution acknowledgment is - requested in the telecommand headers (applicable only for IMA) IMA will send an acknowledgment to the Main Unit which is waiting for that. This will then be forwarded to the s/c. Although this process is more acceptance than execution type of acknowledgment, it has to be used. Due to the acceptance acknowledgment time-out criteria (20s) and the 32-second acquisition period of IMA, it is not possible to have acceptance acknowledgments on IMA.

1.4.3 On error conditions

Error conditions are reported as event packets. If the error is such that automatic recovery process in the MU s/w cannot be executed, the software will shut down erroneous services. S/w won't enter safe mode unless it's absolutely necessary.



2 USING IMA

2.1 General

IMA commands (type 194 and 195, and memory management service 6 for PID 62) are first received in MU. MU convert commands to valid IEEE1355 link packets and then send these to IMA. There is separate command queues for MU and IMA and MU specific commands are executed simultaneously with command transmission to IMA. Therefore, if for some reason IMA fails to receive command at all MU can be commanded without further problems. The command acknowledgments scheme is explained in chapter 1.4.2.

2.2 IMA Server

There is separate server for IMA. It works in parallel to other parts of the software and does not require any specific modes on MU. Acquisition period of 16 sec and is independent of MU modes. Also, TM sent by IMA is reformatted (to standard ESA packets) in parallel with other activities in MU. IMA command sent to MU will be passed to IMA server so that other MU commands can be executed before IMA command is really transmitted to IMA. To allow parallel TM and TC handling for IMA and MU there is a buffer for both IMA TC and TM.



3 TELECOMMANDS

3.1 General

The general structure of telecommands is defined in SGICD.

3.2 Field descriptions

<i>Field name</i>	<i>Form</i>	<i>Description</i>
Parameter	=X	Parameter is constant with value X
	X => Y	Parameter can vary in range from X to Y
	(X) * n	X is repeated n times

Parameters are listed in the same order that they appear in the telecommand or telemetry packet so that first parameter to be sent is listed first.

Some terminology: Immediate response means immediate answer for the telecommand, like event reporting about success of the command. Related effect is effect that can be seen in telemetry, but it is not immediate answer for the command. Examples of this are starting of generation of some packet type, changed reference field in housekeeping packet or change in monitor value in housekeeping packet.

NOTE: Related effect is often something that can't be seen at all in some circumstances. For example, changing NPI bias voltage can't be seen in hk or science data packets if these are not generated at all.

3.3 Telecommand set Part I - commands defined in SGICD

3.3.1 TC(3,5) Enable HK Packet generation

<i>Generic description</i>			
Acronym		aspmHKEnable	
Type	3	PID	61
Subtype	5	Packet Category	12
16 bit parameters	1		
<i>General description</i>			
Description		Enable HK generation in ASPERA-4 Main Unit	
Note		Only housekeeping packet generation of Main Unit can be switched on by this TC	
<i>Parameter description</i>			
Name	Size (bytes)	Value	Note
None	2	=0	
<i>Response</i>			
Immediate response			
Related effect		Generation of MU HK report packet TM(3,25) starts	



3.3.2 TC(3,6) Disable HK Packet generation

Generic description			
Acronym		aspmHKDisable	
Type	3	PID	61
Subtype	6	Packet Category	12
16 bit parameters	1		
General description			
Description		Disable HK generation in ASPERA-4 Main Unit	
Note		Only housekeeping packet generation of Main Unit can be switched off by this TC	
Parameter description			
Name	Size (bytes)	Value	Note
None	2	0	
Response			
Immediate response			
Related effect		Generation of MU HK report packet TM(3,25) stops	

3.3.3 TC(6,2) Load memory using absolute addresses

Generic description			
Acronym		aspmMEMLoad	
Type	6	PID	61
Subtype	2	Packet Category	12
16 bit parameters	varies		
General description			
Description		Load memory to an absolute address	
Note		Any patch to be loaded to EEPROM must be loaded to mass memory. It can be transferred to EEPROM by TC (193,10) which is available only in safe mode.	
Parameter description			
Name	Size (bytes)	Value	Note
Memory id	1	0x80 => 0x83	0x80: N/A 0x81: RAM 0x82: N / A 0x83: MASSMEMORY
Number of blocks (=nb)	1	1=>	Number of blocks to load
Data block Address (repeated nb times)	4	0 => 0x7FFFF	Address of first word in block
Length of block (=lb)	2	1 => 0xffff	Number of words in this block
Data	2*lb	(1=> 0xffff) * lb	lb times data words
Response			
Immediate response			
Related effect			



3.3.4 TC(6,5) Dump memory using absolute addresses

<i>Generic description</i>			
Acronym		AspmMEMDump	
Type	6	PID	61
Subtype	5	Packet Category	12
16 bit parameters	varies		
<i>General description</i>			
Description		Dump memory from an absolute address	
Note			
<i>Parameter description</i>			
<i>Name</i>	<i>Size (bytes)</i>	<i>Value</i>	<i>Note</i>
Memory id	1	0x80 => 0x83	0x80: ROM 0x81: RAM 0x82: EEPROM 0x83: MASMEMORY
Number of blocks (=nb)	1	1=>	Number of blocks to dump
Data block Address (repeated nb times)	4	0 => 0x7FFFF	Address of first word in block
Length of block (=lb)	2	1 => 0xffff	Number of words in this block
<i>Response</i>			
Immediate response		At least one memory dump report packet TM(6,6)	
Related effect			

3.3.5 TC(9,1) Accept Time update

<i>Generic description</i>			
Acronym		AspmTime	
Type	9	PID	61
Subtype	1	Packet Category	12
16 bit parameters	0		
<i>General description</i>			
Description		Accept time update	
Note			
<i>Name</i>	<i>Size (bytes)</i>	<i>Value</i>	<i>Note</i>
None	-	-	
<i>Response</i>			
Immediate response			
Related effect		The clock is updated	



3.3.6 TC(17,1) Request connection test response

<i>Generic description</i>			
Acronym		aspmConn	
Type	17	PID	61
Subtype	1	Packet Category	12
16 bit parameters	0		
<i>General description</i>			
Description		Test Connection	
Note			
<i>Parameter description</i>			
<i>Name</i>	<i>Size (bytes)</i>	<i>Value</i>	<i>Note</i>
None	-	-	-
<i>Response</i>			
Immediate response		Connection Test Report TM(17,2)	
Related effect			

3.3.7 TC(20,1) Enable Science Report Packet Generation on RTU Link

<i>Generic description</i>			
Acronym		aspmSCIEnable	
Type	20	PID	61
Subtype	1	Packet Category	12
16 bit parameters	0		
<i>General description</i>			
Description		Enable Science report packet generation in Main Unit. Set instrument in scientific mode.	
Note		This command must be executed before Scanner can be operated or science data can be produced. This is due to fact that timing of Scanner is tightly coupled with handling of measurement modes.	
<i>Parameter description</i>			
<i>Name</i>	<i>Size (bytes)</i>	<i>Value</i>	<i>Note</i>
None	-	-	-
<i>Response</i>			
Immediate response		Generation of Science data will be enabled. All scanner operations can be performed after execution of this command.	
Related effect			



3.3.8 TC(20,2) Disable Science Report Packet Generation on RTU Link

<i>Generic description</i>			
Acronym		AspmSCIDisable	
Type	20	PID	61
Subtype	2	Packet Category	12
16 bit parameters	0		
<i>General description</i>			
Description		Disables Science report packet generation in Main Unit.	
Note		Science data production will be disabled. Data that has already been measured will be handled and sent.	
<i>Parameter description</i>			
<i>Name</i>	<i>Size (bytes)</i>	<i>Value</i>	<i>Note</i>
None	-	-	-
<i>Response</i>			
Immediate response			
Related effect		Generation of Science data will be disabled.	



3.4 Telecommand set Part II - commands of type 191

3.4.1 TC(191,1) Switch ELS +30V on/off

<i>Generic description</i>			
Acronym		aspmELS30	
Type	191	PID	61
Subtype	1	Packet Category	12
16 bit parameters	1	Hazardous	No
<i>General description</i>			
Description		Switch ELS +30V on/off	
Note		The +30V for ELS controls the high voltages of the deflection plates and MCP.	
<i>Parameter description</i>			
Name	Size (bytes)	Value	Note
On/off	2	0 => 1	0=off, 1=on
<i>Response</i>			
Immediate response			
Related effect		Corresponding power indicator changes in HK packet.	

3.4.2 TC(191,2) Set ELS Screen Grid Voltage

<i>Generic description</i>			
Acronym		AspmELSGrid	
Type	191	PID	61
Subtype	2	Packet Category	12
16 bit parameters	1	Hazardous	No
<i>General description</i>			
Description		Set ELS Screen grid voltage	
Note		Screen grid value define the minimum energy of particles detected by ELS.	
<i>Parameter description</i>			
Name	Size (bytes)	Value	Note
PAD	1	= 0	
Grid voltage	1	0 => 0xFF	Sets screen grid reference voltage
<i>Response</i>			
Immediate response			
Related effect		Set screen grid reference fields in HK telemetry packet and in ELS Engineering Information packet.	

The MU generate a voltage which is linear from 0 to +5 V. These values are represented by the parameter limits 0x0000 and 0x00FF respectively.



3.4.3 TC(191,3) Set ELS Deflection Voltage

Generic description			
Acronym		aspmELSDef1	
Type	191	PID	61
Subtype	3	Packet Category	12
16 bit parameters	1	Hazardous	No
General description			
Description	Set ELS deflection plate voltage and deflection power supply range.		
Note	Set a constant value for deflection plate voltage.		
Parameter description			
Name	Size (bytes)	Value	Note
PAD	3 bits (msb)	=0	
ELS HV Supply Range	1 bit	0 => 1	0 = Low, 1 = High
Deflection voltage	12 bits (lsb)	0 => 0x0FFF	
Response			
Immediate response			
Related effect	Set ELS deflection reference to a constant value, reflected in ELS Engineering telemetry packet.		

The Deflection HV supply range has two states, low range and high range. The control of each supply voltage is generated by the MU. The values linearly range from 0 to +5 V and are represented by the parameter limits of 0x0000 and 0x0FFF respectively.

3.4.4 TC(191,4) Enable ELS High Voltages

Generic description			
Acronym		AspmELSHV	
Type	191	PID	61
Subtype	4	Packet Category	12
16 bit parameters	1	Hazardous	Yes
General description			
Description	Switch ELS High voltages off/on		
Note	Command must be verified with TC(191,255)		
Parameter description			
Name	Size (bytes)	Value	Note
On/off	2	0 => 1	0=off, 1=on
Response			
Immediate response			
Related effect	ELS high voltage enable telemetry state changes in HK packet.		



3.4.5 TC(191,5) Set ELS MCP Bias Voltage

<i>Generic description</i>			
Acronym		AspmELSMcp	
Type	191	PID	61
Subtype	5	Packet Category	12
16 bit parameters	1	Hazardous	No
<i>General description</i>			
Description	Set ELS MCP bias voltage		
Note			
<i>Parameter description</i>			
Name	Size (bytes)	Value	Note
PAD	1	=0	
MCP bias voltage	1	0 => 0xFF	
<i>Response</i>			
Immediate response			
Related effect	ELS MCP bias reference field is reflected in HK packet and in ELS Engineering Information packet.		

The MU generates a reference voltage to control the ELS MCP voltage. The range varies linearly from 0 to +5 V and the values are represented by the parameter limits of 0x000 and 0x00FF respectively.

3.4.6 TC(191,7) Switch IMA +30V on/off

<i>Generic description</i>			
Acronym		aspmIMA30	
Type	191	PID	61
Subtype	7	Packet Category	12
16 bit parameters	1	Hazardous	No
<i>General description</i>			
Description	Switch IMA +30V on/off		
Note	The +30V for IMA controls the high voltages of the deflection and MCP.		
<i>Parameter description</i>			
Name	Size (bytes)	Value	Note
IMA +30V	2	0 => 1	0=off, 1=on
<i>Response</i>			
Immediate response			
Related effect	IMA +30V power state indicator field changes in HK packet.		



3.4.7 TC(191,9) Switch IMA on/off ($\pm 5V$ and $\pm 12V$ on/off)

<i>Generic description</i>			
Acronym		AspmIMApow	
Type	191	PID	61
Subtype	9	Packet Category	12
16 bit parameters	1	Hazardous	No
<i>General description</i>			
Description		Switch IMA $\pm 5V$ and $\pm 12V$ on/off	
Note		Switch on low voltage power to IMA	
<i>Parameter description</i>			
Name	Size (bytes)	Value	Note
IMA $\pm 5V$ and $\pm 12V$	2	0 => 1	0=off, 1=on
<i>Response</i>			
Immediate response			
Related effect		IMA $\pm 12V$ and $\pm 5V$ power state indicator field change in HK packet.	

3.4.8 TC(191,10) Switch NPD Heaters on/off

<i>Generic description</i>			
Acronym		AspmNPDheaters	
Type	191	PID	61
Subtype	10	Packet Category	12
16 bit parameters	1	Hazardous	No
<i>General description</i>			
Description		Switch NPD Start surface heaters on/off	
Note		Activate NPD heaters to control the temperature of the NPD instrument. Simultaneously for both NPD1 and NPD2.	
<i>Parameter description</i>			
Name	Size (bytes)	Value	Note
NPD Heaters on/off	2	0 => 1	0=off, 1=on
<i>Response</i>			
Immediate response			
Related effect		NPD heater status field changes in HK packet.	

3.4.9 TC(191,11) Switch NPD1 +30V on/off

<i>Generic description</i>			
Acronym		aspmNPD130	
Type	191	PID	61
Subtype	11	Packet Category	12
16 bit parameters	1	Hazardous	No
<i>General description</i>			
Description		Switch NPD1 +30V on/off	
Note		The +30V for NPD1 controls the high voltages of the deflection and MCP supplies.	
<i>Parameter description</i>			
Name	Size (bytes)	Value	Note
NPD +30V on/off	2	0 => 1	0=off, 1=on
<i>Response</i>			
Immediate response			
Related effect		Power indicator field changes in HK packet.	



3.4.10 TC(191,12) Set NPD1 Bias Voltage

<i>Generic description</i>			
Acronym		aspmNPD1bias	
Type	191	PID	61
Subtype	12	Packet Category	12
16 bit parameters	1	Hazardous	No
<i>General description</i>			
Description		Set NPD1 bias voltage	
Note		Set the value of the MCP bias supply for NPD1.	
<i>Parameter description</i>			
Name	Size (bytes)	Value	Note
PAD	1	= 0	
NPD1 bias voltage	1	0 => 0xFF	
<i>Response</i>			
Immediate response			
Related effect		NPD1 bias reference and monitor fields change in HK packet.	

The MU generates a reference voltage to control the NPD1 MCP Bias voltage. The range varies linearly from 0 to +5 V and the values are represented by the parameter limits of 0x000 and 0x00FF respectively.

3.4.11 TC(191,13) Set NPD1 Deflection Voltage

<i>Generic description</i>			
Acronym		aspmNPD1defl	
Type	191	PID	61
Subtype	13	Packet Category	12
16 bit parameters	1	Hazardous	No
<i>General description</i>			
Description		Set NPD1 deflection voltage	
Note		Set the value of the deflection voltage for NPD1.	
<i>Parameter description</i>			
Name	Size (bytes)	Value	Note
PAD	1	= 0	
NPD1 Deflection voltage	1	0 => 0xFF	
<i>Response</i>			
Immediate response			
Related effect		NPD1 deflection supply reference and monitor fields change in HK packet.	

The MU generates a reference voltage to control the NPD1 Deflection voltage. The range varies linearly from 0 to +5 V and the values are represented by the parameter limits of 0x000 and 0x00FF respectively.



3.4.12 TC(191,14) Set NPD1 Start MCP Bias Voltage

Generic description			
Acronym		aspmNPD1start	
Type	191	PID	61
Subtype	14	Packet Category	12
16 bit parameters	1	Hazardous	No
General description			
Description		Set NPD1 start MCP bias voltage	
Note		Set the bias reference for the NPD1 start MCP.	
Parameter description			
Name	Size (bytes)	Value	Note
PAD	1	= 0	
NPD1 Start MCP bias voltage	1	0 => 0xFF	
Response			
Immediate response			
Related effect		NPD1 start MCP bias reference and monitor fields change in HK packet.	

The MU generates a reference voltage to control the NPD1 Start MCP Bias voltage. The range varies linearly from 0 to +5 volts and the values are represented by the parameter limits of 0x000 and 0x00FF respectively.

3.4.13 TC(191,15) Set NPD1 Stop MCP Bias Voltage

Generic description			
Acronym		aspmNPD1stop	
Type	191	PID	61
Subtype	15	Packet Category	12
16 bit parameters	1	Hazardous	No
General description			
Description		Set NPD1 stop MCP Bias Voltage	
Note		Set the bias reference for the NPD1 stop MCP.	
Parameter description			
Name	Size (bytes)	Value	Note
PAD	1	= 0	
NPD1 Stop MCP bias voltage	1	0 => 0xFF	
Response			
Immediate response			
Related effect		NPD1 stop MCP bias reference and monitor fields change in HK packet.	

The MU generates a reference voltage to control the NPD1 Stop MCP Bias voltage. The range varies linearly from 0 to +5 V and the values are represented by the parameter limits of 0x000 and 0x00FF respectively.



3.4.14 TC(191,16) Switch NPD2 +30V on/off

<i>Generic description</i>			
Acronym		aspmNPD230	
Type	191	PID	61
Subtype	16	Packet Category	12
16 bit parameters	1	Hazardous	No
<i>General description</i>			
Description		Switch NPD2 +30V on/off	
Note		The +30V for NPD2 controls the high voltages of the deflection and MCP supplies.	
<i>Parameter description</i>			
Name	Size (bytes)	Value	Note
NPD2 +30V on/off	2	0 => 1	0=off, 1=on
<i>Response</i>			
Immediate response			
Related effect		Power indicator fields changes in HK packet.	

3.4.15 TC(191,17) Set NPD2 Bias Voltage

<i>Generic description</i>			
Acronym		AspmNPD2bias	
Type	191	PID	61
Subtype	17	Packet Category	12
16 bit parameters	1	Hazardous	No
<i>General description</i>			
Description		Set NPD2 bias voltage	
Note		Set the value of the MCP bias supply for NPD2.	
<i>Parameter description</i>			
Name	Size (bytes)	Value	Note
PAD	1	= 0	
NPD2 Bias voltage	1	0 => 0xFF	
<i>Response</i>			
Immediate response			
Related effect		NPD2 bias reference and monitor fields change in HK packet.	

The MU generates a reference voltage to control the NPD2 Bias voltage. The range varies linearly from 0 to +5 V and the values are represented by the parameter limits of 0x000 and 0x00FF respectively.



3.4.16 TC(191,18) Set NPD2 Deflection Voltage

<i>Generic description</i>			
Acronym		aspmNPD2defl	
Type	191	PID	61
Subtype	18	Packet Category	12
16 bit parameters	1	Hazardous	No
<i>General description</i>			
Description		Set NPD2 deflection voltage	
Note		Set the value of the deflection voltage for NPD2.	
<i>Parameter description</i>			
Name	Size (bytes)	Value	Note
PAD	1	= 0	
NPD2 Deflection voltage	1	0 => 0xFF	
<i>Response</i>			
Immediate response			
Related effect		NPD2 deflection supply reference and monitor fields change in HK packet.	

The MU generates a reference voltage to control the NPD2 Deflection voltage. The range varies linearly from 0 to +5 V and the values are represented by the parameter limits of 0x000 and 0x00FF respectively.

3.4.17 TC(191,19) Set NPD2 Start MCP Bias Voltage

<i>Generic description</i>			
Acronym		aspmNPD2start	
Type	191	PID	61
Subtype	19	Packet Category	12
16 bit parameters	1	Hazardous	No
<i>General description</i>			
Description		Set NPD2 start MCP bias voltage	
Note		Sets the bias reference for the NPD2 start MCP.	
<i>Parameter description</i>			
Name	Size (bytes)	Value	Note
PAD	1	= 0	
NPD2 Start mcp bias voltage	1	0 => 0xFF	
<i>Response</i>			
Immediate response			
Related effect		NPD2 start MCP bias reference and monitor fields change in HK packet.	

The MU generates a reference voltage to control the NPD2 Start MCP Bias voltage. The range varies linearly from 0 to +5 V and the values are represented by the parameter limits of 0x000 and 0x00FF respectively.



3.4.18 TC(191,21) Switch NPI +30V on/off

<i>Generic description</i>			
Acronym		aspmNPI30	
Type	191	PID	61
Subtype	21	Packet Category	12
16 bit parameters	1	Hazardous	No
<i>General description</i>			
Description		Switch NPI +30V on/off	
Note		The +30V for NPI controls the high voltages of the deflection and MCP supplies.	
<i>Parameter description</i>			
Name	Size (bytes)	Value	Note
NPI +30V on/off	2	0 => 1	0=off, 1=on
<i>Response</i>			
Immediate response			
Related effect		Power indicator field changes in HK packet.	

3.4.19 TC(191,22) Set NPI Bias Voltage

<i>Generic description</i>			
Acronym		aspmNPIBias	
Type	191	PID	61
Subtype	22	Packet Category	12
16 bit parameters	1	Hazardous	No
<i>General description</i>			
Description		Set NPI bias voltage	
Note		Set the value of the MCP bias supply for NPI.	
<i>Parameter description</i>			
Name	Size (bytes)	Value	Note
PAD	1	= 0	
NPI Bias voltage	1	0 => 0xFF	
<i>Response</i>			
Immediate response			
Related effect		NPI bias reference and monitor fields change in HK packet.	

The MU generates a reference voltage to control the NPD2 Stop MCP bias voltage. The range varies linearly from 0 to +5 V and the values are represented by the parameter limits of 0x000 and 0x00FF respectively.



3.4.20 TC(191,23) Set NPI Deflection Voltage

<i>Generic description</i>			
Acronym		aspmNPIdefl	
Type	191	PID	61
Subtype	23	Packet Category	12
16 bit parameters	1	Hazardous	No
<i>General description</i>			
Description		Set NPI deflection voltage	
Note		Set the value of the deflection voltage for NPI.	
<i>Parameter description</i>			
<i>Name</i>	<i>Size (bytes)</i>	<i>Value</i>	<i>Note</i>
PAD	1	= 0	
NPI Deflection voltage	1	0 => 0xFF	
<i>Response</i>			
Immediate response			
Related effect		NPI deflection supply reference and monitor fields change in HK packet.	

The MU generates a reference voltage to control the NPI Bias voltage. The range varies linearly from 0 to +5 V and the values are represented by the parameter limits of 0x000 and 0x00FF respectively.

3.4.21 TC(191,24) Set NPI Deflection Switch

<i>Generic description</i>			
Acronym		aspmNPIswitch	
Type	191	PID	61
Subtype	24	Packet Category	12
16 bit parameters	1	Hazardous	No
<i>General description</i>			
Description		Set NPI Deflection switch on/off	
Note		Turn on/off NPI deflection voltage.	
<i>Parameter description</i>			
<i>Name</i>	<i>Size (bytes)</i>	<i>Value</i>	<i>Note</i>
NPI Deflection switch on/off	2	0 => 1	0=off, 1=on
<i>Response</i>			
Immediate response			
Related effect		NPI deflection switch indicator telemetry point changes in HK packet.	



3.4.22 TC(191,25) Set Scanner Setup

<i>Generic description</i>			
Acronym		aspmSCANSetup	
Type	191	PID	61
Subtype	25	Packet Category	12
16 bit parameters	1	Hazardous	No
<i>General description</i>			
Description		Defines the operation of the Scanner.	
Note		Scanner +30V on/off and select IRQ operation	
<i>Parameter description</i>			
<i>Name</i>	<i>Size (bytes)</i>	<i>Value</i>	<i>Note</i>
PAD	12 bits	=>0	
Scanner error handler	1 bit	0 => 1	0=enabled, 1=disabled
Auto-switchoff mode	1 bit	0 => 1	0=enabled, 1=disabled
Scan IRQ	1 bit	0 => 1	0=disabled, 1=enabled
Scanner +30V on/off	1 bit	0 => 1	0=off, 1=on
<i>Response</i>			
Immediate response			
Related effect		Scanner +30V power state indicator telemetry point changes in HK packet.	

3.4.23 TC(191,26) Set Scanner Voltages

<i>Generic description</i>			
Acronym		aspmSCANVolts	
Type	191	PID	61
Subtype	26	Packet Category	12
16 bit parameters	3	Hazardous	No
<i>General description</i>			
Description		Set Scanner voltages and currents	
Note			
<i>Parameter description</i>			
<i>Name</i>	<i>Size (bytes)</i>	<i>Value</i>	<i>Note</i>
VREFMC	1	0 => 0xFF	
Coast current	1	0 => 0xFF	
Ramp current	1	0 => 0xFF	
Threshold CW	1	0 => 0xFF	
Threshold CCW	1	0 => 0xFF	
Threshold Wheel	1	0 => 0xFF	
<i>Response</i>			
Immediate response			
Related effect		Scanner voltage and current reference telemetry points change in HK packer.	

The MU generates voltages to control different Scanner functions. The ranges varies linearly from 0 to +5 V and the values are represented by the parameter limits of 0x000 and 0x00FF respectively. All except VREFMC are passed to Scanner controller board as digital values.



3.4.24 TC(191,27) Scanner String Heaters

Generic description			
Acronym		aspmSCANStrHeat	
Type	191	PID	61
Subtype	27	Packet Category	12
16 bit parameters	1	Hazardous	Yes
General description			
Description		Release scanner locking mechanism by using string heater 1 or 2 for 15sec. Hazardous command on database level.	
Note			
Parameter description			
Name	Size (bytes)	Value	Note
Pad	14 bits	= 0	
Stringheater	2 bits	0x1 => 0x2	Number of string heater to be used. 0 = N / A 1 = String Heater 1 2 = String Heater 2 3 = N / A
Response			
Immediate response			
Related effect		Scanner locking mechanisms should be released. The release can be verified by trying to initialize Scanner (i.e by rotating it)	

3.4.25 TC(191,30) Enable ASPERA-4 Main Unit watch dog

Generic description			
Acronym		AspmWatchdog	
Type	191	PID	61
Subtype	30	Packet Category	12
16 bit parameters	1	Hazardous	No
General description			
Description		Enable Watchdog timer	
Note: May contain disable option		*Watchdog cannot be disabled. * With current version of s/w wd is enabled as a default	
Parameter description			
Name	Size (bytes)	Value	Note
Security code	2	=0x2704	
Response			
Immediate response			
Related effect			



3.4.26 TC(191,32) NPD1 High Voltage Switch

<i>Generic description</i>			
Acronym		aspmNPD1switch	
Type	191	PID	61
Subtype	32	Packet Category	12
16 bit parameters	1	Hazardous	No
<i>General description</i>			
Description		Enable NPD1 high voltage	
Note			
<i>Parameter description</i>			
<i>Name</i>	<i>Size (bytes)</i>	<i>Value</i>	<i>Note</i>
NPD1 HV	2	0 => 1	0=off, 1=on
<i>Response</i>			
Immediate response			
Related effect			

3.4.27 TC(191,33) NPD2 High Voltage Switch

<i>Generic description</i>			
Acronym		aspmNPD2switch	
Type	191	PID	61
Subtype	33	Packet Category	12
16 bit parameters	1	Hazardous	No
<i>General description</i>			
Description		Enable NPD2 high voltages	
Note			
<i>Parameter description</i>			
<i>Name</i>	<i>Size (bytes)</i>	<i>Value</i>	<i>Note</i>
NPD2 HV	2	0 => 1	0=off, 1=on
<i>Response</i>			
Immediate response			
Related effect			

3.4.28 TC(191,34) Set NPD1 Counter Thresholds

<i>Generic description</i>			
Acronym		aspmNPD1Tresholds	
Type	191	PID	61
Subtype	34	Packet Category	12
16 bit parameters	2	Hazardous	No
<i>General description</i>			
Description		Set NPD1 counter thresholds	
Note			
<i>Parameter description</i>			
<i>Name</i>	<i>Size (bytes)</i>	<i>Value</i>	<i>Note</i>
Start	1	0 => 0xFF	
Stop0	1	0 => 0xFF	
Stop1	1	0 => 0xFF	
Stop2	1	0 => 0xFF	
<i>Response</i>			
Immediate response			
Related effect		NPD1 start count and stop count fields change in the NPD1 Science packets.	



3.4.29 TC(191,35) Set NPD2 Counter Thresholds

<i>Generic description</i>			
Acronym		aspmNPD2Tresholds	
Type	191	PID	61
Subtype	35	Packet Category	12
16 bit parameters	2	Hazardous	No
<i>General description</i>			
Description		Set NPD2 counter thresholds	
Note			
<i>Parameter description</i>			
Name	Size (bytes)	Value	Note
Start	1	0 => 0xFF	
Stop0	1	0 => 0xFF	
Stop1	1	0 => 0xFF	
Stop2	1	0 => 0xFF	
<i>Response</i>			
Immediate response			
Related effect		NPD2 start count and stop count fieldschange in the NPD2 Science packets.	

3.4.30 TC(191,255) Confirm Hazardous Command

<i>Generic description</i>			
Acronym		aspmLaunch	
Type	191	PID	61
Subtype	255	Packet Category	12
16 bit parameters	1	Hazardous	No
<i>General description</i>			
Description		Confirms previous hazardous command.	
Note		This command must follow immediately after command to be confirmed (i e this must be next command).	
<i>Parameter description</i>			
Name	Size (bytes)	Value	Note
Packet Type	1	191 => 193	Packet type of the confirmable command.
Packet Subtype	1	0 => 255	Packet subtype of the confirmable command.
<i>Response</i>			
Immediate response			
Related effect			



3.5 Telecommand set Part III - commands of type 192

3.5.1 TC(192,1) Select ELS mode

<i>Generic description</i>			
Acronym		aspmELSmode	
Type	192	PID	61
Subtype	1	Packet Category	12
16 bit parameters	2	Hazardous	No
<i>General description</i>			
Description		Select ELS measurement mode.	
Note			
<i>Parameter description</i>			
<i>Name</i>	<i>Size (bytes)</i>	<i>Value</i>	<i>Note</i>
Spare	1 bit		
Rice Compression Enabled	1 bit	0 => 1	0=disabled, 1=enabled
Log Compression Enabled	1 bit	0 => 1	0=disabled, 1=enabled
Energy Compression	2 bits	0 => 2	0 = 1 step 1 = 2 steps 2 = 4 steps
Time Compression	3 bits	0 =>4	0 = 1 sweep 1 = 2 sweeps 2 = 4 sweeps 3 = 8 sweeps 4 = 16 sweeps
Sweep Table Number	5 bits		
PAD	1 bit	0	
Deflection Voltage Sweep Disabled	1 bit	0 => 1	
None	1 bit	0 => 1	0 = inactive 1 = active
Sector Mask	2	0 => 0xFFFF	
<i>Response</i>			
Immediate response			
Related effect		ELS information changes in the HK packet and the ELS Science telemetry packet	



3.5.2 TC(192,6) Set NPI Mode

<i>Generic description</i>			
Acronym		aspmNPImode	
Type	192	PID	61
Subtype	6	Packet Category	12
16 bit parameters	3	Hazardous	No
<i>General description</i>			
Description		Set NPI measurement mode	
<i>Parameter description</i>			
<i>Name</i>	<i>Size (bytes)</i>	<i>Value</i>	<i>Note</i>
Stepping Mode	1	0=>255	0 = normal mode (no voltage stepping) 1-255 = number of samples in one step
Accumulation Time	4 bits	0 => 15	Accumulation Time (n) so that one period is 31.25ms * (2 ^ n)
PAD	1 bit	0	
Log Compression Enabled	1 bit	0 => 1	0=disabled, 1=enabled
Rice Compression Enabled	1 bit	0 => 1	0=disabled, 1=enabled
None	1 bit	0 => 1	0 = inactive, 1 = active
Sector Mask	4	0 => 0xFFFFFFFF	
<i>Response</i>			
Immediate response			
Related effect		NPI information changes in the HK packet and the NPI Science telemetry packet	

3.5.3 TC(192,7) Set NPD Mode

<i>Generic description</i>			
Acronym		aspmNPDmode	
Type	192	PID	61
Subtype	7	Packet Category	12
16 bit parameters	3	Hazardous	No
<i>General description</i>			
Description		Set NPD measurement mode	
Note			
<i>Parameter description</i>			
<i>Name</i>	<i>Size (bytes)</i>	<i>Value</i>	<i>Note</i>
Integration Factor	4 bits		Reserved for TOF mode
Accumulation Time	4 bits		Accumulation Time (n) so that one period is 31.25ms * (2 ^ n)
PAD	1 bit	0	
Measurement Mode	3 bits	0 => 3	0 = Raw Array Mode 1 = Bin Matrix Mode 2 = TOF Mode 3 = PHD Mode
Log Compression Enabled	1 bit	0 => 1	0=disabled, 1=enabled
Rice Compression Enabled	1 bit	0 => 1	0=disabled, 1=enabled
NPD2 active	1 bit	0 => 1	0=inactive, 1=active
NPD1 active	1 bit	0 => 1	0=inactive, 1=active
NPD1 Bin Matrix	2	0 => 0x0FFF	Bits 12-15 = PAD
Reduction Tables			Bits 8 - 11 = Dir 2 Bits 4 - 7 = Dir 1 Bits 0 - 3 = Dir 0



ASPERA-4



Venus
Express

Reference : VE-ASP-MA-0005
Issue : 1 Rev. : 0
Date : 2004-05-05
Volume : - Page: 36

Generic description			
NPD2 Bin Matrix	2	0 => 0x0FFF	Bits 12-15 = PAD
Reduction Tables			Bits 8 - 11 = Dir 2
			Bits 4 - 7 = Dir 1
			Bits 0 - 3 = Dir 0
Response			
Immediate response			
Related effect		NPD information changes in the HK packet and the NPD Science telemetry packet	

3.5.4 TC(192,12) Set MU HK Packet Generation Frequency

Generic description			
Acronym		AspmHKDelay	
Type	192	PID	61
Subtype	12	Packet Category	12
16 bit parameters	1	Hazardous	No
General description			
Description		Set HK Generation Frequency	
Note			
Parameter description			
Name	Size (bytes)	Value	Note
None	2	0 => 0xffff	Delay in seconds
Response			
Immediate response			
Related effect			



3.5.5 TC(192,13) Set Scanner mode

<i>Generic description</i>			
Acronym		AspmSCANmode	
Type	192	PID	61
Subtype	13	Packet Category	12
16 bit parameters	2	Hazardous	No
<i>General description</i>			
Description		Set Scanner mode	
Note		In scanning mode (mode = 1), second parameter must be sent but doesn't affect anything.	
		Mu unit will accept scanner mode commands leading the scanner to rotate into b-positions (ie.positions from 0xB0 to 0xBF). If command is for standing mode scanner is simply no moving. In stepping mode next step not in b-positions is commanded instead.	
<i>Parameter description</i>			
Name	Size (bytes)	Value	Note
PAD	7 bits	0	0 = Standing (scanner on)
Scanner mode	1 bits	0 => 3	1 = Scanning 2 = Stepping 3 = Not in use (Scanner off)
Scanner speed	1	0 => 3	0 = Shutdown 1 = 32 sec per scan 2 = 64 sec per scan 3 = 128 sec per scan
Scanner cycle duration	1	0 => 0xFF	Length of measurement cycle (n) so that cycle lasts for 31.25ms * (2^n).
Scanner step angle or Scanner position (based upon Mode Setting)	1	0 => 0xFF	Standing mode => Position Stepping mode => Step Angle
<i>Response</i>			
Immediate response			
Related effect		Scanner information changes in the HK packet and the Scanner Information telemetry packet	



3.5.6 TC(192,14) Initialize Scanner

Generic description			
Acronym		AspmSCANinit	
Type	192	PID	61
Subtype	14	Packet Category	12
16 bit parameters	1	Hazardous	No
General description			
Description		Initialize Scanner	
Parameter description			
Name	Size (bytes)	Value	Note
PAD	7 bits	0	0 = test communication and initialization
Scanner init	1 bit	0 => 1	1 = test communication only
Communication test value	1	0 => 0xFF	test value
Response			
Immediate response			
Related effect			

3.5.7 TC(192,16) Set High Voltage Shutter Reduced Voltages

Generic description			
Acronym		AspmHVShutVolts	
Type	192	PID	61
Subtype	16	Packet Category	12
16 bit parameters	3	Hazardous	No
General description			
Description		Set HV shutter reduced voltages Set HV shutter reduced voltages	
Note			
Parameter description			
Name	Size (bytes)	Value	Note
PAD	1	0	
NPI Bias	1	0 => 0xFF	
NPD1 Stop Bias	1	0 => 0xFF	
NPD1 Start Bias	1	0 => 0xFF	
NPD2 Stop Bias	1	0 => 0xFF	
NPD2 Start Bias	1	0 => 0xFF	
Response			
Immediate response			
Related effect		Bias reference fields values change in the HK packet	



3.5.8 TC(192,15) Set High Voltage Shutter Mode

<i>Generic description</i>			
Acronym		aspmHVShut	
Type	192	PID	61
Subtype	15	Packet Category	12
16 bit parameters	varies	Hazardous	No
<i>General description</i>			
Description		Set HV shutter mode	
<i>Parameter description</i>			
<i>Name</i>	<i>Size (bytes)</i>	<i>Value</i>	<i>Note</i>
Test mode	1 bit	0 off 1 on	In solar sensor mode only
Mode	3 bits	0 off 1 Solar sensor with init 2 Test scan only 3 NPD Countrate 4 External	
Others, varies with mode	12 bits		
Others, varies with mode	8		
Command interpretation in solar sensor mode:			
Test mode	1 bit	0 off 1 on	
Mode	3 bits	1 Solar sensor with init	
Re-init period	8 bits	Number of measurement cycles	
PAD	2 bits		
Scanner speed	2 bits	0 default (32s) 1 32s 2 64s 3 128s	
Solarsensor 1 CW limit	1		Valid if test mode specified
Solarsensor 1 CCW limit	1		Valid if test mode specified
Solarsensor 2 CW limit	1		Valid if test mode specified
Solarsensor 2 CCW limit	1		Valid if test mode specified
PAD	4		
Command interpretation in NPD countrate mode:			
Test mode	1 bit	N/A	
Mode	3 bits	3 NPD Countrate	
Duration	12bits	Duration (n) so that reduced voltages are used for 31.25 * (n+1) ms	
Countrate criteria for NPD1	2		
Countrate criteria for NPD2	2		
PAD	4		
Command interpretation in Ext mode:			
Test mode	1 bit	0 off	
Mode	3 bits	4 Ext Countrate	
Duration for NPI shutter	12 bits	Duration (n) so that reduced voltages are used for 31.25 * (n+1) ms	
CW position for NPI shutter	1		
CCW pos for NPI shutter	1		



<i>Generic description</i>	
PAD	4 bits
Duration for NPD1 and NPD2 shutter	12 bits
	Duration (n) so that reduced voltages are used for 31.25 * (n+1) ms
CW position for NPD1 shutter	1
CCW position for NPD1 shutter	1
CW position for NPD2 shutter	1
CCW position for NPD2 shutter	1
<i>Response</i>	
Immediate response	
Related effect	Values in corresponding fields change in the HK packet

3.5.9 TC(192,20) Run Macro

<i>Generic description</i>			
Acronym	aspmMacroRun		
Type	192		
Subtype	20		
16 bit parameters	1		
PID	61		
Packet Category	12		
Hazardous	No		
<i>General description</i>			
Description	Run macro		
<i>Parameter description</i>			
Name	Size (bytes)	Value	Note
PAD	1	= 0	
Macro Number	1	0 =>0xFF	0 – 191 range of values
<i>Response</i>			
Immediate response			
Related effect	Corresponding macro is loaded from EEPROM and executed		

3.5.10 TC(192,21) Terminate Current Macro

<i>Generic description</i>			
Acronym	aspmMacroTerminate		
Type	192		
Subtype	21		
16 bit parameters	0		
PID	61		
Packet Category	12		
Hazardous	No		
<i>General description</i>			
Description	Terminate current macro		
Note	This command cannot be used in a macro.		
<i>Parameter description</i>			
Name	Size (bytes)	Value	Note
None	-	-	-
<i>Response</i>			
Immediate response			
Related effect			



3.5.11 TC(192,22) Run Single Macro Command

Generic description			
Acronym		aspmMacroRunCmd	
Type	192	PID	61
Subtype	22	Packet Category	12
16 bit parameters	varies	Hazardous	No
General description			
Description		Run single macro command	
Parameter description			
Name	Size (bytes)	Value	Note
None	2	= 0x2704	
Confirm Word	2		type+subtype as in aspmLaunch
Type	1	0=>0xFF	
SubType	1	0=>0xFF	
None	2	= 0x0	
Number of Parameters	1	0=>0xFF	
None	1	= 0x0	
Parameters	varies		as many as specified above
Response			
Immediate response			
Related effect			



3.6 Telecommand set Part IV - commands of type 193

3.6.1 TC(193,1) Pipe Telecommand

<i>Generic description</i>			
Acronym		aspmPipe	
Type	193	PID	61
Subtype	1	Packet Category	12
16 bit parameters	Varies	Hazardous	No
<i>General description</i>			
Description		Pipe TC to TM Send parameters back to telemetry	
Note			
<i>Parameter description</i>			
<i>Response</i>			
Immediate response		Piped TC report packet TM (193, 128)	
Related effect			

3.6.2 TC(193,2) Relax (do nothing)

<i>Generic description</i>			
Acronym		aspmRelax	
Type	193	PID	61
Subtype	2	Packet Category	12
16 bit parameters	0	Hazardous	No
<i>General description</i>			
Description		Relax i e do nothing	
Note			
<i>Parameter description</i>			
Name	Size (bytes)	Value	Note
None	-	-	-
<i>Response</i>			
Immediate response			
Related effect			

3.6.3 TC(193,3) Generate simulated data

<i>Generic description</i>			
Acronym		AspmSim	
Type	193	PID	61
Subtype	3	Packet Category	12
16 bit parameters	1	Hazardous	No
<i>General description</i>			
Description		Generate simulated data	
Note			
<i>Parameter description</i>			
Name	Size (bytes)	Value	Note
Simulation enabled	2	0 => 1	0: simulation disabled 1: simulation enabled
<i>Response</i>			
Immediate response			
Related effect			



3.6.4 TC(193,4) Write word to address

<i>Generic description</i>			
Acronym		aspmWrite	
Type	193	PID	61
Subtype	4	Packet Category	12
16 bit parameters	2	Hazardous	Yes
<i>General description</i>			
Description		Write word to address	
Note		Command must be verified with TC(191, 255)	
<i>Parameter description</i>			
<i>Name</i>	<i>Size (bytes)</i>	<i>Value</i>	<i>Note</i>
Address	2	0 => 0xFFFF	
Data word	2	0 => 0xFFFF	
<i>Response</i>			
Immediate response			
Related effect			

3.6.5 TC(193,5): Read word from address

<i>Generic description</i>			
Acronym		aspmRead	
Type	193	PID	61
Subtype	5	Packet Category	12
16 bit parameters	1	Hazardous	No
<i>General description</i>			
Description		Read word from address	
Note			
<i>Parameter description</i>			
<i>Name</i>	<i>Size (bytes)</i>	<i>Value</i>	<i>Note</i>
Address	2	0 => 0xFFFF	
<i>Response</i>			
Immediate response		Read word report packet TM(193,6)	
Related effect			

3.6.6 TC(193,10) Patch EEPROM

<i>Generic description</i>			
Acronym		aspmPatch	
Type	193	PID	61
Subtype	10	Packet Category	12
16 bit parameters	6	Hazardous	No
<i>General description</i>			
Description		Patch EEPROM (starting from absolute address) using specified number of words found from massmemory at specified absolute address.	
Note			
<i>Parameter description</i>			
<i>Name</i>	<i>Size (bytes)</i>	<i>Value</i>	<i>Note</i>
Massmemory address	4	0 => 0x0007 FFFF	
Eeprom address	4	0 => 0x0003 FFFF	
Patch Mode	1 bit	0 => 1	0 = Patch without using paging mode 1 = Patch using paging mode
Patch length	15 bits	1 => 0x7FFF	Length of patch in 16bit words



Generic description			
Patch CRC checksum	2	0 => 0xFFFF	CRC checksum calculated over whole patch
Response			
Immediate response	EVENT: - EEPROM programmed or - EEPROM programming not successful or - EEPROM programming CRC error		
Related effect			

3.6.7 TC(193,11): Load Module

Generic description			
Acronym		aspmModule	
Type	193	PID	61
Subtype	11	Packet Category	12
16 bit parameters	3	Hazardous	No
General description			
Description		Load Module	
Note			
Parameter description			
Name	Size (bytes)	Value	Note
Address	4	0 => 0x0007 FFFF	
PAD	6 bits	= 0	
Execution Flag	1 bit	0 => 1	0 = Load and run module 1 = Load but don't run module
CRC Verify	1 bit	0 => 1	0 = Verify crc 1 = Don't verify crc
Memory ID	1	= 0x82	(EEPROM)
Response			
Immediate response	EVENT: - Module loaded or - Module load failed		
Related effect			

3.6.8 TC(193,12) Select Boot Mode

Generic description			
Acronym		aspmBootMode	
Type	193	PID	61
Subtype	12	Packet Category	12
16 bit parameters	1	Hazardous	No
General description			
Description		Select boot mode	
Note			
		No use after boot process	
Parameter description			
Name	Size (bytes)	Value	Note
Boot Mode	1	1 => 2	1 = Safe Mode 2 = Normal Mode
Response			
Immediate response			
Related effect			

3.6.9 TC(193,16) Watchdog reset

Generic description



ASPERA-4



Venus
Express

Reference : VE-ASP-MA-0005
Issue : 1 Rev. : 0
Date : 2004-05-05
Volume : - Page: 45

<i>Generic description</i>			
Acronym		aspmWDRreset	
Type	193	PID	61
Subtype	16	Packet Category	12
16 bit parameters	1	Hazardous	No
<i>General description</i>			
Description		Force watchdog reset	
Note			
<i>Parameter description</i>			
Name	Size (bytes)	Value	Note
Security code	2	=0x2704	
<i>Response</i>			
Immediate response		EVENTS: - I'm alive and - Watchdog reset	
Related effect			



3.7 List of telecommands

<i>Telecommand</i>	<i>Acronym</i>	<i>Description</i>	<i>Number of Parameters</i>
TC (3, 5)	aspmHKEnable	Enable HK generation	1
TC (3, 6)	aspmHKDisable	Disable HK generation	1
TC (6, 2)	aspmMEMLoad	Load memory	4
TC (6, 5)	aspmMEMDump	Dump memory	4
TC (9, 1)	aspmTime	Accept Time Update	0
TC (17, 1)	aspmConn	Connection Test	0
TC (20, 1)	aspmSCIRnable	Enable Science on RTU link	0
TC (20, 2)	aspmSCIDisable	Disable Science on RTU link	0
TC (191, 1)	aspmELS30	Switch ELS +30V on/off	1
TC (191, 2)	aspmELSGrid	Set ELS Screen Grid voltage	1
TC (191, 3)	aspmELSDefl	Set ELS Deflection voltage and switch	1
TC (191, 4)	aspmELSHV	Switch ELS high voltage on/off	1
TC (191, 5)	aspmELSMcp	Set ELS MCP bias voltage	1
TC (191, 7)	aspmIMA30	Switch IMA +30V on/off	1
TC (191, 9)	aspmIMAPow	Switch MA \pm 5V and \pm 12V on/off	1
TC (191, 10)	aspmNPDheaters	Switch NPD heaters on/off	1
TC (191, 11)	aspmNPD130	Switch NPD1 +30V on/off	1
TC (191, 12)	aspmNPD1bias	Set NPD1 bias	1
TC (191, 13)	aspmNPD1defl	Set NPD1 Deflection bias	1
TC (191, 14)	aspmNPD1start	Set NPD1 Start bias	1
TC (191, 15)	aspmNPD1stop	Set NPD1 Stop bias	1
TC (191, 16)	aspmNPD230	Switch NPD2 +30V on/off	1
TC (191, 17)	aspmNPD2bias	Set NPD2 bias	1
TC (191, 18)	aspmNPD2defl	Set NPD2 Deflection bias	1
TC (191, 19)	aspmNPD2start	Set NPD2 Start bias	1
TC (191, 20)	aspmNPD2stop	Set NPD2 Stop bias	1
TC (191, 21)	aspmNPI30	Switch NPI +30V on/off	1
TC (191, 22)	aspmNPIBias	Set NPI Bias	1
TC (191, 23)	aspmNPIDefl	Set NPI Deflection voltage	1
TC (191, 24)	aspmNPISwitch	Set NPI Switch	1
TC (191, 25)	aspmSCANSetup	Set Scanner setup	1
TC (191, 26)	aspmSCANVolts	Set Scanner voltages	3
TC (191, 27)	aspmSCANStrHeat	Switch stringheaters on/off	1
TC (191, 30)	aspmWatchdog	Enable Watchdog	1
TC (191, 32)	aspmNPD1switch	Set NPD1 high voltages	1
TC (191, 33)	aspmNPD2switch	Set NPD2 high voltages	1
TC (191, 34)	aspmNPD1Tresholds	Set NPD1 counter tresholds	2
TC (191, 35)	aspmNPD2Tresholds	Set NPD2 counter tresholds	2
TC (191, 255)	aspmLaunch	Confirm Hazardous Command	1
TC (192, 1)	aspmELSmode	Set ELS mode	2
TC (192, 6)	aspmNPImode	Set NPI mode	3
TC (192, 7)	aspmNPDmode	Set NPD mode	3
TC (192, 12)	aspmHKDelay	Set HK generation frequency	1
TC (192, 13)	aspmSCANmode	Set Scanner mode	2
TC (192, 14)	aspmSCANinit	Initialize Scanner	1
TC (192, 15)	aspmHVShut	Set HV shutter mode	Varies
TC (192, 16)	aspmHVShutVolts	Set HV shutter reduced voltages	3
TC (192, 20)	aspmMacroRun	Run macro	1
TC (192, 21)	aspmMacroTerminate	Terminate current macro	0
TC (192, 22)	aspmMacroRunCmd	Run single macro command	Varies
TC (193, 1)	aspmPipe	Pipe TC to TM	Varies
TC (193, 2)	aspmRelax	Relax, I e do nothing	0
TC (193, 3)	aspmSim	Generate simulated data	1
TC (193, 4)	aspmWrite	Write to address	2



ASPERA-4



**Venus
Express**

Reference : VE-ASP-MA-0005
Issue : 1 Rev. : 0
Date : 2004-05-05
Volume : - Page: 47

<i>Telecommand</i>	<i>Acronym</i>	<i>Description</i>	<i>Number of Parameters</i>
TC (193, 5)	aspmRead	Read from address	1
TC (193, 10)	aspmPatch	Patch eeprom	6
TC (193, 11)	aspmModule	Load module	3
TC (193, 12)	aspmBootMode	Select boot mode	1
TC (193, 16)	aspmWDRreset	Watchdog reset	1



4 TELEMETRY

4.1 General

4.2 Telemetry packages

4.2.1 TM(1,1) Telecommand Acceptance report - Success

<i>Generic description</i>			
Acronym		ASPMTCAck	
Type	1	PID	61
Subtype	1	Packet Category	1
16 bit parameters	4		
<i>General description</i>			
Description		Telecommand acceptance report	
Note			
<i>Parameter description</i>			
<i>Name</i>	<i>Size (bytes)</i>	<i>Value</i>	<i>Note</i>
Telecommand packet ID	2	0 => 0xFFFF	
Telecommand packet sequency control	2	0 => 0xFFFF	
<i>Long description</i>			
In SGICD			

4.2.2 TM(1,2) Telecommand Acceptance report - Failure

<i>Generic description</i>			
Acronym		ASPMTCNack	
Type	1	PID	61
Subtype	2	Packet Category	1
16 bit parameters	Varies		
<i>General description</i>			
Description		Telecommand acceptance report - failure	
Note			
<i>Parameter description</i>			
<i>Name</i>	<i>Size (bytes)</i>	<i>Value</i>	<i>Note</i>
<i>Long description</i>			
In SGICD - No changes or additions to that definition has been made			

4.2.3 TM(1,7) TM Execution acknowledgment report – Success

As specified in SGICD

4.2.4 TM(1,8) TM Execution acknowledgment report – Failure

As specified in SGICD



4.2.5 TM(3,25) Housekeeping report

<i>Generic description</i>			
Acronym		ASPMHKRep / ASPIHKRep	
Type	3	Subtype	25
APID	61 => 62		
16 bit parameters	Varies		
<i>General description</i>			
Description		Housekeeping report	
Note			
<i>Parameter description</i>			
<i>Name</i>	<i>Size (bytes)</i>	<i>Value</i>	<i>Note</i>
<i>Long description</i>			
Description later in this document			

4.2.6 TM(6,6) Memory dump report packet (as specified in SGICD)

<i>Generic description</i>			
Acronym		aspmMemDump	
Type	6	Subtype	6
APID	61		
16 bit parameters	Varies		
<i>General description</i>			
Description		Memory dump report packet.	
Note			
<i>Parameter description</i>			
<i>Name</i>	<i>Size (bytes)</i>	<i>Value</i>	<i>Note</i>
<i>Long description</i>			

4.2.7 TM(17,2) Connection test report

<i>Generic description</i>			
Acronym		ASPMConnRep	
Type	17	Subtype	2
APID	61		
16 bit parameters			
<i>General description</i>			
Description		Connection test report	
Note			
<i>Parameter description</i>			
<i>Name</i>	<i>Size (bytes)</i>	<i>Value</i>	<i>Note</i>
<i>Long description</i>			
In SGICD			



4.2.8 TM(20,3) Science data report

<i>Generic description</i>			
Acronym		ASPMScienceRep	
Type	20	Subtype	3
APID	61		
16 bit parameters	Varies		
<i>General description</i>			
Description		Science data report	
Note			
<i>Parameter description</i>			
<i>Name</i>	<i>Size (bytes)</i>	<i>Value</i>	<i>Note</i>
<i>Long description</i>			
Definition later in this document			

4.2.9 TM(193,6) Read word report packet

<i>Generic description</i>			
Acronym		ASPMReadRep	
Type	193	Subtype	6
APID	61		
16 bit parameters	2		
<i>General description</i>			
Description		Word read from address specified in packet TC(193,5)	
Note			
<i>Parameter description</i>			
<i>Name</i>	<i>Size (bytes)</i>	<i>Value</i>	<i>Note</i>
Address	2	Any	Address of word
Data	2	Any	Word read from address
<i>Long description</i>			

4.2.10 TM(193,128) Piped TC report packet

<i>Generic description</i>			
Acronym		ASPMPipeRep	
Type	193	Subtype	128
APID	61		
16 bit parameters	Varies		
<i>General description</i>			
Description		Piped Telecommand	
Note			
<i>Parameter description</i>			
<i>Name</i>	<i>Size (bytes)</i>	<i>Value</i>	<i>Note</i>
<i>Long description</i>			
Parameters should be exact copy of source data field (without checksum) of received telecommand aspmPipe			



4.3 Telemetry list

<i>Telecommand</i>	<i>Acronym</i>	<i>Description</i>	<i>Note</i>
TM (1, 1)	aspmTCAck	Telecommand acceptance report – Success	
TM (1, 2)	AspmTCNack	Telecommand acceptance report – Failure	
TM (1, 7)	AspiTCEAck	Telecommand execution report – Success	Only from IMA
TM (1, 8)	aspiTCENAck	Telecommand execution report – Failure	Only from IMA
TM (6,6)	AspmMemDumpRep / aspiMemDumpRep	Memory dump report packet for MU / IMA	
TM (6, X)	AspiMemCheckRep	Memory check report for IMA	Only for iMA
TM (3, 25)	AspmHKRep / AspmHKRep	Housekeeping packet fro MU / IMA	
TM (17, 2)	aspmConnRep	Connection Test response	
TM (20, 3)	AspmScienceRep / aspiScinceRep	Enable Science on RTU link for MU/IMA	
TM (193,6)	ASPMReadRep		
TM (193,128)	aspmSCIDisable	Disable Science on RTU link	



5 EVENT REPORTING

5.1 General

All events from the MU are formatted according to the same scheme. First word (after headers, i.e. word number 8) is the event number. The following two words are freely chosen extra information about the event, typically just zeros. Events generated by the MU are of type TM(5,1) to TM(5,2), as specified in the SGICD. Subtype 1 corresponds to normal progress and subtype 2 corresponds to a warning.

5.2 Event List

The following table defines all events produced by the MU. If extra parameters are not specified, these are constant zeros.

<i>Event number</i>	<i>Event name</i>	<i>Parameter 1</i>	<i>Parameter 2</i>	<i>Description</i>
40001	I'm Alive			Generated after normal boot process as a first event
40003	Going to reboot			
40004	Watchdog reset	wd mask	wd mask cleared	
40005	Going to safe mode			
40006	Going to normal mode			
40007	Telecommand buffer overflow			
40010	Eeprom programmed			
40011	Eeprom programming - nonsuccess	CRC check sum in patch	CRC checksum in programmed EEPROM area	
40012	CRC error in Eeprom patch	CRC check sum in patch	CRC checksum specified in TC	
40013	Module loaded			
40014	Module load failed	Error code defining exact type of error	Optional extra information	
40015	Default boot module loaded			
40016	Default boot module loading failed	Error code defining exact type of error	Optional extra information	
40020	Command handler error	1: command not confirmed properly 16: other error 0xffff: command not found	Seq count of command raising error	
40021	Invalid confirmation by TC(191,255)	For Command to be confirmed: Bit 8-15: type bit 0-7: Subtype	From the confirmation parameters: Bit 8-15: type bit 0-7: Subtype	
40022	Invalid mode definition	Upmost address for the data storage of invalid mode		
40026	Macro execution succesful	Macro number		
40027	Macro terminated by TC	Macro number	Command index in macro command buffer	
40028	Macro Checksum error in EEPROM	Calculated checksum	Checksum in EEPROM	
40029	Macro Can't start			
40074	IMA command buffer full			



ASPERA-4



**Venus
Express**

Reference : VE-ASP-MA-0005
Issue : 1 Rev. : 0
Date : 2004-05-05
Volume : - Page: 53

<i>Event number</i>	<i>Event name</i>	<i>Parameter 1</i>	<i>Parameter 2</i>	<i>Description</i>
40092	Scanner initialized			
40097	Scanner error	2: Communication test failed before initialization 3: Initialization failed. 4: Can't start scanner properly 5: Scanner not stopped properly 6: Scanner not initialized 7: Can't escape endposition on initialization 8: Science not enabled		



6 HOUSEKEEPING TELEMETRY

6.1 General

The ASPERA-4 Main Unit have one type of housekeeping (HK) packet which contains all HK signals and parameters.

6.2 HK packet source data field

6.2.1 Source data field for Main Unit

6.2.1.1 Generic structure

After headers, there will be the source data field. For the HK report packet, it will be as shown below.

<i>Byte</i>	<i>Bits</i>	<i>Field</i>	<i>Note</i>
Source data field			
16		PAD	for TM(3,25) always 0
17		SID	
18-119		Parameters	Full HK packet

The SID field contains an identifier telling which type of HK packet is being sent. For the Main Unit the full Housekeeping packet is identified by setting SID to 0. For IMA SID=10. They can also be recognised by examining the application id field.

6.2.1.2 Full Housekeeping Packet

The full HK packet will have the following format. Bit number 0 will be the LSB (i e numbering is NOT the same as defined in the SGICD). If not otherwise stated, the fields will contain exactly the value read from hardware.

<i>Byte</i>	<i>Bits</i>	<i>Field</i>	<i>Note</i>
18		els_temp	
19		npd1_temp	
20		npd2_temp	
21		npi_temp	
22		scanner_temp_sensor	
23		PAD	
24-25		sw_version	Software version
26		els_minus_5v_screen_grid_ref	sw monitored
27		els_minus_5v_screen_grid_mon	
28		els_bias_mcp_ref	sw monitored
29		els_bias_mcp_mon	
30-31	13-15	PAD	
	12	els_plus_30v_on_off	
	11	els_enable_hv	sw monitored
	9	PAD	
	8	els_range	sw monitored
	0-7	ELS deflection voltage sweep table number	sw_monitored
32		hk_i_plus_30v	
33		hk_i_plus_5v	



ASPERA-4



Venus
Express

Reference : VE-ASP-MA-0005
Issue : 1 Rev. : 0
Date : 2004-05-05
Volume : - Page: 55

Byte	Bits	Field	Note
34		hk_v_plus_12v	
35		hk_v_plus_30v	
36		hk_v_plus_5v	
37		hk_v_minus_12v	
38		hk_v_minus_5v	
39	7	NPD1_defl_switch	
	6	NPD2_defl_switch	
	5	Sun sensor 2	
	4	Sun sensor 1	
	3	PAD	
	2	npd_heaters_on_off	sw monitored
	1	npd1_plus_30v_on_off	
	0	npd2_plus_30v_on_off	
40		npd1_bias_mon	
41		npd1_bias_ref	sw monitored
42		npd1_defl_mon	
43		npd1_defl_ref	sw monitored
44		npd1_start_bias_mon	
45		npd1_start_bias_ref	sw monitored
46		npd1_stop_bias_mon	
47		npd1_stop_bias_ref	sw monitored
48		npd1_frontctrl	
49		npd1_mainctrl	
50-51		npd1_stat	
52-53		npd1_tdcrd	
54-55		npd1_calib11	
56-57		npd1_calib12	
58-59		npd1_calib21	
60-61		npd1_calib22	
62-63		npd1_sefcnt	
64-65		npd1_defcct	
66		npd2_bias_mon	
67		npd2_bias_ref	sw monitored
68		npd2_defl_mon	
69		npd2_defl_ref	sw monitored
70		npd2_start_bias_mon	sw monitored
71		npd2_start_bias_ref	
72		npd2_stop_bias_mon	
73		npd2_stop_bias_ref	sw monitored
74		npd2_frontctrl	
75		npd2_mainctrl	
76-77		npd2_stat	
78-79		npd2_tdcrd	
80-81		npd2_calib11	
82-83		npd2_calib12	
84-85		npd2_calib21	
86-87		npd2_calib22	
88-89		npd2_sefcnt	
90-91		npd2_defcct	
92		npi_bias_ref	sw monitored
93		npi_bias_mon	
94		npi_defl_ref	sw monitored
95		npi_defl_mon	
96	7	npi_plus_30v_on_off	sw monitored
	6	npi_defl_switch	sw monitored
	5	npi_defl_mode	sw monitored
	3-4	SPARE4	



ASPERA-4



Venus
Express

Reference : VE-ASP-MA-0005
Issue : 1 Rev.: 0
Date : 2004-05-05
Volume : - Page: 56

Byte	Bits	Field	Note
	2	ima_plus_minus_12v_on_off	sw monitored
	1	ima_plus_30v_on_off	sw monitored
	0	ima_plus_minus_5v_on_off	sw monitored
97		scanner_vrefmc	
98	7	scanner_status_ccw_end_pos	
	6	scanner_status_cw_end_pos	
	5	scanner_status_pos_clock	
	4	scanner_status_direction	0: 0 - 180 1: 180 - 0
	2-3	scanner_status_state	0: Not busy 1: ramp up 2: Full speed move 3: Ramp down
	1	Lost step	
	0	scanner_initialized	
99	7	scanner_plus_30v_on_off	
	5-6	PAD	
	4	scanner_setup_mode	0: normal 1: manual
	3	scanner_setup_direction	0: 0 - 180 1: 180 - 0 for manual mode speed command only
	2	PAD	
	0-1	scanner_speed	0: STOP 1: 32s scan 2: 64s scan 2: 128s scan
100		scanner_coast_current_ref	
101		scanner_ramp_current_ref	
102		scanner_treshold_cw_ref	
103		scanner_treshold_ccw_ref	
104		scanner_treshold_wheel_ref	
105		scanner_position	
106		sw_mode	sw monitored
107		cpu_load	sw monitored
108-109		ELS sector mask	sw monitored
110-111	8-15	ELS compression scheme (ie. defines mode)	sw monitored
	0-7	ima_link_status	Bitfield is best explained in document called 'Rosetta RPC PIU Interfaces document. Part II - Data handling interfaces'. In short, it contains status register of IEEE 1355 LINK Chip. Bit 7: ndata0A Bit 6: crdMEM Bit 5: datav Bit 4: resetm Bit 3: ffrx Bit 2: EOP1 Bit 1: ndata0 Bit 0: nm1 In typical nominal operation one should find value 0x41 on the link when link is working properly.
112-115		NPI Sector mask	
116-117	7-15	PAD	
	6	NPI Mode	
	2-5	NPI Accumulation time	$31.25ms * 2^{n-1}$
	1	NPI Log compression enabled	
	0	NPI RICE compression enabled	
118	7	PAD	



ASPERA-4



Venus
Express

Reference : VE-ASP-MA-0005
Issue : 1 Rev.: 0
Date : 2004-05-05
Volume : - Page: 57

Byte	Bits	Field	Note
	6	NPD RICE compression enabled	
	5	NPD Log compression enabled	
	0-4	NPD Accumulation time	
119	4-7	NPD2 mode	0: not in use 1: raw data 2: bin matrix (0 0 0) 3: bin matrix (0 0 1), (0 1 0) or (1 0 0) 4: bin matrix (0 0 2), (0 2 0) or (2 0 0) 5: bin matrix (0 1 1), (1 0 1) or (1 1 0) 6: bin matrix (0 1 2), (1 0 2), (0 2 1), (1 2 0), (2 0 1) or (2 1 0) 7: bin matrix (0 2 2), (2 0 2) or (2 2 0) 8: bin matrix (1 1 1) 9: bin matrix (1 1 2), (1 2 1) or (2 1 1) 10: bin matrix (1 2 2), (2 1 2) or (2 2 1) 11: bin matrix (2 2 2) 12: phd mode 13: tof mode NOTE: Although reduction tables for bin matrixc can be defined independently all default modes in macros are defined so that bin matrix is of type (0 0 0), (1 1 1) or (2 2 2) for both NPDs simultaneously.
	0-3	NPD1 mode	

There are a few spare bits. They are used to align 8 bit signals to 8 bit fields. Spare bits can be allocated later for some other use.

Software signal fields:

*ref: All values named *ref are monitored by software. They represent values written to some hardware register, typically values commanded by TC.

sw_version: sw_version is one 16-bit number defining the software version. It is included in every private tecommand packet originating in MU and in MU HK packets. S/W mode is constructed as follows:

Bits	Name	Description
14-15	Release class	0: N/A 1: D (development) 2: T (Testing version) 3: R (Release, official and stable revision)
9-13	Major	
4-8	Minor	
0-3	Patch number	

For example, Version number 0xC871 means s/w version R-4.7.1 (Release, major=4,minor=7, and patch number =1)

cpu_load: N/A

sw_mode: sw_mode defines software mode



7 INSTRUMENT SOFTWARE MODES

<i>SW Mode</i>	<i>Mode name</i>
1	Booting
2	Safe
3	Prom
4	Normal

7.1 Instrument modes

Instrument modes are defined in housekeeping packet just by reporting corresponding settings one by one.



8 IMA TELEMETRY

8.1 Source data field for IMA

After headers, there will be the source data field. For the HK report packet, it will be as shown below:

Byte	Bits	Field	Note
Source data field			
16	8-15	PAD	PAD=0
	0-7	SID	SID=10
18-41		IMA Housekeeping packet data (24 bytes)	

The content of the IMA Housekeeping packet data is defined by the IMA team and can be found in the ICA-IMA TC/TM Data Formats and Related Software Aspects Document issued by Hans Borg at IRF dated 2002-04-07 . The content of the source data field is exactly the same as the data fields of 4 link packets sent by IMA to the MU.

8.2 IMA HK definition

Word offs.	Bits.	Content.	Table pos.	Parameter.		
0	15-10	Mode. See below.	0	mode		
	9-8	Cmd status			9	hk_prm
		0=Ok (OK)				
		1=Invalid (Inv)				
		2=Out of range (Out)				
		3=Erroneous (Err)				
	7-0	HV switches		10	ad_prm	
	7	Deflection HV logical (ref)				
	6	Deflection LV logical (ref)				
	5	Entrance HV logical (ref)				
	4	Grid LV logical (ref)				
	3	Pacc HV logical (ref)				
	2	+28V main				
1	+28V opto					
0	+28V mcp					
1	15	Cmd toggle (Numeric 0/1)		12	hk_prm	
	14-12	SID no		1	Sid_nr	
	0	Minimum (Min)				
	1	Normal (Nrm)				
	2	Burst (Bst)				
	3	Calibration (Cal)				
	4	Special (Spc)				
	5	Test (Tst)				
	11-8	+28V presence		11	ad_prm	
	11	HV enable/disable				
	10	Main				
	9	Opto				
	8	Mcp				
7-0	Fifo filling (F8)		2	fifo_fill		
2	Cmd return (Numeric hex)			direct from tc_decoder		
3	15-8	Opto HV monitor		13	ad_prm	
	7-0	Mcp HV monitor		14	ad_prm	
4	15-8	Deflection HV monitor		15	ad_prm	



ASPERA-4



Venus
Express

Reference : VE-ASP-MA-0005
Issue : 1 Rev. : 0
Date : 2004-05-05
Volume : - Page: 60

<i>Word offs.</i>	<i>Bits.</i>	<i>Content.</i>	<i>Table pos.</i>	<i>Parameter.</i>
	7-0	Deflection LV monitor	16	ad_prm
5	15-8	Pacc HV monitor	17	ad_prm
	7-0	Grid LV monitor	18	ad_prm
6	15-8	Sensor temperature. (Sns)	19	ad_prm
	7-0	DPU temperatur. (Dpu)	20	ad_prm
7	15	Direct command switch	3	switches
	14-12	Pacc low level (ref.)	4	dta_12bit[3]
	11-0	Deflection HV reference	21	dig_dflhv
8	15	Alt. Pacc (Opera=Fix/Alt)	5	switches
	14-12	Pacc high level ref.	6	dta_12bit[4]
	11-0	Deflection LV reference	22	dig_dfllv
9	15	Pacc level (High/Low)	23	ms.flag
	14-12	Grid LV reference	24	dta_12bit[2]
	11-0	Entrance HV reference	25	dig_entr
10	15	Deflection HV (Opera=Stp/Fix)	26	switches
	14-12	Opto default reference	7	dta_12bit[0]
	11-9	Mcpdefault reference	8	dta_12bit[1]
	8-0	Entrance upper HV monitor	27	ad_prm
11	15	Entrance HV (Opera=Stp/Fix)	28	switches
	14-12	Opto current reference	29	Optocur
	11-9	Mcp current reference	30	Mcpcur
	8-0	Entrance lower HV monitor	31	ad_prm



ASPERA-4



Venus
Express

Reference : VE-ASP-MA-0005
Issue : 1 Rev. : 0
Date : 2004-05-05
Volume : - Page: 61

8.3 IMA scientific TM modes

<i>Mode</i>	<i>Mnemonic</i>	<i>Comments</i>
Minimum		
0	Idle	
1	Mmom	Moments only
2	Mspo	Spectras only
3	Mmsp	Moments and Spectras
4	Msis	Selected Ion Species
5	Mexm	Energy Mass matrix
6	Void	
7	Void	
Normal		
8	Nrm0	Normal 0
9	Nrm1	
10	Nrm2	
11	Nrm3	
12	Nrm4	
13	Nrm5	
14	Nrm6	
15	Nrm7	
Burst		
16	Har0	High angular resolution 0
17	Har1	
18	Har2	
19	Har3	
20	Har4	
21	Har5	
22	Har6	
23	Har7	
24	Exm0	Energy Mass matrix 0
25	Exm1	
26	Exm2	
27	Exm3	
28	Exm4	
29	Exm5	
30	Exm6	
31	Exm7	
Special		
32	Test	
33	Cal1	Calibration 1
34	Cal2	Calibration 2
35	Fake	Faked science data
36	Void	
37	Void	
38	Void	
39	Void	



Fifo filling must be unpacked by int unpack_f8 (int acc)

```
int Astat5a::unpack_f8(int acc)
{
int exp;

    exp=(acc >>4) &0xF;
    if(exp>1) {
        acc=(acc & 0xF) | 0x10;
        acc=acc<< (exp-1);
    }
    return acc;
}
```



9 SCIENCE DATA

9.1 Science data production modes

9.2 Science data packet formats

All packages will have the normal TM header and Data field header in front of the package.

The Lossy compression scheme will be used only if the RICE (lossless) compressed package is larger than the packet size.

If the measurement mode is changed before the data for one packet is completely measured, the packet will be cut on the starting place of invalidity. Hence, the data sent to the ground is valid (in this sense) but the set is not necessarily complete. This can be identified by the packet length (in the uncompressed case it's smaller than normal) or as a smaller amount of decompressed data (in compressed case). Of course, this kind of recovery is not always possible.

9.3 Science data packet types

The Science packets produced in the Main Unit have data types and subtypes. The data Type (4bits) defines mainly an instrument the packet is related to and the subtype (4bits) specifies the packet type within an instrument packet. Packet types and subtypes are allocated as follows.

The Main Unit will also format telemetry packets coming from IMA. These will be formatted to the ESA packet TM format and sent to the s/c. Science data coming from IMA is not analyzed by any means in the Main Unit.

<i>Data Type</i>	<i>Data subtype</i>	<i>Data type name</i>	<i>Description</i>
0	0	Dummy	Doesn't contain anything meaningful
<i>ELS Data Packages</i>			
1	0	ELS Engineering information	First ELS packet within one scan cycle. Contains engineering information needed for analysis of ELS data. No science data included
	1	ELS Complete sweep	Data from one complete sweep included
	2	ELS Sweep step 0-63	Data from first 64 steps in one sweep
	3	ELS Sweep step 64-127	Data from latter 64 steps in one sweep
<i>NPD1 data packages</i>			
2	0	NPD raw data	NPD1 data produced in raw data mode
	1	NPD binning data	NPD1 data produced in bin matrix mode
	2	NPD TOF mode	NPD1 data in Time-of-Flight mode
	3	NPD PHD mode	NPD1 data in Pulse height distribution mode
<i>NPD2 data packages</i>			
3	0	NPD raw data	NPD2 data produced in raw data mode
	1	NPD binning data	NPD2 data produced in bin matrix mode
	2	NPD TOF mode	NPD2 data in Time-of-Flight mode
	3	NPD PHD mode	NPD2 data in Pulse height distribution mode
<i>NPI data packages</i>			
4	0	NPI Normal mode data	NPI data in normal mode
	1	NPI Stepping mode	NPI data in deflection voltage stepping mode
<i>Engineering data packages</i>			
5	0	Solar sensor information	Status of Solar sensor 1&2 in each sample irq during one scan.
	1	Scanner information	Scanner position on each sample irq in one scan.



9.3.1 IMA telemetry packets

IMA telemetry packets will be sent almost as they are received in the Main Unit. The structure of the IMA telemetry packets are as follows. The time tag of the TM packet will be the time of receiving the first link packet from IMA. Time will be the same for all packets built from the same IMA packet.

Byte	Bits	Field	Subfield	Remark
16		Error status	0: No errors identified by MU others: first invalid word in IMA data	
17		IMA SID		
18-last		IMA packet		Maximum 2046 words of IMA telemetry packet

9.3.2 ELS telemetry packets

An ELS data packet can contain a maximum of 128 steps*16 sectors = 2048 words of (16-bit) raw data. Based upon whether compression is enabled or not, the data may fit in a single packet or may have to be split into 2 packets, with each packet comprised of 64 steps. The following table represents the ELS packet header that is common to all ELS packets.

Byte	Bits	Field	Subfield	Remark
16-17		Science data Header	SW version	
18-19	8-15		Spare	
	4-7		Data type	1 = ELS Packet
	2-3		PAD	
	0-1		ELS packet subtype	0 = ELS engineering information 1 = ELS data steps 0-127 2 = ELS data steps 0-63 3 = ELS data steps 64-127
20-25		SCET Time	On start of first sweep (i e 'engineering' sweep) in this scan	
26-27			ELS sector mask	
28	7	ELS compression scheme	Spare	
	6		Rice compression	
	5		Log compression (16 to 8 bit)	Note: If RICE compression is used, values will be 16bits in width, but the range for the value is 0-255. This is to optimize both performance and compression.
	3-4		Energy compression	0= 1 step, 1=2 steps, 2=4 steps , 3= undefined
	0-2		Time compression	0=1 sweep, 1=2 sweeps, 2=4 sweeps, 3=8 sweeps, 4=16 sweeps, 5-7=undefined
29			spare	



9.3.2.1 ELS engineering information

In the beginning of every scan cycle, some engineering information is sent in a separate ELS science packet. This information is needed for the analysis of the ELS science data that is returned during that scan cycle. This packet is built in the following way, starting from byte 30.

Byte	Bits	Field	Subfield	Remark
30	3-7		Spare	
	2		Scanner direction	0 = 0 – 180 1 = 180 – 0
	0-1		Scanner speed	0 = standing 1 = 32s scan 2 = 64s scan 3 = 128s scan
31			Scanner position	On start of scan (or step) period
32		ELS Status	PAD	
33			ELS temperature	
34			ELS MCP reference	
35			ELS MCP monitor	
36			ELS Screen grid reference	
37			ELS Screen grid monitor	
38-39			ELS Deflection reference step1	
40-41			ELS Deflection monitor step 1	
42-43			ELS Deflection ref. step 2	
44-45			ELS Deflection mon. step 2	
Etc				
546-547			ELS Deflection ref. step 128	
548-549			ELS Deflection mon. step 128	

9.3.2.2 ELS data

After the first packet of ELS engineering data is sent, the remaining ELS packets will contain ELS science data. There are three types of packets: (1) one containing data from one complete sweep (128 steps), (2) one containing the first 64 steps from one sweep, and (3) one containing the latter 64 steps from one sweep. All ELS packets will be sent in a row so it's possible to find the order of these packet from the Packet sequence count field. In this case, the packet will be as follows:

Byte	Bits	Field	Subfield	Remark
30	3-7		Spare	
	2		Scanner direction	0 = 0 - 180 1 = 180 - 0
	0-1		Scanner speed	0 = standing 1 = 32s scan 2 = 64s scan 3 = 128s scan
31			Scanner position	On start of scan (or step) period
32		Data	Sector 0, step 1, sweep 1	Data from one sweep. If no log, energy nor sectormask type of compression is applied to the data it will be divided to two parts. (ELS data packet subtypes 2 and 3) . In this case both packets will have same time tag on packet bytes 6-11. However, sequence count will differ between these two packets.
			Sector 1, step 1, sweep 1	
			
			Sector 0, step 2, sweep 1	
			Sector 1, step 2, sweep 1	



Byte	Bits	Field	Subfield	Remark
------	------	-------	----------	--------

9.3.3 NPD telemetry packets

Byte	Bits	Field	Subfield	Remark
16-17		Science data Header	SW version	
18			spare	
19	4-7		Data type	2 = NPD1 packet 3 = NPD2 packet
	0-3		NPD packet subtype	0 = NPD raw data 1 = NPD binning data 2 = NPD TOF mode 3 = NPD PHD mode

9.3.4 NPD Raw data packet

Because raw data events are 25 bit in width and the compression scheme used is 16 bit RICE, one has to do a trick in order to make the compression as effective as possible. These 25 bit events are divided in the packet into two separate 'data streams', both containing 512 words.

Stream_1 words will have following structure.

Byte	Bits	Field	Subfield	Remark
0-1	5-15	Stream_1 word	TOF	
	3-4		Direction	
	0-2		Coincidence	

Stream_2 words will have the following structure.

Byte	Bits	Field	Subfield	Remark
0-1	8-15	Stream_2 word	PAD	
	0-7		Stop PH	

The overall structure for the NPD raw data packet will be as follows.

Byte	Bits	Field	Subfield	Remark
20-25			Sample start time (SCET)	
26-27	8-15	Scanner information block	Scanner position	In the beginning of sample
	3-7		PAD	
	2		Scanner direction	
	0-1		Scanner speed	
28			PAD	
29	4-7	NPD bit information	Accumulation time	Time = 2^N * 31.25ms
	2-3		PAD	
	1		Log compression enabled	Always 0 for raw data mode (0 = disabled)
	0		RICE Compression enabled	
30		NPD Registers	FRONTCTRL	
31			MAINCTRL	
32-33			STAT	
34-35			TDCRD	
36-37			CALIB11	
38-39			CALIB12	
40-41			CALIB21	
42-43			CALIB22	



ASPERA-4



Venus
Express

Reference : VE-ASP-MA-0005
Issue : 1 Rev. : 0
Date : 2004-05-05
Volume : - Page: 67

Byte	Bits	Field	Subfield	Remark
44-45			STARTCNT	
46-47			STOP0CNT	
48-49			STOP1CNT	
50-51			STOP2CNT	
52-53			TOFCNT	
54-55			RAWCNT	
56-		Data	Stream 1: 512 * Stream_1 words Stream 2: 512 * Stream_2 words	If applied, RICE compression is used in 'one-shot' over both streams. If applied, RICE compression is used in 'one-shot' over both streams.

9.3.4.1 NPD Bin matrix data packet

The NPD Bin matrix data packet will contain data from 768 bin counters. The data will be ordered so that bin number 0 is the first one found in the packet.

Byte	Bits	Field	Subfield	Remark
20-25			Sample start time (SCET)	
26		Scanner block information	Scanner position	In the beginning of this sample.
27	3-7		PAD	
	2		Scanner direction	
	0-1	Scanner speed		
28			PAD	
29	4-7	NPD Bit information	Accumulation time	Time = $2^N * 31.25\text{ms}$
	2-3		PAD	
	1		Log compression enabled	0 = disable 1 = enable
	0		RICE Compression enabled	0 = disable 1 = enable
30-31	12-15	Threshold values	PAD	
	8-11		Threshold 3	0 = Matrix 0, 16x16
	4-7		Threshold 2	1-14 = Matrix 1, 2x16
	0-3		Threshold 1	15 = Matrix 2, 1x16
32-33		NPD Registers	CALIB11	
34-35			CALIB12	
36-37			CALIB21	
38-39			CALIB22	
40-41			STARTCNT	
42-43			STOP0CNT	
44-45			STOP1CNT	
46-47			STOP2CNT	
48-		Data	Bin number 0x000	Might be RICE compressed
			Bin number 0x001	Number of bins returned is dependent upon the threshold mode, so the
			Etc ...	



ASPERA-4



Venus
Express

Reference : VE-ASP-MA-0005
Issue : 1 Rev. : 0
Date : 2004-05-05
Volume : - Page: 68

Byte	Bits	Field	Subfield	Remark
			Bin number 0x2ff	<p>maximum number of bins returned would be $16 \times 16 \times 3 = 300$ bins (0x000 to 0x2ff). The 3 represents the number of directions. In case of 1x16 matrices count for lowest tof value is sent first.</p> <p>In case of 2x16 matrices lowest tof value in hydrogen region is sent first. 16th element is lowest tof value in oxygen region.</p>

9.3.4.2 NPD TOF mode data packet

When NPD is run in the special TOF mode, the data will be packeted into TOF mode packets which contain 3 different 'TOF' tables.

Byte	Bits	Field	Subfield	Remark
20-25			Sample start time (SCET)	
26-27	8-15	Scanner information block	Scanner position	In the beginning of sample
	3-7		PAD	
	2		Scanner direction	
	0-1		Scanner speed	
28			PAD	
29	4-7	NPD bit information	Accumulation time	$\text{Time} = 2^N * 31.25\text{ms}$
	2-3		PAD	
	1		Log compression enabled	0 = disable 1 = enable
	0		RICE Compression enabled	0 = disable 1 = enable
30			Number of (valid) samples integrated to the matrix	Latchups may happen during integration. Affected samples are not integrated to the matrix.
31			PAD	
32-33		NPD Registers	CALIB11	
34-35			CALIB12	
36-37			CALIB21	
38-39			CALIB22	
40-41			STARTCNT	
42-43			STOP0CNT	
44-45			STOP1CNT	
46-47			STOP2CNT	
48-		Data	First data word in TOF mode	768 data words (or bytes), Might be RICE compressed



9.3.4.3 NPD PHD mode data packet

When NPD is run in the special PHD mode, the data will be packeted into PHD mode packets which contain the least significant bytes of the stoparray.

Byte	Bits	Field	Subfield	Remark
20-25			Sample start time (SCET)	
26-27	8-15	Scanner information block	Scanner position	In the beginning of sample
	3-7		PAD	
	2		Scanner direction	
	0-1		Scanner speed	
28			PAD	
29	4-7	NPD bit information	Accumulation time	Time = $2^N * 31.25ms$
	2-3		PAD	
	1		Log compression enabled	Always 0 for PHD mode (0 = disabled)
	0		RICE Compression enabled	
30-31			PAD	
32-33		NPD Registers	CALIB11	
34-35			CALIB12	
36-37			CALIB21	
38-39			CALIB22	
40-41			STARTCNT	
42-43			STOP0CNT	
44-45			STOP1CNT	
46-47			STOP2CNT	
48-		Data	Least significant byte of STOPARRAY channel 0	48 data bytes (or bytes), Might be RICE compressed
			Least significant byte of STOPARRAY channel 1	
			...	
			Least significant byte of STOPARRAY channel 47	

9.3.5 NPI telemetry packets

One NPI telemetry packet will consist of 32 samples. This leads to 32 samples*32sectors = 1024 words of raw 16 bit data. This data can be compressed. Whether the packet is compressed or uncompressed can be determined using the NPI compression flags that are returned in the MU full housekeeping packet and in byte 28 of the NPI science packet.

Byte	Bits	Field	Subfield	Remark
16-17		Science data Header	SW version	
18			PAD	
19	4-7		Data type	4 = NPI packet
	0-3	NPI packet subtype	0 = NPI data (normal mode) 1 = NPI data (defl stepping mode)	



9.3.5.1 NPI normal mode data packet

Byte	Bits	Field	Subfield	Remark
20-25			Sample start time (SCET)	
26-27	8-15	Scanner information block	Scanner position	In the beginning of sample
	3-7		PAD	
	2		Scanner direction	
	0-1		Scanner speed	
28	4-7	NPI bit information	Accumulation time	Time = 2^N * 31.25ms
	2-3		PAD	
	1		Log compression enabled	0=disabled 1=enabled
	0		RICE Compression enabled	0=disabled 1=enabled
29			Sample Number	Number of samples in packet (max=32)
30-33			NPI Sector mask	
34-		Data	Sample 0, sector 0	Might be RICE compressed
			Sample 0, sector 1	
			...	
			Sample 31, Sector 31	

9.3.5.2 NPI Deflection stepping mode data packet

Byte	Bits	Field	Subfield	Remark
20-25			Sample start time (SCET)	
26-27	8-15	Scanner information block	Scanner position	In the beginning of sample
	3-7		PAD	
	2		Scanner direction	
	0-1		Scanner speed	
28	4-7	NPI bit information	Accumulation time	Time = 2^N * 31.25ms
	2-3		PAD	
	1		Log compression enabled	0=disabled 1=enabled
	0		RICE Compression enabled	0=disabled 1=enabled
29			Sample Number	Number of samples in packet (max=32)
30-33			NPI Sector mask	
34-37			NPI deflection status mask	
38-		Data	Sample 0, sector 0	Might be RICE compressed
			Sample 0, sector 1	
			...	
			Sample 31, Sector 31	



9.3.6 Engineering telemetry packets

There are two packets of 'engineering type' packets; the solar sensor information packet and the scanner information packet. Solar sensor information is a readout of the solar sensors in each sample interrupt during one scan cycle. The Scanner position packet reports on the scanner position on each sample irq during one scan cycle.

Byte	Bits	Field	Subfield	Remark
16-17		Science data Header	SW version	
18			PAD	
19	4-7		Data type	5 = Engineering packet
	0-3		Engineering packet subtype	0 = Solar sensor information 1 = Scanner information

9.3.6.1 Solar sensor information packet

Byte	Bits	Field	Subfield	Remark
20-25			Sample start time (SCET)	
26			Scanner position	At start
27	7		PAD	
	6		Scanner direction	
	4-5		Scanner speed	
	1-3		PAD	
	0		RICE compression enabled	
28-	7		Solar sensor 1 status pos 0	
	6		Solar sensor 2 status pos 0	
	...			
	1		Solar sensor 1 status pos 3	
	0		Solar sensor 2 status pos 3	
...				
Last	7		Solar sensor 1 status pos last-3	
	6		Solar sensor 2 status pos last-3	
	...			
	1		Solar sensor 1 status pos last	
	0		Solar sensor 2 status pos last	

9.3.6.2 Scanner information packet

Byte	Bits	Field	Subfield	Remark
20-25			Sample start time (SCET)	
26			Scanner position	At start
27	7		PAD	
	6		Scanner direction	
	4-5		Scanner speed	
	1-3		PAD	
	0		RICE compression enabled	
28-		Data	Scanner position 0	Up to 2048 positions (each is 1 byte), which corresponds to 64sec. Can be RICE compressed.
			Scanner position 1	
			...	
			Scanner position last	



ASPERA-4



**Venus
Express**

Reference : **VE-ASP-TN-060402**
Issue : **1** Rev. : **1**
Date : **2006-06-17**
Volume : **-** Page: **8**

APPENDIX 5. NPD RAW DATA STRUCTURE

DigTOF in ASPERA/NPD

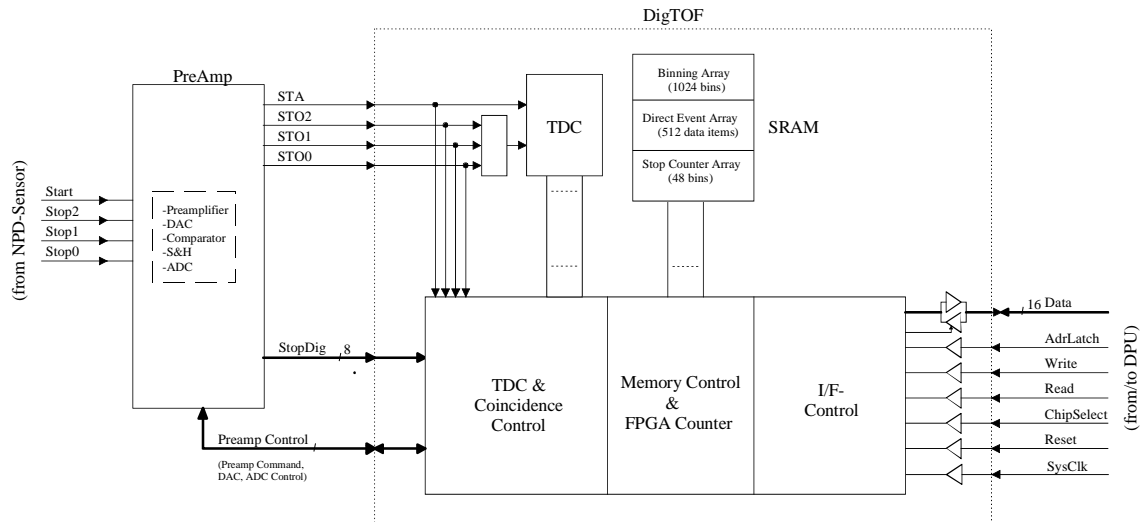
This documents contains a description of the DigTOF-electronics for ASPERA/NPD.

Version 1.0

History

Issue	Pg.	Date	Changes	Orig
0.1	all	04/09/00	first edition	cd
0.2	all	11/06/01	typos corrected reset of single FPGA counters replaced by common reset Register ADCRST added flag STAT. TDCWRERR added flag STAT. TDCRDERR added flag STAT. TDCCMDERR added flag STAT. ADCERR added switch FRONTCTRL.ADCCALDIS added flag MAINCTRL. LATCHUP added Register LURST added Register IFTEST added SRAM burst readouts: exceeding of read accesses are shown now coincidence changed, also default value for COINBDRS has changed CALNO: precision increased DACCMD: Channel numbering changed from 1,2,3,.. to A, B, C,... Burst Readout: range overflow is shown by 0x5555 now Appendix entries deleted LATCHUP implemented	cd
0.3	All	17/01/02	Hamming-Code Error Correction for memory data on FM board added Switch MAINCTRL.ECENA added Counter SEFCCNT implemented Counter DEFCCNT implemented	cd
1.0	All	17/01/02	numbering of document sides corrected	cd

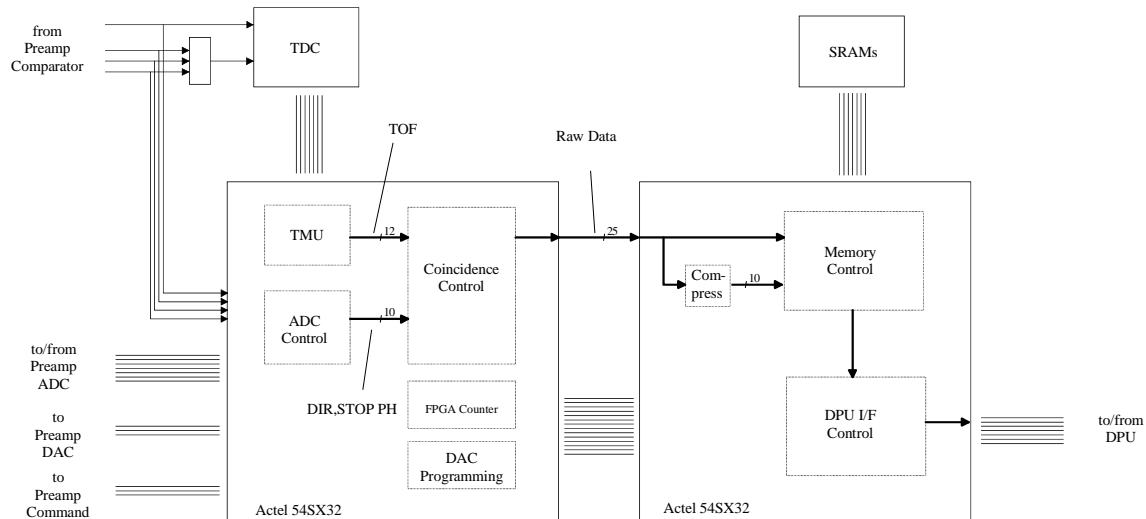
Overview



The tasks of the DigTOF-electronics are:

- TOF measuring from one start to one out of three stop signals
- serving of the preamplifier board and initiating analog/digital conversion of stop pulseheight
- coincidence check and selection of valid TOF - Stop pulseheight pairs
- counting of events
- buffering of three different data types in SRAM
- interfacing DigTOF to the DPU

Logic Implementation



The occurrence of a start, followed by a stop signal leads to a Δt -measurement in the TDC (Time to digital converter) and a pending generation of a data item with uncorrected Δt -information. The task of the TMU (TDC management unit) is to handle the TDC, mainly read data from this and correct these values. Prior to any correction process, the necessary parameters have to be determined. This will be done with the calibration process (see calibration). The output of the TMU is a TOF value with 12 bit binary time information. In parallel to this, the occurrence of a stop signal will be followed by a sampling process to the preamplifier ADC, thus a 10-bit data item with information of both direction and 8-bit stop pulseheight will be generated. The coincidence control then checks for a valid coincidence of these two data items and additionally flags the occurrence of more than one start or stop signal during Δt -measurement. This now leads to a 25-bit raw data item that will be used for the pending storing process. The memory control has to handle three different memory areas in the SRAM. For the binning array, the raw data will be compressed to a 10 bit data (see compression), that represents the bin number inside the destined array. The respective bin will be incremented by one up to the bin depth of 65536 (16 bit). For the raw data array, incoming raw data items will sequentially be stored until this array is filled completely. The stop counter array will be filled in the same way as the binning array, but with the compressed stop pulseheight together with the respective direction. All data arrays will be filled in parallel (binning array will be excluded if coincidence level does not fit). Readout and the following initialization of these arrays will be done with burst read access from the DPU. Besides the stop counter array, 16-bit event counters and two registers facing the preamplifier board are implemented in the FPGA. One of this registers will be used to program the DAC on the preamplifier board, the other for directly commanding the preamplifier electronics. All control-, counter- and memory- data will be accessed from the DPU over 16-bit registers (see registers), physically the connection to the DPU is a 16-bit bus (see description of the DPU-Interface).

Calibration

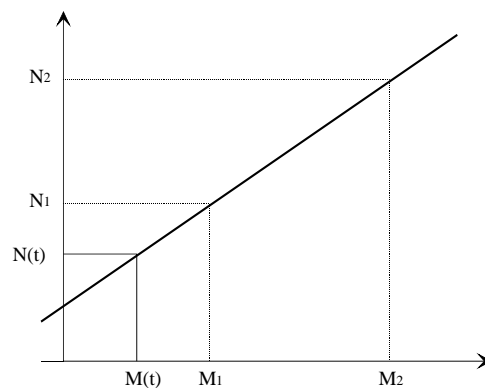
There is a linear relationship between the TDC values and the TOF, with parameters mainly depending on temperature and voltage. They have to be known to the DigTOF electronics, in order to perform correction of the TDC values. Determination of these parameters will be done by stimulation the TDC with two known time differences from a calibration clock. The resulting TDC values will then be used in the DPU to calculate gain and offset, which afterwards will be written into DigTOF. This calibration process has to be repeated within a given time to obtain a specified precision.

The goal is to obtain a binary TOF data

$$N = \frac{T}{1ns},$$

this originates from the TDC value M with following relation:

$$N(t) = O + G \cdot M(t).$$



With the measured TDC calibration values

$$M1 = CAL12 + \frac{CAL11}{16384},$$

$$M2 = CAL22 + \frac{CAL21}{16384},$$

$$N1 = \frac{TCAL}{1ns},$$

$$N2 = 2 \cdot \frac{TCAL}{1ns},$$

the gain G and offset O to transform the TOF-values can be calculated:

$$G = \frac{N2 - N1}{M2 - M1},$$

$$O = N_v - G \cdot M_v \quad ; v = 1;2$$

With respect to the position of the comma (see registers), these two values have to be written into DigTOF.

Data buffering

DigTOF buffers three different data items in dedicated memory areas:

1. Binning Array

This array contains 1024 bins, each with a depth of 65536 (16-bit). Data items fitting a dedicated bin will increment its counter by one up to the upper limit of 65536. Readout of this area will be done by write access to the respective register, followed by 1024 read accesses.

The bin number has following relation to its contents:

Bin Array [1023..0]		
Bit[9:8]	Bit[7:4]	Bit[3:0]
DIR[1:0]	STOP PH COMPRESSED[3:0]	TOF COMPRESSED[3:0]

(see compression)

2. Raw Data Array

This array contains 512 data places, each with a width of 32-bit. Incoming raw data items will sequentially be stored until this array is filled completely. Readout of this area will be done by write access to the respective register, followed by 1024 read accesses.

Storing sequence: upper 16-bit, lower 16-bit

Raw Data[31..0]				
Bit[31:25]	Bit[24:22]	Bit[21:20]	Bit[19:12]	Bit[11:0]
n.c.	COIN[2:0]	DIR[1:0]	STOP PH [7:0]	TOF [11:0]
	00 1 Start, 1 Stop 01 n Start, 1 Stop 02 1 Start, n Stop 03 n Start, n Stop 04 0 Start, 1 Stop n = 2, 3, ...	0 Stop0 1 Stop1 2 Stop2		in 0.5ns steps

3. Stop Counter Array

This array contains 48 bins, each with a depth of 65536 (16-bit). Data items fitting a dedicated bin will increment its counter by one up to the upper limit of 65536. Readout of this area will be done by write access to the respective register, followed by 48 read accesses.

The bin number has following relation to its contents.

Stop Counter Array [47..0]	
Bit[5:4]	Bit[3:0]
DIR[1:0]	STOP PH COMPRESSED[3:0]

Data Compression

To reduce the amount of data, the 12-bit TOF and the 8-bit Stop values are compressed according to the following rule:

TOF:	TOF[11:0]		TOF COMPRESSED[3:0]
	100 - 124	→	0
	125 - 156	→	1
	157 - 197	→	2
	198 - 248	→	3
	249 - 311	→	4
	312 - 391	→	5
	392 - 491	→	6
	492 - 617	→	7
	618 - 774	→	8
	775 - 972	→	9
	973 - 1220	→	10
	1221 - 1532	→	11
	1533 - 1923	→	12
	1924 - 2413	→	13
	2414 - 3028	→	14
	3029 - 3800	→	15

STOP:	STOP PH[7:0]		STOP PH COMPRESSED[3:0]
	0 - 15	→	0
	16 - 31	→	1
	32 - 47	→	2
	48 - 63	→	3
	64 - 79	→	4
	80 - 95	→	5
	96 - 111	→	6
	112 - 127	→	7
	128 - 143	→	8
	144 - 159	→	9
	160 - 175	→	10
	176 - 191	→	11
	192 - 207	→	12
	208 - 223	→	13
	224 - 239	→	14
	240 - 255	→	15

DigTOF-handling / Software

The handling of the DigTOF-electronics will be done with a few macros. This chapter gives a rough overview over the steps to be made when performing special tasks. The extracts (appendix) from the EGSE S/W @ IDA give more specified information.

Setup

- Reset NPD electronics (H/W reset)
- Initialize Actel control register
- Initialize TDC Glob register
- Set TDC into measurement mode 1
- Write max and min borders for coincidence part
- Program DAC 0
- Program DAC 1
- Program DAC 2
- Program DAC 3
- Write Preamp Control Register
- (Perform calibration)
- Enable TDC

Main DPU Task (Calibration+HK+Science data readout)

- Enable TDC input for calibration
- Disable Storing into SRAM
- Read Start Counter
- Read Stop0 Counter
- Read Stop1 Counter
- Read Stop2 Counter
- Read TOF Counter
- Read RAW Counter
- Reset FPGA Counter
- Read Stop Counter array
- Set TDC into calibration mode
- Read Binning array (if this is desired)
- Read Raw data array (if this is desired)
- Read Calibration register
- Calculate Gain and Offset
- Write Gain and Offset
- Set TDC back into measurement mode 1
- Enable TDC input for measurement
- Enable Storing into SRAM

Calibration

- Enable TDC input for calibration
- Set TDC into calibration mode
- Wait
- Read Calibration register
- Calculate Gain and Offset
- Write Gain and Offset
- Set TDC back into measurement mode 1
- Enable TDC input for measurement

Binning Data

- Disable Storing into SRAM
- If desired: disable simultaneously deleting of both Binning and Raw Data array (debug)
- Read Binning array
- Enable Storing into SRAM

Raw Data

- Disable Storing into SRAM
- If desired: disable simultaneously deleting of both Binning and Raw Data array (debug)
- Read Raw data array
- Enable Storing into SRAM

Main DPU Task

- Disable Storing into SRAM
- Disable FPGA Counter
- Read Start Counter
- Read Stop0 Counter
- Read Stop1 Counter
- Read Stop2 Counter
- Read TOF Counter
- Read RAW Counter
- Read Stop Counter array
- Reset FPGA Counter
- Enable Storing into SRAM
- Enable FPGA Counter

Note:

- after power on, the first SRAM access delivers unvalid data and will be used to initialize the respective memory cells
- later in the flight S/W there will be one main task with performing calibration and all data readout tasks (storing into SRAM will be disabled during complete readout)

Register

All control-, counter- and memory- data will be accessed from the DPU over 16-bit registers. Before accessing a designated register, the respective address has to be written into the electronics (see description of the DPU-Interface).

Address (hex)	Read	CS_BUS	Write	CS_BUS
0	FRONTCTRL	F7	FRONTCTRL	F9
1	STAT	F8	TDCCMD	F10
2	TDCRD	F12	TDCWR	F11
3	CALIB11	F3	CALNG	F16
4	CALIB12	F4	CALNO	F17
5	CALIB21	F5	COINBDRS	F44
6	CALIB22	F6	TDCRST	-
7	-	-	-	-
8	STARTCNT	F30	CNTRST	F36
9	STOP0CNT	F31	ADCRST	F37
A	STOP1CNT	F32	-	-
B	STOP2CNT	F33	-	-
C	TOFCNT	F34	-	-
D	RAWCNT	F35	-	-
E	-	-	DACCMD	F42
F	-	-	PREAMPCTRL	F43
10	BINARRAY	M3	BINARRAY	M0
11	RAWARRAY	M4	RAWARRAY	M1
12	STOPARRAY	M5	STOPARRAY	M2
13	MAINCTRL	M7	MAINCTRL	M6
14	SEFCCNT	M13	RAWDBGHIGH	M8
15	DEFCCNT	M14	RAWDBGLOW	M9
16	-	-	LURST	M10
17	IFTEST	M11	IFTEST	M12

Name: FRONTCTRL

Description: This register is used to as a common control register

Address: see register table

Group: common

Access: Read/Write

Note: · see below

Bit-Position	Name		Description
0	TDCINENA		TDCINENA = 1 enables attention of TDC to the input signals start, stop and calibration clock
1	TDCOUTDIS		TDCOUTDIS = 1 disables readout of valid data from the TDC
2	CALWAITENA		CALWAITENA=1 enables wait for calibration values
3	AUTORSTDIS		AUTORSTDIS = 1 disables automatic TDC-reset when SYSERR occurs
4	STOARTDIS		STOARTDIS =1 disables generation of artificial stop signal
5	CNTDIS		CNTDIS = 1 disables FPGA-counter
6	STADIS		STADIS = 1 disables start signal going into the TDC
7	ADCCALDIS		ADCCALDIS=1 disables using of ADC calibration
15-8	-	-	

Name: MAINCTRL

Description: This register is used to as a common control register

Address: see register table

Group: common

Access: Read/Write

Note: · see below

Bit-Position	Name		Description
1-0	LVL[1:0]		Level for storing as binning data, storing into binning array will be omitted if COIN[2:0] > LVL[1:0]
2	STOREDIS		STOREDIS = 1 disables storing into SRAM
3	DEBUGENA		DEBUGENA = 1 enables simulation of rawdata (debug)
4	DELSIMDIS		DELSIMDIS = 1 disables simultaneously deleting of both Binning and Raw Data array (after each read access on data)
5	LATCHUP		LatchUp occurred, if LATCHUP = 1
6	ECENA		Hamming-Code Error Correction on SRAM data enabled, if ECENA=1
15-7	n.c.		

Name: STAT

Description: This register is used to reflect some TDC and FPGA status signals

Address: see register table

Group: common

Access: Read

Note: · see below

Bit-Position	Name		Description
0	TDCSYSERR		SYSEERR-Flag from TDC
1	TDCREADY		READY-Flag from TDC
2	TDCVALID		VALID-Flag from TDC
3	TDCCALM		CALM-Flag from TDC
4	TDCBUSDIR		BUSDIR-Flag from TDC
8-5	-		
9	TDCWRERR		TDC write access error – Flag
10	TDCRDERR		TDC read access error – Flag
11	TDCCMDERR		TDC command error – Flag
12	CMDBUSY		Commanding TDC active, if CMDBUSY=1
13	DACBUSY		Programming DAC active, if DACBUSY=1
14	NEWCAL		new calibration data available, if NEWCAL=1; any read-access to the CALIBxx registers resets this flag
15	ADCERR		ADC error occurred, if ADCERR=1

Name: TDCCMD

Description: After being written with an TDC-opcode, the contents of this register will be written into the TDC

Address: see register table

Group: TDC handling

Access: Write

Note: · dependent on the TDC-opcode, a respective parameter value has to be written into TDCWR before

Name: TDCRD

Description: After the transmission of an appropriate TDC-opcode, the contents of the requested TDC register is available in this register

Address: see register table

Group: TDC handling

Access: Read

Note: ·

Name: TDCWR

Description: Together with an appropriate TDC-opcode, the contents of this register will be used as a parameter value and will be written into the TDC

Address: see register table

Group: TDC handling

Access: Write

Note: ·

Name: CALIB11

Description: This register contains part1 of the calibration data from the TDC (CAL11)

Address: see register table

Group: Calibration

Access: Read

Note: · New calibration data will be shown with STAT.NEWCAL=1

Name: CALIB12

Description: This register contains part2 of the calibration data from the TDC (CAL12)

Address: see register table

Group: Calibration

Access: Read

Note: · New calibration data will be shown with STAT.NEWCAL=1

Name: CALIB21

Description: This register contains part3 of the calibration data from the TDC (CAL21)

Address: see register table

Group: Calibration

Access: Read

Note: · New calibration data will be shown with STAT.NEWCAL=1

Name: CALIB22

Description: This register contains part4 of the calibration data from the TDC (CAL22)

Address: see register table

Group: Calibration

Access: Read

Note: · New calibration data will be shown with STAT.NEWCAL=1

Name: CALNG

Description: With respect to the position of the comma, this register has to be written with the calculated gain G from the calibration process

Address: see register table

Group: Calibration

Access: Write

Note: · 11 digits after decimal point

Name: CALNO

Description: With respect to the position of the comma, this register has to be written with the calculated offset O from the calibration process

Address: see register table

Group: Calibration

Access: Write

Note: · 4 digits after decimal point

Name: COINBDRS

Description: This register contains both lower and upper time borders for the coincidence part

Address: see register table

Group: Miscellaneous

Access: Write

Note: · This register has to be written with a hardware-specific value

Name: DACCMD

Description: This register will be used to program the DAC on the preamplifier board (serial link)

Address: see register table

Group: Miscellaneous

Access: Write

Note: · programming of one DAC channel needs about 4 μ s

15	14	13	12	11	10	9	8	7	6	5	4	3	2	1	0
-				DACCHN[3:0]				DACVAL[7:0]							

DACVAL[7:0]: 8-bit DAC value

DACCHN[3:0]: DAC Channel to be programmed, 0x01 \equiv Channel A, 0x02 \equiv Channel B, 0x03 \equiv Channel C etc.

Name PREAMPCTRL

Description: This lower 8 bit of this register are directly connected to the preamplifier board and will be used to control this (tbd)

Address: see register table

Group: Miscellaneous

Access: Write

Note: · PREAMPCTRLVAL[7:0] = 0xff after power up

15	14	13	12	11	10	9	8	7	6	5	4	3	2	1	0
-								PREAMPCTRLVAL[7:0]							

Name: ADCRST

Description: Write access to this register resets the ADC control unit and performs new calibration of the ADC ('internal mid-scale error calibration')

Address: see register table

Group: Miscellaneous

Access: Write

Note:

Name: STARTCNT

Description: This register counts the start-signals from the NPD-sensor up to the upper limit of 65536

Address: see register table

Group: FPGA Counter

Access: Read

Note:

- Write access to CNTRST sets counter to zero
- FPGA counters should be disabled (FRONTCTRL.CNTDIS = 1) before read access

Name: STOP0CNT

Description: This register counts the stop0-signals from the NPD-sensor up to the upper limit of 65536

Address: see register table

Group: FPGA Counter

Access: Read

Note:

- Write access to CNTRST sets counter to zero
- FPGA counters should be disabled (FRONTCTRL.CNTDIS = 1) before read access

Name: STOP1CNT

Description: This register counts the stop1-signals from the NPD-sensor up to the upper limit of 65536

Address: see register table

Group: FPGA Counter

Access: Read

Note:

- Write access to CNTRST sets counter to zero
- FPGA counters should be disabled (FRONTCTRL.CNTDIS = 1) before read access

Name: STOP2CNT

Description: This register counts the stop2-signals from the NPD-sensor up to the upper limit of 65536

Address: see register table

Group: FPGA Counter

Access: Read

Note:

- Write access to CNTRST sets counter to zero
- FPGA counters should be disabled (FRONTCTRL.CNTDIS = 1) before read access

Name: TOFCNT

Description: This register counts the generated TOF values up to the upper limit of 65536

Address: see register table

Group: FPGA Counter

Access: Read

Note:

- Write access to CNTRST sets counter to zero
- FPGA counters should be disabled (FRONTCTRL.CNTDIS = 1) before read access
- For debugging/evaluating purpose only

Name: RAWCNT

Description: This register counts the generated RAW values up to the upper limit of 65536

Address: see register table

Group: FPGA Counter

Access: Read

Note:

- Write access to CNTRST sets counter to zero
- FPGA counters should be disabled (FRONTCTRL.CNTDIS = 1) before read access
- For debugging/evaluating purpose only

Name: CNTRST

Description: This register is used to reset the 6 FPGA counters

Address: see register table

Group: FPGA Counter

Access: Write

Note: Write access sets all 6 FPGA counters to zero

Name: BINARRAY

Description: This register will be used to link the binning array (from SRAM) to the DPU

Address: see register table

Group: SRAM Data

Access: Read/Write

Note:

- Readout of the binning data must be initiated by a write access to this register, after that 1024 read access have to be performed.
- This register automatically reflects the next valid data item from the binning array
- The respective memory cells will be set to zero automatically after read access on BINARRAY or RAWARRAY, latter only if MAINCTRL.DELSIMDIS = 0
- Time between two read accesses should not be less than 1.2 μ s (tpd)
- Storing into SRAM must be disabled (MAINCTRL.STOREDIS = 1) bevor any access to this register
- exceeding the amount of read accesses is shown by Data=0x5555

Name: RAWARRAY

Description: This register will be used to link the raw data array (from SRAM) to the DPU

Address: see register table

Group: SRAM Data

Access: Read/Write

Note:

- Readout of the binning data must be initiated by a write access to this register, after that 1024 read access have to be performed.
- This register automatically reflects the next valid data item from the binning array
- The respective memory cells will be set to zero automatically after read access on RAWARRAY or BINARRAY, latter only if MAINCTRL.DELSIMDIS = 0
- Time between two read accesses should not be less than 1.2 μ s (tpd)
- Storing into SRAM must be disabled (MAINCTRL.STOREDIS = 1) bevor any access to this register
- exceeding the amount of read accesses is shown by Data=0x5555

Name: STOPARRAY

Description: This register will be used to link the stop array (from SRAM) to the DPU

Address: see register table

Group: SRAM Data

Access: Read/Write

Note:

- Readout of the binning data must be initiated by a write access to this register, after that 48 read access have to be performed.
- This register automatically reflects the next valid data item from the binning array
- The respective memory cells will be set to zero automatically after read access on STOPARRAY
- Time between two read accesses should not be less than 1.2 μ s (tpd)
- Storing into SRAM must be disabled (MAINCTRL.STOREDISEN = 1) before any access to this register
- exceeding the amount of read accesses is shown by Data=0x5555

Name: SEFCCNT

Description: This registers counts the occurrence and correction of single bit errors of the SRAM up to the upper limit of 65536.

Address: see register table

Group: SRAM Data

Access: Read

Note:

- Register is cleared by hardware-reset to DigTOF

Name: DEFCCNT

Description: This registers counts the occurrence of double bit errors of the SRAM data from up to the upper limit of 65536.

Address: see register table

Group: SRAM Data

Access: Read

Note:

- Register is cleared by hardware-reset to DigTOF

Name: TDCRST

Description: This register will be used to reset the TDC and the error-flags

Address: see register table

Group: Miscellaneous

Access: Write

Note: · For debugging/evaluating purpose only

Name: RAWDBGHIGH

Description: This register will be used to simulate RAW-data (these are the upper 16 bits)

Address: see register table

Group: Miscellaneous

Access: Write

Note: · to see any effect, MAINCTRL.DEBUGEN has to be set to 1 before
· pending write access to RAWDBGLOW is needed
· For debugging/evaluating purpose only

Name: RAWDBGLOW

Description: This register will be used to simulate RAW-data (these are the lower 16 bits)

Address: see register table

Group: Miscellaneous

Access: Write

Note: · to see any effect, MAINCTRL.DEBUGEN has to be set to 1 before
· RAWDBGHIGH have to be written before
· For debugging/evaluating purpose only

Name: IFTEST

Description: This 16-bit register is implemented to simplify the DPU I/F-tests (single Write and Read accesses)

Address: see register table

Group: Miscellaneous

Access: Read/Write

Note: · For debugging/evaluating purpose only

Appendix

The following pages previously contained extracts from the EGSE-S/W @IDA. Now these extracts are available within single files.



ASPERA-4



**Venus
Express**

Reference : **VE-ASP-TN-060402**
Issue : **1** Rev. : **1**
Date : **2006-06-17**
Volume : **-** Page: **9**

APPENDIX 6. HK CHANNEL CONVERSION FACTORS

Extract from the ASPERA-4 VEX HK calibration database.

Date 2005-11-22

Values are taken from VE-ASP-DS-0012 (VERDI Database - I1R3).xls

The "CPOI" type of calibration data consists of x,y pairs that define the calibration curve. The "SVAL" type describes the meaning of the specific value of that HK parameter. The raw HK value is converted to engineering value when calibration is applied.

X-value

Y-value

Type CPOI : polynom, SVAL : Value to nemonic

Description

X-value	Y-value	Type	Description
0	-264,68	CPOI	ELS Temp
255	114,07	CPOI	ELS Temp
0	-268,18	CPOI	NPD1 Temp
255	116,74	CPOI	NPD1 Temp
0	-271,88	CPOI	NPD2 Temp
255	118,76	CPOI	NPD2 Temp
0	-265,38	CPOI	NPI Temp
255	154,56	CPOI	NPI Temp
0	-267,27	CPOI	Scanner Temp
255	115,84	CPOI	Scanner Temp
0	0	CPOI	HK_V_-12V
255	-13,22	CPOI	HK_V_-12V
0	0	CPOI	HK_V_-5V
255	-5,17	CPOI	HK_V_-5V
0	0	CPOI	HK_V_+5V
255	5,24	CPOI	HK_V_+5V
0	0	CPOI	HK_V_+12V
255	13,0769	CPOI	HK_V_+12V
0	0	CPOI	HK_V_+30V
255	30,165	CPOI	HK_V_+30V
0	0	CPOI	HK_I_+5V
255	2961,06	CPOI	HK_I_+5V
0	0	CPOI	HK_I_+30V
255	368,985	CPOI	HK_I_+30V
0	-149,6	CPOI	NPD1 Bias
255	4406,23	CPOI	NPD1 Bias
0	-149,6	CPOI	NPD1 Start
255	4406,23	CPOI	NPD1 Start
0	-34,402	CPOI	NPD1 Stop
255	4431,923	CPOI	NPD1 Stop
0	-41,42	CPOI	NPD2 Bias
255	4428,985	CPOI	NPD2 Bias
0	-41,42	CPOI	NPD2 Start
255	4428,985	CPOI	NPD2 Start
0	-70,65	CPOI	NPD2 Stop
255	4366,095	CPOI	NPD2 Stop
0	-30,659	CPOI	NPD1 Defl
255	5694,346	CPOI	NPD1 Defl
0	46,719	CPOI	NPD2 Defl
255	5612,859	CPOI	NPD2 Defl
0	27,885	CPOI	NPI Bias
255	-4654,935	CPOI	NPI Bias

0	-37,866 CPOI	NPI Defl
255	5696,574 CPOI	NPI Defl
0	0 CPOI	ELS MCP bias
255	3000 CPOI	ELS MCP bias
0	0 CPOI	Scanner Position
223	180 CPOI	Scanner Position
0,612	-200 CPOI	ASPERA 118MF PT2000 acq by RTU
0,898	-180 CPOI	ASPERA 118MF PT2000 acq by RTU
1,158	-160 CPOI	ASPERA 118MF PT2000 acq by RTU
1,4	-140 CPOI	ASPERA 118MF PT2000 acq by RTU
1,634	-120 CPOI	ASPERA 118MF PT2000 acq by RTU
1,86	-100 CPOI	ASPERA 118MF PT2000 acq by RTU
2,058	-80 CPOI	ASPERA 118MF PT2000 acq by RTU
2,248	-60 CPOI	ASPERA 118MF PT2000 acq by RTU
2,429	-40 CPOI	ASPERA 118MF PT2000 acq by RTU
2,6	-20 CPOI	ASPERA 118MF PT2000 acq by RTU
2,766	0 CPOI	ASPERA 118MF PT2000 acq by RTU
2,898	20 CPOI	ASPERA 118MF PT2000 acq by RTU
3,052	40 CPOI	ASPERA 118MF PT2000 acq by RTU
3,207	60 CPOI	ASPERA 118MF PT2000 acq by RTU
3,342	80 CPOI	ASPERA 118MF PT2000 acq by RTU
3,478	100 CPOI	ASPERA 118MF PT2000 acq by RTU
3,605	120 CPOI	ASPERA 118MF PT2000 acq by RTU
3,713	140 CPOI	ASPERA 118MF PT2000 acq by RTU
3,771	150 CPOI	ASPERA 118MF PT2000 acq by RTU
176	0 CPOI	Boot EEP incl. Context
191	15 CPOI	Boot EEP incl. Context
192	0 CPOI	Test pattern
207	15 CPOI	Test pattern
208	0 CPOI	Boot EEP excl. Context
223	15 CPOI	Boot EEP excl. Context
224	0 CPOI	IMA Internal SID nr
230	6 CPOI	IMA Internal SID nr
240	0 CPOI	Default boot section
255	15 CPOI	Default boot section
256	0 CPOI	Deflection level
351	95 CPOI	Deflection level
512	0 CPOI	Entrance level
527	15 CPOI	Entrance level
768	0 CPOI	SW start level
832	64 CPOI	SW start level
1024	0 CPOI	Spare level
1279	255 CPOI	Spare level
2560	0 CPOI	Mode cmd
2599	39 CPOI	Mode cmd
3072	0 CPOI	Reprog. all EEP sections
3087	15 CPOI	Reprog. all EEP sections
4096	0 CPOI	Opto reference
4103	7 CPOI	Opto reference
8192	0 CPOI	Mcp reference
8207	15 CPOI	Mcp reference
12288	0 CPOI	Grid reference
12295	7 CPOI	Grid reference
16384	0 CPOI	Pacc low ref.
16391	7 CPOI	Pacc low ref.
20480	0 CPOI	Pacc high ref.

20487	7 CPOI	Pacc high ref.
24576	0 CPOI	Deflection LV ref.
28671	4095 CPOI	Deflection LV ref.
28672	0 CPOI	Deflection HV ref.
32767	4095 CPOI	Deflection HV ref.
32768	0 CPOI	Entrance ref.
36863	4095 CPOI	Entrance ref.
36864	0 CPOI	Noise reduction
40959	4095 CPOI	Noise reduction
40960	0 CPOI	Fifo low mark
45055	4095 CPOI	Fifo low mark
45056	0 CPOI	Fifo high mark
49151	4095 CPOI	Fifo high mark
49152	0 CPOI	Fifo force mark
53247	4095 CPOI	Fifo force mark
53248	0 CPOI	Fifo clear mark
57343	4095 CPOI	Fifo clear mark
57344	0 CPOI	Ima scale factor
61439	4095 CPOI	Ima scale factor
0	0 CPOI	Opto HV monitor
255	5 CPOI	Opto HV monitor
0	0 CPOI	Deflection LV monitor
255	100 CPOI	Deflection LV monitor
0	0 CPOI	Grid LV monitor
255	12 CPOI	Grid LV monitor
0	-60 CPOI	DPU temperature
255	60 CPOI	DPU temperature
0	-5 CPOI	Upper entrance HV mon
511	5 CPOI	Upper entrance HV mon
0 OFF	SVAL	Generic ON/OFF
1 ON	SVAL	Generic ON/OFF
2 OFF	SVAL	Mcp 28V switch
3 ON	SVAL	Mcp 28V switch
4 OFF	SVAL	Opto 28V switch
5 ON	SVAL	Opto 28V switch
6 OFF	SVAL	Main 28V switch
7 ON	SVAL	Main 28V switch
8 OFF	SVAL	Pacc Hv switch
9 ON	SVAL	Pacc Hv switch
10 OFF	SVAL	Grid LV switch
11 ON	SVAL	Grid LV switch
12 OFF	SVAL	Entr HV switch
13 ON	SVAL	Entr HV switch
14 OFF	SVAL	Defl LV switch
15 ON	SVAL	Defl LV switch
16 OFF	SVAL	Defl HV switch
17 ON	SVAL	Defl HV switch
18 OFF	SVAL	Direct cmd sw.
19 ON	SVAL	Direct cmd sw.
20 OFF	SVAL	WD enabel sw.
21 ON	SVAL	WD enabel sw.
28 OFF	SVAL	Compr. switch
29 ON	SVAL	Compr. switch
30 OFF	SVAL	Alt.Pacc switch
31 ON	SVAL	Alt.Pacc switch
32 LOW	SVAL	Pacc. level

33	HIGH	SVAL	Pacc. level
34	OFF	SVAL	Auto red. sw.
35	ON	SVAL	Auto red. sw.
36	OFF	SVAL	Shadow masking
37	ON	SVAL	Shadow masking
38	OFF	SVAL	Bad. HV masking
39	ON	SVAL	Bad. HV masking
40	OFF	SVAL	Bad mass masking
41	ON	SVAL	Bad mass masking
0	Fixed	SVAL	Pacc.Op. Mode
1	Alternating	SVAL	Pacc.Op. Mode
0	No	SVAL	No/Yes
1	Yes	SVAL	No/Yes
0	Ok	SVAL	Ok/Overflow
1	Overflow	SVAL	Ok/Overflow
0	Ok	SVAL	Cmd status
1	Invalid	SVAL	Cmd status
2	Out of rang	SVAL	Cmd status
3	Erroneous	SVAL	Cmd status
0	Min	SVAL	IMA Internal Sid type
1	Norm	SVAL	IMA Internal Sid type
2	Burst	SVAL	IMA Internal Sid type
3	Cal	SVAL	IMA Internal Sid type
4	Spec	SVAL	IMA Internal Sid type
5	Test	SVAL	IMA Internal Sid type
6	Ima	SVAL	IMA Internal Sid type
0	Idle	SVAL	Mode
1	Void1	SVAL	Mode
2	Mspo	SVAL	Mode
3	Void2	SVAL	Mode
4	Msis	SVAL	Mode
5	Mexm	SVAL	Mode
6	Void3	SVAL	Mode
7	Void4	SVAL	Mode
8	Nrm0	SVAL	Mode
9	Nrm1	SVAL	Mode
10	Nrm2	SVAL	Mode
11	Nrm3	SVAL	Mode
12	Nrm4	SVAL	Mode
13	Nrm5	SVAL	Mode
14	Nrm6	SVAL	Mode
15	Nrm7	SVAL	Mode
16	Har0	SVAL	Mode
17	Har1	SVAL	Mode
18	Har2	SVAL	Mode
19	Har3	SVAL	Mode
20	Har4	SVAL	Mode
21	Har5	SVAL	Mode
22	Har6	SVAL	Mode
23	Har7	SVAL	Mode
24	Exm0	SVAL	Mode
25	Exm1	SVAL	Mode
26	Exm2	SVAL	Mode
27	Exm3	SVAL	Mode
28	Exm4	SVAL	Mode
29	Exm5	SVAL	Mode

30 Exm6	SVAL	Mode
31 Exm7	SVAL	Mode
32 Test	SVAL	Mode
33 Cal1	SVAL	Mode
34 Cal2	SVAL	Mode
35 Fake	SVAL	Mode
36 Void5	SVAL	Mode
37 Void6	SVAL	Mode
38 Void7	SVAL	Mode
39 Vcal8	SVAL	Mode
0 OFF	SVAL	dummy for ON/OFFs
1 ON	SVAL	dummy for ON/OFFs



ASPERA-4



**Venus
Express**

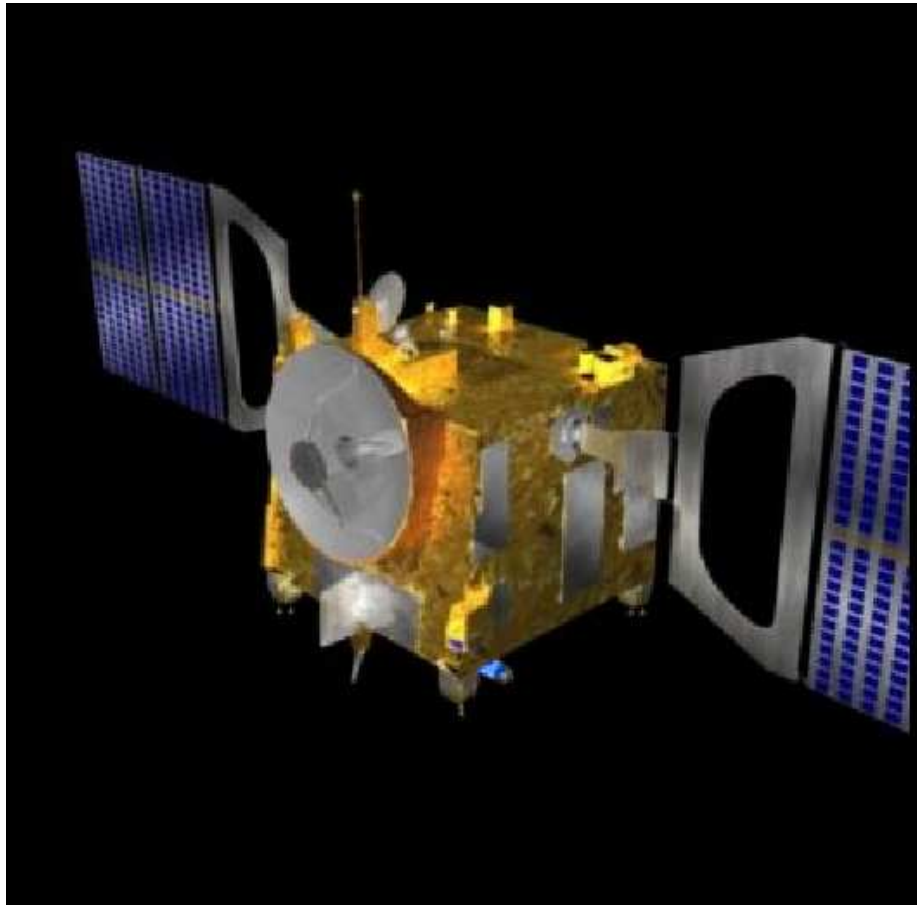
Reference : **VE-ASP-TN-060402**
Issue : **1** Rev. : **1**
Date : **2006-06-17**
Volume : **-** Page: **10**

APPENDIX 7. ASPERA-4 SENSOR NUMBERING

Aspera 4 : Frame definitions and sensors attitudes

PÈNE Nicolas
Centre d'Etude Spatiale des Rayonnements
Toulouse, France

21st December 2005



Contents

1	Introduction	3
2	IMA	4
2.1	definition	4
2.2	IMA variables	7
2.3	IMA \vec{u} definition	8
2.4	IMA sector looking direction	9
3	Main Unit	11
3.1	Main Unit orientation	11
3.2	the spacecraft coordinates	13
3.3	Main Unit variables	15
3.4	Rotation matrix	16
3.5	<i>DVV</i> definition in the Main Unit system	17
3.6	<i>DVV</i> definition in the satellite system	18
3.7	ELS sector looking direction	20
3.8	NPI sector looking position	22
3.9	NPD sector looking position	24
3.10	Scanner datas	26
4	The VEXLIB	28

1 Introduction

The purpose of the document is to determine an algorithm of calculation of the *direction of the velocity vector (DVV)* of incidence particles.

Particle velocity vector is defined in the satellite frame of reference X_s, Y_s, Z_s . Present document considers two separated packages : Mass spectrometer **IMA** and **Main Unit**.

Figure 1 shows the location of **IMA** and **Main Unit** with respect to the satellite frame.

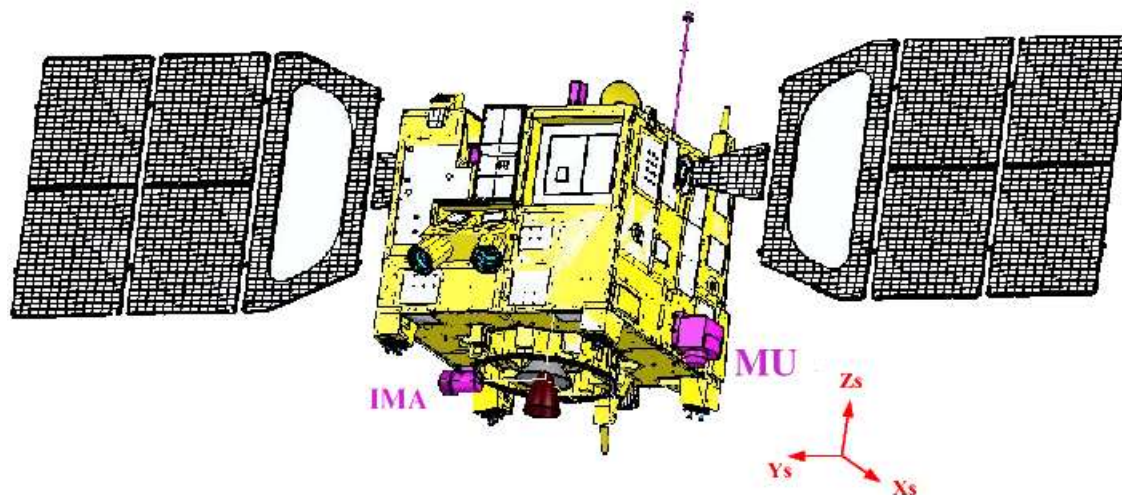


Figure 1: Satellite system ($X_s Y_s Z_s$)

2 IMA

2.1 definition

Figures 2, 3, 4 and 5 shows location of IMA in the $X_s Y_s Z_s$ VEX reference frame :

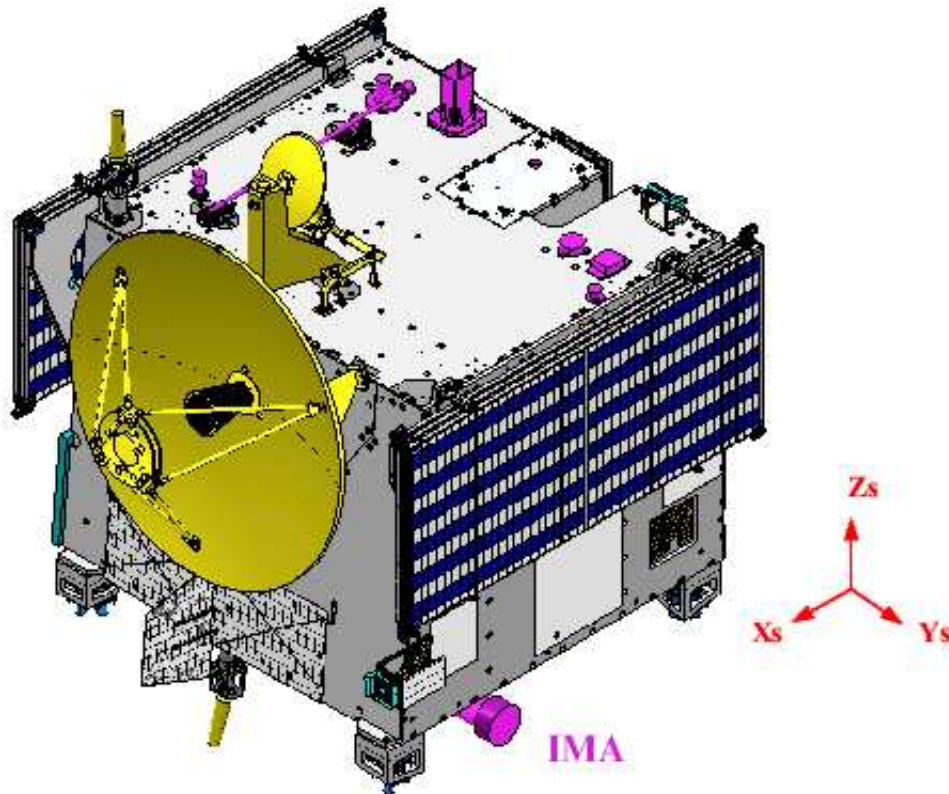
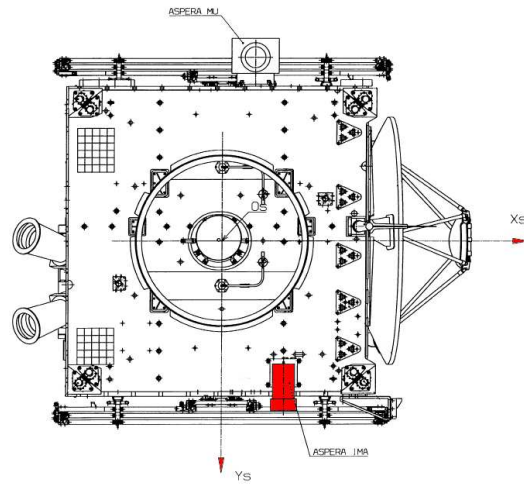
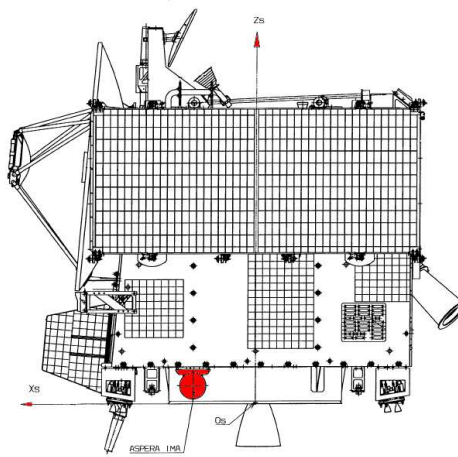


Figure 2: IMA location

Figure 3: IMA location in $x_s y_s$ planeFigure 4: IMA location in $x_s z_s$ plane

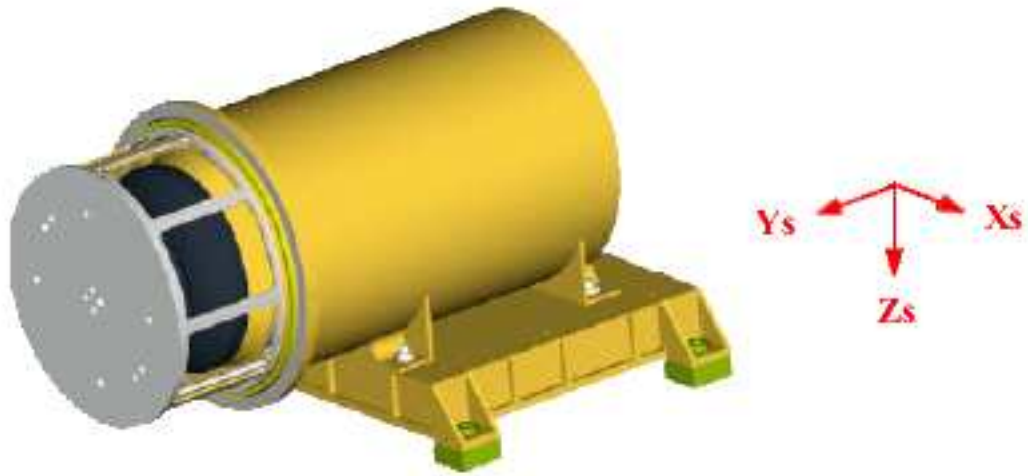


Figure 5: IMA orientation in $x_s y_s z_s$ plane

2.2 IMA variables

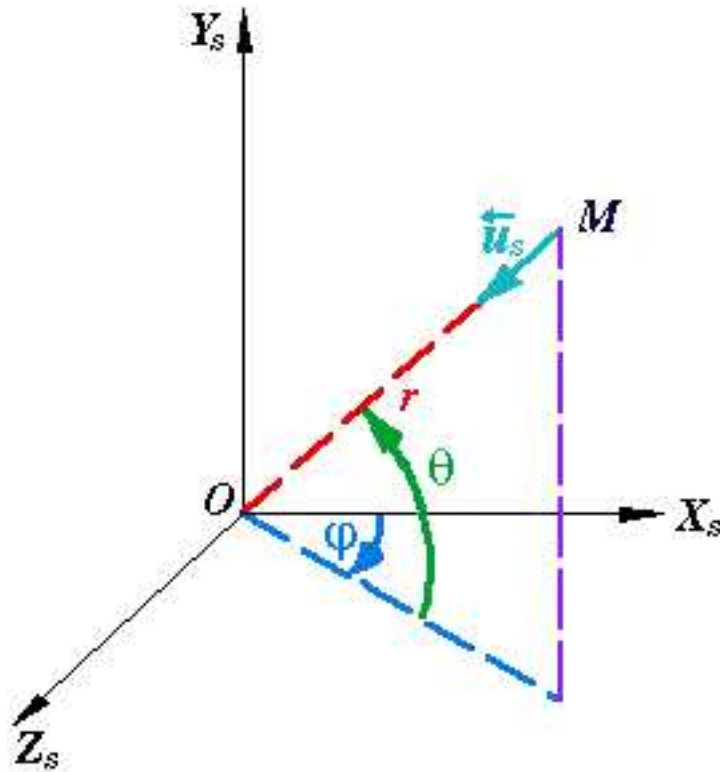
This section introduces the variables used for IMA instrument.

θ is the **elevation angle** of the incident ion counted from the $X_s Z_s$ plane towards $+Y_s$.

According to the calibration report, the maximum elevation angle is $\theta_{max} = 46$ degrees, and the lowest value for the elevation angle is $\theta_{min} = -43.7$ degrees.

ϕ is the **azimuthal angle** counted from the $+X_s$ axis towards the $+Z_s$ axis.

\vec{u} is the *DVV* of the incident particle (unity vector) defined by θ and ϕ .

2.3 IMA \vec{u} definitionFigure 6: DVV in $X_s Y_s Z_s$ plane

θ : elevation angle

ϕ : azimuthal angle

\overrightarrow{MO} : DVV

\vec{u} follow the direction of \overrightarrow{MO} :

$$\vec{u} = \frac{\overrightarrow{MO}}{|\overrightarrow{MO}|} = \frac{\overrightarrow{MO}}{r}$$

Then \vec{u} components in the X_s, Y_s, Z_s plane are:

$$\vec{u} = \begin{bmatrix} -\cos\theta \cos\phi \\ -\sin\theta \\ -\cos\theta \sin\phi \end{bmatrix}$$

2.4 IMA sector looking direction

Figure 7 shows the layout of 16 fields-of-view of azimuthal sectors of IMA. This view doesn't correspond to the physical sectors position.

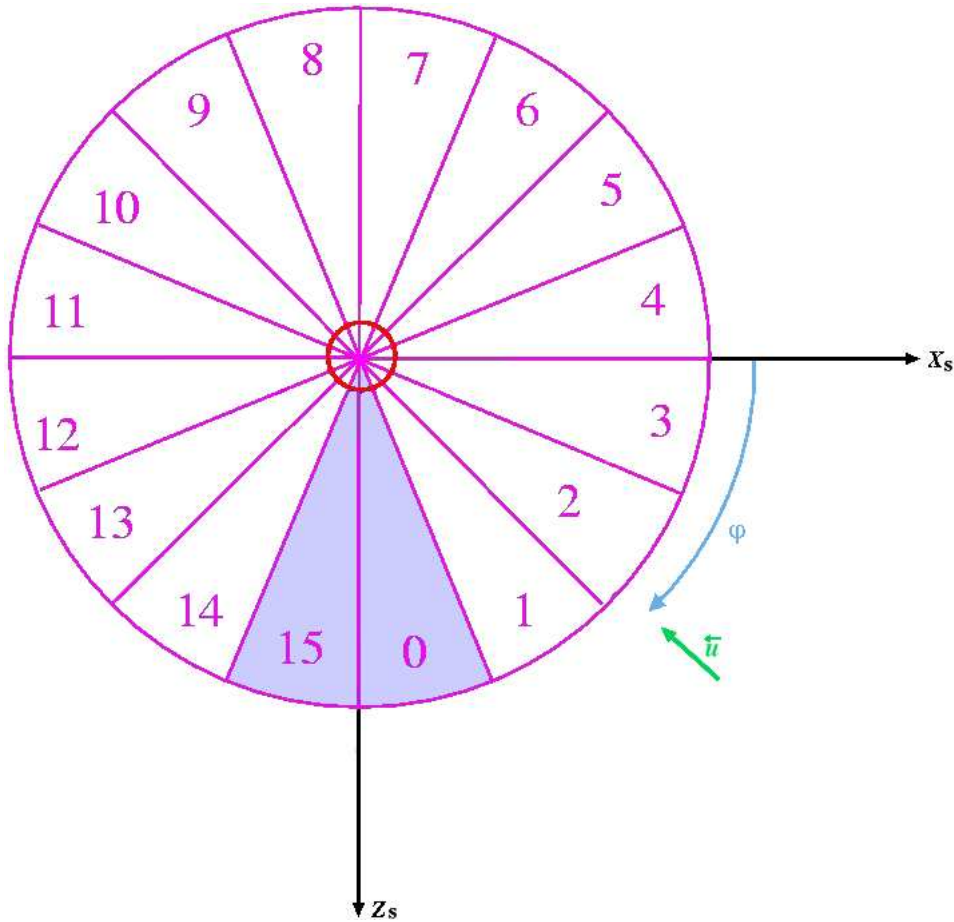


Figure 7: IMA sector looking direction in $X_s Z_s$ plane

For example, an ion with \vec{u} DVV shown in figure 7 by green arrow will be registered in the azimuthal sector 2.

The following table displays the ϕ values at the beginning, the middle and the end of each sector.

It also indicates the value of $\vec{u}_{X_s Z_s}$ coming in the middle of each sector.

Sector	Begin	Middle	End	$\vec{u}_{X_s Z_s} (*)$
0	90.00	78.75	67.50	(-0.195 , -0.981)
1	67.50	56.25	45.00	(-0.556 , -0.831)
2	45.00	33.75	22.50	(-0.831 , -0.556)
3	22.50	11.25	0.00	(-0.981 , -0.195)
4	0.00	348.75	337.50	(-0.981 , 0.195)
5	337.50	326.25	315.00	(-0.831 , 0.556)
6	315.00	303.75	292.50	(-0.556 , 0.831)
7	292.50	281.25	270.00	(-0.195 , 0.981)
8	270.00	258.75	247.50	(0.195 , 0.981)
9	247.50	236.25	225.00	(0.556 , 0.831)
10	225.00	213.75	202.50	(0.831 , 0.556)
11	202.50	191.25	180.00	(0.981 , 0.195)
12	180.00	168.75	157.50	(0.981 , -0.195)
13	157.50	146.25	135.00	(0.831 , -0.556)
14	135.00	123.75	112.50	(0.556 , -0.831)
15	112.50	101.25	90.00	(0.195 , -0.981)

3 Main Unit

3.1 Main Unit orientation

Main Unit (MU) is the common frame for four sensors : ELS, NPI, NPD1 and NPD2.

Main Unit (MU) can turn around Y_s axis.

To describe the instance attitudes of each sensor, we have to introduce a new reference frame $X_{mu}Y_{mu}Z_{mu}$ attached to MU.

We define $X_{mu}Y_{mu}Z_{mu}$ as a system equivalent to $X_sY_sZ_s$ when MU is in a *parking position* shown in *figure 8*.

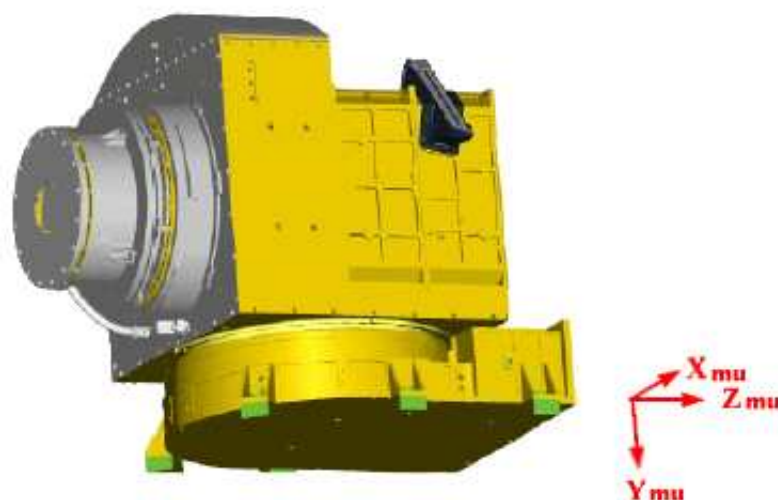
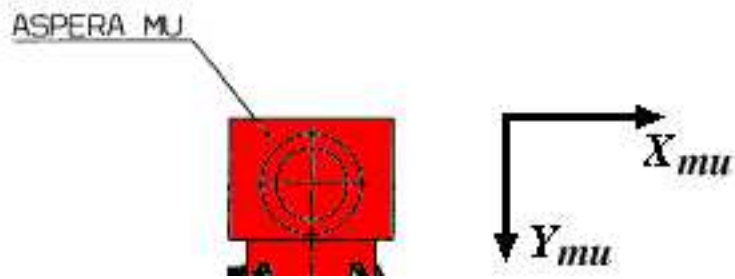
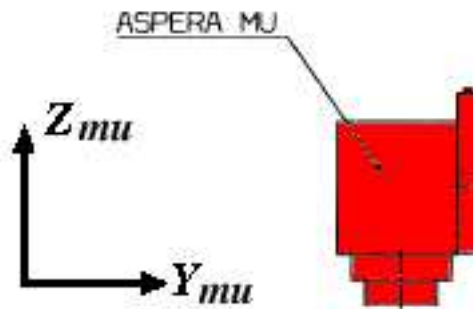


Figure 8: MU location

Figure 9: MU location in $x_{mu}y_{mu}$ planeFigure 10: MU location in $y_{mu}z_{mu}$ plane

3.2 the spacecraft coordinates

Figure 12 shows MU position onto the spacecraft.
Here, main Unit is in a **parking position**.

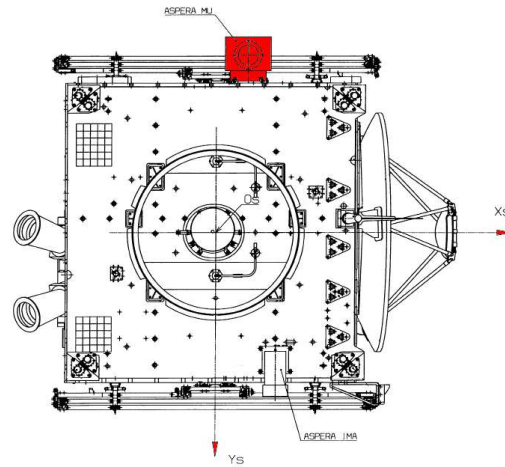


Figure 11: MU parking position in $x_s y_s$ plane

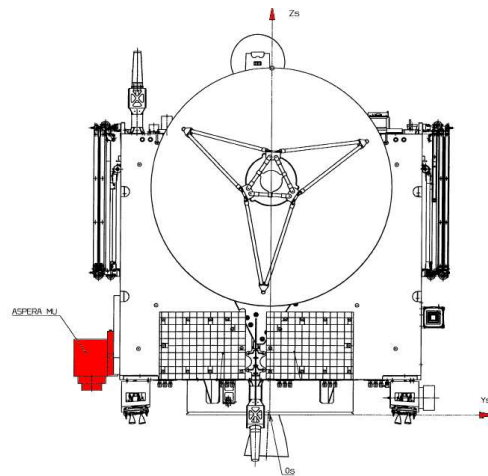


Figure 12: MU parking position in $y_s z_s$ plane

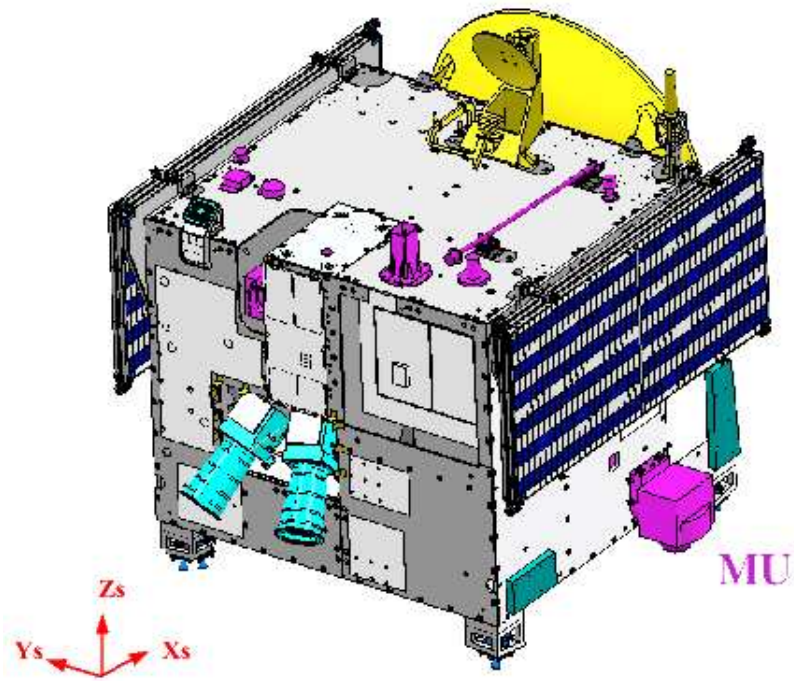


Figure 13: MU parking position in $x_{mu}y_{mu}z_{mu}$ plane

3.3 Main Unit variables

The following variables are used to determine DVV of particles measured by MU.

$$Y_{mu} = Y_s$$

θ is the **scanner angle** in the $X_s Z_s$ plane of the satellite frame. We define θ as the angle between Z_s and X_{mu} . When MU turns around Y_s , θ is varying from 0 to 180 degrees.

At parking position $\theta = 90$.
Then, for $\theta = 90$ degrees :

$$X_{mu} = X_s$$

$$Y_{mu} = Y_s$$

$$Z_{mu} = Z_s$$

Figure 14 represents X_{mu} and Z_{mu} in the $X_s Z_s$ plane:

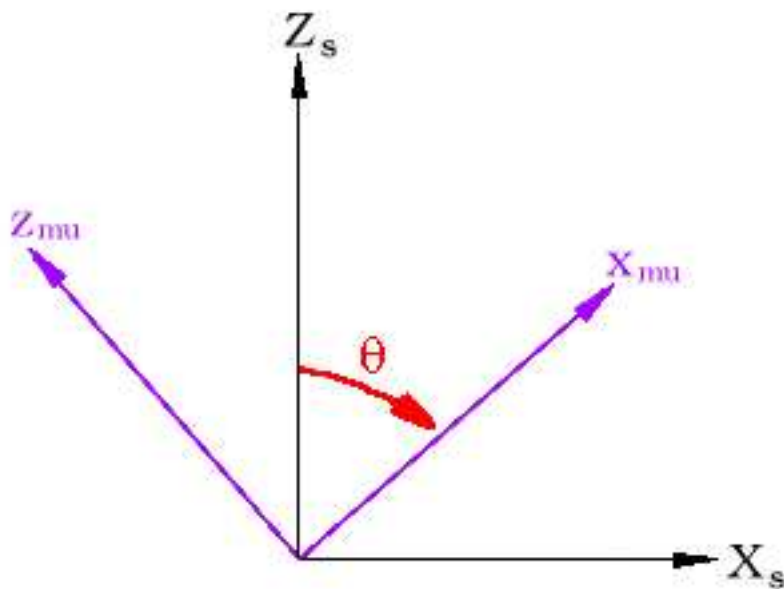


Figure 14: X_{mu} and Z_{mu} in the $X_s Z_s$ plane

3.4 Rotation matrix

In $X_s Z_s$ system, X_{mu} and Z_{mu} are defined by:

$$X_{mu} = \cos\theta Z_s + \sin\theta X_s$$

$$Z_{mu} = \sin\theta Z_s - \cos\theta X_s$$

$$Y_{mu} = Y_s$$

so:

$$\begin{bmatrix} X_s \\ Y_s \\ Z_s \end{bmatrix} = \begin{bmatrix} \sin\theta & 0 & -\cos\theta \\ 0 & 1 & 0 \\ \cos\theta & 0 & \sin\theta \end{bmatrix} \cdot \begin{bmatrix} X_{mu} \\ Y_{mu} \\ Z_{mu} \end{bmatrix}$$

The rotation matrix to translate from the MU system to the satellite system is :

$$M = \begin{bmatrix} \sin\theta & 0 & -\cos\theta \\ 0 & 1 & 0 \\ \cos\theta & 0 & \sin\theta \end{bmatrix}$$

3.5 DVV definition in the Main Unit system

ϕ is the **azimuthal angle** counted from the $+X_{mu}$ axis towards the $+Y_{mu}$ axis.

\vec{u}_{mu} is an unity vector corresponding of DVV of the incident particle.

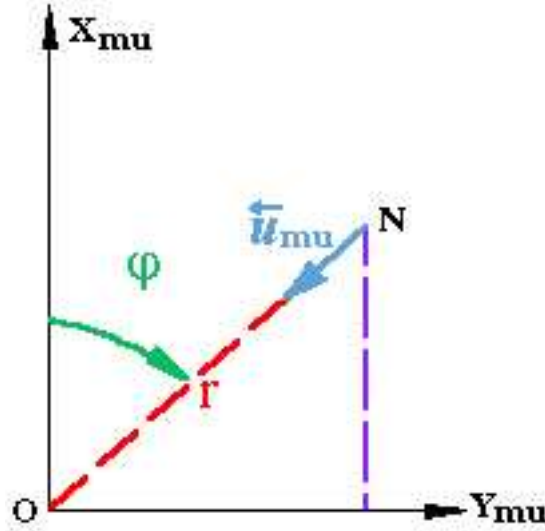


Figure 15: DVV in $X_{mu}Y_{mu}$ plane

\vec{u}_{mu} follow the direction of \vec{NO} :

$$\vec{u}_{mu} = \frac{\vec{NO}}{|\vec{NO}|} = \frac{\vec{NO}}{r}$$

note, that $u_{z_{mu}} = 0$

Thus, \vec{u}_{mu} coordinates in the X_{mu}, Y_{mu}, Z_{mu} plane are:

$$\vec{u}_{mu} = \begin{bmatrix} -\cos\phi \\ -\sin\phi \\ 0 \end{bmatrix}$$

3.6 DVV definition in the satellite system

\vec{u}_s defines the particle direction in the satellite system.

To obtain \vec{u}_s we have to apply the rotation matrix M to convert the \vec{u}_{mu} from the MU system to the satellite system:

$$\begin{bmatrix} u_{x_s} \\ u_{y_s} \\ u_{z_s} \end{bmatrix} = \begin{bmatrix} \sin\theta & 0 & -\cos\theta \\ 0 & 1 & 0 \\ \cos\theta & 0 & \sin\theta \end{bmatrix} \cdot \begin{bmatrix} u_{x_{mu}} \\ u_{y_{mu}} \\ u_{z_{mu}} \end{bmatrix}$$

$$\begin{bmatrix} u_{x_s} \\ u_{y_s} \\ u_{z_s} \end{bmatrix} = \begin{bmatrix} \sin\theta & 0 & -\cos\theta \\ 0 & 1 & 0 \\ \cos\theta & 0 & \sin\theta \end{bmatrix} \cdot \begin{bmatrix} -\cos\phi \\ -\sin\phi \\ 0 \end{bmatrix}$$

Thus :

$$\vec{u}_s = \begin{bmatrix} -\cos\phi \sin\theta \\ -\sin\phi \\ -\cos\phi \cos\theta \end{bmatrix}$$

Figure 16 shows an interpretation of the \vec{u}_s in the X_s, Y_s, Z_s frame, where \vec{u}_s is equal to $\frac{\overrightarrow{MO}}{|\overrightarrow{MO}|}$:

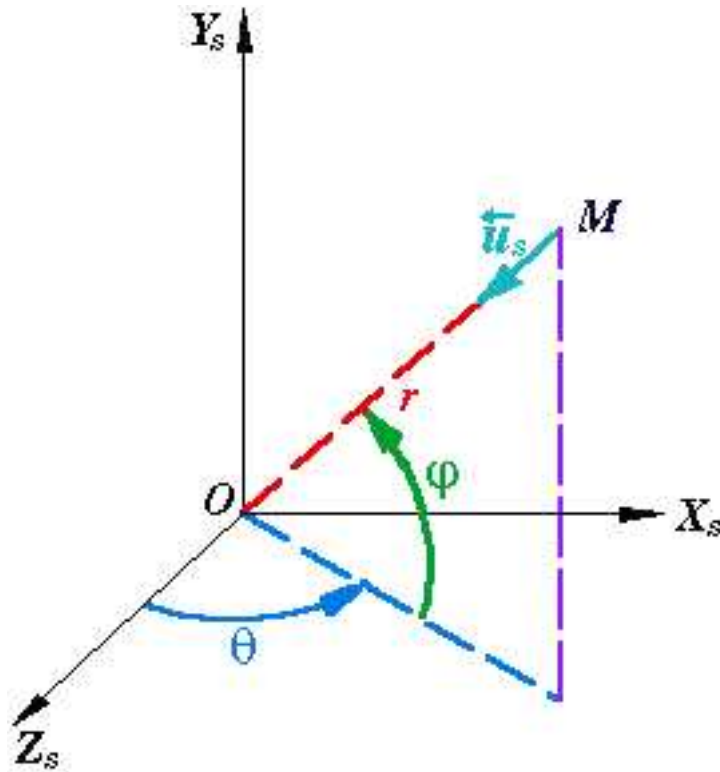


Figure 16: particle direction in $X_s Y_s Z_s$ plane

θ : scanner angle
 ϕ : azimuthal angle
 \overrightarrow{MO} : DVV

3.7 ELS sector looking direction

The next picture defines fields-of-view of 16 ELS sectors in the X_{mu}, Y_{mu} frame.

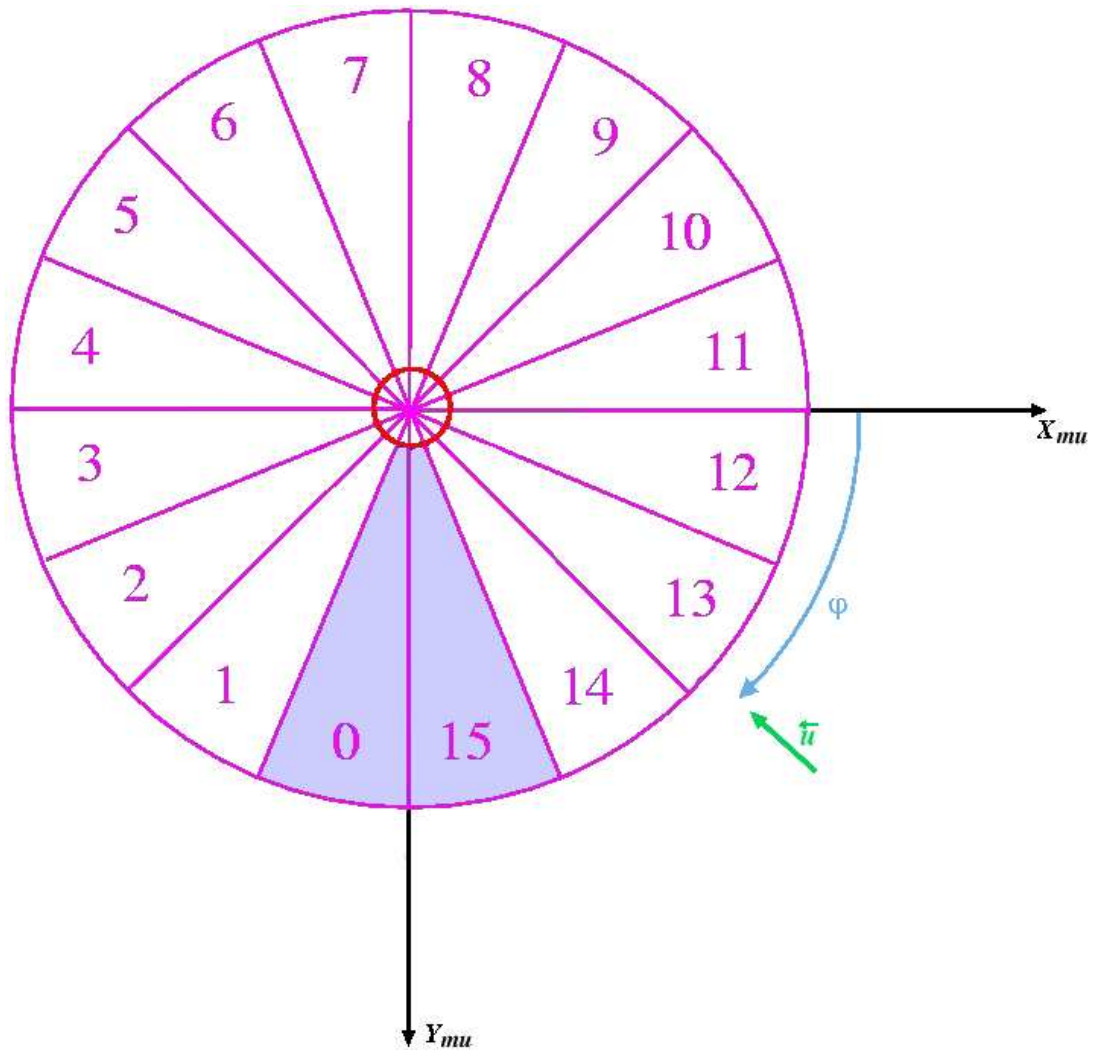


Figure 17: ELS sector looking direction in $X_{mu}Y_{mu}$ plane

ϕ : azimuthal angle

\vec{u} : unity vector corresponding to DVV

For example, a particle with \vec{u} DVV shown in *figure 17* by green arrow will be registered by sector 13.

The following table displays the ϕ values at the beginning, the middle and the end of each sector.

It also indicates the value of $\vec{u}_{X_{mu}Y_{mu}}$ coming in the middle of each sector.

Sector	Begin	Middle	End	$\vec{u}_{X_{mu}Y_{mu}} (*)$
0	90.00	101.25	112.50	(0.195 , -0.981)
1	112.50	123.75	135.00	(0.556 , -0.831)
2	135.00	146.25	157.50	(0.831 , -0.556)
3	157.50	168.75	180.00	(0.981 , -0.195)
4	180.00	191.25	202.50	(0.981 , 0.195)
5	202.50	213.75	225.00	(0.831 , 0.556)
6	225.00	236.25	247.50	(0.556 , 0.831)
7	247.50	258.75	270.00	(0.195 , 0.981)
8	270.00	281.25	292.50	(-0.195 , 0.981)
9	292.50	303.75	315.00	(-0.556 , 0.831)
10	315.00	326.25	337.50	(-0.831 , 0.556)
11	337.50	348.75	0.00	(-0.981 , 0.195)
12	0.00	11.25	22.50	(-0.981 , -0.195)
13	22.50	33.75	45.00	(-0.831 , -0.556)
14	45.00	56.25	67.50	(-0.556 , -0.831)
15	67.50	78.75	90.00	(-0.195 , -0.981)

3.8 NPI sector looking position

The next picture defines fields-of-view of 32 sectors of NPI in the X_{mu}, Y_{mu} frame.

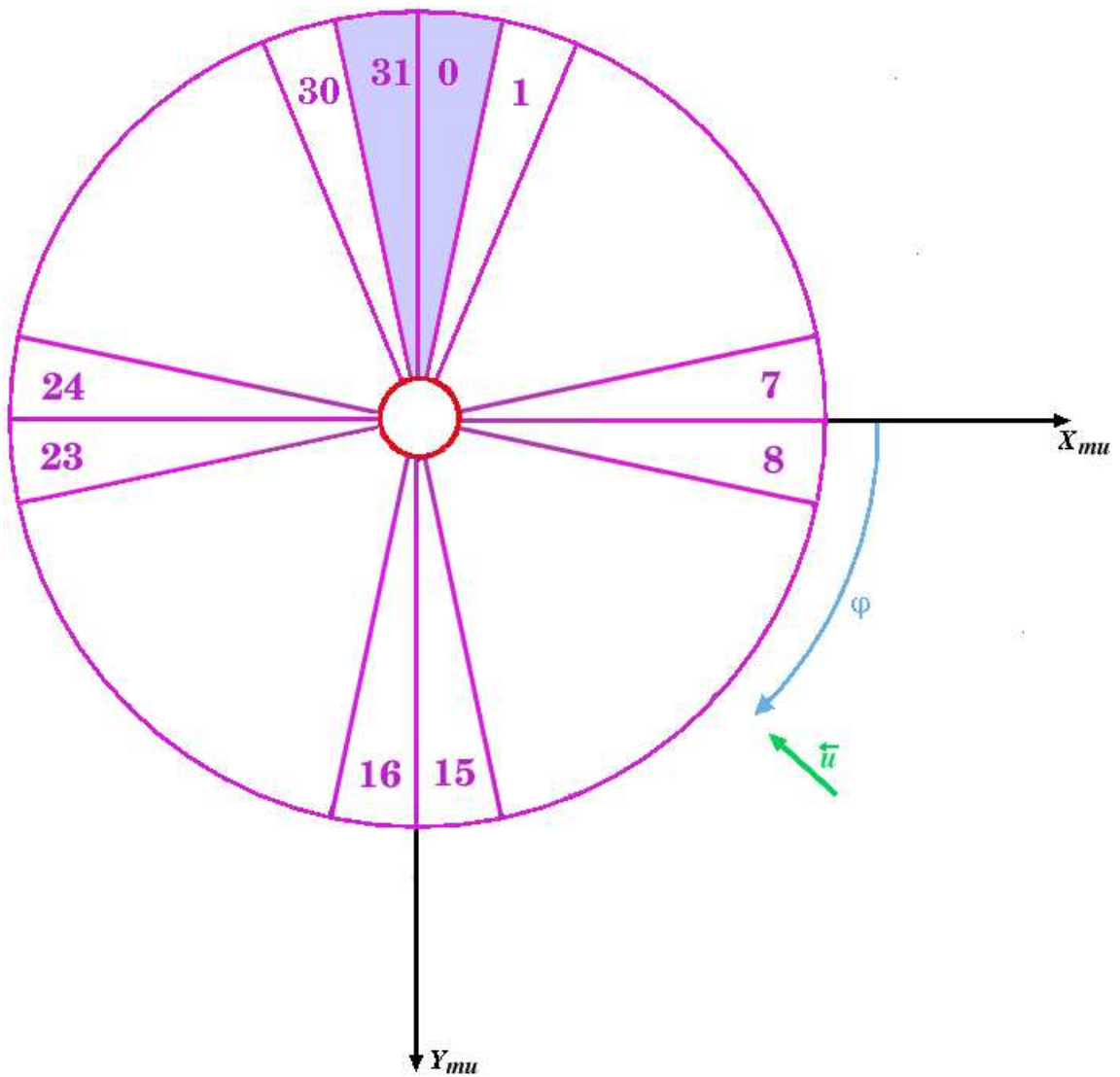


Figure 18: NPI sector looking direction in $X_{mu}Y_{mu}$ plane

ϕ : azimuthal angle

\vec{u} : unity vector corresponding to DVV .

The following table displays the ϕ values at the beginning, the middle and the end of each sector. It also indicates the value of $\vec{u}_{X_{mu}Y_{mu}}$ coming in the middle of each sector.

Sector	Begin	Middle	End	$\vec{u}_{X_{mu}Y_{mu}} (*)$
0	270.00	275.62	281.25	(-0.098 , 0.995)
1	281.25	286.88	292.50	(-0.290 , 0.957)
2	292.50	298.12	303.75	(-0.471 , 0.882)
3	303.75	309.38	315.00	(-0.634 , 0.773)
4	315.00	320.62	326.25	(-0.773 , 0.634)
5	326.25	331.88	337.50	(-0.882 , 0.471)
6	337.50	343.12	348.75	(-0.957 , 0.290)
7	348.75	354.38	0.00	(-0.995 , 0.098)
8	0.00	5.62	11.25	(-0.995 , -0.098)
9	11.25	16.88	22.50	(-0.957 , -0.290)
10	22.50	28.12	33.75	(-0.882 , -0.471)
11	33.75	39.38	45.00	(-0.773 , -0.634)
12	45.00	50.62	56.25	(-0.634 , -0.773)
13	56.25	61.88	67.50	(-0.471 , -0.882)
14	67.50	73.12	78.75	(-0.290 , -0.957)
15	78.75	84.38	90.00	(-0.098 , -0.995)
16	90.00	95.62	101.25	(0.098 , -0.995)
17	101.25	106.88	112.50	(0.290 , -0.957)
18	112.50	118.12	123.75	(0.471 , -0.882)
19	123.75	129.38	135.00	(0.634 , -0.773)
20	135.00	140.62	146.25	(0.773 , -0.634)
21	146.25	151.88	157.50	(0.882 , -0.471)
22	157.50	163.12	168.75	(0.957 , -0.290)
23	168.75	174.38	180.00	(0.995 , -0.098)
24	180.00	185.62	191.25	(0.995 , 0.098)
25	191.25	196.88	202.50	(0.957 , 0.290)
26	202.50	208.12	213.75	(0.882 , 0.471)
27	213.75	219.38	225.00	(0.773 , 0.634)
28	225.00	230.62	236.25	(0.634 , 0.773)
29	236.25	241.88	247.50	(0.471 , 0.882)
30	247.50	253.12	258.75	(0.290 , 0.957)
31	258.75	264.38	270.00	(0.098 , 0.995)

The sectors 14,15,16 and 17 are blocked by satellite body for any values of θ . Other sectors can be blocked for certain θ values.

3.9 NPD sector looking position

NPD consists of two sensors, NPD1 and NPD2.

Each sensor has 3 detectors in the azimuthal plane.

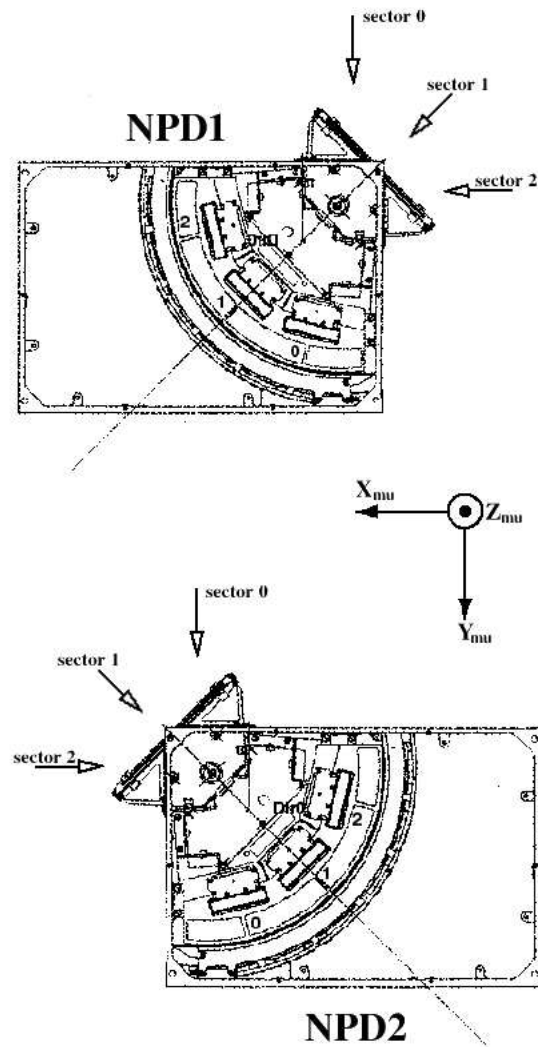


Figure 19: NPD sector looking direction in $X_{\mu}Y_{\mu}Z_{\mu}$ plane

The following tables display for NPD1 and NPD2 the ϕ values at the beginning, the middle and the end of each sector. It also indicates the value of $\vec{u}_{X_{mu}Y_{mu}}$ coming in the middle of each sector.

- NPD1 table :

Sector	Begin	Middle	End	$\vec{u}_{X_{mu}Y_{mu}} (*)$
0	270.00	255.00	240.00	(0.259 , 0.966)
1	240.00	225.00	210.00	(0.707 , 0.707)
2	210.00	195.00	180.00	(0.966 , 0.259)

- NPD2 table :

Sector	Begin	Middle	End	$\vec{u}_{X_{mu}Y_{mu}} (*)$
0	270.00	285.00	300.00	(-0.259 , 0.966)
1	300.00	315.00	330.00	(-0.707 , 0.707)
2	330.00	345.00	0.00	(-0.966 , 0.259)

Moreover the deflector is declined on 15° from the start surface plane :

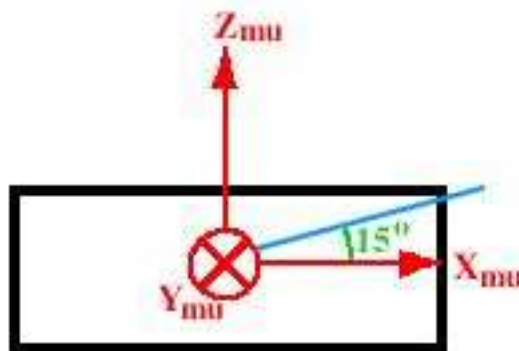


Figure 20: NPD deflection

3.10 Scanner datas

The scanner angle θ is determined in the telemetry files for each main unit sensor (ELS, NPI, NPD1 and NPD2).

In the header of this file, we find scanner direction, scanner speed and scanner position.

The following example shows how those information appear into the data file :

```
Scanner_Direction 1
Scanner_Speed 32
Scanner_Position 0
```

Telemetry frames are generated if $\theta \geq 0^\circ$ and $\theta \leq 180^\circ$. Nevertheless, the scanner can move between -10° and 190° .

position	CCW stop	CCW	CW	CW stop
deg	-10°	0°	180°	190°
count	0	0	223	≤ 231

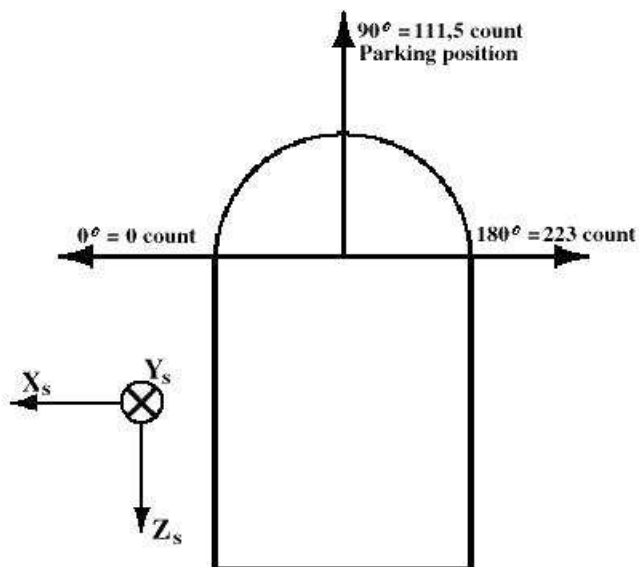


Figure 21: Scanner count

There is 3 allowed speeds for the scanner : 32 *sec*/180°, 64 *sec*/180° and 128 *sec*/180°.

Scanner direction is defined as follows :

- *Scanner_direction 0* : θ is counted up from 0 to 180 degrees.
- *Scanner_direction 1* : θ is counted down from 180 to 0 degrees.

4 The VEXLIB

To switch to the VSO (Venus-Sun-Orbit) sytem, we have to use the **VEXLIB**. VEXLIB is developed by *GFI* (Daniel Popescu) and is using the SPICE LIB and OASW provided by *ESA*.

- *initSPICE*(*&ier*, *errtxt*) : initialisation of the SPICE lib

- *errtxt* : error message if *ier!* = 0
- *ier* : error code
 - 0 : Ok
 - 1 : error

- *initOrbJ2000*(*int *iunit*, *char *fname*, *int iorder*,*int *nvars*, *int *iframe*,
*int *ibody* ,*int *itscal*, *double *tbeg*, *double *tend*, *int *ifid*,
*int *ier*) : open an ESA binary orbit file created with *as2bin*

- *iunit* : number of the unit associated to the orbit file.
- *fname* : name of the orbit file.
- *nvars* : number of vars in the orbit file.
 - 3 : position
 - 6 : position and velocity
 - 42 : position, velocity and derivative
- *iframe* : default location.
 - 0 : mean equator and equinox of j2000
 - 1 : mean ecliptic and equinox of j2000
 - 2 : mean equator and equinox of b1950
 - 3 : mean ecliptic and equinox of b1950
- *ibody* : system of reference.
 - 0 : bary-centre of the solar system
 - 2 : Venus
 - 3 : Earth
 - 11 : Sun
- *itscal* : time ladder.
 - 0 : barycentric dynamic time (*MJD2000* format)
- *tbeg* : beginning time of the orbit file.
- *tend* : ending time of the orbit file.
- *ifid* : orbit file id.
 - 0 : opening failed
- *ier* : error code
 - 0 : Ok
 - 1 : unable to open file

2 : unable to get additional parameters

- *CalcStateJ2000*(*int ifid*, *double time*, *double *state*, *int *iframe*, *int *ibody*, *int *ier*) : calculate VEX state vector.

- *ifid* : orbit file id.
- *time* : time (barycentric dynamic time *MJD2000* format)
- *state* : state vector in the *iframe* location and compared to *ibody*.
- *iframe* : default location.
 - 0 : mean equator and equinox of j2000
 - 1 : mean ecliptic and equinox of j2000
 - 2 : mean equator and equinox of b1950
 - 3 : mean ecliptic and equinox of b1950
- *ibody* : system of reference.
 - 0 : bary-centre of the solar system
 - 2 : Venus
 - 3 : Earth
 - 11 : Sun
- *ier* : error code
 - 0 : Ok
 - 1 : time to early
 - 2 : time to late
 - 3 : time in a gap
 - 4 : error getting additional parameters
 - 5 : error can't read block header
 - 6 : invalid identifier

- *closeOrbJ2000*(*int ifid*, *int *ier*) : close an ESA binary orbit file.

- *ifid* : orbit file id.
- *ier* : error code
 - 0 : Ok
 - 1 : unable to close file
 - 2 : invalid identifier

-
- *initAttJ2000*(*int *iunit, char *fname, int iorder, int *nvars, int *iframe, int *itscal, double *tbeg, double *tend, int *ifid, int *ier*) : open an ESA binary attitude file.
 - *iunit* : number of the unit associated to the attitude file.
 - *fname* : name of the attitude file.
 - *iorder* : interpolation order (6 to 12; 8 recommended).
 - *nvars* : number of vars in the orbit file.
 - 3 : position
 - 6 : position and velocity
 - 42 : position, velocity and derivative
 - *iframe* : default location.
 - Only *EMEJ2000* available in this version.
 - *itscal* : time ladder.
 - 0 : barycentric dynamic time (*MJD2000* format)
 - *tbeg* : beginning time of the attitude file.
 - *tend* : ending time of the attitude file.
 - *ifid* : attitude file id.
 - 0 : opening failed
 - *ier* : error code
 - 0 : Ok
 - 1 : unable to open file
 - 2 : unable to get additional parameters

 - *CalcAttQuatJ2000*(*int ifid, double time, double *state, int *iframe, int *ibody, int *ier*) : calculate VEX quaternion attitude and angular velocity.
 - *ifid* : attitude file id.
 - *time* : time (barycentric dynamic time *MJD2000* format)
 - *state* : state vector in the *iframe* location and compared to *ibody*.
 - *iframe* : attitude reference.
 - 0 : J2000
 - *ibody* : system of reference.
 - 0 : bary-centre of the solar system
 - 2 : Venus
 - 3 : Earth
 - 11 : Sun
 - *ier* : error code
 - 0 : Ok
 - 1 : time to early
 - 2 : time to late
 - 3 : time in a gap

- 4 : error getting additional parameters
- 5 : error can't read block header
- 6 : invalid identifier

- *CalcAttMatJ2000*(*int ifid*, *double time*, *double amat*[3][3], *double omega*[3], *int *iframe*, *int *ier*): calculate the angular velocity and the rotation matrix from the satellite location to the EMEJ2000 location.

- *ifid* : attitude file id.
- *time* : time (barycentric dynamic time *MJD2000* format)
- *iframe* : attitude reference.
 - 0 : J2000
- *ibody* : system of reference.
 - 0 : bary-centre of the solar system
 - 2 : Venus
 - 3 : Earth
 - 11 : Sun
- *ier* : error code
 - 0 : Ok
 - 1 : time too early
 - 2 : time too late
 - 3 : time in a gap
 - 4 : error getting additional parameters
 - 5 : error can't read block header
 - 6 : invalid identifier

- *closeAttJ2000*(*int ifid*, *int *ier*) : close an ESA binary attitude file.

- *ifid* : attitude file id.
- *ier* : error code
 - 0 : Ok
 - 1 : unable to close file
 - 2 : invalid identifier

-
- *CalcJD2000*(*double *mjday, int year, int month, int day, int hour, int minute, double second*): convert a calendar date into a julian day.
 - *mjday* : Julian day modified.

 - *CalcDJ2000*(*double mjday, int *year, int *month, int *day, int *hour, int *minute, double *second*): convert a julian day into a calendar date.
 - *mjday* : Julian day to modify.

 - *eme2000vso*(*double date, double pmat[3][3], double pmatt[3][3], int* ier, char *errtxt*): changeover matrix of the EME2000 towards VSO.
 - *date* : barycentric dynamic time (*MJD2000* format)
 - *pmat* : changeover matrix (3 * 3) EME2000 to VSO
 - *pmatt* : transposed matrix of *pmat*
 - *ier* : error code
 - 0 : Ok
 - 1 : error
 - *errtxt* : error message if *ier*! = 0

 - *eme2000uai*(*double date, double pmat[3][3], double pmatt[3][3], int* ier, char *errtxt*): changeover matrix of the EME2000 towards UAI.
 - *date* : barycentric dynamic time (*MJD2000* format)
 - *pmat* : changeover matrix (3 * 3) EME2000 to Venus fixed
 - *pmatt* : transposed matrix of *pmat*
 - *ier* : error code
 - 0 : Ok
 - 1 : error
 - *errtxt* : error message if *ier*! = 0

 - *eme2000gse*(*double date, double pmat[3][3], double pmatt[3][3], int* ier, char *errtxt*): changeover matrix of the EME2000 towards GSE.
 - *date* : barycentric dynamic time (*MJD2000* format)
 - *pmat* : changeover matrix (3 * 3) EME2000 to GSE
 - *pmatt* : transposed matrix of *pmat*
 - *ier* : error code

0 : Ok

1 : error

- *errtxt* : error message if *ier!* = 0

- *MxV(double matrix[3][3], double vin[3], double vout[3])*
: Multiplication of a vector (3) by a matrix (3x3).

- *matrix* : Matrix (3 * 3)

- *vin* : incoming vector (3)

- *vout* : result of the multiplication; vector (3).

- *calcStateGSE(double date, int target, double *state, int* ier, char *errtxt)*
: position and velocity of an object in GSE.

- *date* : barycentric dynamic time (*MJD2000* format)

- *target* : id NAIF of the object

- *state* : state vector in the *iframe* location and compared

- *ier* : error code

0 : Ok

1 : error

- *errtxt* : error message if *ier!* = 0



ASPERA-4



**Venus
Express**

Reference : **VE-ASP-TN-060402**
Issue : **1** Rev. : **1**
Date : **2006-06-17**
Volume : **-** Page: **11**

APPENDIX 8. ASPERA-4 CALIBRATION REPORT



ASPERA-4



**Venus
Express**

Reference : **VE-ASP-CR-050530**
Issue : **1** Rev. : **1**
Date : **2005-05-30**
Volume : **-** Page: **1**

ASPERA – 4 CALIBRATION REPORT

	Name and function	Date	Signature
Prepared by:	Stas Barabash	2005-05-30	
Verified by:			
Approved by:			
Issued by:			



1 SCOPE AND STRUCTURE OF THE DOCUMENT

The document provides calibration reports on four ASPERA-4 individual sensors, ELS (Electron Spectrometer), NPI (Neutral Particle Imager), NPD (Neutral Particle Detector), and IMA (Ion Mass Analyzer). In the calibration overview the sensor performance is summed up vs. proposal “Venus Express. Response to ESA’s Call for Ideas for the Re-Use of the Mars Express Platform”. Four Appendixes contain the individual calibration reports. The calibrations have been performed at

- ELS: Mullar Space Science Laboratory, UK
- NPI: Swedish Institute of Space Physics, Kiruna, Sweden
- NPD: Swedish Institute of Space Physics, Kiruna, Sweden
- IMA: CESR /CNRS, Toulouse, France

2 CALIBRATION RESULTS OVERVIEW

Four tables below shows the instrument performance vs. proposal. Note that for the sensors mounted on the scanner, ELS, NPI, NPD the full 3D resolution is provided by the fastest scanning speed which is 32s per 180° scan.

Table 1. NPI performance (see Appendix 1)

Parameters	As proposed	As calibrated
Energy range, keV	≈0.1 - 60	0.2 ¹ – 60 ²
Energy resolution, ΔE/E	No	No
Mass resolution	No	No
Intrinsic field of view	9° x 344°	9° x 344°
Angular resolution (FWHM)	4.6° x 11.5°	3.5° x 13°
G-factor/pixel, cm ² sr (w/o effic.)	2.5 x 10 ⁻³	2.5 x 10 ⁻³
Efficiency,	10 ⁻²	10 ⁻⁵ – 6·10 ⁻³ (0.2 – 5 keV)
Time resolution / spectrum (*)	N/A	65 ms – 128s ³
Time resolution for 3D, s	32	32

(*) not in the proposal

¹ – at efficiency 10⁻⁵ for oxygen and 2.47 kV MCP bias

² – Cut-off deflector at 5 kV

³ – Commandable

Table 2. NPD (see Appendix 2)

Parameters	As proposed	As calibrated
Energy range, keV	0.1 - 10	0.006 – 18 (H) ¹ 0.19 - 10 keV (O) ²
Energy resolution, ΔE/E	80	50
Mass resolution	H, O	H, O
Intrinsic field of view	9° x 180°	9° x 180°
Angular resolution (FWHM)	5° x 30°	NPD1 NPD2 Dir0 3.5° x 34.1° 3.7° x 32.5° Dir1 4.3° x 51.7° 4.6° x 60.8° Dir2 4.5° x 40.0° 4.0° x 41.3°
G-factor/pixel, cm ² sr (inc. effic.)	(0.62 – 15.5) x 10 ⁻⁴	(0.024 – 3.8) x 10 ⁻⁴ (H) ³ (0.03 – 10.7) x 10 ⁻⁴ (O) ³
Efficiency, %	1 - 25	0.013 – 6.0 (H) ³ 0.005 – 11.8 (O) ³
Time resolution / spectrum (*)	N/A	65 ms – 128s ⁴
Time resolution for 3D	32	32

(*) not in the proposal



- ¹ – based on the 50 ns – 2400 ns TOF window. Calibrated efficiency for 100 eV H is 10^{-3} .
² – based on 2400 ns upper TOF limit and calibrated efficiency $(8.5 - 10.3) \cdot 10^{-2}$ for 10 keV O.
³ – for all directions and for the energy range 0.3 – 10 keV for O and 0.1 – 5.0 for H.
⁴ – Commandable

Table 3. ELS (see Appendix 3)

Parameters	As proposed	As calibrated
Energy range, keV	0.001 - 20	0.001 - 20
Energy resolution, $\Delta E/E$	7%	6% – 10%
Mass resolution	No	No
Intrinsic field of view	$10^\circ \times 360^\circ$	$10^\circ \times 360^\circ$
Angular resolution (FWHM)	$5^\circ \times 22.5^\circ$	$5^\circ \times 22.5^\circ$
G-factor/pixel, $\text{cm}^2 \text{sr}$ (inc. effic.)	3×10^{-4}	TBD, close to MEX
Time resolution / spectrum (*)	N/A	4s (128 steps)
Time resolution for 3D	32	32

(*) not in the proposal

Table 4. IMA (see Appendix 4)

Parameters	As proposed	As calibrated
Energy range, keV	0.01 - 40	0.03 - 31.8 ¹
Energy resolution, $\Delta E/E$	10%	4%
Mass resolution, $M/\Delta M$	5	M/q : 1, 2, 16, 32 (see Appendix 4)
Intrinsic field of view	$90^\circ \times 360^\circ$	$90^\circ \times 360^\circ$ ²
Angular resolution (FWHM)	$5^\circ \times 22.5^\circ$	$5^\circ \times 22.5^\circ$ (programmed) ²
G-factor/pixel, $\text{cm}^2 \text{sr eV/eV}$ (inc. effic.)	3.5×10^{-4}	$(0.6 - 2) \cdot 10^{-4}$ (at 600 eV, for the other see Table 1 in Appendix 4) ²
Time resolution / spectrum (*)	N/A	196s / energy – elevation sweep
Time resolution for 3D	32	196

(*) not in the proposal

1 – lower limit is extrapolated from calibrations at the lower limit at 300 eV

2 – function of energy and mass (see report)

3 CONCLUSION

The instrument performance is in line with Proposal.



ASPERA-4



**Venus
Express**

Reference : **VE-ASP-CR-050530**
Issue : **1** Rev. : **1**
Date : **2005-05-30**
Volume : **-** Page: **5**

APPENDIX 1. NPI CALIBRATION REPROT

ASPERA-4 NPI Calibration Report

K. Brinkfeldt, S. Barabash, A. Grigoriev, K. Asamura, B. Sandel, C. Curtis

May 26, 2005

Abstract

This report treats the functional test and calibration of the Neutral Particle Imager (NPI), which is a part of the instrument ASPERA-4 to be flown on Venus Express. For the functional test the detector MCP (Micro Channel Plate) saturation voltage and dark current are measured. For the calibration part the sensor efficiency and response to azimuth and elevation scans are presented. The NPI was also calibrated against Lyman- α photons ($\lambda = 121.6$ nm). The results of these measurements are included. The ASPERA-4 NPI is the flight spare of the ASPERA-3 NPI on Mars Express.

1 Introduction

The ASPERA-4 instrument will investigate plasma-neutral interactions near Venus as part of the Venus Express mission scheduled for launch 2005. ASPERA-4 includes the Neutral Particle Imager (NPI) which will image energetic neutral atoms (ENA) with an angular resolution of $9^\circ \times 11.25^\circ$. The NPI is a cylindrical tophat type instrument with 32 apertures. A high voltage deflection system will remove charged particles from the measured flux so that only neutral particles can pass and impact a tilted target block. Secondary and reflected particles are converted to a current pulse with a Multi Channel Plate (MCP) chevron configuration. At the MCP output a sectioned anode is connected to front end electronics.

1.1 Description of the Calibration Facility at IRF

The system in the IRF laboratory is the Model 2751 50 keV Ion Source from Peabody Scientific. It is capable of producing a parallel and even ion beam with an energy of up to 50 keV/q. The system can be run in three different modes to be able to achieve the three energy ranges 0 - 1 keV/q, 1 - 15 keV/q and 15 - 50 keV/q. Ions are produced in the duoplasmatron from arcing between an anode and an oxide coated mesh filament. There is a funnel-shaped electrode constricting the gas and generated plasma cloud to a volume that is converging toward the axial aperture exit. This restricts the plasma to a narrow beam emerging from the aperture. To increase the ionization efficiency, a strong magnetic field is applied in the axial direction of the duoplasmatron. Electrons generated will then spiral along the magnetic field lines towards the anode and produce longer ionization tracks. The ion beam is then extracted through an extraction gap by an extraction electrode and then accelerated through a three-element Einzel focusing lens, which also helps to collimate the diverging ion beam into a parallel beam. The focal length can be optimized by adjusting the lens voltage. The ions then enter an ExB filter. This consists of a perpendicular magnetic and an electrical field. The elec-

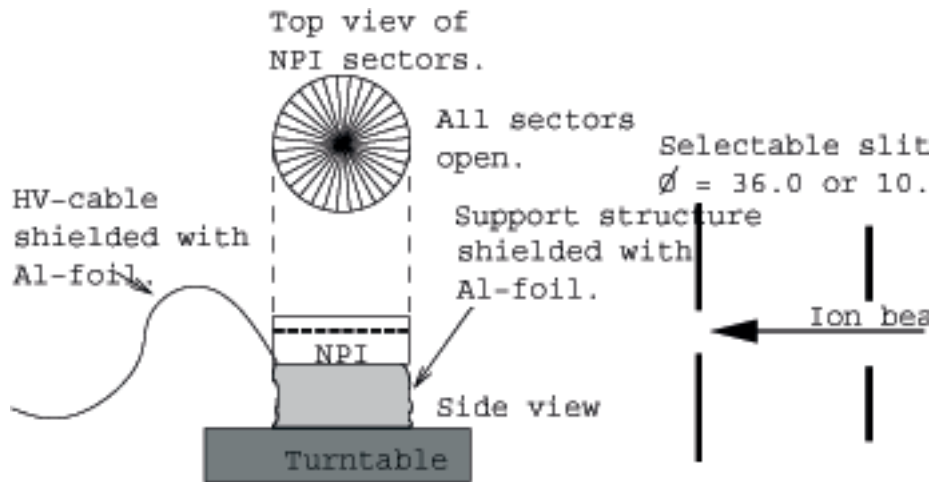
trical field strength can be varied to filter out the desired ion mass according to the formula: The electrode voltage is divided between the voltage on the top electrode (V_{ExB}^+) and the voltage on the bottom electrode (V_{ExB}^-). These are not perfectly symmetrical. After exiting the ExB filter the ions are accelerated in an acceleration gap to achieve the final beam energy. The beam is then further filtered through the electrostatic analyzer, which is a 90 degree spherical electrode with a radius of 5 ". Ions with energies different from the energy selected by setting the electric field inside the analyzer will not make the turn. The electrostatic analyzer at the IRF facility has an energy resolution of 1 %. To permit widening of the ion beam emerging from the electrostatic analyser, a defocus lens first diverges the beam and then a focus lens collimates the diverging beam into a parallel beam leaving the system. Both lenses are three-element Einzel lenses of different size. The retractable Faraday cup provides measurements of the beam intensity and because of this also indirectly the beam location. It is mounted inside the vacuum tank.

1.2 Measurement configuration

Fig. 1 shows the instrument measurement configuration for the particle calibration used in this report. The UV calibration set up was similar. The sensor electrical configuration was identical for the UV calibration.

2 Functional Test of the NPI Flight Model

The functional test of the NPI sensor was designed to verify the basic functionality of the sensor, measure the MCP-bias saturation voltage and measure the sensor dark response. The functionality of the sensor was satisfactory. The sector priority effect with increasing MCP bias observed in the ASPERA-3 NPI was found to be negligible in the ASPERA-4 NPI.



Electrical configuration:

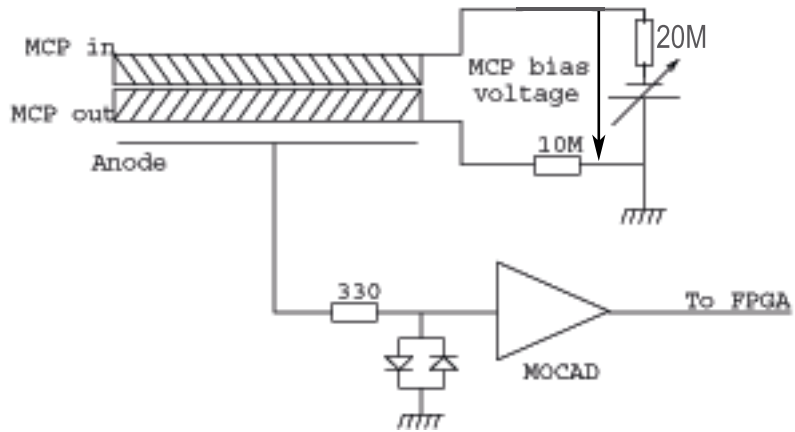


Figure 1: Calibration configuration of the sensor.

Table 1: Beam parameters for the saturation measurement.

Species:	H_2O^+
Energy:	4.8 keV
Intensity:	$0.097 \cdot 10^{-11} \text{ A}$
Sector:	4
Sampling time:	1 s (averaged over 60 s)

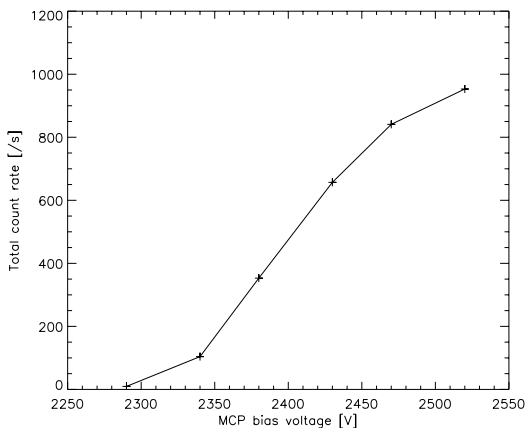


Figure 2: Measured total count rate with MCP bias voltage. This measurement was made with a 4.8 keV, H_2O^+ beam.

2.1 MCP Saturation

Micro channel plates have a saturation bias, at which the count rate from the plate no longer increase with bias. The optimal operation bias is just prior to the saturation bias. This measurement was done to find the optimal operation bias. The measurement setup for the saturation measurement is in Fig. 1. The measurement beam parameters are in Table 1: A

plot of the measured total count rate with increasing MCP bias voltage is in Fig. 2. From the figure the optimal operating MCP bias voltage should be in the shoulder region of 2420 - 2520 V. The nominal operating MCP bias voltage is set to 2430 V.

2.2 MCP Dark Current

MCPs have a dark current associated with them. A plot of the NPI dark count at nominal MCP bias is in Fig. 3. There is a clear anomaly in sector 22. Another dark current measurement was made after the calibration and the anomaly had decreased some. It is therefore believed to be caused by some impurity on, or within the MCP plates at the position corresponding to sector 22. The effect is reduced after operation effectively during several hours in the calibration. It is believed that the anomaly will continue to reduce and eventually disappear. The instrument setup for the dark count measurement is in Fig. 1. No beam was used in this measurement. The sampling time was 1 s and the measurement was averaged over 60 samples. Table 2 lists the total dark count for each NPI sector during 60 seconds for different MCP bias.

3 Particle Calibration of the Flight Model

3.1 Calibration Plan

The calibration plan of the NPI sensor includes a full investigation of the response of one sector only and then an investigation of the relative response of the other sectors. Thorough investigation of all 30 open sectors would be too time consuming. An investigation of one reference sector should include the angular response (scans of azimuth and elevation angles) at different beam energies. Also, the efficiency should be calculated for different energies. Suggested beam energies are 0.5, 0.75, 1.0, 5.0 and 10 keV.

When the response from the reference sector is known, a relative response of the other sectors is found from a 360° azimuth scan with elevation angle fixed at the maximum response of the reference sector.

3.2 Angular response

Full azimuth and elevation scans were performed on sector 4 and responses for nominal MCP bias (2430

Table 2: Dark count at different MCP bias. Sampling time is 60 seconds.

Sector	MCP bias 2340 V	MCP bias 2380 V	MCP bias 2430 V	MCP bias 2470 V
0	0	0	4	5
1	2	3	5	2
2	0	5	5	5
3	0	1	6	10
4	1	2	4	5
5	2	3	2	3
6	1	0	6	4
7	0	2	4	4
8	1	1	3	4
9	1	1	4	6
10	2	2	2	9
11	0	2	2	4
12	1	2	6	5
13	0	0	3	5
14	0	2	2	11
15	0	1	2	3
16	3	0	5	6
17	1	3	4	3
18	1	3	3	7
19	1	3	3	7
20	0	3	4	4
21	0	2	5	5
22	0	4	23	59
23	1	2	2	6
24	2	0	1	4
25	1	3	1	4
26	1	2	1	4
27	1	1	3	3
28	1	2	3	3
29	0	1	5	4
30	2	1	5	6
31	3	4	3	5
Total	29	61	131	215

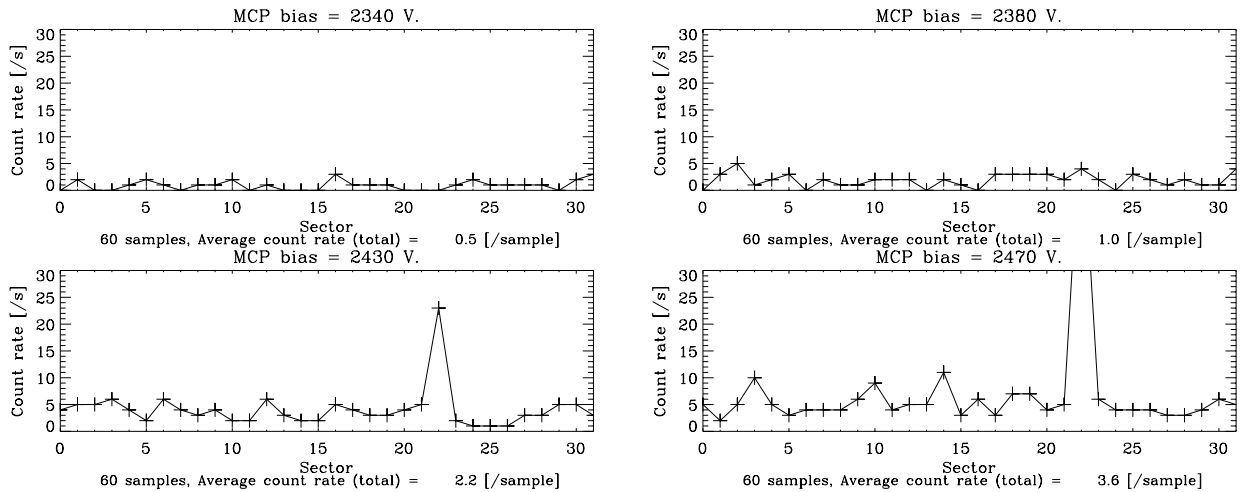


Figure 3: Normalized dark count for all sectors at different MCP bias.

Table 3: Beam parameters for the angular scans.

Species:	H_2O^+
Energy:	4.8 keV
Intensity:	$\approx 0.14 \cdot 10^{-11} - 1.2 \cdot 10^{-11} \text{ A}$
Sector:	4 (full scan : $\Delta\varphi = 1^\circ$ and $\Delta\theta = 1^\circ$)
Sampling time:	1 s

Table 5: Beam parameters for the azimuth scans.

Species:	H_2^+
Energy:	4.8 keV
Intensity:	$\approx 1.5 \cdot 10^{-11} \text{ A}$
Sector:	0-31 (full scan : $\Delta\varphi = 2^\circ$)
Sampling time:	1 s

V) and an additional two MCP bias settings (2380 V and 2470 V) were recorded. The normalized responses are in Fig. 4. The measurement configuration is shown in Fig. 1. The ion beam configurations for these measurements are in Table 4.

3.3 Azimuth scan

The azimuth scan response for the NPI sensor at nominal MCP bias (2430 V) is in Fig. 5. The instrument configuration for this measurement is in Fig. 1 and the beam parameters for this measurement is in Table 5. The relative response of the different sectors are in table 3. It shows the averaged response of the sector centers (azimuth center $\pm 2^\circ$) for each sector

relative to sector 4 and should be used to normalize the different sector responses prior to data analysis.

3.4 Efficiency Measurement

The particle efficiency ε of the NPI sensor is measured as a count rate C over beam current I for the ratios of the beam profile area A_{beam} and the effective sector target block area of the NPI, A_{eff} :

$$\varepsilon = \frac{C \cdot A_{beam}}{I \cdot A_{eff}}, \quad (1)$$

Here, the target block area, A_{eff} , is 0.128 cm^2 and A_{beam} is limited to 10.1 mm using a slit. The beam current is:

$$I = \frac{I_{faraday}}{e}, \quad (2)$$

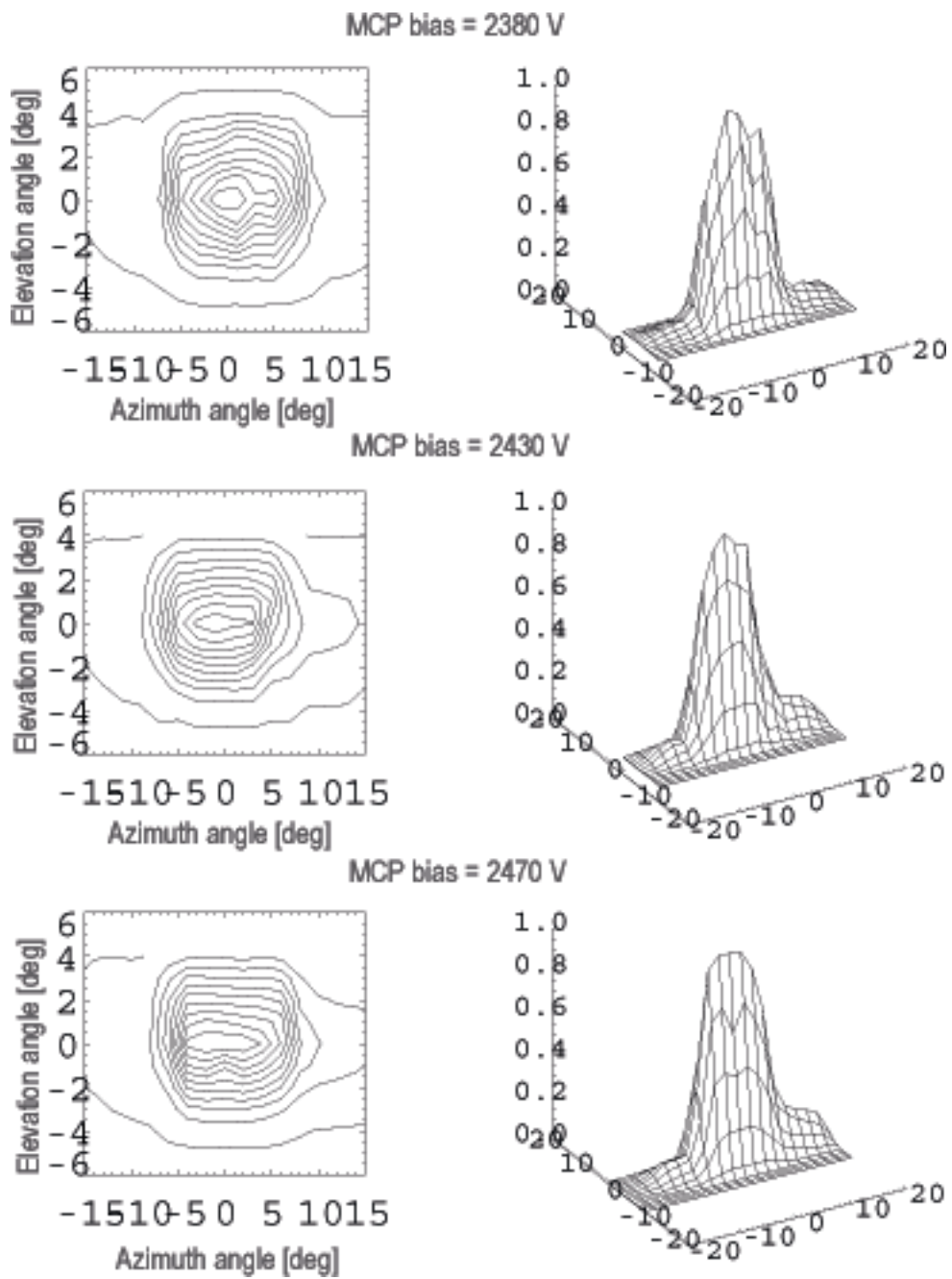


Figure 4: Angular scan of sector 4 at MCP bias 2380 V (top left and right) with corresponding fits (bottom left and right).

Table 4: The data points of the angular response of particles for MCP bias 2430 V.

	-16	-14	-12	-10	-8	-6	-4	-2	0	2	4	6	8	10	12	14	16	18
7	0.0000	0.0002	0.0007	0.0000	0.0002	0.0000	0.0005	0.0003	0.0003	0.0002	0.0002	0.0000	0.0002	0.0004	0.0002	0.0000	0.0002	0.0004
6	0.0000	0.0002	0.0000	0.0004	0.0002	0.0003	0.0009	0.0005	0.0002	0.0002	0.0000	0.0000	0.0002	0.0000	0.0000	0.0002	0.0002	0.0000
5	0.0000	0.0002	0.0002	0.0002	0.0007	0.0009	0.0000	0.0005	0.0002	0.0002	0.0003	0.0002	0.0003	0.0002	0.0000	0.0002	0.0002	0.0000
4	0.0000	0.0012	0.0009	0.0026	0.0061	0.0201	0.0181	0.0408	0.0972	0.0387	0.0449	0.0193	0.0191	0.0052	0.0049	0.0043	0.0016	0.0015
3	0.0000	0.0028	0.0074	0.0182	0.0225	0.0697	0.1340	0.2114	0.2103	0.2221	0.2091	0.0705	0.0703	0.0280	0.0336	0.0255	0.0093	0.0038
2	0.0000	0.0082	0.0242	0.0474	0.0494	0.1292	0.3649	0.4605	0.4929	0.5073	0.3778	0.2071	0.1438	0.0695	0.0760	0.0657	0.0414	0.0082
1	0.0000	0.0184	0.0522	0.0778	0.0780	0.2418	0.6249	0.7563	0.7948	0.7526	0.7042	0.3733	0.2420	0.1415	0.1208	0.1062	0.0726	0.0191
0	0.0000	0.0240	0.0645	0.0854	0.0811	0.3209	0.7612	0.8349	1.0000	0.9382	0.9249	0.4656	0.3023	0.1618	0.1548	0.1399	0.0929	0.0298
-1	0.0000	0.0238	0.0641	0.0756	0.0564	0.2954	0.6589	0.7473	0.7932	0.7691	0.7675	0.5950	0.2427	0.1367	0.1252	0.1138	0.0875	0.0218
-2	0.0000	0.0196	0.0473	0.0522	0.0470	0.2354	0.4610	0.4919	0.5309	0.5321	0.5058	0.4438	0.2001	0.0878	0.0806	0.0691	0.0648	0.0241
-3	0.0000	0.0182	0.0296	0.0258	0.0243	0.1277	0.2660	0.2694	0.2857	0.2949	0.2888	0.2496	0.1209	0.0514	0.0412	0.0346	0.0421	0.0143
-4	0.0000	0.0059	0.0074	0.0065	0.0094	0.0228	0.0615	0.0716	0.0784	0.0817	0.0737	0.0549	0.0371	0.0074	0.0098	0.0089	0.0085	0.0045

Table 6: Response (measured count/s) to particles for all sectors relative to the response of sector 4.

Sector	0	1	2	3	4	5	6	7	8	9	10
Relative sensitivity	0.45	0.60	0.74	0.88	1.00	0.95	0.41	0.28	0.41	1.0.23	0.22
Sector	11	12	13	14	15	16	17	18	19	20	21
Relative sensitivity	0.27	0.46	0.46	0.44	0.00	0.00	0.52	0.47	0.49	0.49	0.47
Sector	22	23	24	25	26	27	28	29	30	31	
Relative sensitivity	0.47	0.29	0.36	0.26	0.40	0.39	0.37	0.63	0.48	0.58	

where $I_{faraday}$ is the Faraday cup reading and e is the elementary charge.

The measurement configuration is found in Fig. 1. Efficiency measurements were made for different MCP bias using H_2O^+ and H^+ ions of different energies. An efficiency measurement with blocked neighboring sectors were also made. The measurement beam parameters were:

Species:	H_2O^+
Energy:	0.29, 0.48, 0.96 and 4.8 keV
Intensity:	$\approx 1 \cdot 10^{-14} - 7 \cdot 10^{-11}$ A
Sector:	4
Sampling time:	30 s

Fig. 6 is a plot of the efficiency to H_2O^+ and H^+ ions with and without neighboring sectors blocked.

3.5 Estimation of geometrical factor

The response of each sector on the NPI is defined as a count rate $C = \text{counts/s}$. If the effective area (area of the target block visible from the sector aperture) of one NPI sector is A_{eff} the The measured geometrical factor G is defined as:

$$G = \frac{A_{eff}(\theta_0, \varphi_0)}{C_{meas}(\theta_0, \varphi_0)} \int_{\varphi} \int_{\theta} C_{meas}(\theta, \varphi) \cos \theta d\theta d\varphi, \quad (3)$$

where A_{eff} is the effective areal size, C is the measured count rate, θ is the elevation angle and φ is the azimuth angle. The calibration data from sector

14 on MEX NPI was used for the geometrical factor calculation. From the calibration measurements in the center of sector 14 $C(0,0) \approx 68$ and the effective target area of one sector in the NPI is $A_{eff} = 0.128 \text{ cm}^2$. Calibration measurements of instrument elevation and azimuth response gives:

$$\int_{\varphi} \int_{\theta} C(\theta, \varphi) \cos \theta d\theta d\varphi = 1.46$$

and from equation 3 this results in a geometrical factor of:

$$G_{sector} \approx \frac{0.128}{68} \cdot 1.46 = 2.7 \cdot 10^{-3} \text{ cm}^2 \text{ sr}$$

4 UV calibration of the flight model

An MCP is also a good detector of photons in the UV range. The response efficiency is a function of UV wavelength with a higher efficiency towards lower wavelengths. This is a problem when operating the sensor in space because the UV output of the Sun. The predominately abundant wavelength from the the Sun in the UV range is the hydrogen Lyman- α (L_{α}) line at 121.6 nm. For photons in this region the sensitivity of the MCPs is about 1 percent. To estimate the effect of the Solar UV contamination on the particle measurements we measured the response from the sensor to L_{α} . As for the particle calibration the approach was to find the detailed UV response of only one of the 32 sectors of the NPI. Then make a relative measurement of the central position of the

other 31 sectors. Also the response linearity with UV intensity was checked. Only the VEX NPI was calibrated against UV.

To be able to produce a count in the NPI a photon will have to get through a number of steps. First, obviously, it has to hit the aperture within a specific angular range. The deflection plate surfaces are coated with copper sulfide. It creates a powdery surface that is uneven on a small scale to prevent reflections. Assuming that it impacts the NPI target block it may be absorbed, in which case there will not be any count associated with the photon, or reflected towards the MCP stack. The target block is coated with DAG-213, which is resin based graphite solution. The VEX NPI UV calibration is, to our knowledge, the first time DAG-213 UV reflection efficiency is measured. Expected efficiency (ε_{tb}) is around 10^{-5} . There could also be small variations in the coating over the area of the target block of the NPI. The efficiency of the MCP itself for UV of the Lyman-alpha wavelength (ε_{Ly}) is $\approx 1\%$. So the combined expected efficiency of the NPI for L_α photons is

$$\varepsilon = \varepsilon_{tb} \cdot \varepsilon_{Ly} = (10^{-5}) \cdot (10^{-1}) = 10^{-6} \quad (4)$$

We estimate the UV-intensity in the calibration beam using an absolutely calibrated channeltron. A beam map (Fig. 7) was acquired using the channeltron and the result is then compared to the continuous measurements with the beam monitor. This way we can get an estimate of how many photons are entering the NPI aperture at different readings of the beam monitor (the scaling factor turned out to be $k = 386$). This is only a rough estimation, in which the beam map in Fig. 7 has been approximated to a linear rise, a plateau and linearly decrease. During the measurements a common beam monitor reading was $C_{bm} = 18$ kHz. Applying our rather gross approximation gives a number for the estimated count rate of the NPI when the beam is pointed into an aperture:

$$R_{UV} = C_{bm} k \varepsilon = (18 \cdot 10^3) \times (386) \times (10^{-6}) = 7 \text{ s}^{-1}$$

The linearity of the UV response is important to understand the UV contamination measured in space.

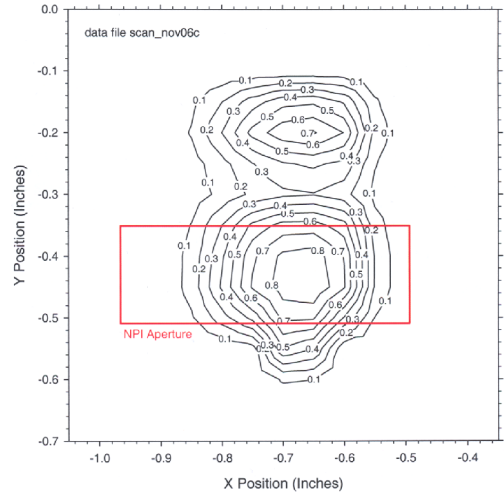


Figure 7: The measured beam map with the aperture used during the UV calibration of VEX NPI.

Table 7: Recorded count rate for different intensities.

$R_{BeamMonitor}$ [kHz]	I [s^{-1}]	C_{NPI} [s^{-1}]
3.4	$1.4 \cdot 10^6$	5.5
9.0	$3.5 \cdot 10^6$	18.0
18.0	$6.9 \cdot 10^6$	31.9

If we know that the response is more or less linear within certain intensities we can scale the response against what is present in space to determine how much Sun contamination we can expect. Measurements were made at three different L_α intensities. The beam monitor read out, UV intensity and NPI count rate recorded are in Table 2 and the result is shown in Fig. 10a.

It is also important to know what the UV response is at different incident angles to an NPI aperture. The angular scan reveals how wide the UV response is, but also if there are any reflections off of the deflection plates or the spokes in the deflection system that can reach the MCP. Because of limited space and the movement of the control yoke in the calibra-

tion tank, the angular scan was made with respect to the aperture plane of the NPI (sector 4). We should thus expect not to see any counts in any other sector than number 4. If we do, this must be a result of internal reflections since all photons from the beam is directed into sector 4 for all angles. The result of the angular scan is shown in Fig. 8 and listed in Table 8.

The response to L_α photons in sector 4 response of other sectors was measured only in the center-aperture of each sector. The geometry of the calibration tank allowed only six sectors to be measured at a time. Then the vacuum had to be broken and the NPI remounted. Measurements of all 32 sectors required six remountings with pumping time in between. The relative measurements was thus a rather lengthy process. The beam intensity varied somewhat between mountings. The intensity is compensated for in Fig. 9. Compensation is based on continuous beam monitor read outs during the measurements.

Fig 10b shows the sum of all counts during the angular scan in alla sectors. There are visible counts in sectors 3,4,and 5. However, the total count into the neighboring sectors are less than ten percent of that in sector 4.

To ensure that there are no reflections from the spokes of sectors other than the sector in the direction of the UV source a translation measurement was made. Sector aperture number 4 was centered on the UV beam and the NPI was then horisonally translated according to Fig. 10c. The space in the tank limited the translation to less than the full diameter of the NPI. However, reflections from aperture spokes further away than the translation range is highly unlikely as it would require a multitude of reflections to reach even the target block. The resulting count in sector 4 is shown in Fig. 10d.

In conclusion the UV efficiency of the VEX NPI sensor is around 10^{-5} .

Table 8: The data points of the angular response of UV for MCP bias 2430 V.

	-10	-8	-6	-4	-2	0	2	4	6	8	10
4	0.0000	0.0071	0.0000	0.0000	0.0357	0.0143	0.0071	0.0000	0.0071	0.0000	0.0071
2	0.0000	0.0000	0.0430	0.1434	0.4230	0.4158	0.1936	0.0860	0.0215	0.0143	0.0072
0	0.0000	0.0216	0.0504	0.4101	0.8705	1.0000	0.5540	0.1295	0.0216	0.0072	0.0000
-2	0.0000	0.0000	0.0361	0.2743	0.4187	0.5414	0.2888	0.0505	0.0072	0.0000	0.0072
-4	0.0000	0.0072	0.0000	0.0507	0.1376	0.1087	0.0797	0.0072	0.0000	0.0072	0.0000
-6	0.0000	0.0073	0.0073	0.0073	0.0073	0.0073	0.0000	0.0073	0.0145	0.0000	0.0073

Table 9: Response (measured count/s) to UV for all sectors relative to the response of sector 4.

Sector	0	1	2	3	4	5	6	7	8	9	10
Relative sensitivity	1.18	0.84	1.014	1.03	1.00	0.88	0.53	0.54	0.78	0.69	0.84
Sector	11	12	13	14	15	16	17	18	19	20	21
Relative sensitivity	0.77	0.77	0.62	0.88	0.00	0.00	1.00	0.87	0.77	0.84	0.74
Sector	22	23	24	25	26	27	28	29	30	31	
Relative sensitivity	0.67	0.50	0.68	0.57	0.81	0.98	0.96	1.05	0.93	1.50	

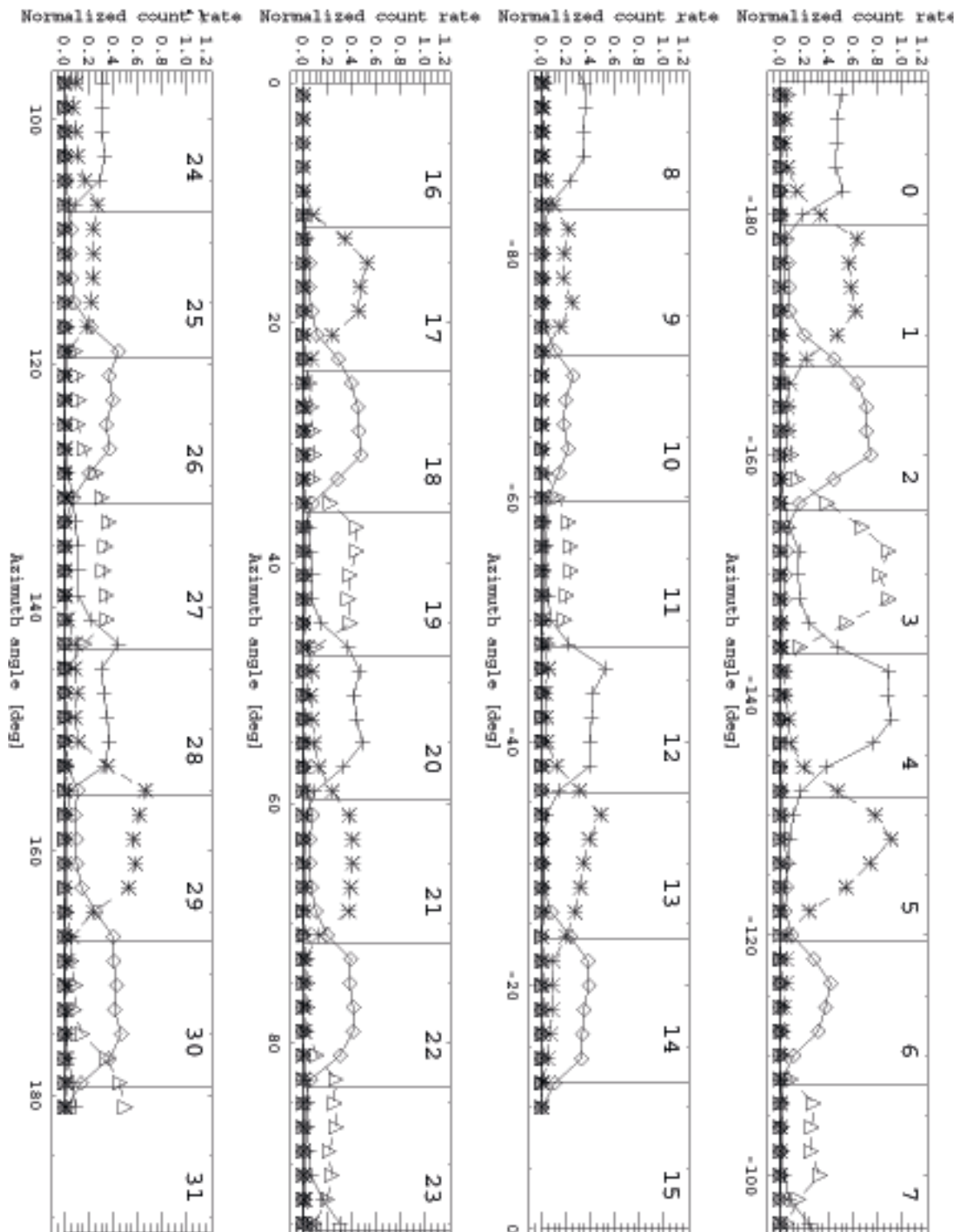


Figure 5: 360° azimuth scan of normalized sector response. The sector numbers are displayed. Measurement was made with MCP bias of 2300 V and a deflector voltage of 1000 V.

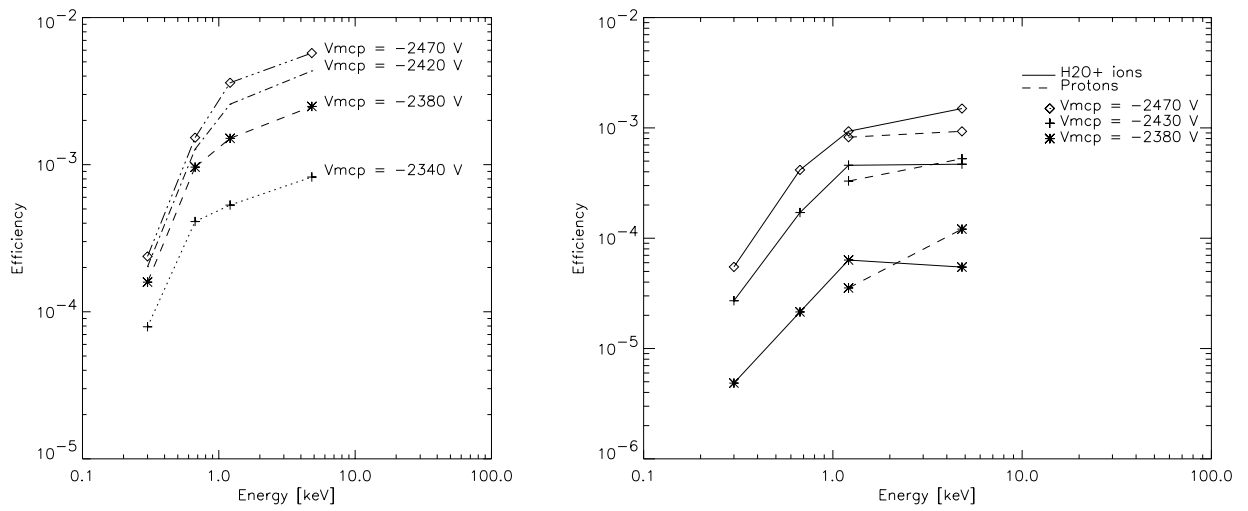


Figure 6: (Left) Efficiency using H_2O^+ ions with neighboring sectors open. (Right) Efficiency using H_2O^+ and H^+ ions with neighboring sectors mechanically blocked.

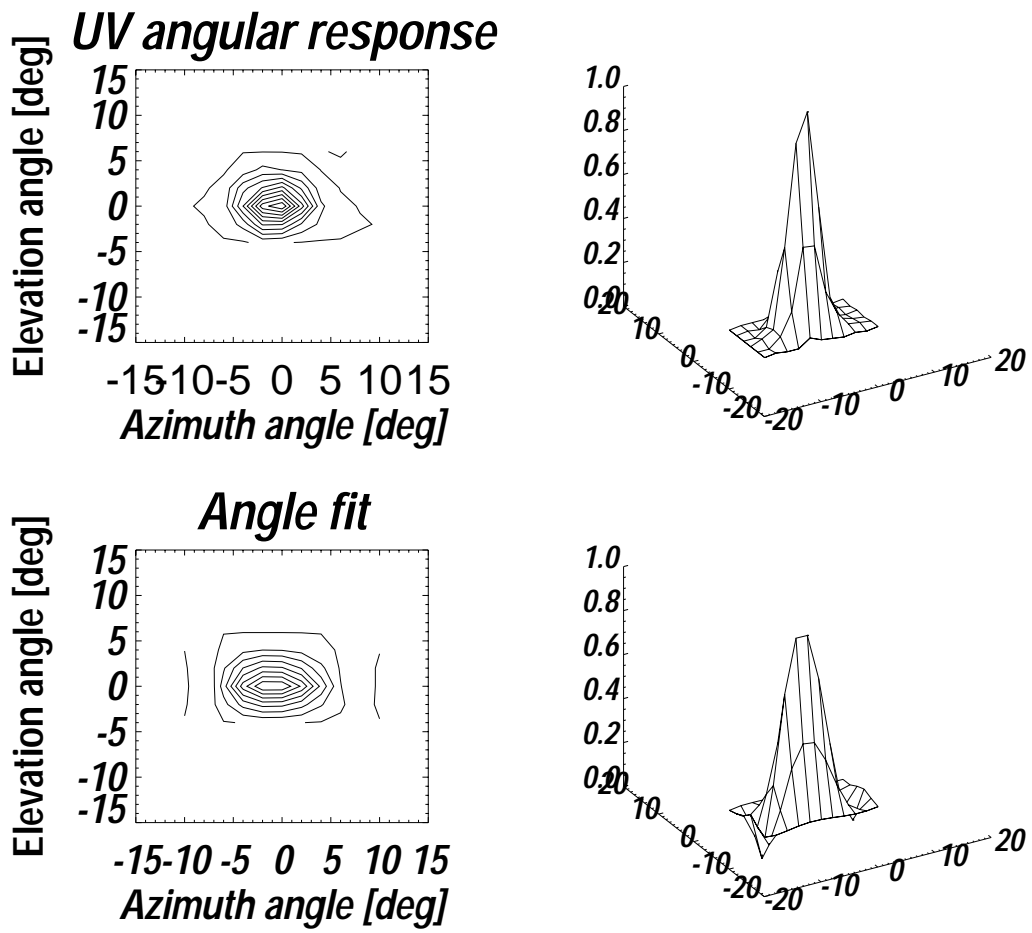


Figure 8: Angular scan of sector 4.

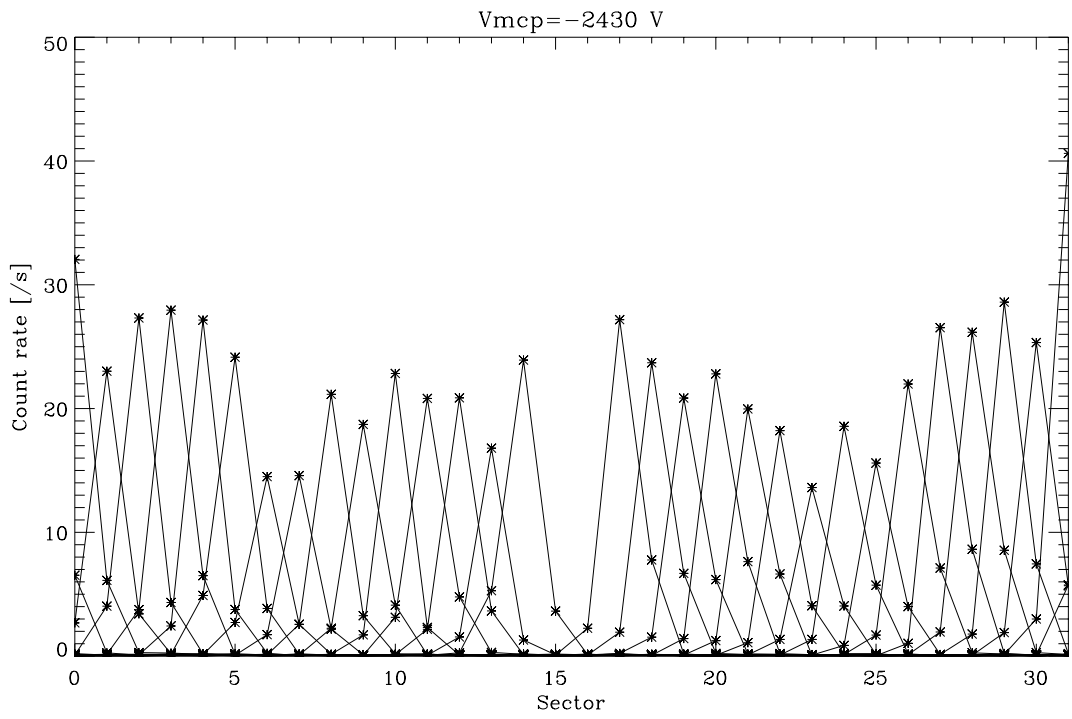
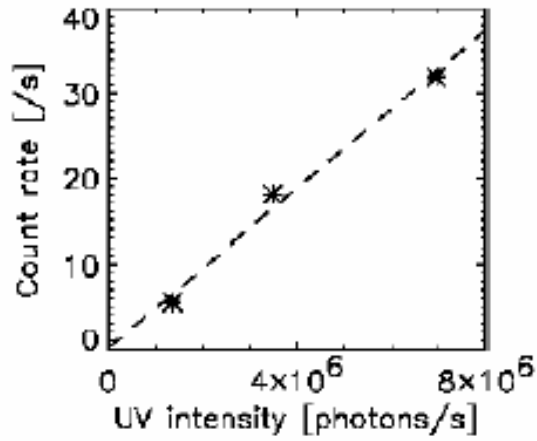
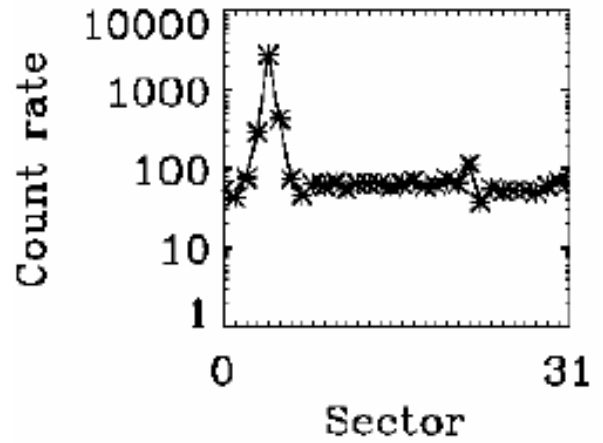


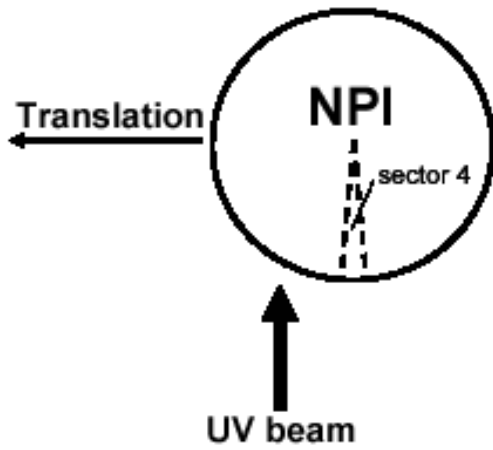
Figure 9: Response with the UV beam directed into the centers of all sectors.



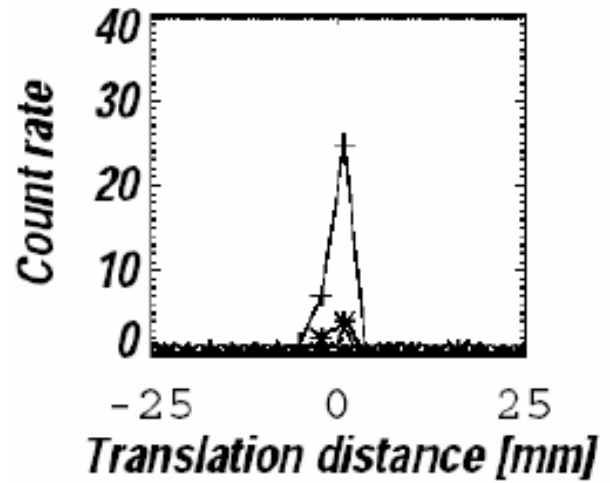
a



b



c



d

Figure 10: (a) UV intensity versus the NPI count rate. (b) The total sum of the angular scans. (c) Translation measurement set up with $\Delta x = 3$ mm. (d) Count during translation measurement.



ASPERA-4



**Venus
Express**

Reference : **VE-ASP-CR-050530**
Issue : **1** Rev. : **1**
Date : **2005-05-30**
Volume : **-** Page: **6**

APPENDIX 2. NPD CALIBRATION REPROT

Calibration report on NPD1 / NPD2 ASPERA-4
Venus-Express
Ver 1.0

A. Grigoriev, S. Barabash, A. Fedorov

May 24, 2005

Contents

1	NPD general description	4
2	NPD calibration setup. Coordinate system. Technical details.	4
2.1	Technical details	4
2.2	Calibration facilities	7
2.3	Calibration setup	7
2.4	Calibration plan	9
3	Calibration of the VEX NPD1 / NPD2 Flight Models.	10
3.1	MCP characterization	10
3.2	Efficiency	11
3.2.1	Results	11
3.2.2	Measurements process	15
3.3	Angular response of NPD sensor	20
3.4	Geometrical Factor calculation	20
3.5	ToF spectra	24
3.6	Energy resolution	25
3.7	Heater and temperature sensor.	28
3.8	Noise	28

List of Tables

1	NPD1 efficiencies in dependency on ion mass and energy and direction.	13
2	NPD2 efficiency	13
3	Table shows the values of elevation and azimuthal correction coefficients for each of NPD1 detectors.	16
4	Table shows the values of elevation and azimuthal correction coefficients for each of NPD2 detectors.	16
5	Table shows the correction koefficients K_1 and K_2 which describes the pinhole normal declination from the ion beam direction for NPD1 and NPD2 detectors.	19
6	Correction koefficients K_{meas} to correct efficiency calculations for both NPD1 and NPD2 sensors.	19
7	Table shows the geometrical constants of all detectors of NPD1 and NPD2 instruments	24
8	Table shows the NPD1 sensor geometrical factor G dependency on ion species mass and energy.	24

9	Table shows the NPD2 sensor geometrical factor G dependency on ion species mass and energy.	24
---	---	----

List of Figures

1	The principle design of NPD sensor.	5
2	The Instrument directions definition.	6
3	The Instrument's cross section.	7
4	NPD calibration mechanical set up.	8
5	The count rates of Start, Stop0, Stop1, Stop2 detectors (MCP) in dependency on MCP bias for NPD1 (left panel) and NPD2 (right panel) are shown.	10
6	The figure shows the NPD1 sensor absolute efficiency curves in dependency on ions mass and energy for different directions.	12
7	The figure shows the NPD2 sensor absolute efficiency curves in dependency on ions mass and energy for different directions.	14
8	The upper part of the figure shows a scan procedure for NPD sensor during calibration. The lower rectangulars show the pinhole open area in dependency on azimuthal and elevation angles.	17
9	The figure shows the beam images as its are seen by NPD sensor.	18
10	Angular response of the NPD1 sensor. The left column shows the measured 2D angular response for all directions Dir0/Dir1/Dir2. The middle column consists of curves of angular response integrated over the elevation angle. The right column shows the curves of the angular response integrated over the azimuthal angle.	21
11	Angular response of the NPD2 sensor. The left column shows the measured 2D angular response for all directions Dir0/Dir1/Dir2. The middle column consists of curves of angular response integrated over the elevation angle. The right column shows the curves of the angular response integrated over the azimuthal angle.	22
12	The figure shows the TOF discription curves for NPD1 dir1 for H in dependency on beam energy	25
13	The figure shows the TOF discription curves for NPD1 dir1 for O in dependency on beam energy	26
14	The figure shows the TOF dependency on beam energy of different ion species (H^+ , O^+) for direction 1	27

1 NPD general description

- NPD sensor is developed for VenusExpress mission ASPERA-4 experiment
- Calibrated: 2004
- Launch date October, 2005 (launch to Venus)
- Integrated into ASPERA-4. NPD1 - closer to the Digital Processing Unit (DPU), NPD2 - outermost one.

Neutral Particle Detector (NPD) developed for the ESA Mars-Express and Venus-Express missions is a compact low weight (650g) high efficiency sensor to image low Energy Neutral Atoms (ENA) resulted from the solar wind interaction with the Martian exosphere. NPD provides measurements of the ENA differential flux over the energy range 100 eV - 10 keV resolving H and O with a coarse $5 \times 30^\circ$ angular resolution and total efficiency $1 \div 50\%$. The sensor consists of two identical detectors each with a $9 \times 90^\circ$ intrinsic field of view placed on a scanning platform which performs 180° scans to cover a hemisphere. The measurement principle is based on surface interaction technique.

Principle design of the NPD sensor, see Figure 1

ENA incident on a start surface at a grazing angle of 15° are reflected under approximately a mirror angle and cause secondary electron emission in the Start Surface. The secondary electrons are transported to an Start MicroChannel Plate (MCP) assembly, which gives the START signal. The reflected ENA hit the stop surface and again produce the secondary electrons used to generate the STOP signal in the Stop MCP assembly. The Time-of-Flight (TOF) measurements give ENA velocity, the STOP signal is also used to identify mass (H or O). Coincidence technique as well as properties of the START and STOP surface coating provide Ultra-Violet (UV) suppression to the level sufficient to achieve the required signal-to-noise ratio.

2 NPD calibration setup. Coordinate system. Technical details.

2.1 Technical details

As it is seen on the Figure 1, the sensor has 3 detectors in the azimuthal plane. The detector directions definition are presented on the Fig. 2. The basic position of the NPD sensor, integrated into ASPERA-4 is such, that its long side is placed in the horizontal

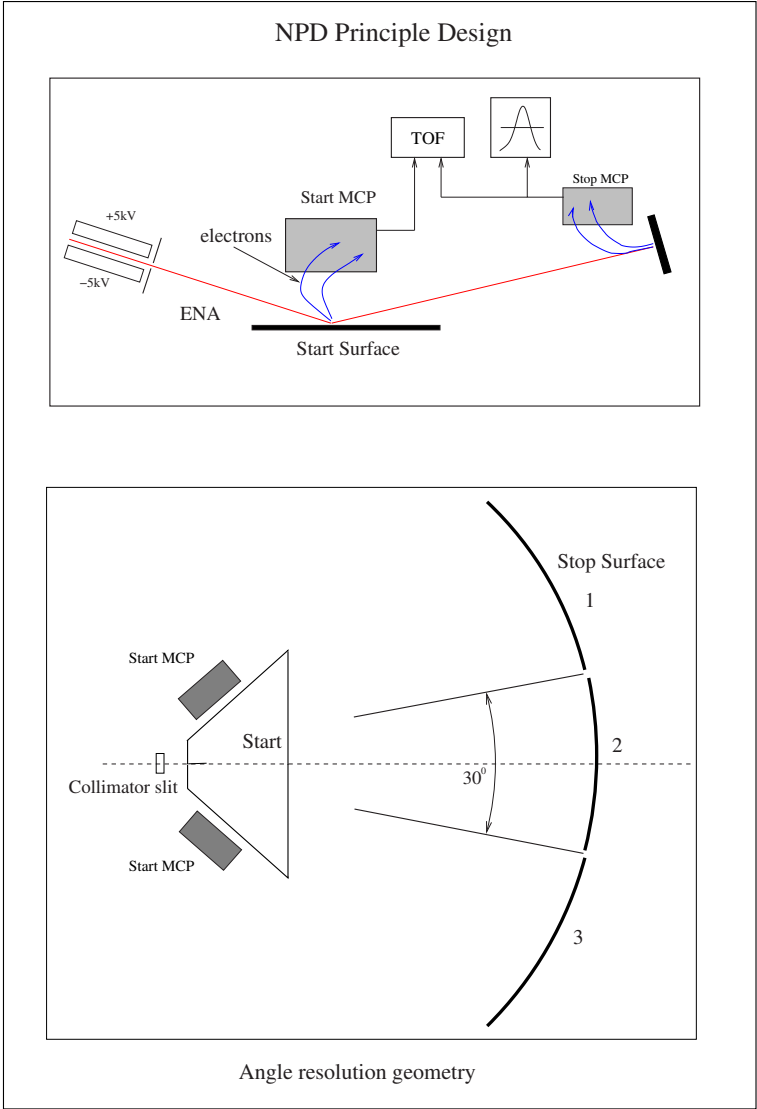


Figure 1: The principle design of NPD sensor.

plane, along the scanner platform. While scanning it will scan in the NPD's elevation plane.

Figure 2 describes the directions of view of each of NPD detectors. The "zero" direction is set to correspond to the detector placed in the vertical plane, which is along the short side of the chassi. The direction 2 corresponds to the detector placed in the horizontal plane with the pinhole position. The detector 1 is the detector in-between the 0 one and the number 2.

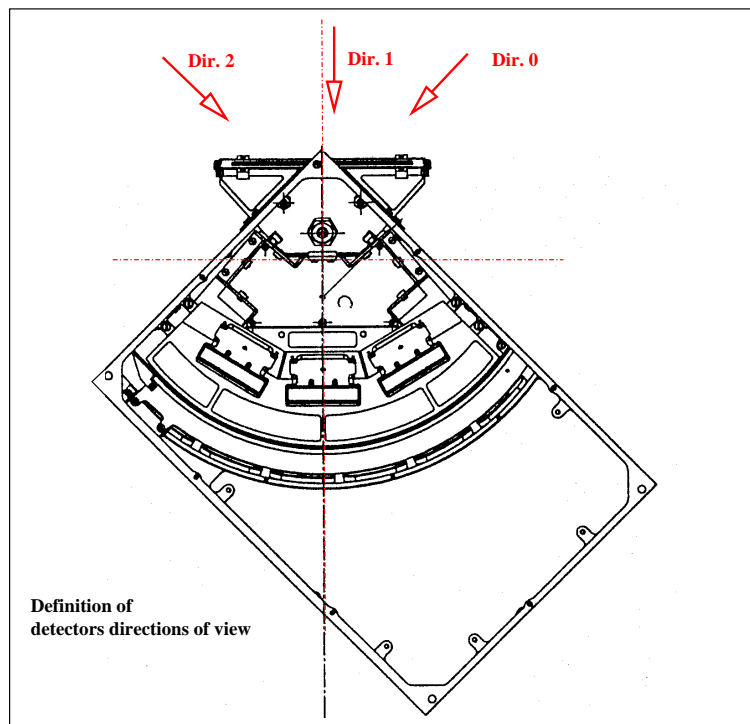


Figure 2: The Instrument directions definition.

The cross-section of the sensor along the plane "pinhole – Detector 1" is shown on Figure 3. The deflector is declined on 15° from the Start Surface plane. The incoming beam comes through the collimator slit, between deflector electrodes, through a pinhole and incident on a Start Surface. The collimator slit has dimensions $4.5 \times 70.0 \text{ mm}^2$. The distance between deflector electrodes is 4.5 mm . They are biased with $+/- 5 \text{ kV}$ to deflect charged particles with energy less than the deflector energy cut-off 60 keV . Deflector provides field of view of the sensor $9^\circ \times 90^\circ$. Pinhole has dimensions $3.0 \times 4.5 \text{ mm}^2$. On the sensor cross-section on the Figure 3 Deflector, Start Surface, Stop Surface and the middle Stop MCP detector are clearly seen.

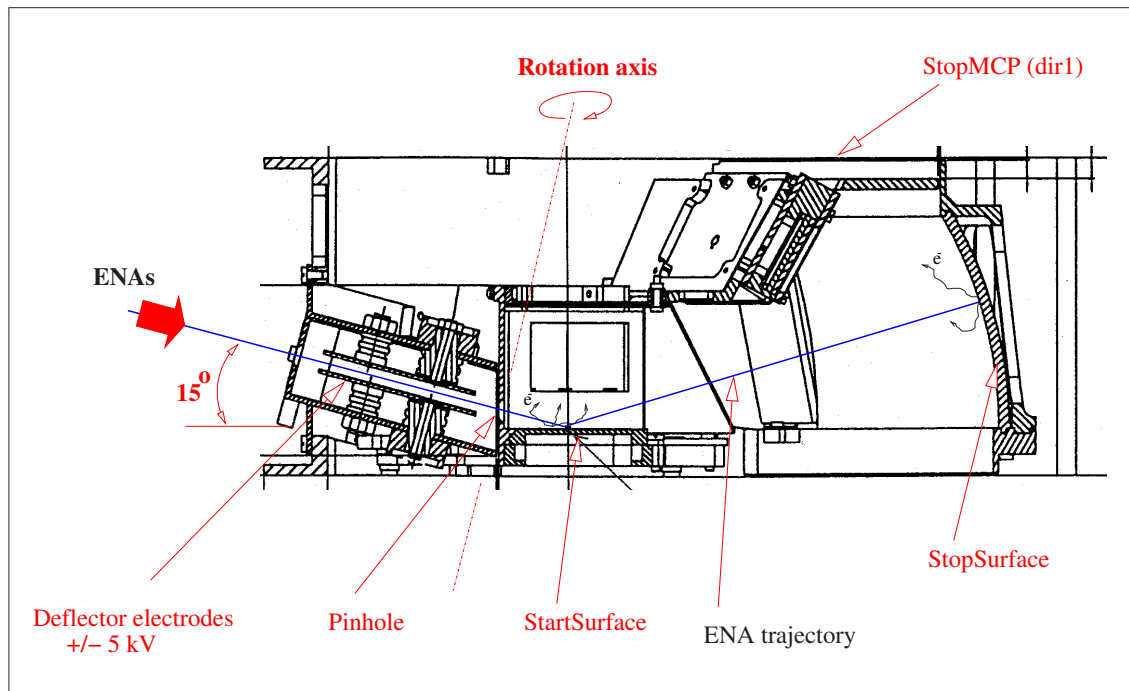


Figure 3: The Instrument's cross section.

2.2 Calibration facilities

Each NPD sensor has been calibrated in the Swedish Institute of Space Physics (IRF, Kiruna).

2.3 Calibration setup

Each sensor has been calibrated in a stand-alone configuration.

On the Figure 4 NPD calibration mechanical setup is shown. NPD is placed into the vacuum chamber on the turntable at the distance $\sim 1.7m$ from the output aperture of the ion beam source. It can be swept in both azimuthal and elevation directions in the wide range of angles, $> 90^\circ$ in both directions with an accuracy better than 1° . Also the turntable can be translated across the incident beam in the vertical and horizontal directions to align the sensor's aperture and the ion beam. The ion source aperture diameter is 36 mm.

A Faraday cup is used to measure the ion beam intensity. As the Faraday cup entirely covers the aperture it is not possible to monitor the ion beam intensity continuously. The beam intensity is measured before and after measurement cycle. The system produces quite stable ion beam with intensity variation time scale larger than a measurement cycle. During the calibration period the parallel ion beam is to be used. But sometimes to de-

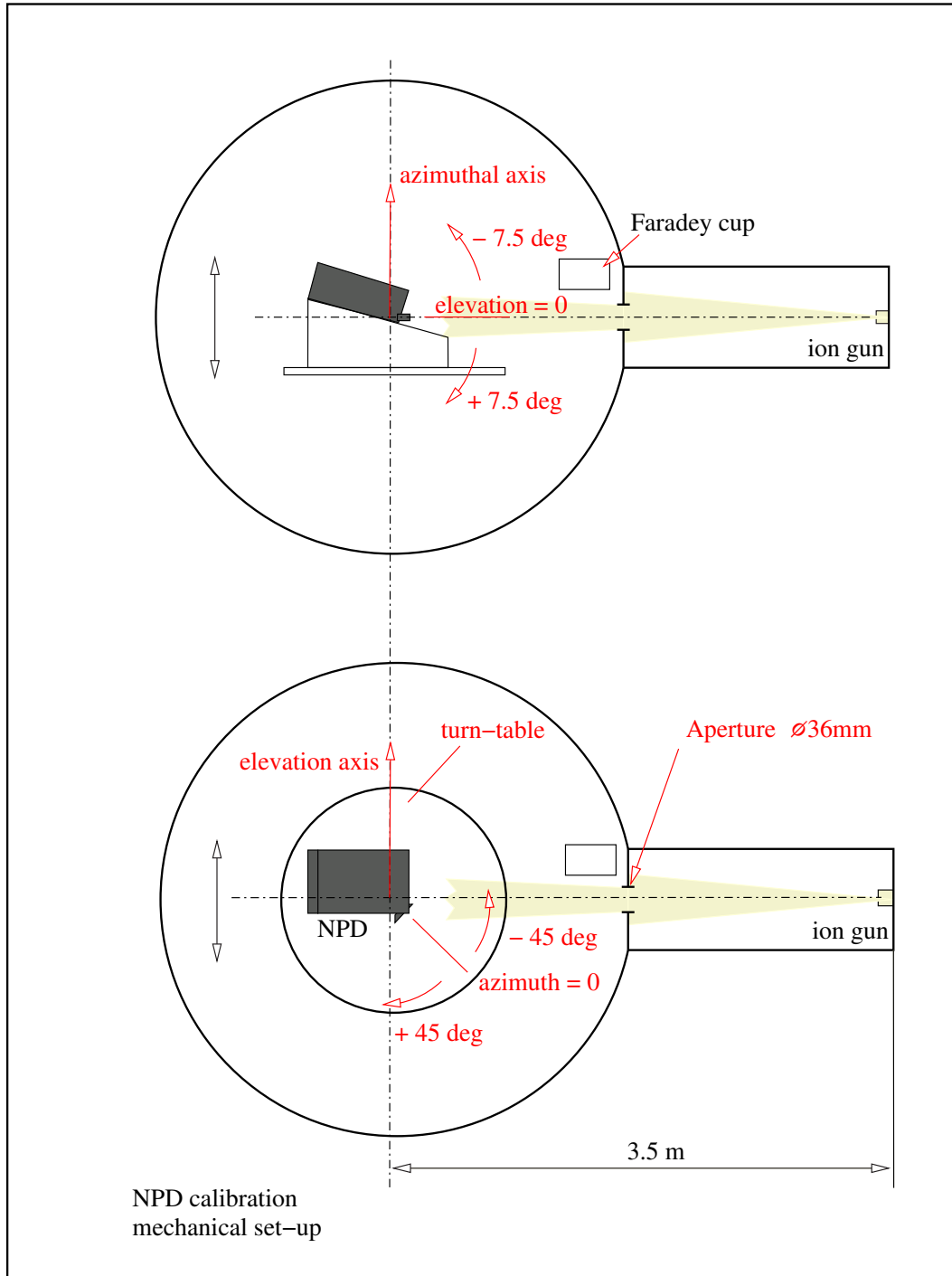


Figure 4: NPD calibration mechanical set up.

crease its density or to make a beam profile smoother (means more homogenous ion beam) the ion beam focusing/defocusing could be done. The maximum beam divergence is estimated to be less than 2%. Therefore the ion beam spot at the NPD location can vary about 36 to 60 mm in cross section. The scanning across the ion beam spot procedure is invented to take the ion beam spot diameter variation into account. The procedure is describe in details later on.

Sensor calibration is done under next conditions:

- Beam intensity in general case is set to keep a count rate on the StartMCP about $(1 \div 3) \times 10^3$ count/sec.
- Integration time: 1 sec
- Deflector electrodes are grounded. So the sensor is calibrated using the charged ion beam. It is done to provide the proper beam current. Note: the neutral part of the ion beam is about a few percent of the initial beam current. The results are comparable with the measurements with ENA beam.
- The pressure in the vacuum chamber was kept approximately 4×10^{-7} mbar

During the measurements NPD sensors produced data in RAW and BIN matrix modes. Details about NPD modes can be found in '*DigTOFinASPERA/NPD*' document (see '*NPD_description03.pdf*').

2.4 Calibration plan

In order to get the relative and absolute characteristics of the instrument the next calibration procedure has been developed:

1. MCP characterization to obtain the nominal bias.
2. Efficiency measurements.
3. Angular response measurements.
4. Geometrical Factor calculation.
5. TOF distributions and Pulse Height (PH) distributions analysis.
6. Energy and Mass resolution.
7. Heater test. Temperature sensor response.
8. Noise of the NPD sensors integrated with ASPERA-4 instrument.

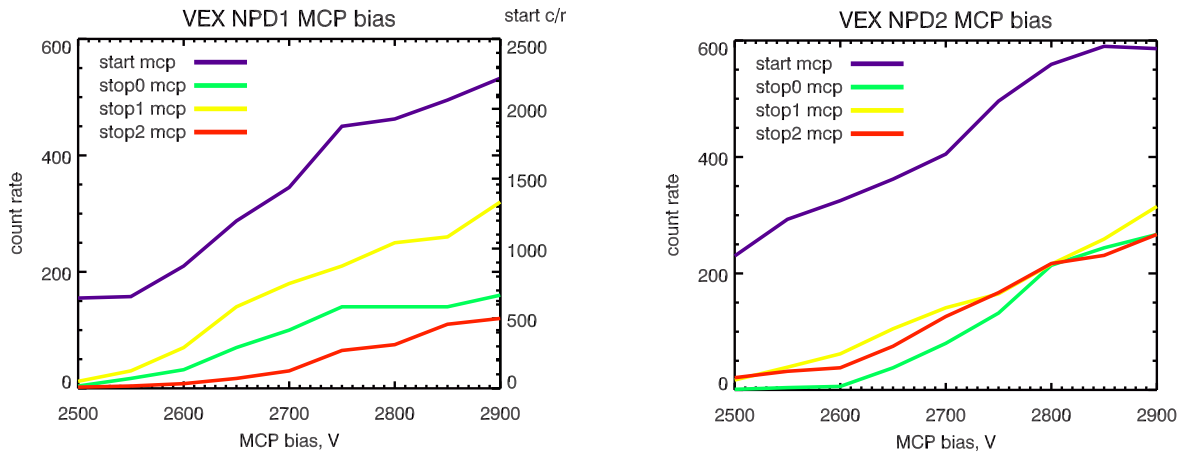


Figure 5: The count rates of Start, Stop0, Stop1, Stop2 detectors (MCP) in dependency on MCP bias for NPD1 (left panel) and NPD2 (right panel) are shown.

3 Calibration of the VEX NPD1 / NPD2 Flight Models.

Calibration of NPD units has been done in order to estimate the different parameters of the sensor, such as efficiency, geometrical factor, angular and energy resolution. The calibration results fully correspond to the specified performance.

3.1 MCP characterization

To find out the nominal bias for all detectors the MCP characterization is done for the next conditions:

- Ion beam:
 - > Species: H_2O^+ ions
 - > Energy: 5 KeV
 - > Intensity: Beam intensity is set to keep count rate on Start MCP about $\sim (1 \div 3) \times 10^3$ count/sec
- The MCP bias range 2.3 to 2.9 kV. Count rate measurement at every 50 V steps
- Integration time: ~ 1 sec
- The full count of Start and Stop counters without TOF validation is taken into account

Figure 5 shows the count rates of Start, Stop0, Stop1, Stop2 detectors (MCP) in dependency on MCP bias for both NPD1 (left panel) and NPD2 (right panel). The count of counters without TOF correlation is presented. Start, Stop0, Stop1, Stop2 counters are color-coded by dark-blue, green, yellow and red colors correspondingly.

NPD1

Calibration of the NPD1 sensor is done at nominal bias voltages on MCP detectors. Nominal Start MCP bias is set to 2750V, Stop MCP bias is set to 2750 V. MCP gain degradation compensation margin is about 250 V.

NPD2

Calibration of the NPD2 sensor is done at nominal bias voltages on MCP detectors. Nominal Start MCP bias is set to 2800V, Stop MCP bias is set to 2800 V. MCP gain degradation compensation margin is about 200 V.

3.2 Efficiency

3.2.1 Results

The absolute efficiency of the NPD1 and NPD2 sensors is measured during the calibration process. Measurements are done for the different ion species H and O, for a set of ion beam energies 0.1 to 10.0 KeV, for every NPD direction.

The efficiency of the NPD1 and NPD2 sensors for different ion mass, energy and for every direction are shown in the Table 1 and Table 2 correspondingly. – means no data.

Efficiency graphs for NPD1 and NPD2 are presented on Figure 6 and Figure 7.

Least-square polynomial fit of a next function 1 is performed.

$$\varepsilon = \exp\left(\sum_{k=0}^3 a_k \cdot \ln^k(E)\right) \quad (1)$$

where

ε – efficiency

E – ion energy, KeV

a_k – coefficients

Function to calculate NPD efficiency is valid within the next energy range: 0.1 to 5.0 KeV for H and 0.3 to 10.0 KeV for O.

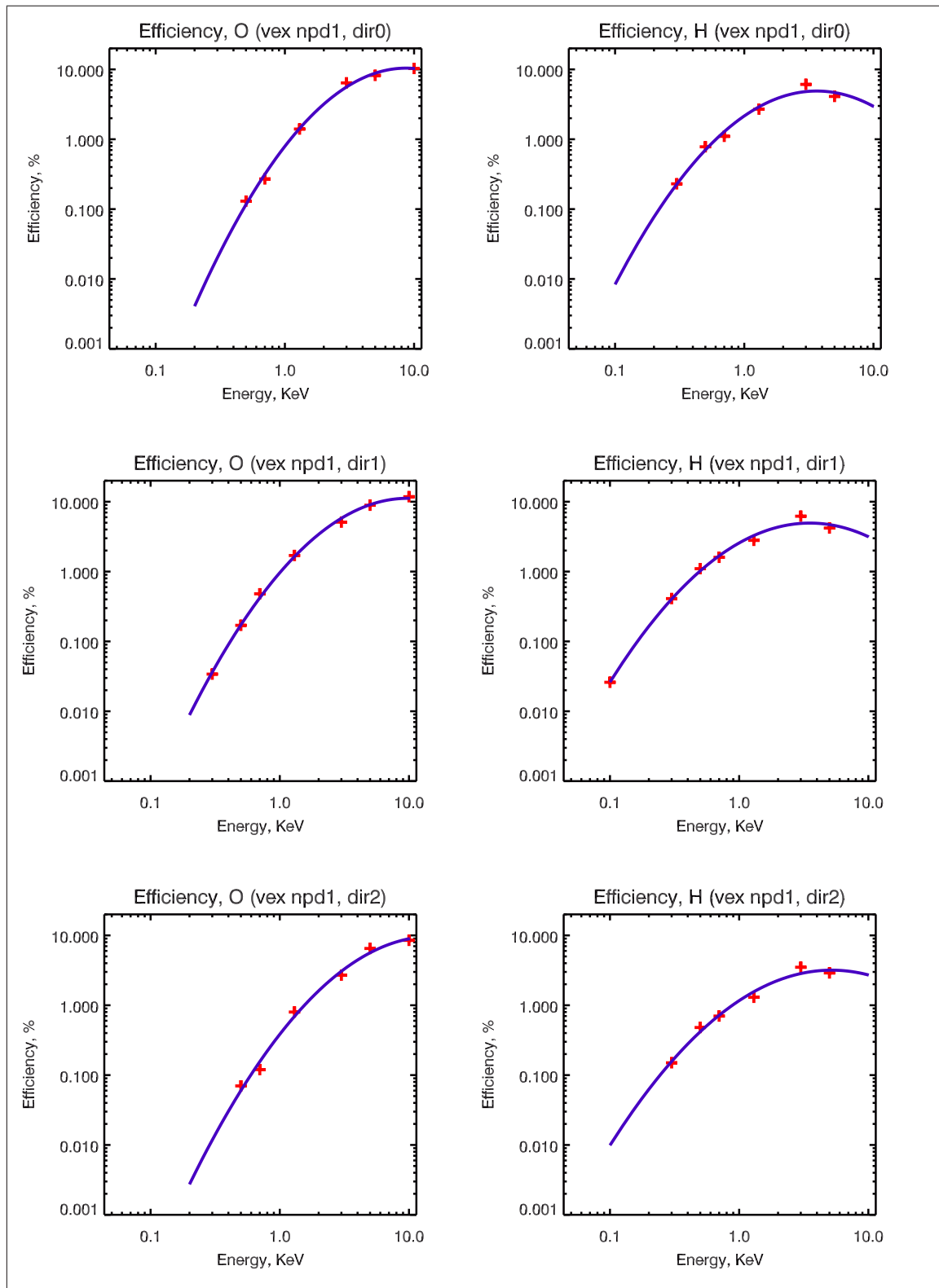


Figure 6: The figure shows the NPD1 sensor absolute efficiency curves in dependency on ions mass and energy for different directions.

		$\varepsilon, \%$							
	E, KeV	10.0	5.0	3.0	1.3	0.7	0.5	0.3	0.1
O^+	Dir0	10.3	8.2	6.4	1.4	0.27	0.13	—	—
	Dir1	11.8	8.9	5.1	1.7	0.48	0.17	0.034	—
	Dir2	8.5	6.5	2.7	0.8	0.12	0.07	—	—
H^+	Dir0	—	4.1	6.1	2.7	1.1	0.78	0.23	—
	Dir1	—	4.2	6.2	2.8	1.6	1.1	0.41	0.026
	Dir2	—	2.9	3.5	1.3	0.7	0.48	0.15	—

Table 1: NPD1 efficiencies in dependency on ion mass and energy and direction.

		$\varepsilon, \%$						
	E, KeV	5.0	3.0	1.3	0.7	0.5	0.3	0.1
O^+	Dir0	6.63	4.5	0.85	0.15	0.037	0.005	—
	Dir1	6.1	4.6	0.95	0.25	0.08	0.014	—
	Dir2	10.7	8.9	2.2	0.49	0.14	0.019	—
H^+	Dir0	3.6	3.4	1.62	0.59	0.31	0.092	—
	Dir1	3.9	3.6	2.1	0.86	0.48	0.16	0.013
	Dir2	6.0	6.3	3.4	1.55	0.82	0.3	—

Table 2: NPD2 efficiency

Table shows the NPD2 efficiencies in dependency on ion species and energy and direction

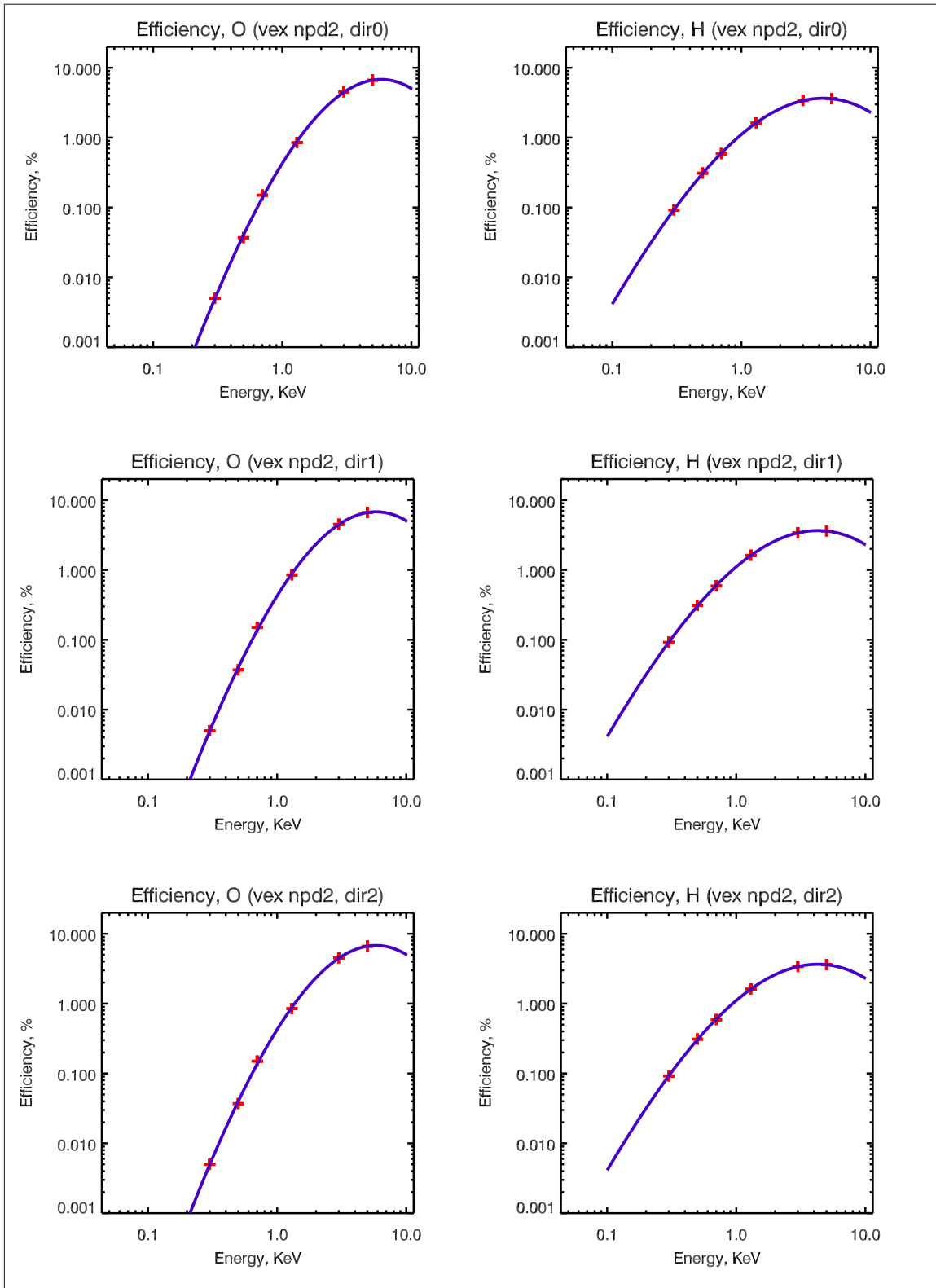


Figure 7: The figure shows the NPD2 sensor absolute efficiency curves in dependency on ions mass and energy for different directions.

3.2.2 Measurements process

Absolute efficiencies had been calculated using BINning array data (coincidence flag equals 0).

NPD sensor efficiency depends on a set of factors such as ion species mass and energy, MCP bias voltage, azimuthal and elevation angles, so on.

Beam Energy: 10.0, 5.0 keV, 3.0 keV, 1.3 keV, 0.7 keV, 0.5 keV

Species: H^+ , H_2O^+

Direction: Dir0, Dir1, Dir2

To measure the sensor's absolute efficiency the next conditions should be fulfilled:

- Count rate measurement at α_0, β_0 - angles at which the detectors count rate has a maximum value.
- Ion beam is parallel and stable
- Ion beam spatial distribution is homogeneous.
- MCP bias voltage is stable.

The default position of NPD sensor during efficiency measurements is $\alpha = 0, \beta = 0$. But as it is seen from angular response measurements, the maximal count rate is achieved at $\beta_e = 1.5^\circ$. The ratio between detector's count rate at α, β : $C(\alpha, \beta)$ and count rate at α, β_e : $C(\alpha, \beta_e)$ is K_e :

$$K_e = \frac{C(\alpha, \beta_e)}{C(\alpha, \beta)}$$

where

K_e - elevation coefficient

The efficiency values are to be corrected by using the K_e coefficient.

Measurements by the detector Dir1 are performed at $\alpha = 0^\circ$. Measurements by the directions Dir0 and Dir2 are performed at $\alpha = +/-40^\circ$ for NPD1 and $\alpha = +/-35^\circ$ for NPD2 (see Figure 4). For the azimuthal angle α equal to 45° , count rate drops drastically. The maximum azimuthal response is achieved with the next α angles:

Dir0 $\alpha_a = -35^\circ$

Dir1 $\alpha_a = 0^\circ$

Dir2 $\alpha_a = +35^\circ$

The ratio between detector's count rate at α, β : $C(\alpha, \beta)$ and count rate at α_a, β : $C(\alpha_a, \beta)$ is K_a :

$$K_a = \frac{C(\alpha_a, \beta)}{C(\alpha, \beta)}$$

where

K_a - azimuthal correction coefficient

The efficiency values are to be corrected by using the K_a coefficient also.

The table 3 and table 4 show the values of elevation and azimuthal correction coefficients for each of NPD sensors.

NPD1	K_e	K_a
<i>Dir0</i>	1.0	1.0
<i>Dir1</i>	1.0	1.0
<i>Dir2</i>	1.0	1.0

Table 3: Table shows the values of elevation and azimuthal correction coefficients for each of NPD1 detectors.

NPD2	K_e	K_a
<i>Dir0</i>	1.0	1.0
<i>Dir1</i>	1.0	1.0
<i>Dir2</i>	1.0	1.0

Table 4: Table shows the values of elevation and azimuthal correction coefficients for each of NPD2 detectors.

To minimize the ion beam not uniform spatial distribution effect on efficiency measurements all ion beam particles have been counted by performing the scan of the area larger than the ion beam spot at the NPD location. Scan procedure is shown on Figure 8. First of all by scanning along x-axis and/or y-axis beam borders had been found. Meanwhile it was checked if beam is homogeneous. Beam profile could be tuned if necessary. Sensor was translated along the vertical and horizontal axes by steps $dV = 3.0\text{mm}$, $dH = 4.5\text{mm}$. Pinhole zigzagged covering the spot area A equals to:

$$A = 60 \times 63\text{mm}^2$$

Pinhole should cover whole beam spot area, therefore steps are chosen according to the pinhole sides lengths. This is valid for all sensors and every direction. The integration time at each measurement point is about 1 sec. Figure 9 shows the number of beam profile images got by the instrument for different ion masses and energy by sensor's detector *Dir1*. Finally the integral count rate is calculated. Beam intensity was checked before and

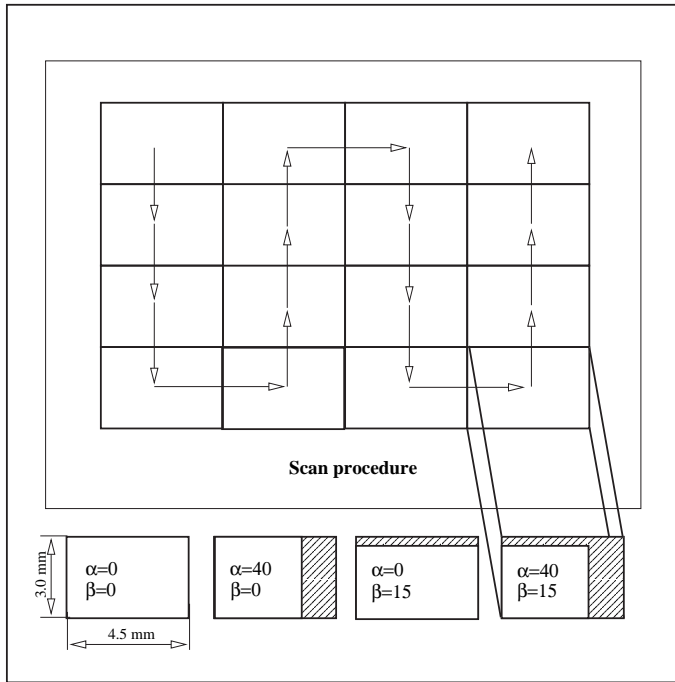


Figure 8: The upper part of the figure shows a scan procedure for NPD sensor during calibration. The lower rectangulars show the pinhole open area in dependency on azimuthal and elevation angles.

after each scan. If beam intensity values has been different arithmetic mean was taking into account. Then efficiency has been calculated according to the Equation 2:

$$\varepsilon = \frac{C \cdot q_e}{J \cdot T_{int}} \quad (2)$$

where

ε - calculated efficiency,

C - measured integral count rate, $\frac{1}{sec}$

q_e - electron charge,

T_{int} - integration time, s

J - beam intensity, A

Also it is necessary to take into account the pinhole area during measurements. The pinhole area dependency on the azimuth and elevation angles is shown on the Figure 8 lower panel. The corresponding coefficients are shown in the Table 5.

- NPD is elevated on 15° , therefore the pinhole area is decreased by $K_1 = \frac{1}{\cos 15^\circ}$
- For $\alpha = \pm 40^\circ$ pinhole area is decreased by $K_2 = \frac{1}{\cos 40^\circ}$. For $\alpha = 40^\circ$ scan steps should not be changed, but we have to take into account covered pinhole area coeffi-

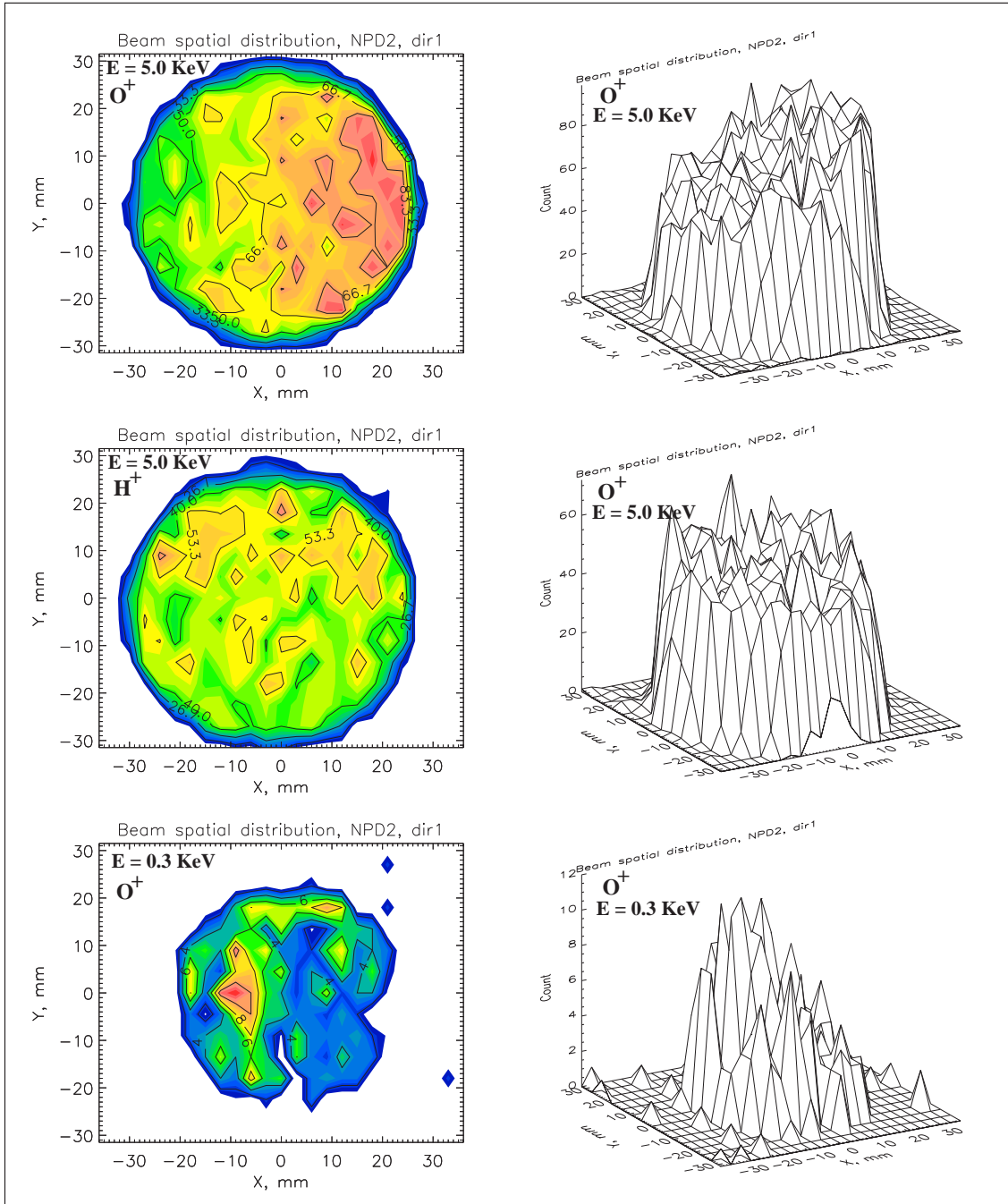


Figure 9: The figure shows the beam images as its are seen by NPD sensor.

cient K_2 to maintain the scan procedure. Otherwise it would require more steps for each scan, therefore much longer. In that case beam intensity long-time variations can take place.

	NPD1	NPD2
K_1	1.04	1.04
K_2	1.31	1.22

Table 5: Table shows the correction coefficients K_1 and K_2 which describes the pinhole normal declination from the ion beam direction for NPD1 and NPD2 detectors.

Finally the corrected efficiency formula is shown by Equation 3

$$\varepsilon_{corr} = \varepsilon \cdot K_{meas} \quad (3)$$

where

ε_{corr} – the corrected absolute efficiency of a detector

K_{meas} – efficiency correction total coefficient (equation 4)

$$K_{meas} = K_e \cdot K_a \cdot K_1 \cdot K_2 \quad (4)$$

where

K_1 - declination coefficient $1/\cos(15)$,

K_2 - (optional) pinhole open area coefficient for side directions,

K_e - elevation correction coefficient

K_a - azimuthal correction coefficient

In the table 6 the correction coefficient K_{meas} for both NPD1 and NPD2 sensors are presented.

	NPD1	NPD2
K_{meas}	1.36	1.27

Table 6: Correction coefficients K_{meas} to correct efficiency calculations for both NPD1 and NPD2 sensors.

The efficiency measurements has been done for the next ion beam settings:

- NPD1
 - Species: H_2O^+ ; Energy, KeV: 10.0, 5.0, 3.0, 1.3, 0.7, 0.5, 0.3
 - Species: H^+ ; Energy, KeV: 5.0, 3.0, 1.3, 0.7, 0.5, 0.3, 0.1
- NPD2
 - Species: H_2O^+ ; Energy, KeV: 5.0, 3.0, 1.3, 0.7, 0.5, 0.3
 - Species: H^+ ; Energy, KeV: 5.0, 3.0, 1.3, 0.7, 0.5, 0.3, 0.1

3.3 Angular response of NPD sensor

Angular response of sensor is obtained under the next conditions:

- The incident beam species: H^+
- The beam Energy: 5 KeV
- Azimuthal scan range -50° to $+50^\circ$ with step 5°
- Elevation scan range -7.5° to $+7.5^\circ$ with step 1.5°
- Exposition time at every point: ~ 1 sec

During the angular response measurements the valid count rate is measured. Valid count rate stands for the count of any Start MCP signal which is followed by a one of Stop detectors signal within the definite time window. In terms of data that type of count rate has a coincidence flag equal to 0.

Figures 10, 11 show the angular response of NPD1 and NPD2 detectors. The left column shows the measured 2D angular response for all directions Dir0/Dir1/Dir2. The middle column consists of curves of angular response integrated over the elevation angle. The right column shows the curves of the angular response integrated over the azimuthal angle. The Full Width on Half of Maximum (FWHM) of the curves is wider than the theoretical calculations. That can be explained by the properties of the Start surface. The Dir0 and Dir2 detectors peaks are sharp at the outermost sides, that is due to the geometrical constraints like position and shape of the baffles, placed between the Start Surface edges and the Stop surface edges. The elevation response curves are looking similar to each other, because they are defined by the deflector configuration (position of deflector electrodes). Table 7 show the geometrical constants G_0 of the instruments.

3.4 Geometrical Factor calculation

Geometrical factor of the instrument is an integral of the entrance effective area over solid angle as shown by Equation 5.

$$G = \int_{\theta} \int_{\varphi} A_{eff}(\theta, \varphi) \cos\theta d\Omega \quad (5)$$

In our case that formula looks as below (Equation 6):

$$G = \int_{\alpha} \int_{\beta} A_{eff}(\alpha, \beta) \cos\alpha d\alpha d\beta \quad (6)$$

where

$A_{eff}(\alpha, \beta)$ - effective area of the sensor's aperture, depends on both azimuthal and elevation angles

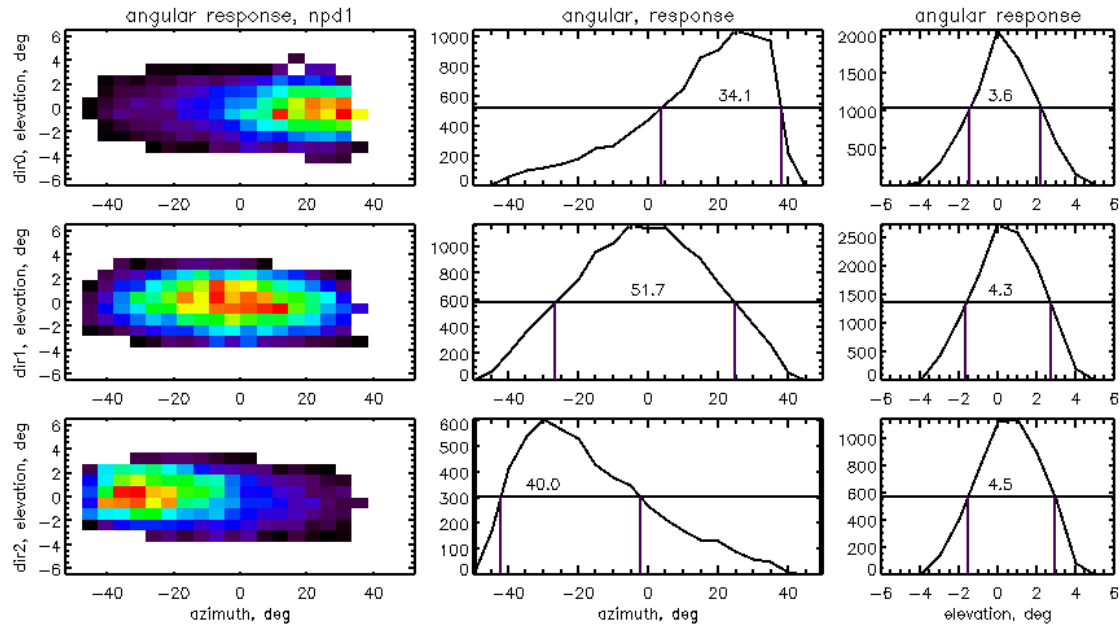


Figure 10: Angular response of the NPD1 sensor. The left column shows the measured 2D angular response for all directions Dir0/Dir1/Dir2. The middle column consists of curves of angular response integrated over the elevation angle. The right column shows the curves of the angular response integrated over the azimuthal angle.

α - azimuthal angle, deg

$d\alpha$ - displacement in an azimuthal plane, deg

β - elevation angle, deg

$d\beta$ - displacement in an elevation plane, deg

Effective area of a sensor's aperture is a measured count rate over ion beam density

$$A_{eff}(\alpha, \beta) = \frac{C(\alpha, \beta)}{P} \quad (7)$$

where

$C(\alpha, \beta)$ - sensor count rate (depends on azimuthal and elevation angle)

P - ion beam density, [$cm^{-2}s^{-1}$]

P can be expressed by ion beam current measured by a Faraday cup and ion source aperture area (Equation 8)

$$P = \frac{J}{q_e \cdot S_s \cdot t} = \frac{C_s}{S_s}, \quad (8)$$

$q_e = 1.6 \times 10^{-19} C$

J - Faraday cup current, A

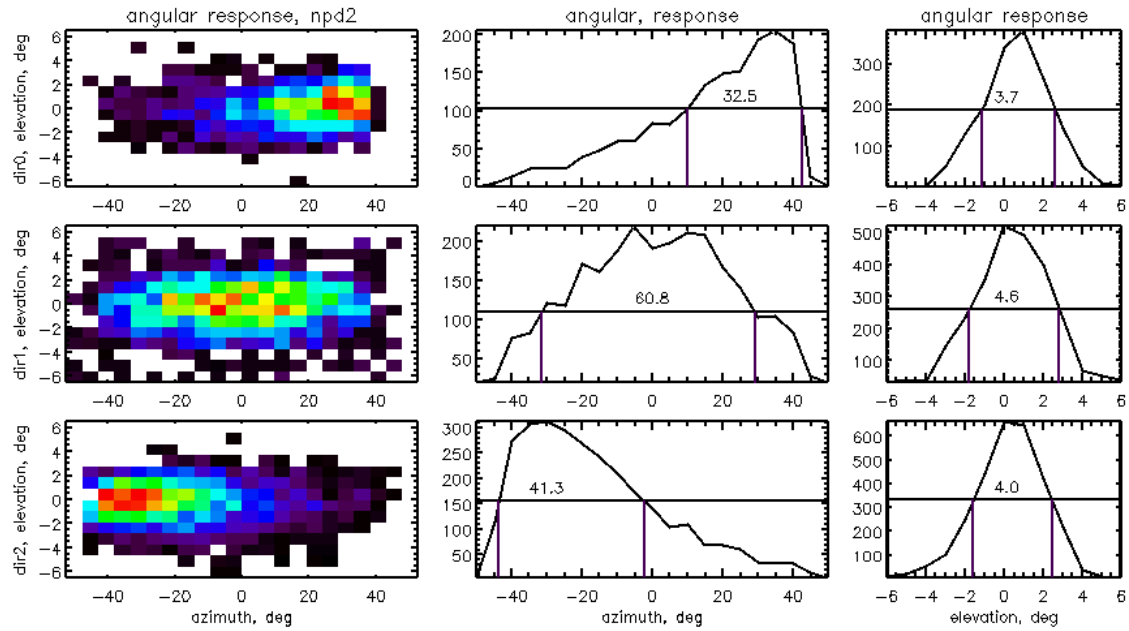


Figure 11: Angular response of the NPD2 sensor. The left column shows the measured 2D angular response for all directions Dir0/Dir1/Dir2. The middle column consists of curves of angular response integrated over the elevation angle. The right column shows the curves of the angular response integrated over the azimuthal angle.

$S_s = 10.18 \text{ cm}^2$ – ion source aperture area, cm^2

t – integration time, sec

C_s – ion source output count rate, s^{-1}

$$C_s = \frac{J}{q \cdot t}$$

Substitute A_{eff} for Equation 6

$$G = \int_{\alpha} \int_{\beta} \frac{C(\alpha, \beta)}{P} \cos \alpha d\alpha d\beta \quad (9)$$

P – a constant, so it goes out of an integral sign. Let's divide and multiply the Equation 9 by $C(\alpha_0, \beta_0)$

$$G = \frac{C(\alpha_0, \beta_0)}{P} \int_{\alpha} \int_{\beta} \frac{C(\alpha, \beta)}{C(\alpha_0, \beta_0)} \cos \alpha d\alpha d\beta \quad (10)$$

where

α_0, β_0 - azimuthal and elevation angles at which the count rate of a sensor is maximal for

the corresponding detector,

$C(\alpha_0, \beta_0)$ – sensor’s count rate, measured at the position (α_0, β_0)

Here an integral part of an Equation 10 is a constant G_0 describing the angular properties of the sensor.

$$G_0 = \int_{\alpha} \int_{\beta} \frac{C(\alpha, \beta)}{C(\alpha_0, \beta_0)} \cos \alpha d\alpha d\beta \quad (11)$$

Equation 11 shows a geometrical constant of the sensor. The geometrical factor equation looks now as follows:

$$G = \frac{C(\alpha_0, \beta_0)}{P} \cdot G_0 \quad (12)$$

Then I substitute the beam density P in Equation 9 by the Equation 8

$$G = \frac{C(\alpha_0, \beta_0) \cdot S_s}{C_s} \cdot G_0 \quad (13)$$

Now let me set the sensor efficiency into geometrical factor calculation.

The sensor efficiency can be expressed by Equation 14

$$\varepsilon = \frac{C(\alpha_0, \beta_0) \cdot S_s}{C_s \cdot S_p} \quad (14)$$

where

$S_p = 0.135 \text{ cm}^2$ – sensors pinhole area, cm^2

ε - detector’s efficiency, calculated by Equation 2

Now ion source output count rate C_s at Equation 13 is to be substituted by the C_s expression from Equation 14. Finally,

$$G = G_0 \cdot S_p \cdot \varepsilon \quad (15)$$

where

G - geometrical factor of an instrument, $[\text{sr}^{-1} \text{cm}^{-2} \text{s}^{-1}]$

Calculated geometrical constants of NPD1 and NPD2 detectors are presented in the Table 7

The table 8 and table 9 show the geometrical factor G of the NPD1 and NPD2 sensors correspondingly in dependency on incident ion beam energy and ion species mass. The efficiency ε is included.

G_0			
	<i>Dir0</i>	<i>Dir1</i>	<i>Dir2</i>
<i>NPD1</i>	0.044	0.067	0.051
<i>NPD2</i>	0.046	0.082	0.051

Table 7: Table shows the geometrical constants of all detectors of NPD1 and NPD2 instruments

$G, \times 10^{-4}$									
	<i>E, KeV</i>	10.0	5.0	3.0	1.3	0.7	0.5	0.3	0.1
O^+	<i>Dir0</i>	6.12	5.02	3.92	0.87	0.17	0.08	—	—
	<i>Dir1</i>	10.67	8.05	4.61	1.54	0.43	0.15	0.03	—
	<i>Dir2</i>	5.85	4.48	1.86	0.55	0.08	0.05	—	—
H^+	<i>Dir0</i>	—	2.44	3.62	1.60	0.65	0.46	0.14	—
	<i>Dir1</i>	—	3.80	5.61	2.53	1.45	1.0	0.37	0.024
	<i>Dir2</i>	—	2.0	2.41	0.90	0.48	0.33	0.10	—

Table 8: Table shows the NPD1 sensor geometrical factor G dependency on ion species mass and energy.

3.5 ToF spectra

The Figure 12 shows the TOF distributions for the ion beam of one specific mass H of different energies taken by NPD1 sensor *Dir1* detector. The different curves are color coded. The covered energy range is 0.1 to 5.0 KeV. The displacement of curves reflects the energy loss of about 34% during the reflection from the START surface. The Figure 13 shows the TOF distributions for the O ion beam of different energies covering the range 0.3 to 10.0 KeV. The energy losses are the same as for H beam. Measurements are done in RAW mode.

$G, \times 10^{-4}$								
	<i>E, KeV</i>	5.0	3.0	1.3	0.7	0.5	0.3	0.1
O^+	<i>Dir0</i>	4.12	2.80	0.53	0.09	0.023	0.003	—
	<i>Dir1</i>	6.75	5.09	1.05	0.28	0.09	0.015	—
	<i>Dir2</i>	7.37	6.13	1.52	0.38	0.09	0.013	—
H^+	<i>Dir0</i>	2.24	2.11	1.01	0.37	0.19	0.057	—
	<i>Dir1</i>	4.32	3.99	2.33	0.95	0.53	0.18	0.014
	<i>Dir2</i>	4.13	4.38	2.34	1.07	0.57	0.21	—

Table 9: Table shows the NPD2 sensor geometrical factor G dependency on ion species mass and energy.

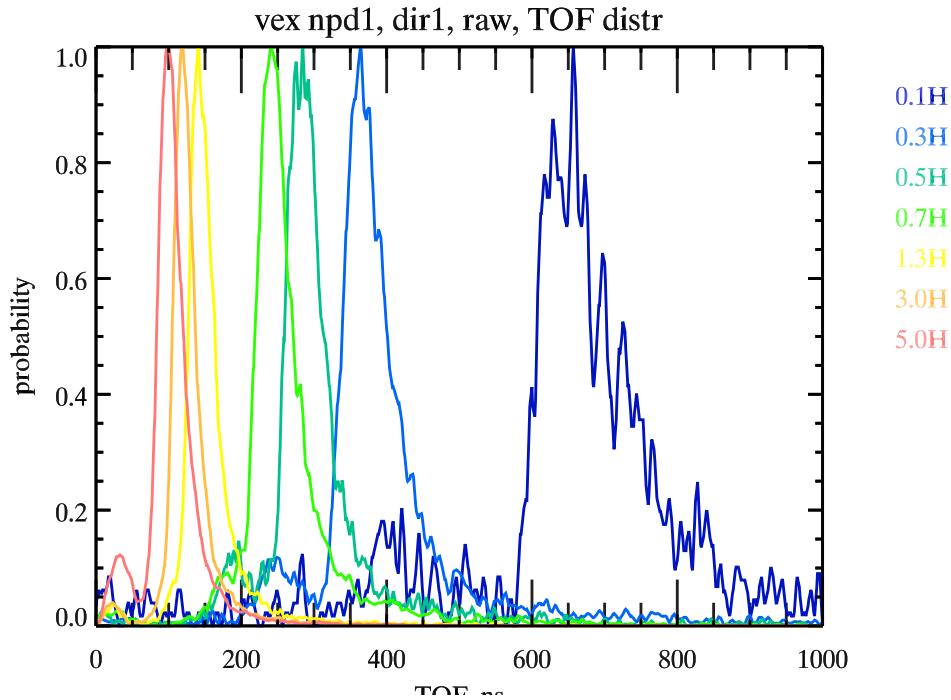


Figure 12: The figure shows the TOF distribution curves for NPD1 dir1 for H in dependency on beam energy

3.6 Energy resolution

Summarizing the TOF measurements the TOF dependency on incident ion energy for the NPD1 sensor is presented on Figure 14. The X-axis – is ion beam energy in log scale. The Y-axis – is particles ToF in log scale. The position of ToF peaks for the set of ion beam energies are plotted by color-coded dots. Error bars show the FWHM of ToF peaks. The lower line (blue) stands for H^+ ions and the upper line (red) stands for O^+ ions. The dashed lines show the theoretical dependence corresponding to the 33% energy loss in the Start Surface. Water molecules produced in the source break-up during the impact but the residual components carry the same initial velocity corrected for the energy loss in the target. This figure shows that within 1 – 10 KeV the TOF measurements give reliable mass identification.

These curves can be expressed by the next equations:

$$T(H) = \exp(5.31 - 0.48 * \ln(E))$$

$$T(O) = \exp(6.94 - 0.48 * \ln(E))$$

where

E – ion particles energy, keV

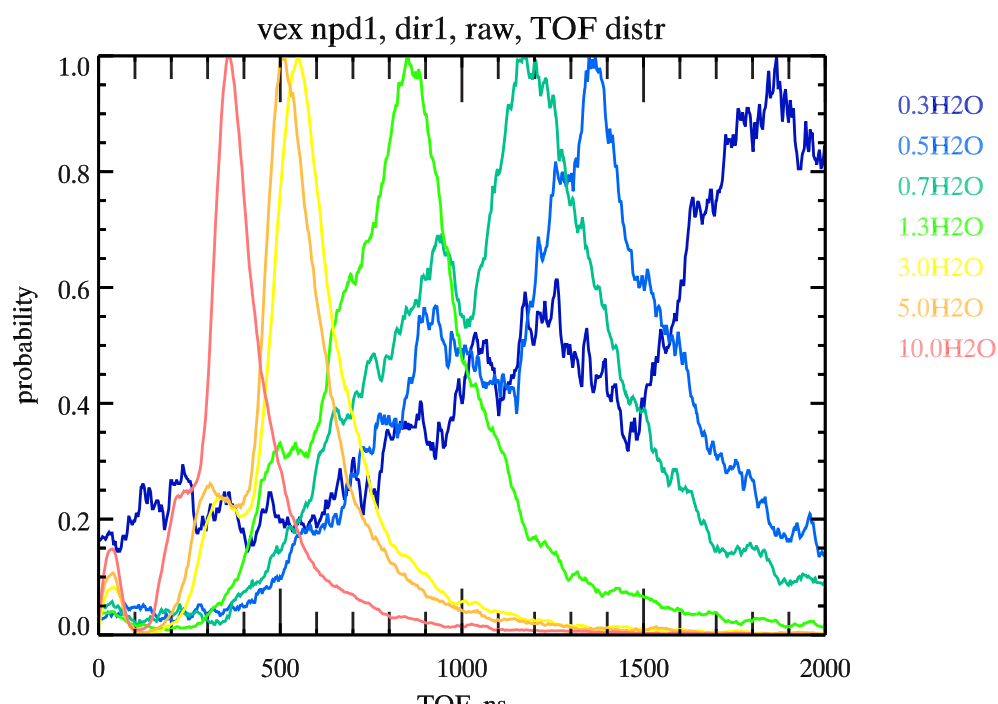


Figure 13: The figure shows the TOF distribution curves for NPD1 dir1 for O in dependency on beam energy

T – ion particles ToF number, ns

Curves are valid for NPD1 Dir1 detector.

One of the important results can be formulated as follows: for the definite energy range (0.1 KeV - 10 KeV) low energy O^+ ions can be distinguished from the high energy H^+ particles by only the ToF values. On the plot (Figure 14) the functions overlap within the TOF window 280 ns – 690ns. So, the particles with ToF more than 690 ns are O type definitely. And the particles with ToF less than 280 ns are H ions. Of course the energy of incoming heavy particles can be more than $10keV$, therefore the curves overlapping TOF window can be extended to lower values. The ions (both light and heavy) with ToF that fit that window have comparable velocities. So to distinguish between these species one has to analyze the PHD of the Stop detectors as well as analyze the TOF distribution shape. In case of O species of higher energy than 10 keV the estimation of particles mass based only on the TOF analysis is not very clear. For such cases the PH analysis can be done additionally.

So we can use ToF analysis to resolve energy of ion species in such mass and energy range:

- O ions

$E < 1.3 \text{ keV}$
 $\text{ToF} > 690 \text{ ns}$

- H ions
 $E > 0.7 \text{ keV}$
 $\text{ToF} < 280 \text{ ns}$

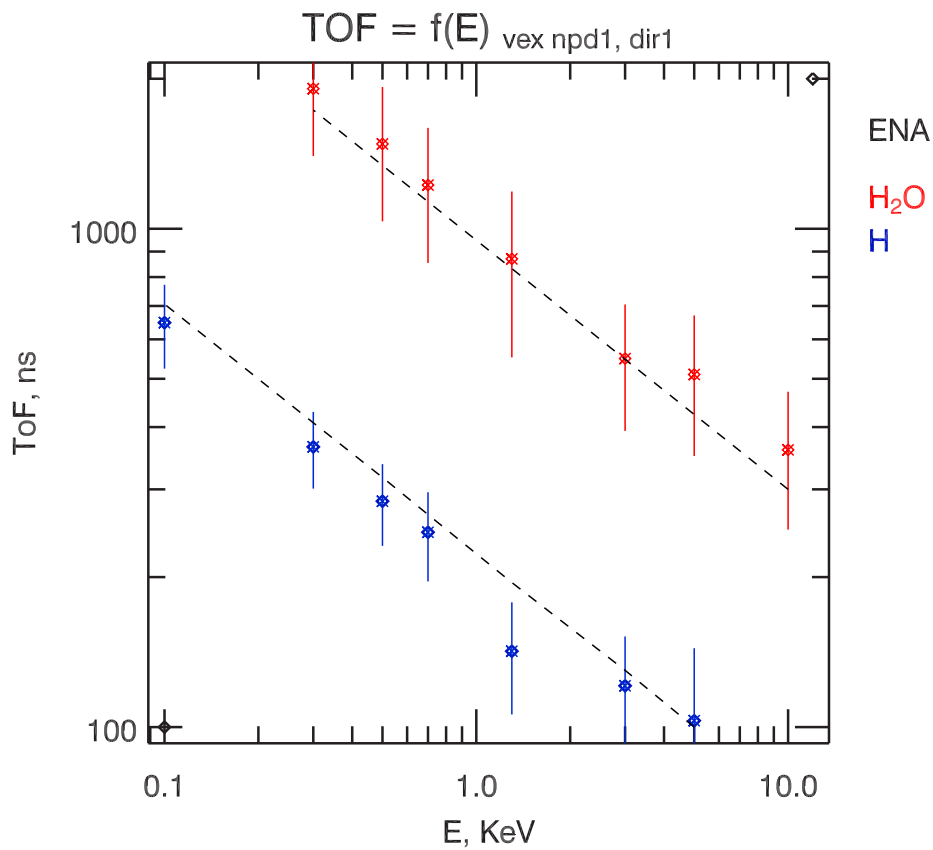


Figure 14: The figure shows the TOF dependency on beam energy of different ion species (H^+ , O^+) for direction 1

And we have to use the PH analysis for ions species with TOF that fit the TOF window $280\text{ns} - 690\text{ns}$ and are within the next mass and energy range:

- TOF window: $280 \text{ ns} - 690 \text{ ns}$
- $E(O) = 1.3 \text{ KeV} - \text{less } 10 \text{ KeV}$
- $E(H) = 0.1 \text{ keV} - 0.7 \text{ keV}$

Lowest limit of light particles energy that can be measured by the NPD sensor is 0.1 keV. For the lower energy ions scattering on the StartSurface is too high as well as ion is not enough energetic to cause a secondary electron yield from the Stop Surface.

By applying the numbers calculated above for the compressed mode data ToF window will have the next values:

- TOF window: 246 ns – 610 ns
- Compressed mode: 7 – 10 steps
- $E(O) = 2.4 \text{ KeV} - 11 \text{ KeV}$
- $E(H) = 0.1 \text{ keV} - 1.0 \text{ keV}$

Heating test has been done during calibration. Heater had been switched on for ≈ 10 hours. TOF measurements have been done before and after Start Surface heating. TOF distribution didn't vary after heating. That can be explained either by too short heating time period or by too low maximum temperature of Start Surface, reached during heating or by the Start Surface cleanness.

3.7 Heater and temperature sensor.

Temperature sensors are calibrated after the NPD integration with the ASPERA-4 instrument. Heater increases temperature of the START unit on 50 degrees over the ambient temperature.

It takes approximately 2 hours to heat a StartSurface to the equilibrium maximum temperature.

3.8 Noise

NPD electronics in its most sensitive state is sensitive enough to pick up the electric noise (even without MCP HV bias). So to decrease the electric noise level electronics' discriminators thresholds are set to maximum values, that level in binary form is 0×00 and corresponds to 5V on DAC.

Finally the noise at biased MCP detectors is less than 20 c/s. The TOF validation removes that uncorrelated noise count.



ASPERA-4



**Venus
Express**

Reference : **VE-ASP-CR-050530**
Issue : **1** Rev. : **1**
Date : **2005-05-30**
Volume : **-** Page: **7**

APPENDIX 3. ELS CALIBRATION REPROT

Venus Express ASPERA ELS

MULLARD SPACE SCIENCE LABORATORY
UNIVERSITY COLLEGE LONDON

Author: Dhiren Kataria

Venus Express ASPERA ELS Calibration Report

Volume 1

DOCUMENT: MSSL/VEX/001

May 26th 2005

1 Introduction

The raw data from the ELS instrument consists of a matrix of counts N , each for an accumulation time T , from the sixteen anodes and to cover the energy range of interest. This needs to be converted into the phase space density $f(\mathbf{v})$ of the electron distribution and the relation between N and $f(\mathbf{v})$ is given by (Johnstone *et al.*, 1987):

$$dN/dt = [\mathbf{GF}]v^4 f(\mathbf{v})$$

where $[\mathbf{GF}]$ is the geometric factor of the sensor, obtained from ground calibration, and \mathbf{v} is the velocity at the centre of the response of the electrostatic analyzer. $f(\mathbf{v})$ is then used to obtain the moments of the distribution as follows:

$$n = \int_{all \mathbf{v}} f(\mathbf{v}) d^3 \mathbf{v}$$

$$\mathbf{V} = \left(\frac{1}{n} \right) \int_{all \mathbf{v}} \mathbf{v} f(\mathbf{v}) d^3 \mathbf{v}$$

$$\mathbf{T} = \left(\frac{m}{n} \right) \int_{all \mathbf{v}} (\mathbf{v} - \mathbf{V})(\mathbf{v} - \mathbf{V}) f(\mathbf{v}) d^3 \mathbf{v}$$

to provide the density, velocity and temperature. The $[\mathbf{GF}]$, in units of $m^2 \text{ sr eV/eV}$, is given by

$$[\mathbf{GF}] = (e \Delta u' \Delta \theta \Delta \phi) / T_C \sum_l \sum_m \sum_n N_{lmn} / I_{lmn}$$

where, Δu =Spacing between calibration points in velocity,

$\Delta \theta$ =Elevation spacing,

$\Delta \phi$ =Azimuth spacing,

T_C =Accumulation time,

I =Beam current in ELS aperture per unit area,

N =ELS counts.

This document reports on the ground calibration tests carried out at MSSL for the ELS instrument. Note that $[\mathbf{GF}]$ incorporates both the purely geometric response of the instrument as well as the detector response.

As the Venus Express instrument was known to be mechanically imperfect and the absolute QE of the detector was not known, it would not be possible to deconvolve the geometric response from the detector response. Hence, the laboratory calibrations define the integrated instrument response and the relative response of the 16 sectors.

2 Calibration details

2.1 Calibration facility

The calibration facility [Johnstone et al., 1997], based on the technique described in Marshall et al (1986), provides a wide area photoelectron beam at energies ranging from a few eV to 15 keV with variable beam intensities from a few Hz to several MHz. The system is fully automated facilitating calibration scans over the complete range of polar and azimuth angles at several instrument voltage settings both for the analyser as well as the MCP. A flexible data acquisition system was integrated into the automation to provide simultaneous measurements from the 16 preamplifier channels, coordinated with the instruments position and voltage settings. Before performing the instrument calibration, a profile of the beam output is recorded at each of the calibration energies by means of a channeltron mounted on an X-Y table. During calibrations, the channeltron is mounted as close as possible to the instrument aperture in order to provide a constant reference to the beam intensity.

The setup for the calibration is identical to the one that was used for the calibration of the Mars Express instrument and is described in further detail in the report mex017_fucal_setup.doc, attached along with this report.

2.2 Details of tests

Tests were carried out to study the following parameters of the instrument:

Analyser: Concentricity, K-factor, Angular acceptance and Energy Resolution

Detector: Operational regime, Rate response, Gain uniformity/QE

UV response

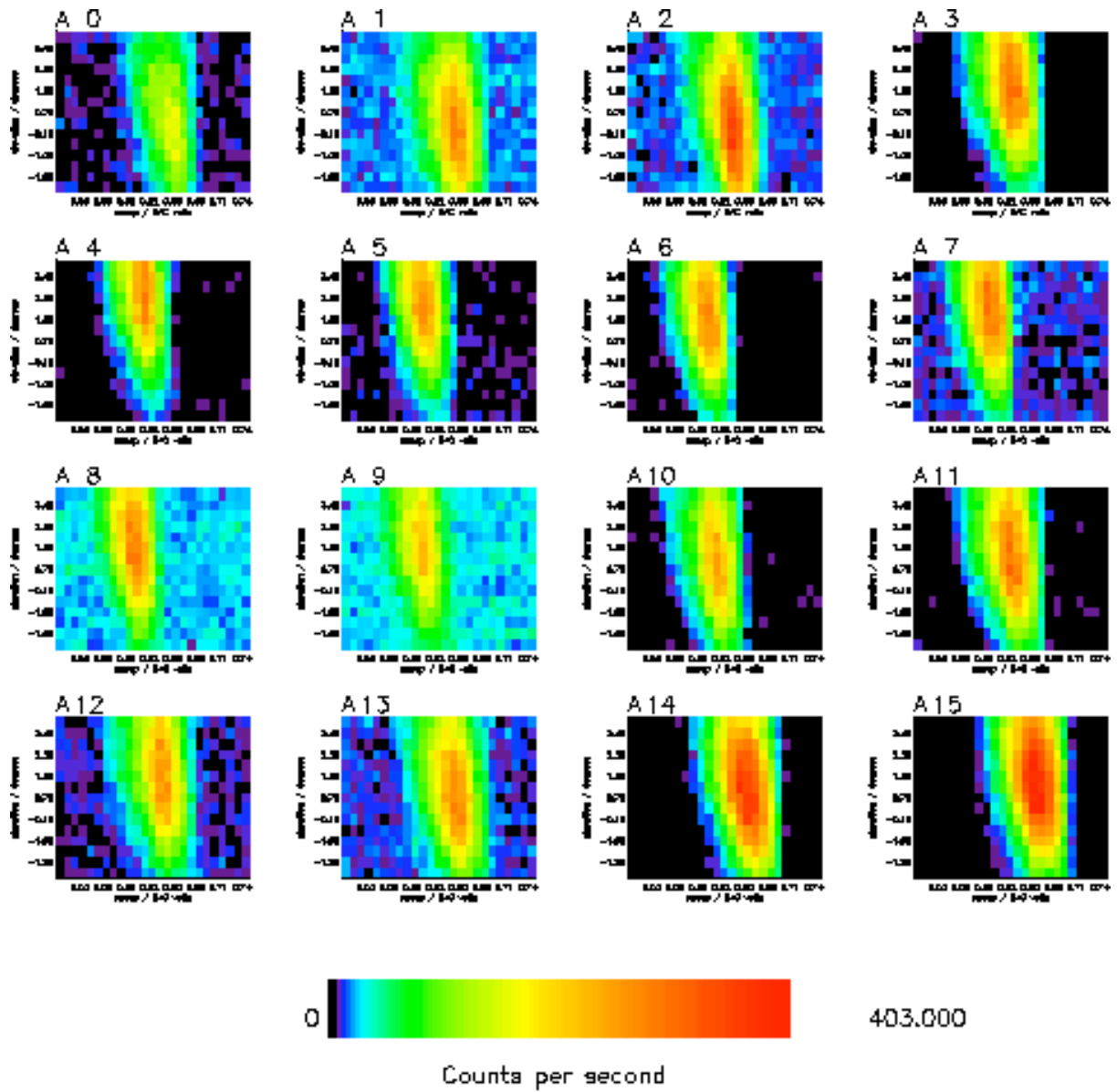
2.2.1 Energy Angle scans

All the analyser parameters are extracted from the Energy (sweep voltage) – Angle scans carried out at the centre of each anode for beam energies of 10eV, 30 eV, 50eV, 70eV, 100eV, 200eV at the low range of the sweep power supply and of 1 keV, 3 keV, 6 keV, 10 keV, 12 keV at the high range. Table 1 lists the details of the scans and figures 1 to 3 are example plots at 30, 200 and 3 keV respectively. Figure 4 is a plot of the k-factor for the 10 energies and Figure 5 is a plot of the energy resolution across the 16 anodes.

Table 1. Summary of Energy angle scans carried out with the beam incident on the centre of each anode.

Date	Energy	MCP voltage	DAC set	Filter	Polar			Elevation		Sweep		
					Angles	Anode	Step	Angles	Step	DAC set	Step	Range
	10 eV	2358	3.93	1.5	-168.75 to 168.75	0 to 15	22.5	-2.7 to 5.7	0.6	0.16 to 0.28	0.005	Low
26/06/2003	30 eV	2358	3.93	1.5	-168.75 to 168.75	0 to 15	22.5	-2.4 to 3.9	0.45	0.51 to 0.75	0.01	Low
	50 eV	"	"	"	"	"	"	"	"	0.93 to 1.17	0.01	Low
	70 eV	"	"	"	"	"	"	"	"	1.28 to 1.64	0.015	Low
	100 eV	"	"	"	"	"	"	"	"	1.8 to 2.4	0.025	Low
	200 eV	"	"	"	"	"	"	"	"	3.6 to 4.8	0.05	Low
	1keV	"	"	"	"	"	"	-1.5 to 2.7	0.3	0.105 to 0.225	0.005	High
	3keV	"	"	"	"	"	"	"	"	0.43 to 0.55	0.005	High
	6keV	"	"	"	"	"	"	"	"	0.86 to 1.1	0.01	High
	10keV	"	"	"	"	"	"	"	"	1.3 to 1.9	0.025	High
	12 keV	"	"	"	"	"	"	"	"	1.72 to 2.2	0.02	High

Figure 1. Energy Angle scans at 30 eV. Data is taken with the beam incident at the centre of each anode.



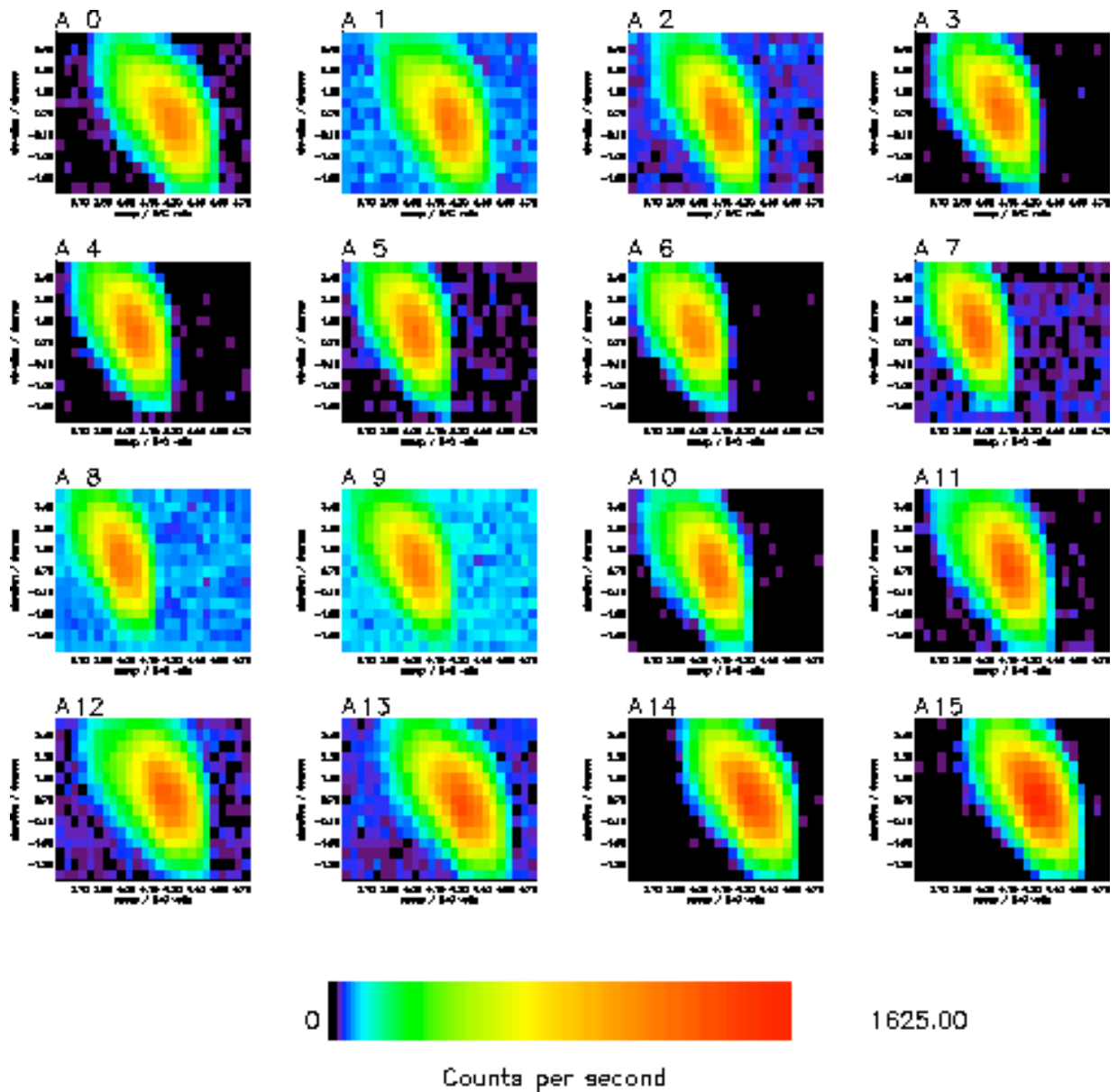
Program: Vex_En_Ang_ver_2.pro

Data file: X:\venusexp\vfaf030a.pdt

1s integrations for MCP 2358 V,filter OD=1.0+0.5, 30 eV, low range

Fri Jul 04 10:16:01 2003

Figure 2. Energy Angle scans at 200 eV. Data is taken with the beam incident at the centre of each anode.



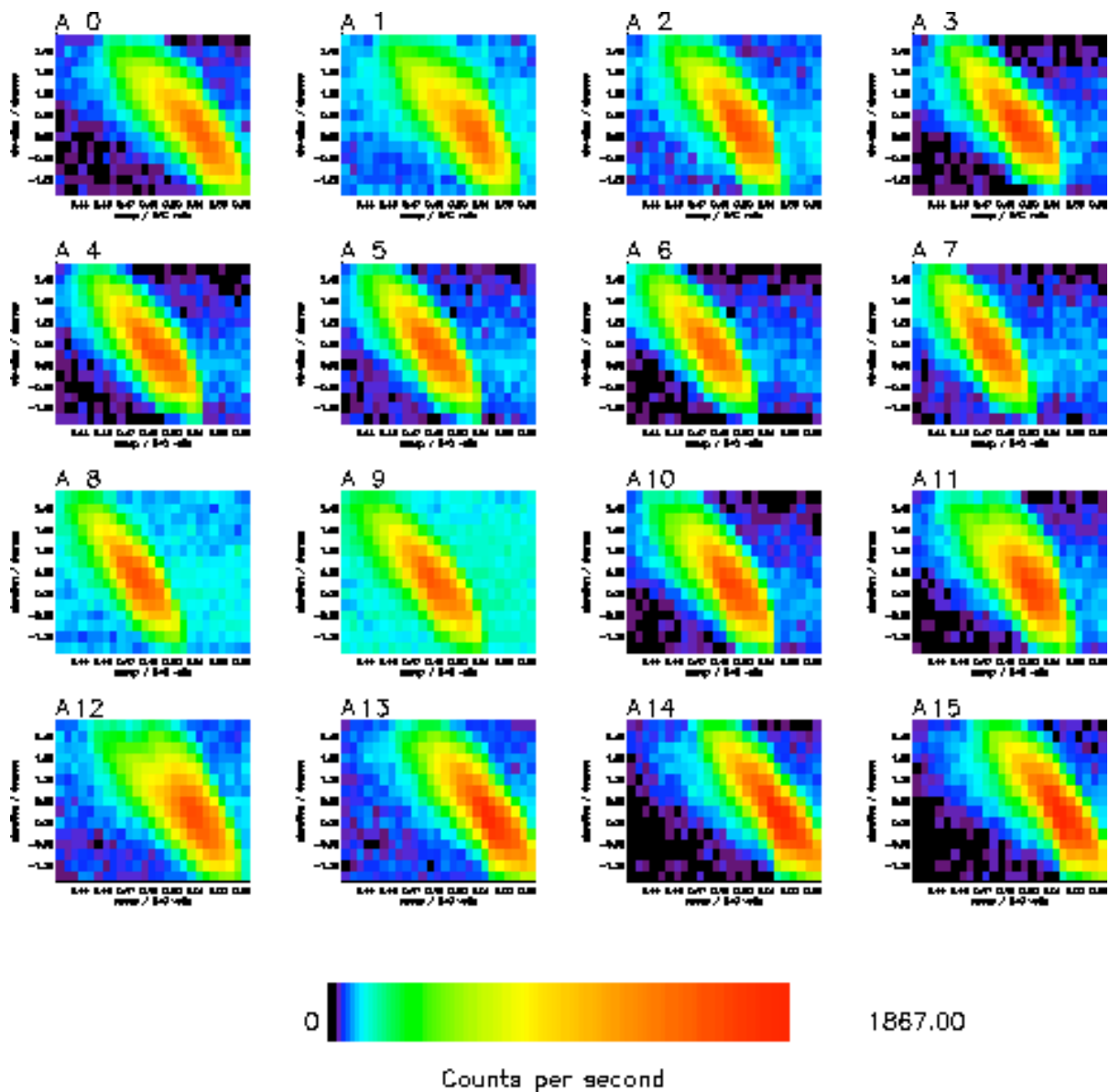
Program: Vex_En_Ang_ver_2.pro

Data file: X:\venusexp\vfaf200a.pdt

1s integrations for MCP 2358 V,filter OD=1.0+0.5, 200 eV, low range

Thu Jul 03 16:02:57 2003

Figure 3. Energy Angle scans at 3 keV. Data is taken with the beam incident at the centre of each anode.



Program: Vex_En_Ang_ver_2.pro

Data file: X:\venusexp\vaf3k0a.pdt

1s integrations for MCP 2358 V,filter OD=1.0+0.5, 3 keV, high range

Thu Jun 26 14:12:59 2003

Figure 4. Plot of k-factor across the 16 anodes for the 10 energies, 30 ev to 12 keV, violet to red.

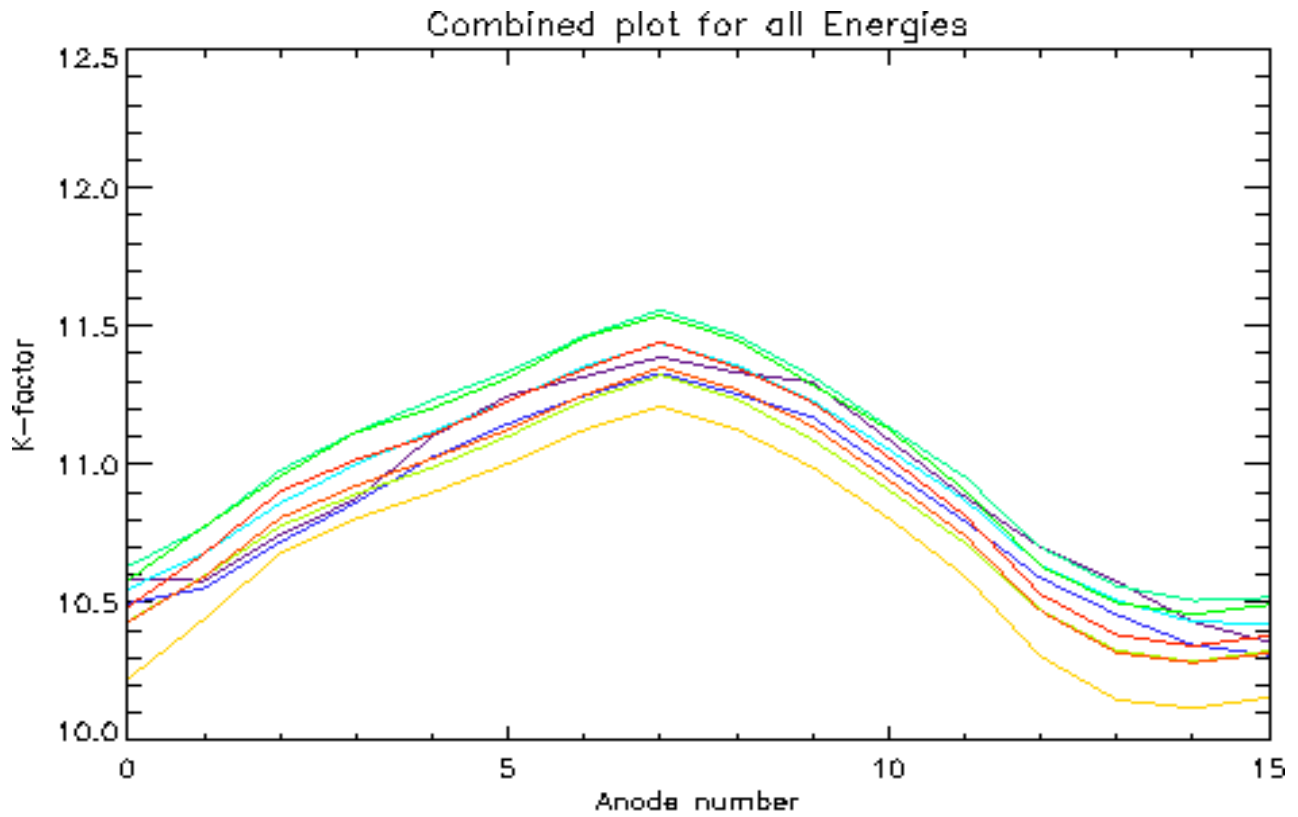
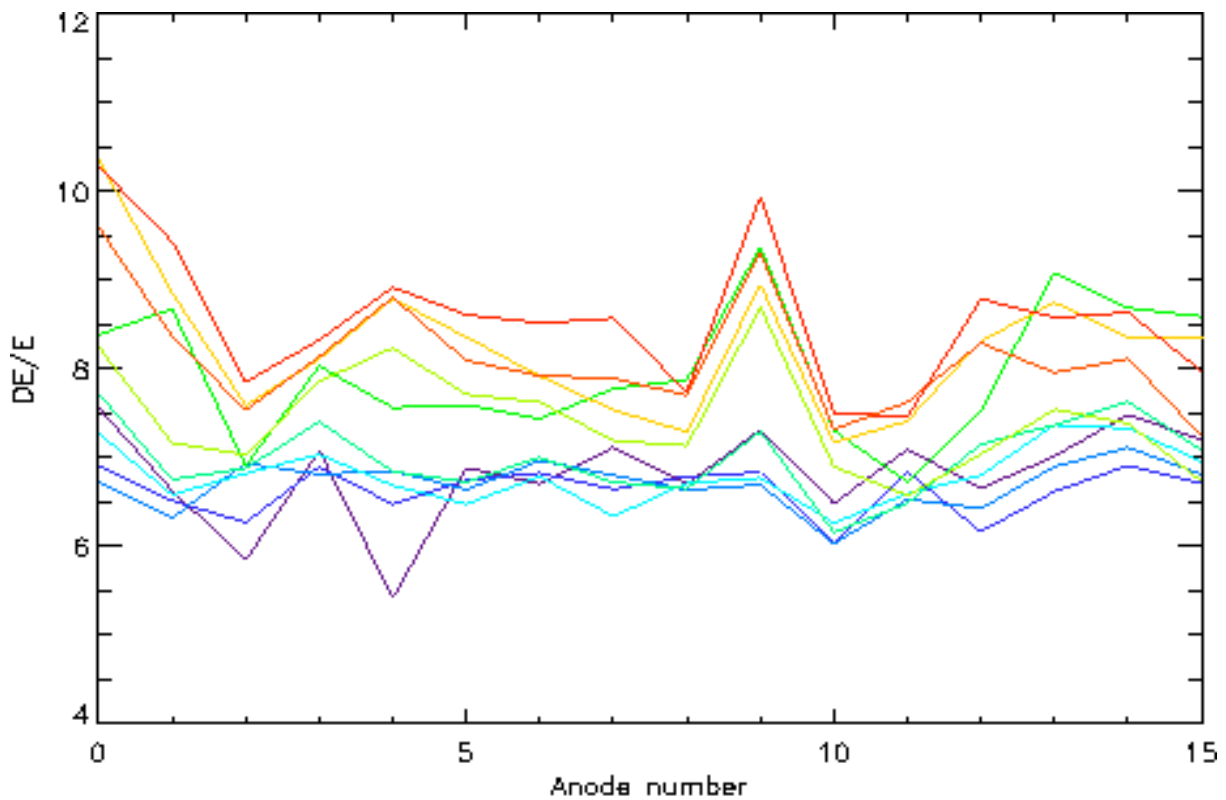


Figure 5. Plot of the energy resolution across the 16 anodes for the 10 energies, 30 ev to 12 keV, violet to red.



2.2.2 Fine polar scans

The energy-angle scans also provide the peak response of the instrument for each energy. In order to get the relative response of the instrument, a fine scan is carried out at polar steps of 0.25 degrees across the polar range of $\pm 168.75^\circ$ at the peak elevation and voltage. The tests carried out are listed in Table 2 and figure 6 is an example of the response at 100 eV.

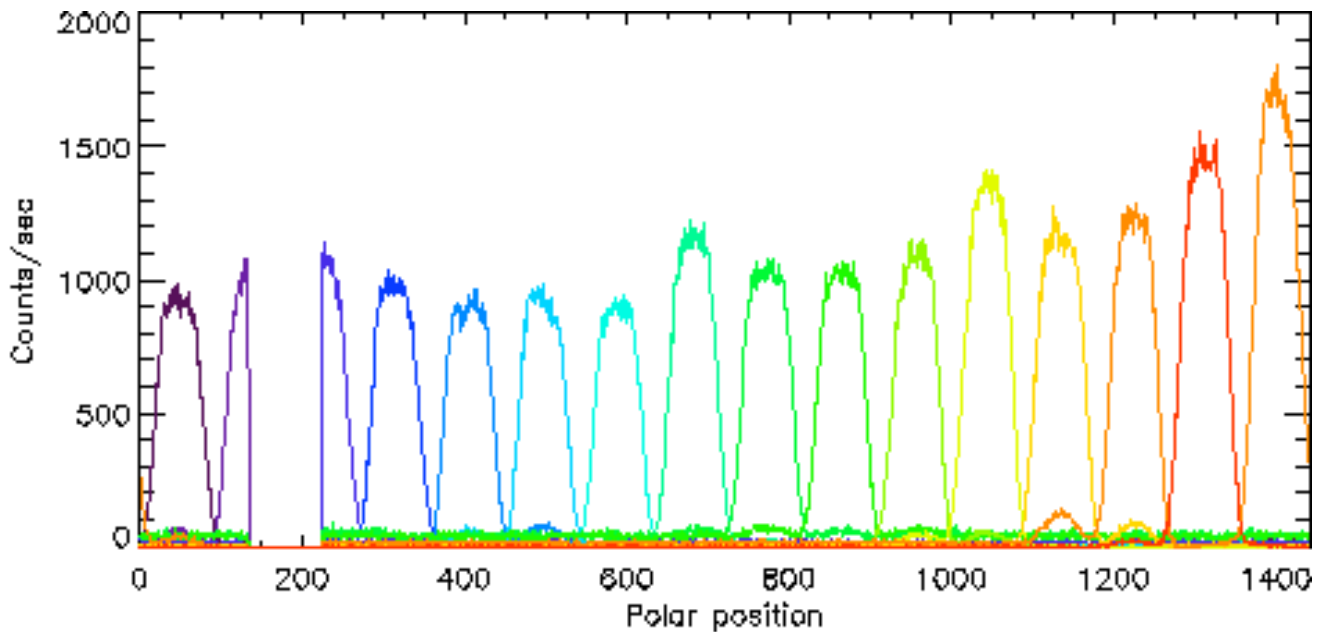


Figure 6. Plot of the response at peak elevation and sweep voltage at fine polar steps of 0.25°

Table 2. Summary of tests carried out at fine polar angles of 0.25° at the peak elevation and sweep voltage response of the instrument .

Date	Energy	MCP voltage	DAC set	Filter	Polar			Elevation		Sweep		Range
					Angles	Anode	Step	Angles	Step	DAC set	Step	
26/06/2003	30 eV	2580	4.3	1.5	-168.75 to 168.75	0 to 15	0.25	Peak	-	Peak	-	Low
	100 eV	"	"	"	"	"	"	"	"	"	"	Low
	200 eV	"	"	"	"	"	"	"	"	"	"	Low
	3 keV	"	"	"	"	"	"	"	"	"	"	High
	10 keV	"	"	"	"	"	"	"	"	"	"	High

2.2.3 MCP voltage response

The next set of tests, summarised in table 3, determine the operational regime of the microchannel plate detector. Tests are carried out with the beam incident on anode 10 and the MCP voltage is raised from 1800V to 2880V. The results for the different energies, normalised to the voltage at 2580V are shown in figure 7.

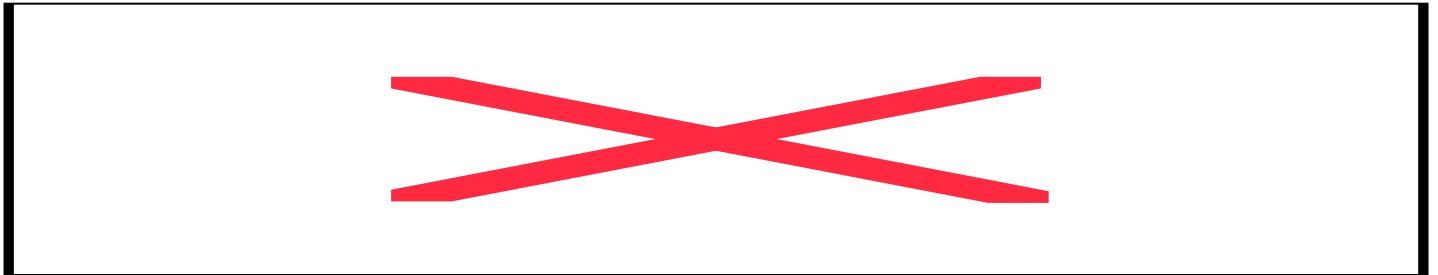
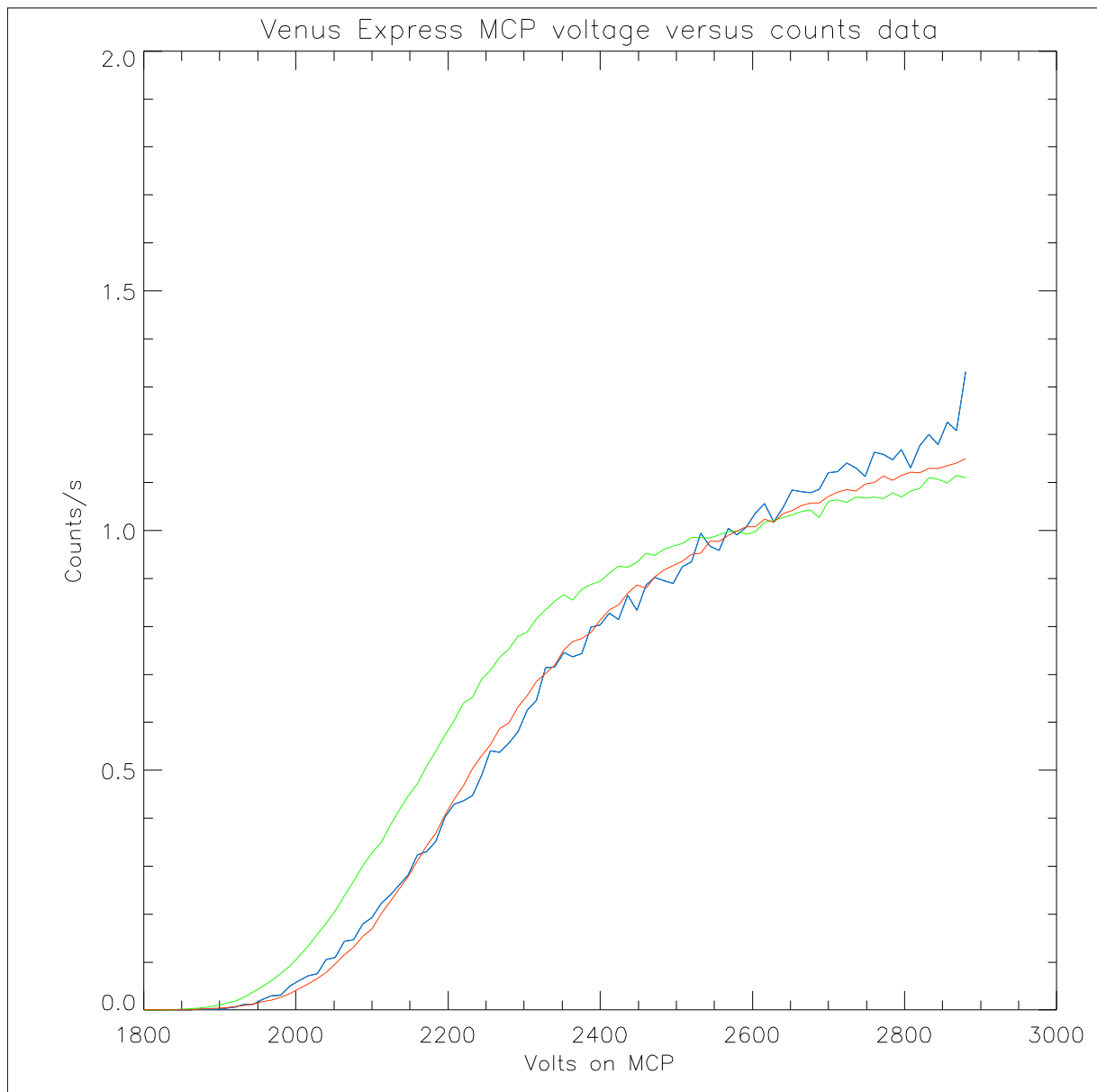


Table 3. Summary of tests carried out at several voltages at different beam energies

Figure 7. MCP voltage versus normalised counts at different energies. 30 eV – blue, 300 eV – green, 10 keV – red.



2.2.4 Energy angle scans at 2580V

Figure 7 suggests an operational voltage of 2580 V in order to minimise the difference in the detector response due to the energy of the incident beam. Hence, energy-angle scans were carried out at additionally at 2580V at a few energies to complement the data at 2358V and characterise and energy dependent features in the relative response of the instrument. Table 4 lists the details.

Date	Energy	MCP voltage	DAC set	Filter	Polar			Elevation		Sweep		Range
					Angles	Anode	Step	Angles	Step	DAC set	Step	
26/06/2003	30 eV	2580	4.3	1.5	-168.75 to 168.75	0 to 15	22.5	-2.4 to 3.9	0.45	0.51 to 0.75	0.01	Low
	200 eV	"	"	"	"	"	"	"	"	3.6 to 4.8	0.05	Low
	1 keV	"	"	"	"	"	"	-1.5 to 2.7	0.3	0.105 to 0.225	0.005	High

Table 4. Summary of energy-angle scans carried out at 2580V on the MCPs

2.2.5 Detector event rate response

Table 5 summarizes the tests performed to study the response of the detector to a varying incident event rate and provides a measure of the deadtime of the instrument.

Date	Energy	MCP voltage	DAC set	Filter	Range	Polar			Elevation		Sweep		Range
						Anode	Step	Range	Step	Range	Step		
17/06/2003	100 eV	2358	3.93	1.5	-11.25	#10	-	1.2	-	1.6	2.8	Low	
	"	"	"	1	"	"	"	"	"	"	"	Low	
	"	"	"	2	"	"	"	"	"	"	"	Low	
	"	"	"	1.3	"	"	"	"	"	"	"	Low	
	"	"	"	1.4	"	"	"	"	"	"	"	Low	
	"	"	"	1.6	"	"	"	"	"	"	"	Low	

2.2.6 UV response

The response of the instrument to UV light incident on has been studied by shining a Krypton UV lamp. Details of the test set up is given in Chris Alsop et al and a summary of the tests carried out are given in table 6. Figure 8 shows the energy angle response of the 16 anodes to UV with the lamp facing anode 1. As can be seen, most of the counts are observed at very low energies and are primarily due to low energy secondary electrons emitted by the incident light which make it to the MCP.

Date	Energy	MCP voltage	DAC set	Filter	Polar			Elevation		Sweep		Range
					Angles	Anode	Step	Angles	Step	DAC set	Step	
11/08/2003	UV	2580	4.3	-	-168.75	1	-	-12.5 to 12.5	0.25	0.0 to 0.2	0.005	Low
	UV	"	"	-	"	"	-	"	"	"	"	Low
	UV	"	"	-	101.25	5	-	"	"	"	"	Low
	UV	"	"	-	"	"	-	"	"	"	"	Low
	UV	"	"	-	-168.75	1	-	"	"	"	"	Low
	UV	"	"	-	"	"	-	"	"	"	"	Low
	UV	"	"	-	101.25	5	-	"	"	"	"	Low
	UV	"	"	-	"	"	-	"	"	"	"	Low

Table 6. Summary of UV tests. The instrument is set up so the source is facing either anode 1 or anode 5. See explanation in text.

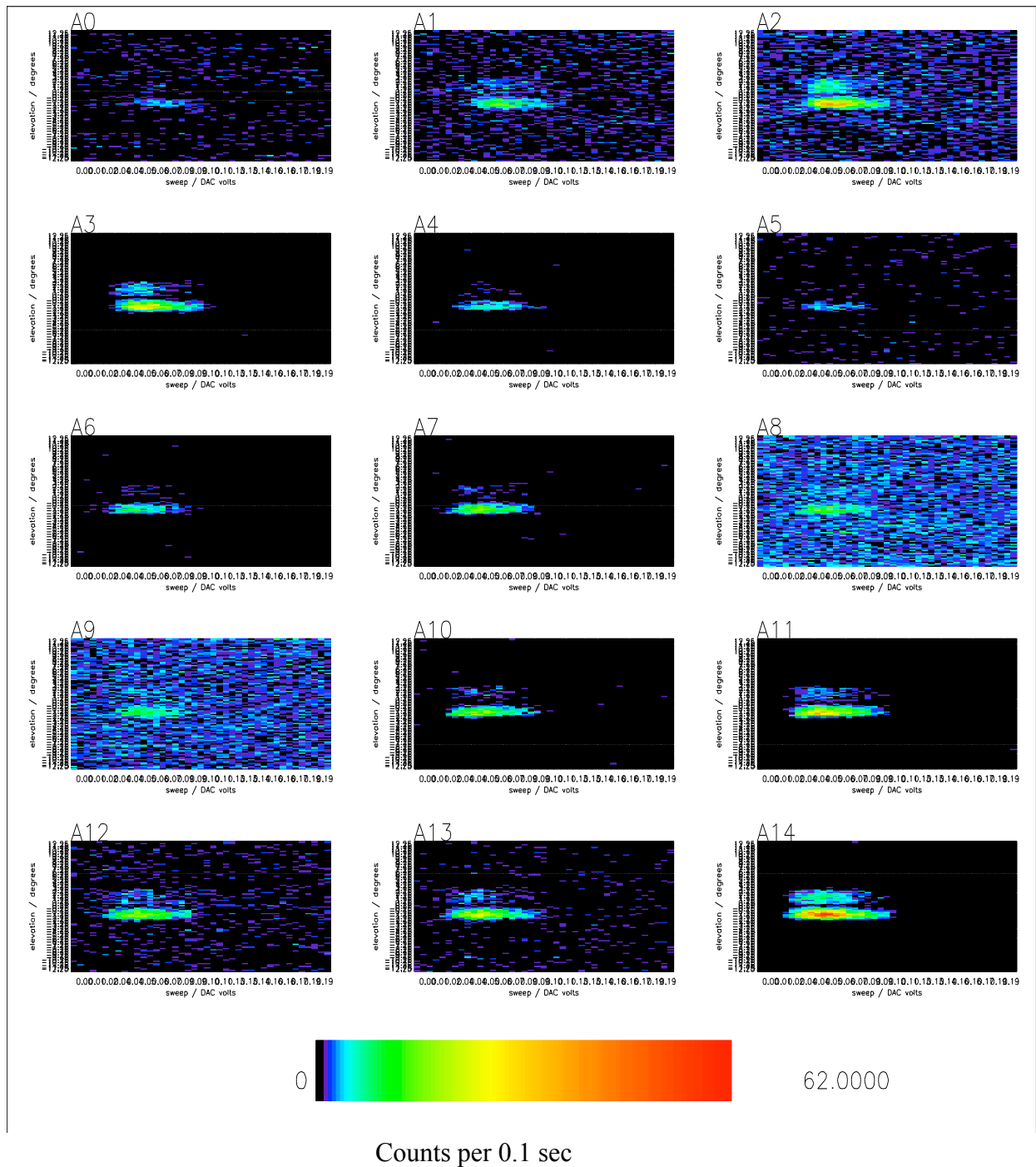


Figure 8. Energy angle scans for UV light incident on the instrument .

3 Note on preliminary results and analysis

Preliminary analysis has been carried out and geometric factors extracted. However, due the complications arising from the mechanical imperfections, a number of discrepancies need to be resolved and further detailed analysis is currently in progress. In addition, the data will need to be corroborated with simulations to reproduce the performance and finally, compared with other instruments in-flight.



ASPERA-4

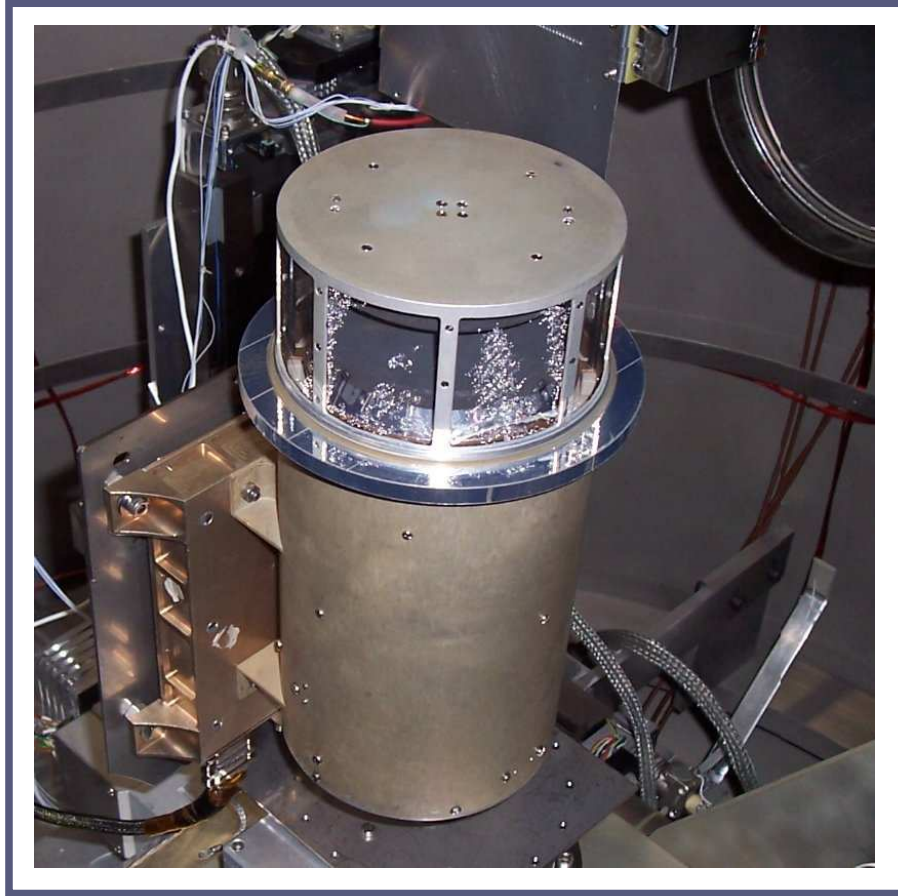


**Venus
Express**

Reference : **VE-ASP-CR-050530**
Issue : **1** Rev. : **1**
Date : **2005-05-30**
Volume : **-** Page: **8**

APPENDIX 4. IMA CALIBRATION REPROT

Venus Express ASPERA-4
IMA Calibration Report.
V.1.0 May 30, 2005



Andrei Fedorov

Centre d'Etude Spatiale Rayonnement, Toulouse, France

Contents

1. Introduction: principal design, calibration objectives, and terms definition.
2. Brief description of calibration facilities
3. K, D-Elevation and Azimuthal properties of the sensor.
4. Mass position and geometrical factor for different masses.
5. Resultant tables.

1 Introduction: principal design, calibration objectives, and terms definition.

IMA is a rather complex mass analyzer. Figure 1 introduces the principal design of the sensor. It consists of the electrostatic scanner, spherical top-hat electrostatic analyzer, followed by the magnet mass analyzer. The ions can be accelerated in the gap between electrostatic analyzer and magnet section. Magnet mass analyzer consists of 16 azimuthal sections followed by 16 sectors (low panel of figure 1) of MCP position sensitive detector. Detector measures the radial position and the angular sector number for each incident particle. For the given particle energy, the radial position of the incident ion on the MCP surface corresponds to its mass. The sector number corresponds to the azimuth of the incident particle.

Sensor performance is controlled by scanner voltage U_{def} , electrostatic analyzer voltage U_{an} , and ion acceleration between analyzer and magnet section U_{PAC} . These voltages are produced by high voltage unit controlled by corresponding reference values. Finally the instrument properties are calculated as the functions of high voltage reference values, particle beam direction, particles energy and mass.

1.1 Terms definition

Instrument geometry is defined as:

X, Y, Z frame has an origin in the center of spherical analyzer. Axis directions are shown in figure 1.

Θ is the **elevation** angle of the incident ion (see top panel of figure 1) counted from the **XY** plane. Positive direction is shown in figure 1.

Φ is the **azimuthal** angle of the incident ion (see bottom panel of figure 1) counted from the middle of the 8th sector of the detector in the **XY** plane. Particles coming with $\Phi = 0$ strike the middle of the sector "0" of the detector. Angle Φ is counting anticlockwise.

S is an azimuthal sector number $0 \div 15$.

R_M is the radial position of the ion on the detector surface which defines the mass of the particle. R_M is coded by detector as a number $0 \div 31$. Low value corresponds to the low R_M (the central part of the detector surface).

Voltages inside instrument are defined as:

EAC_ref is the reference value to control scanner voltage. It is changed from -5000mV up to 5000mV.

EAC_U and **EAC_L** are top and low scanner electrodes voltages controlled by **EAC_ref**. Range of both is $\pm 2600V$.

$U_{def} = \text{EAC_U} - \text{EAC_L}$ is the value which controls Θ angle.

ESC_H_ref is the reference value to control inner analyzer plate high voltage. Value range is $0 \div +5000mV$.

ESC_H is the inner analyzer plate voltage. The range is $0 \div 4000V$.

ESC_L is the exterior analyzer plate voltage. The range is $0 \div 11V$.

$U_{an} = \text{ESC_H} - \text{ESC_L}$ is the analyzer voltage which defines the energy of the particles.

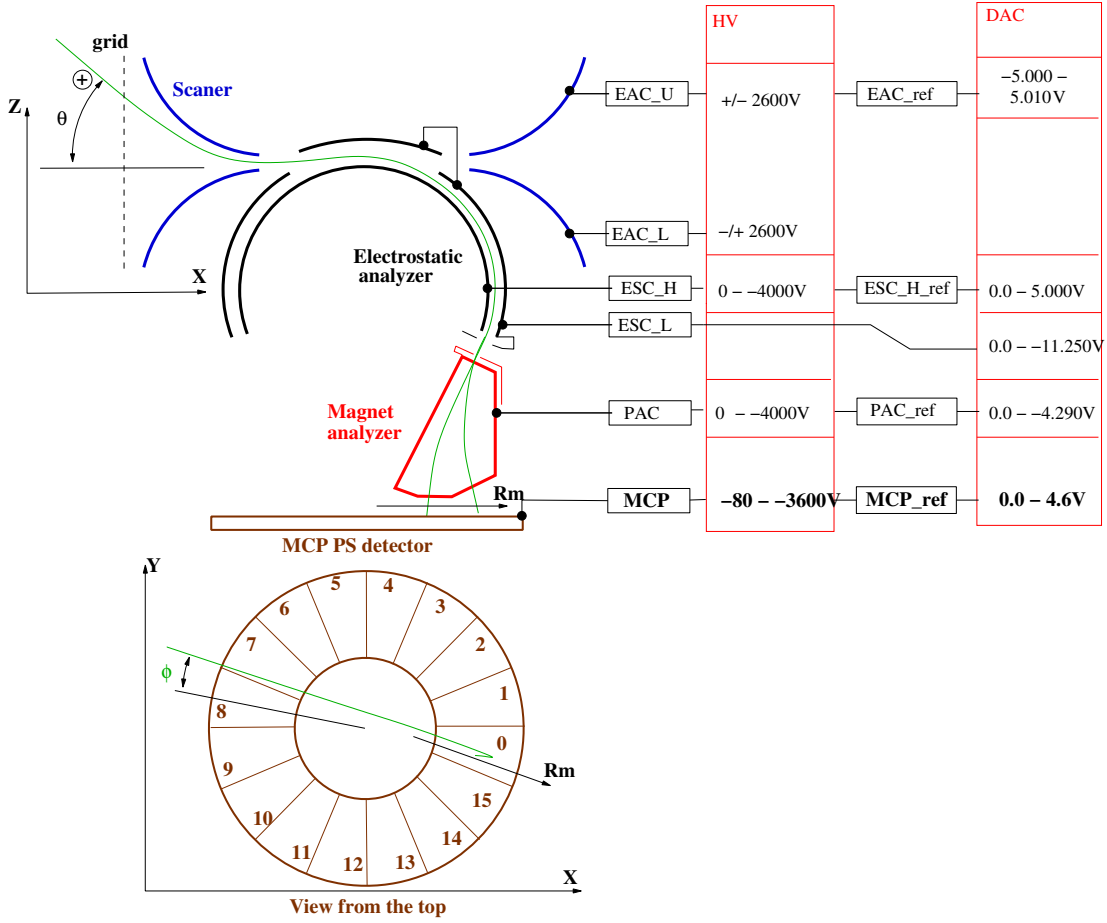


Figure 1: The principal diagram of the IMA mass analyzer. Terms and coordinate system introduction. Green curve in the bottom panel represents the particle trajectory inside the sensor. See text for details.

$U_{PAC} = \mathbf{PAC}$ is the post acceleration voltage between analyzer and magnet sections. Only 3 values are available: ($-39V$, $-1902V$, $-3615V$).

Physical terms used in the present reports are as follows:

$E_q = \langle \text{particle energy} \rangle / \langle \text{particle charge} \rangle$ measured in V .

$K = E_q / U_{an}$ "K" factor of the analyzer.

$K_{ref} = E_q / ESC_H_ref$, this value is useful for calibration tables.

$D = U_{def} / E_q$, this value defines scanner properties (see section 3)

$D_{ref} = EAC_ref / E_q$, this value is useful for calibration tables.

$M_q = \langle \text{particle mass} \rangle / \langle \text{particle charge} \rangle$ measured in $AUM / \langle \text{electron charge} \rangle$.

G_L is the differential geometrical factor measured for given Φ , $cm^2 \text{ rad } eV/eV$.

$GF = \int G_L d\Phi$ is the total geometrical factor $cm^2 \text{ sr } eV/eV$. Note that the last value is useless in the most of cases. The point is that the temperature of the measured ions is usually small, and angular distribution of the ion flow is narrow in comparison with the width of the azimuthal sector 22.5° . Thus the present report is dealing with G_L value.

During calibration the following constants and functions should be defined:

$K_{ref}(\Phi)$ and then $K(\Phi)$.

$\Delta E/E(\Phi)$ - energy resolution of the sensor.

$\Theta(D, \Phi)$ and $\Theta(D_{ref}, \Phi)$.

$\Delta\Theta(\Theta, \Phi)$ - angular resolution of the sensor.

$R_M(E_q, M_q, U_{PAC})$ - position of the center of the mass peak

ΔR_M - width of the mass peak

$G_L(\Theta, \Phi, E_q, M_q)$ for each azimuthal sector.

1.2 Rough estimation of the theoretical geometrical factor

The standard field of view of the sensor is $22.5^\circ \times 4^\circ = 0.027sr$. The aperture of the instrument is defined by slit in the acceleration lens between the spherical analyzer and the magnet. For one azimuthal sector it is $1mm \times 10mm = 0.1cm^2$. $\Delta E/E = 0.04$. In this case very rough estimation of the geometrical factor of one sector is

$$GF_{estim} = 1.0 \cdot 10^{-4} cm^2 sr eV/eV \quad (1)$$

2 Brief description of calibration facilities

2.1 Mechanical setup

The mechanical set up is shown in Figure 2. The sensor is located at about 2.5 m from the ion source. The turnable platform allows to change Φ in $\pm 170^\circ$ range, and Θ in $\pm 90^\circ$ range. Both angles are set with accuracy of 0.01° .

Ion gun allows to choose H^+ , H_2^+ , O^+ , O_2^+ ions in the energy range 500eV - 30 keV. The energy and sort of ions are programmed. To monitor the ion flux one CEM is mounted on the periphery of the beam.

2.2 High voltage setup

High voltage control is shown in Figure 3. All reference voltages for IMA HV units and for Ion Gun HV supply are provided by 16 bits DAC with accuracy 0.2mV. The multichannel ADC provides measurements of HV monitor values with accuracy 0.1 mv.

Calibration of high voltage sources provided by IRF is as follows:

$$ESC_H[V] = -1.933 + ESC_H_ref[mV] \cdot 0.6587 \quad (2)$$

$$U_{def}[V] = -6.16 + 1.920 \cdot EAC_ref[mV] \quad (3)$$

3 K, D-Elevation and Azimuthal properties of the sensor

3.1 K properties of the electrostatic analyzer

Figure 4 shows measurements of H^+ energy versus U_{an} reference value in case when ESC_L is zero. Corresponding formulas are as follows:

$$E_q = 6.37 \cdot (ESC_H_ref - 2.93) \quad (4)$$

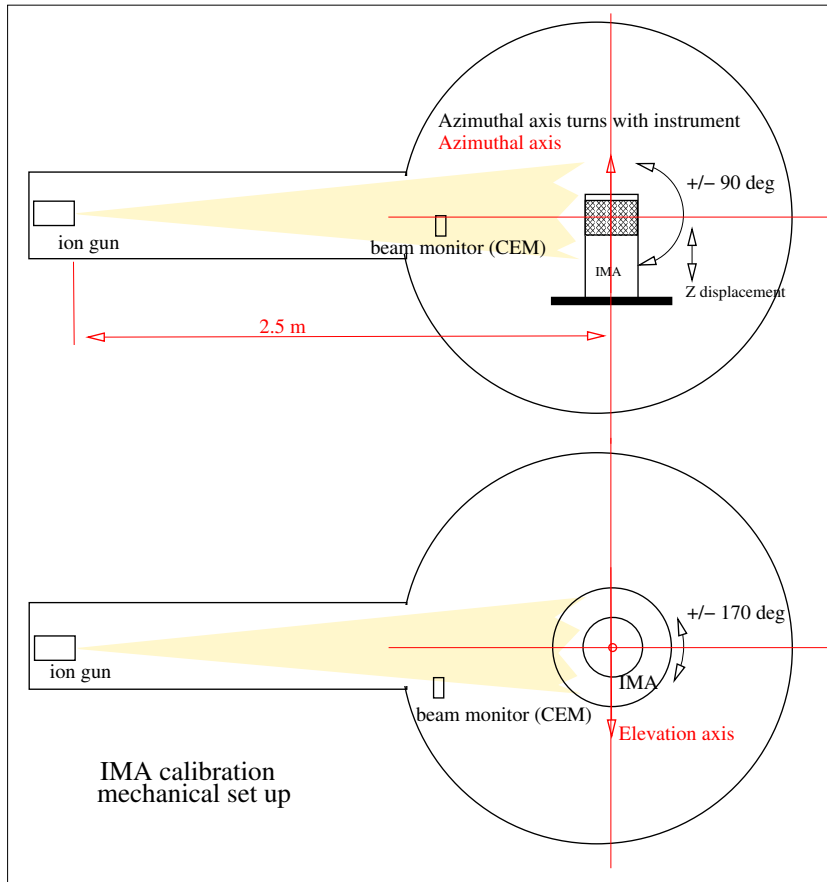


Figure 2: The mechanical set up of IMA in the vacuum chamber

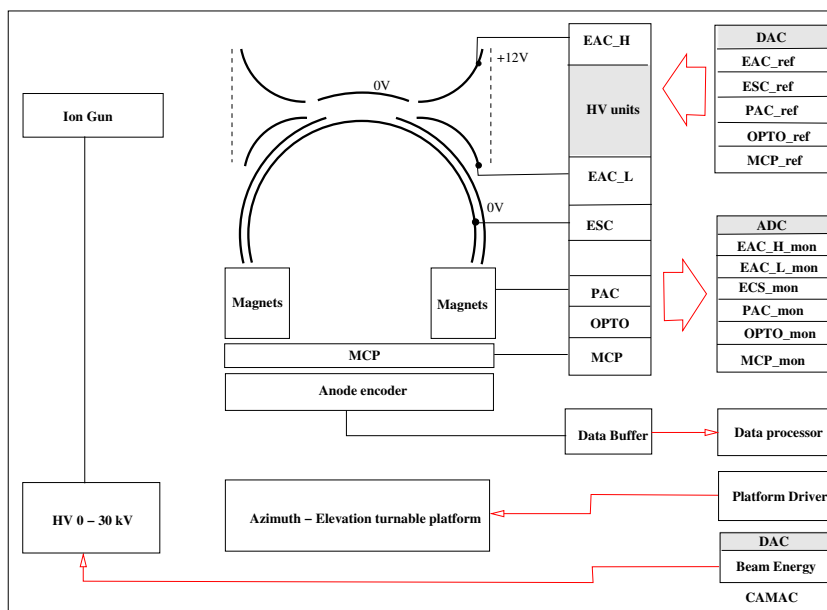


Figure 3: The electrical diagram of IMA calibration

$$ESC_H_ref = 2.93 + 0.157 \cdot E_q \quad (5)$$

$$K = 9.67 \quad (6)$$

$$K_{ref} = 6.37 \quad (7)$$

ESC_H_ref is measured in mV.

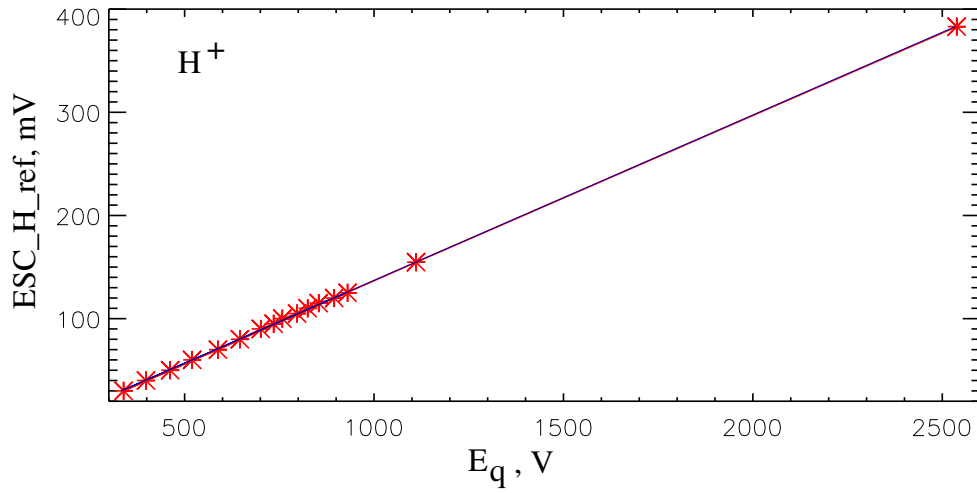


Figure 4: E_q versus ESC_H_ref . Measurements has been made for H^+ ions and for all available PAC values and for all Φ values.

Dependence of the K and K_{ref} values on the Φ angle for $\Theta = 0$ is shown in figure 5. K variation is described as:

$$K_{ref} = 6.37 \cdot \sin(\Phi - 184.0) \cdot 0.11 \quad (8)$$

$$K = 9.67 \cdot \sin(\Phi - 184.0) \cdot 0.11 \quad (9)$$

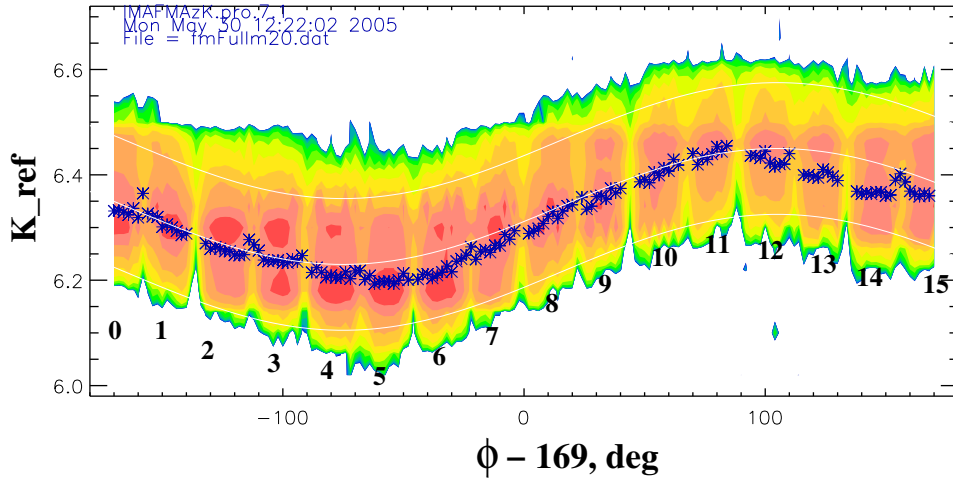


Figure 5: K_{ref} versus azimuth angle Φ . Measurements has been made for H^+ ions 1100 eV energy. Black numbers correspond to the azimuthal sector S .

3.2 D-Elevation properties of the scanner

Measured function of $\Phi(D_{ref})$ is shown in figure 6. Corresponding formulas are as follows:

$$\Theta[deg] = -3.44 - 182.6 \cdot D_{ref} \quad (10)$$

$$D_{ref} = -1.89 \cdot 10^{-2} - 5.47 \cdot 10^{-3} \cdot \Theta[deg] \quad (11)$$

$$\Theta[deg] = -3.44 - 95.1 \cdot D \quad (12)$$

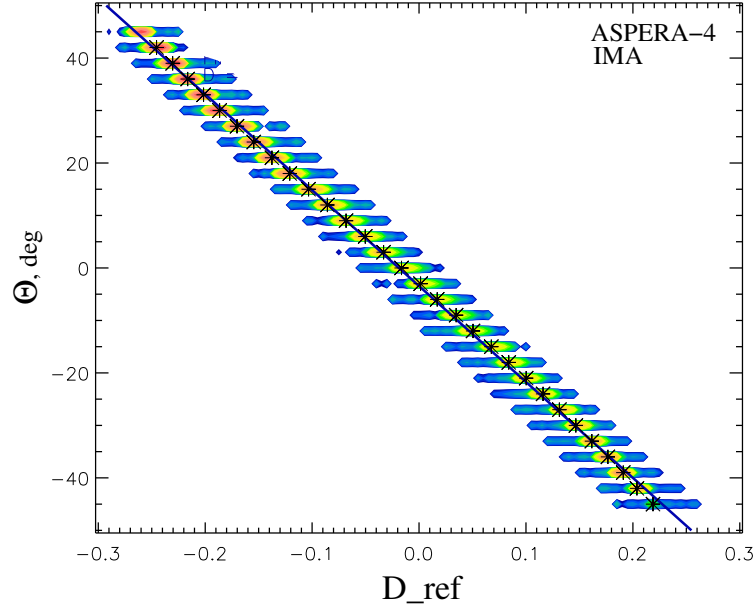


Figure 6: Θ versus D_{ref} . Measurements has been made for O^+ ions and for all available PAC values and for all Φ values.

4 Mass position and geometrical factor for different masses

IMA calibration was made for 4 types of ions, namely: H^+ , H_2^+ , N^+ , and O_2^+ . For each ions type, the peak position and corresponding geometrical factor has been measured for all azimuthal sectors S , in E_q range $[300 \div 10000 \text{ eV}]$, for $\Theta = 0$, and for all possible U_{PAC} values. Peaks for different E_q and different U_{PAC} are shown in figure 7. Vertical axis of each plot is the differential geometrical factor G_L , corresponding to the fixed azimuthal angle Φ . Shown measurements correspond to the centers of each azimuthal sector. Peaks are relatively wide due to the averaging over the all 16 sectors of the sensor.

The differential geometrical factors G_L in $cm^2 \text{ rad eV/eV}$ are given in Table 1. Figure 8 shows G_L of one sector versus azimuthal angle Φ . Values presented in Table 1 correspond to the maximum of the profile.

Finally figure 9 shows interpolation of the mass peak position over entire energy range of the instrument.

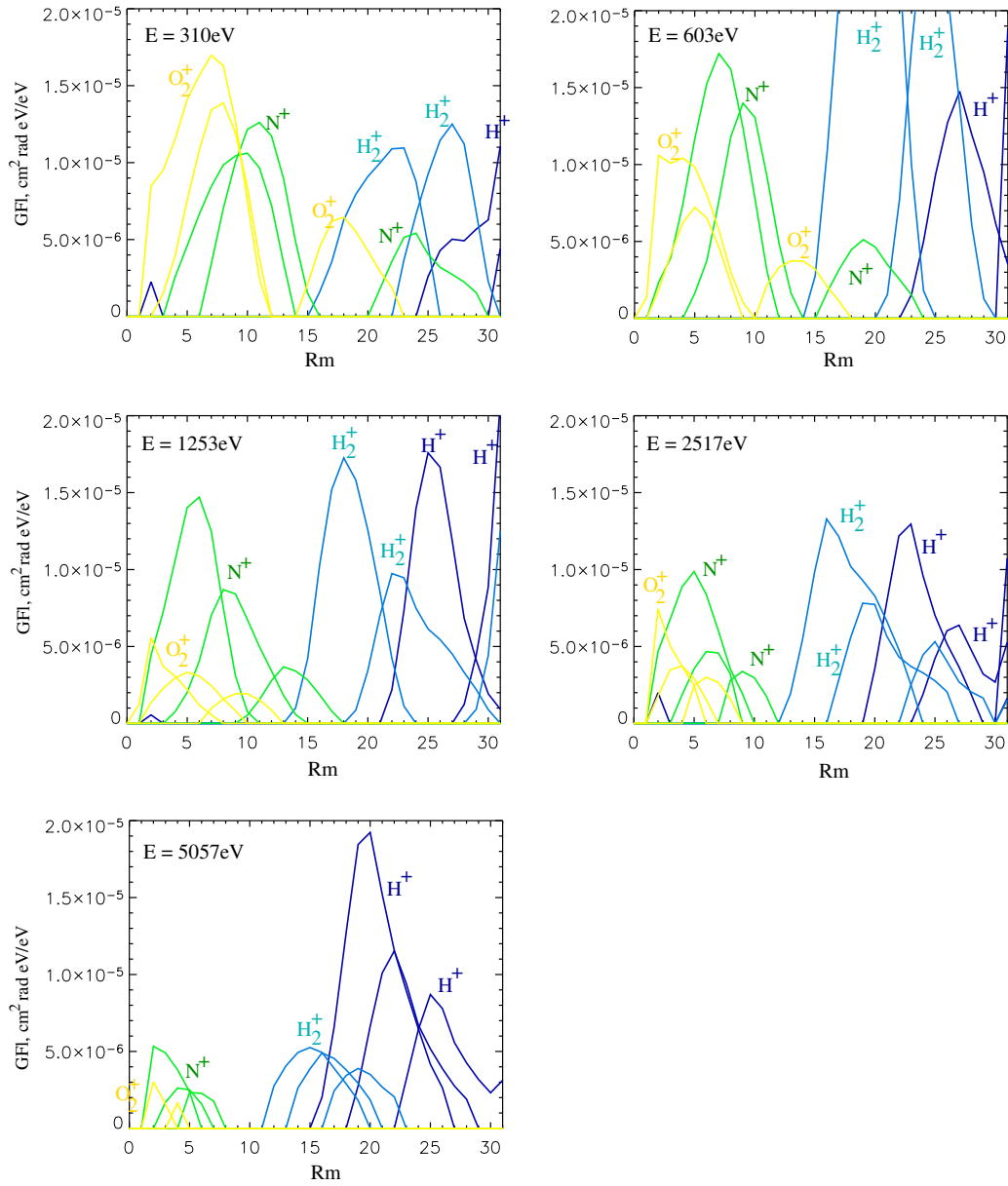


Figure 7: Mass peaks of H^+ , H_2^+ , N^+ , and O_2^+ for different energies. In the each panel the same color peaks correspond to the different U_{PAC} . Left peak corresponds to the maximal acceleration.

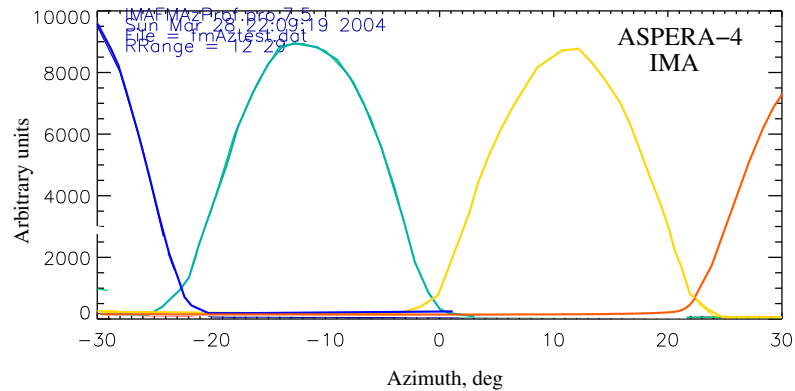


Figure 8: Geometrical factor (in arbitrary units) of one azimuthal sector versus Φ .

E_q, V	U_{PAC} index	$G_L H^+$	$G_L H_2^+$	$G_L N^+$	$G_L O_2^+$
310.	0	0.0E+00	0.0E+00	3.0E-05	3.4E-05
310.	1	4.4E-06	6.4E-05	7.2E-05	7.5E-05
310.	2	4.2E-05	7.4E-05	7.4E-05	1.2E-04
603.	0	0.0E+00	0.0E+00	2.7E-05	1.9E-05
603.	1	1.9E-05	1.2E-04	6.8E-05	3.3E-05
603.	2	7.5E-05	2.0E-04	9.7E-05	6.0E-05
1253.	0	0.0E+00	1.8E-05	1.7E-05	8.8E-06
1253.	1	3.5E-05	6.1E-05	4.9E-05	1.8E-05
1253.	2	8.4E-05	9.0E-05	7.5E-05	1.8E-05
2517.	0	1.1E-05	2.4E-05	1.1E-05	9.7E-06
2517.	1	3.4E-05	4.6E-05	1.8E-05	1.3E-05
2517.	2	6.8E-05	8.4E-05	5.0E-05	1.9E-05
5057.	0	4.5E-05	1.8E-05	6.4E-06	1.6E-06
5057.	1	6.1E-05	2.5E-05	8.4E-06	0.0E+00
5057.	2	1.1E-04	3.1E-05	1.6E-05	4.6E-06

Table 1: Differential geometrical factor G_L versus E_q and U_{PAC} .

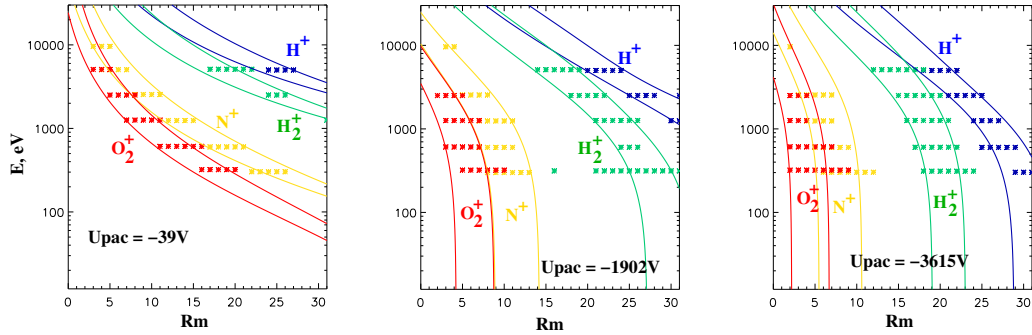


Figure 9: Interpolation of the position of the mass peaks of H^+ , H_2^+ , N^+ , and O_2^+ for entire energy range.



ASPERA-4



**Venus
Express**

Reference : **VE-ASP-TN-060402**
Issue : **1** Rev. : **1**
Date : **2006-06-17**
Volume : **-** Page: **12**

APPENDIX 9. IMA TM / TC DESCRIPTION

The ICA-IMA-VIA TC/TM data formats and related software aspects.

Issue **1.8**
2004-10-28 Hans Borg. IRF- Kiruna.

Document history.

Date	Issue	By	Changes
2002-04-07	Draft	HB	Composed and edited from several partial documents.
2002-04-20	1.2	HB	Added: Related documents. Important NOTE for HK-data change. Corrected standard header status bit.
2002-05-08	1.3	HB	Added: Mass order for table look up. Command status coding.
2003-05-16	1.4	HB	Corrected parameter orders (§5.2.1,§5.2.3) Timing and time tagging. (8.0)
2003-09-07	1.5	HB	Added header (§5.5.1) & HK (§6.1) parameters descriptions. Extra to timing (§8.2)
2003-11-15	1.6	HB	Corrected sampling time in §3.0
2004-05-08	1.7	HB	Added VIA specific definitions. Updated some ICA default settings.
2004-10-28	1.8	HB	Parameter order (§5.2.3 and §5.4).

Related documents.

- 1) ICA – RPC : the Ion Composition Analyser in the Rosetta Plasma Consortium. O Norberg et. al.
Note: “The ICA –RPC: ... should basically be applicable on the IMA - MU configuration”
- 2) ICA command description. Issue 1.5. H Borg.
- 3) IMA command description. Issue 1.4. H Borg.
- 4) CCSDS 120.0-B-1.
- 5) Basics of ICA/IMA embedded software. Issue: 1.3 H Borg
- 6) ICMA_ADC_CAL_yymmdd.doc (Current: yymmdd=030910 by HB)

Table of contents.

1.0 Scope.

2.0 Terminology.

3.0 Experiment basic operation.

4.0 The commanding system.

4.1 General.

4.2 Detailed command list.

5.0 Telemetry/Science modes.

5.1 Telemetry modes.

5.2 Data reduction modes general.

5.2.1 Science data processing.

5.2.2 Shadow and bad HV masking.

5.2.3 Parameter orders.

5.3 The data reduction modes.

5.3.1 Minimum modes.

5.3.1.1 Spectras only.

5.3.1.2 Selected Ion species.

5.3.1.3 Energy-Mass.

5.3.2 Normal modes.

5.3.3 High angular resolution modes.

5.3.4 Energy-Mass modes.

5.4 Special modes.

5.4.1 Test mode.

5.4.2 Calibration 1 mode.

5.4.3 Calibration 2 mode.

5.4.4 Fake mode.

5.4.5 Idle mode.

5.4.6 The 16-bit AD monitors.

5.4.7 The switch bits.

5.5 The standard header.

5.5.1 Header parameters description.

5.6 Telemetry/Data reduction mode combinations.

6.0 Housekeeping data.

6.1 HK parameters description.

7.0 Special data characteristics.

7.1 The F8 code.

7.2 Data compressions.

7.2.1 Compressed data layout.

8.0 Timing and time tagging.

8.1 General.

8.2 Time tagging.

1.0 Scope.

As the ICA (RPC/Rosetta), the IMA (Aspera/Mars Express) and VIA (Aspera/Venus Express) experiments are essentially the same this document treats all three. Differences are explicitly noted. It only briefly describes the operation of the experiments.

It is assumed that the reader has a basic knowledge of the experiments.

The document tries to describe in some detail the tm data return from the experiments.

2.0 Terminology.

If not otherwise stated a byte denotes an 8-bit item and a word a 16-bit item. A nibble is a 4-bit item. Bits are labeled in the power of 2, i.e. 0 (zero) is the least significant bit.

Precaution: ESA uses "octets" for an 8-bit item and "word" for a 16-bit item. ESA also uses 0 as the MS-bit (Mil Std. 1750 convention. Item size dependent).

F8 denotes an experiment 8-bit hybrid floating code used to reduce 32/16 bit parameters to 8 bits.

Notations like ICA/IMA/VIA indicates that all instruments is treated differently, typically default values, while ICA/IMA-VIA means ICA is different than IMA-VIA who are the same. Else notations like ICA only, IMA-VIA only are also used.

3.0 Experiment basic operation.

The basic operation consists of stepping through 32 or 96 energy HV deflection steps for each of 16 entrance HV deflection steps (polar angles). A complete cycle (scan) takes 64 seconds (32 levels) or 192 seconds (96 levels) respectively. The sampling time is 120.9 milliseconds. Each sample produces an imager matrix of 32 mass bins times 16 sectors (azimuth angles).

The data acquisition and transmission is synchronized to an acquisition (start) pulse. For ICA that pulse is received once per 32 seconds and for IMA once per 16 seconds.

All data to and from the experiment is transmitted over a serial 1355-link from/to a central unit that in turn interfaces to the spacecraft systems.

Each format starts with a 16-byte long standard header with a 3-byte long synchronization pattern.

Except for the header and some data in the special modes all data is by default converted to an 8-bit hybrid floating code (F8) followed by a loss less bit data compression.

Thus, most ICA-IMA data formats will float in the ESA telemetry packets. Some may, however, be synchronized (see §5.4).

For a more detailed description of the experiment see ICA – RPC : the Ion Composition Analyser in the Rosetta Plasma Consortium. (Norberg,O. et al.).

4.0 The commanding system.

4.1 General

With a few exceptions all experiment commands consists of a 16-bit word.
The word is subdivided into 4 nibbles n3-n0.

n3	n2	n1	n0
----	----	----	----

The commands are divided into 3(4) classes (types) as:

- Type 3 n3 :. 0 n2,n1,n0 represents a 12-bit variable parameter.
Capacity: 15 sets. n3=1-15.
- Type 2 n3=0 n2.:0 n1,n0 represents an 8-bit variable parameter.
Capacity: 15 sets. n2=1-15.
- Type 1/0 n3=n2=0 n1,n0 is dynamically used for variable length parameters like
4-bit, 1-bit or no parameter commands.
Capacity: 256 sets. n1,n0=0-255.

Note: The combined command words = 0xFFFF or 0x0000 are not used for safety.

The basic experiment internal interpretation of the 16-bit word is given below (§4.2).

For further details about commanding, see ICA/IMA Command Description. Issue 1.4. (H Borg).

4.2 Detailed command list.

The list below gives all the commands in terms of a short description, type, fixed part, parameter mask, acceptable parameter range and when applicable the default value. Note that this is the internal interpretation.

Prm: below stands for parameter. A “-“ below indicates not applicable or not defined.

Short description	Type	Fixed part	Prm. mask	Prm. range	Default
Main +28 volt switch	1/0	0x0002	0x0001	0-1	0
Opto +28 volt switch	1/0	0x0004	0x0001	0-1	0
Mcp +28 volt switch	1/0	0x0006	0x0001	0-1	0
Post acc. HV switch	1/0	0x0008	0x0001	0-1	1
Grid LV switch	1/0	0x000A	0x0001	0-1	1
Entrance HV switch	1/0	0x000C	0x0001	0-1	1
Deflection LV switch	1/0	0x000E	0x0001	0-1	1
Deflection HV switch	1/0	0x0010	0x0001	0-1	1
Direct command switch	1/0	0x0012	0x0001	0-1	0
Watch dog enable/disable	1/0	0x0014	0x0001	0-1	1
Gas pressure HV control. ICAonly	1/0	0x0016	0x0001	0-1	0
Thruster firing HV control. ICA only	1/0	0x0018	0x0001	0-1	0
Compression enable/disable	1/0	0x001C	0x0001	0-1	1
Alternating post acc. enb/dis	1/0	0x001E	0x0001	0-1	0
Post acc. level high/low	1/0	0x0020	0x0001	0-1	1
Auto reduction change enb/dis	1/0	0x0022	0x0001	0-1	1
Shadow masking enb/dis	1/0	0x0024	0x0001	0-1	1
Bad HV masking enb/dis	1/0	0x0026	0x0001	0-1	1
Bad mass clearing enb/dis. VIA only	1/0	0x0028	0x0001	0-1	0
Next command direct	1/0	0x0040	-	-	-
Energy deflection stepping	1/0	0x0041	-	-	-
Entrance deflection stepping	1/0	0x0042	-	-	-
Release V-cal format	1/0	0x0043	-	-	-
Activate debugger. Bench only	1/0	0x0046	-	-	-
Gas-HV timeout test. ICA only	1/0	0x0047	-	-	-
Trigger machine error. Bench only	1/0	0x0048	-	-	-
Test Watch dog reset.	1/0	0x004A	-	-	-
Empty TM fifo	1/0	0x004B	-	-	-
Flush TM fifo	1/0	0x004C	-	-	-
Boot PROM	1/0	0x004D	-	-	-
Imager test	1/0	0x004E	-	-	-
Dummy command	1/0	0x004F	-	-	-
Set HV ref. Range bits. VIA only.	1/0	0x0050	0x0003	0-3	-
Set bad mass index bit MS. VIA only	1/0	0x0060	+ 2:nd wrd	0-0xFFFF	0
Set bad mass index bit LS. VIA only	1/0	0x0070	+ 2:nd wrd	0-0xFFFF	0
Boot EEPROM incl. Context	1/0	0x00B0	0x000F	0-15	-
Set imager test pattern	1/0	0x00C0	0x000F	0-15	-
Boot EEPROM excl. Context	1/0	0x00D0	0x000F	0-15	-
Set ICA/IMA-VIA SID number	1/0	0x00E0	0x000F	0-5/0-6	5
Set EEPROM default boot section	1/0	0x00F0	0x000F	0-15	0

Short description	Type	Fixed part	Prm. mask	Prm. Range	Default
Set energy deflection level	2	0x0100	0x00FF	0-95	-
Set entrance deflection level	2	0x0200	0x00FF	0-15	-
Set ICA/IMA/VIA solar wind start index	2	0x0300	0x00FF	0-64	29/24/22
Set Gas pressure low level. ICA only	2	0x0400	0x00FF	0-255	0x16
Set Gas pressure high level. ICA only	2	0x0500	0x00FF	0-255	0x15
Set data reduction mode	2	0x0A00	0x00FF	0-39	0
Reprog. all EEPROM sections *)	2	0x0C00	0x00FF	0-16	-
Reprog. EEPROM section *)	2	0x0D00	0x00FF	0-255	-
Set ICA/IMA/VIA Opto reference	3	0x1000	0x0FFF	0-7	7/6/6
Set ICA/IMA/VIA Mcp reference	3	0x2000	0x0FFF	0-15	12/13/12
Set ICA/IMA Grid reference	3	0x3000	0x0FFF	0-7	7/7
Set ICA/IMA/VIA post acc. low reference	3	0x4000	0x0FFF	0-7	3/4/3
Set ICA/IMA/VIA post acc. hgh reference	3	0x5000	0x0FFF	0-7	6/7/6
Set energy defl. LV reference	3	0x6000	0x0FFF	0-4095	-
Set energy defl. HV reference	3	0x7000	0x0FFF	0-4095	-
Set entrance defl. HV reference	3	0x8000	0x0FFF	0-4095	-
Set noise reduction level	3	0x9000	0x0FFF	0-4095	0
Set ICA/IMA-VIA Fifo low (min) water mark	3	0xA000	0x0FFF	0-4095	40/20
Set ICA/IMA-VIA Fifo high (max) water mark	3	0xB000	0x0FFF	0-4095	80/40
Set ICA/IMA-VIA Fifo force water mark	3	0xC000	0x0FFF	0-4095	120/60
Set ICA/IMA-VIA Fifo clear water mark	3	0xD000	0x0FFF	0-4095	320/320
Set IMA Tm scaling factor. IMA-VIA only	3	0xE000	0x0FFF	0-4095	180
Start command (combined)	3	0xF000	0x0FFF	0-4095	-

*) Requires a second word reading 0xFEED (security lock key).

5.0 Telemetry/Science modes.

5.1 Telemetry modes.

The experiments have to their disposal a number of telemetry modes (here named Sid, Science ID). The Sid defines the TM rate available. The Sid numbers below are the internal ICA-IMA numbers that is also used in commanding. Note that direct (near real time) TM is mostly not available. The TM data is buffered onboard the S/C. The TM rate below then describes the reasonable amount to create to stay within the buffer allowance allocated for the planned S/C session before tapping to a ground S/C tracking station.

Telemetry modes (Sid+HK).

Sid	Mnemonic	Exp. Pkt. size in bytes	ICA rate	IMA rate
0	Min (Minimum)	618	5.15 bps	10.3 bps
1	Nrm (Normal)	2478	103.25 bps	206.5 bps
2	Bst (Burst)	4092	1023 bps	2046 bps
3	Cal (Calibration)	1074	268.5 bps	537 bps
4	Spc (Special)	3198	799.5 bps	1599 bps
5	Tst (Test)	600	75 bps	150 bps
6	Ima (Ima)	3996 *	NA	3996 bps
HK	Housekeeping	24	6 bps	12 bps

*) For IMA-VIA 2 such packets are sent every acquisition period.

5.2 Data reduction modes general.

The H/W operation of the experiment is always the same but for the 32 or 96 energy level step modes. The number of energy levels is strictly tied to the science mode selected. The experiment produces too much data to be transmitted (~ 80 000 bps). The parametric space measured are 32 mass bins (not true M/q) for 16 azimuths, 16 polar angles and 96 (32) energy levels. To cope with the high production rate versus the available Tm rate capacity the data is first reduced by integrations in the measured parametric space. The resulting (32/16 bit parameters) are then converted to a hybrid 8 bit floating code (F8). The size of the data set (format) is after this mostly still too big. The data therefore passed via a loss less bit compression routine before feeding it to the tm output FIFO.

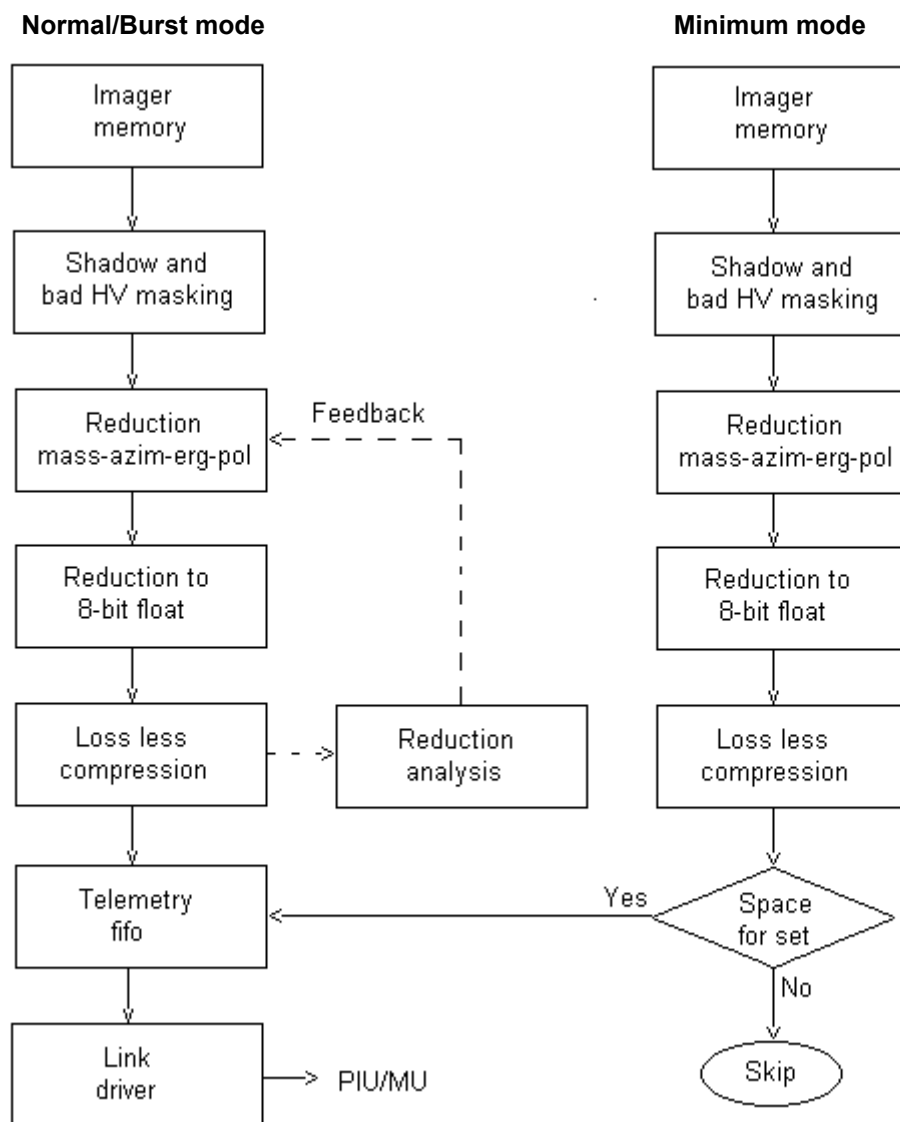
The tm FIFO can take a certain backlog of data due to its size. The backlog is watched by low and high watermarks. When appropriate, the S/W will change the reduction scheme such as to stay (on average) within the allocated tm rate. Thus the watermarks are scaled against the current telemetry mode. A more detailed description is given in § 5.2.1

5.2.1 Science data processing.

The data is read from the imager memory, shadow masked and fed to a data reduction module. The reduction is performed by integrations in the parametric space azimuth*mass*energy*polar-angles. When a full data set is acquired a 32/16 bit to a hybrid 8 bit floating code further reduces the data. The resulting data set is then compressed by a loss less method and fed to the telemetry FIFO for transmission. The TM-FIFO can take a certain backlog with respect to the current TM-rate (SID). The size of the compressed data will vary due to the characteristics of the actual data. For the *Normal* and *Burst* modes the TM-FIFO filling is controlled by analyzing the data set size with respect to the TM-FIFO filling and the actual TM-rate. When appropriate, a feedback is made to the reduction module to change the reduction scheme. The TM-FIFO filling is guided by watermarks. For the *Minimum* modes that create several data sets during the duration of a format, the reduction is fixed but instead the number of sets to transmit is adjusted to match, on the average, the TM-rate (SID).

The automatic data reduction change and data compression can be disabled by commands. It affects both *Minimum* and *Normal/Burst* modes.

Principle data flow.



5.2.2 Shadow and bad HV masking.

It is just the fact that the anticipated field of view of the experiments is not clean. Due to the mounting there are other S/C obstacles in the field of view. The current S/W has built in tables to simply clear out (set to 0) imager sectors that are more or less obscured. This has a two-folded motivation.

- a) A clear knowledge of what data is included (partly obscured may give "funny" effects).
- b) Zeroing out may (not for sure) give a better compression efficiency.

Like wise, due to HV limitations (capacity or accuracy) all polar angles cannot be reached for all energies. They are treated as for shadowed sectors above.

5.2.3 Parameter orders.

Apart from the Special modes (5.4), Science data are always delivered as a matrix azimuth*mass*energy*polar, where **azimuth** (the first) is the fastest varying one.

For masses above or equal to 8, the integration is simply done by adding adjacent mass bins. E.g. 8 mass bins integrate them 4 by 4 from the 32 available.

Note that the Imager addressing is such that the heavier masses comes first and the lighter ones last.

For masses below 8 (i.e. <= 6), the mass bins are integrated according to lookup tables and supposed to represent true M/q. The transmission order of the M/q masses is defined by the lookup tables.

The mass order for ICA and IMA is: H+ >O+ O+ He+ He++ O++
and for VIA: H+ O+ He+ >O+ He++ O++

If less than 6 masses, masses at the end are skipped.

Azimuth, energy and polar angles always come in the same order.

5.3 The data modes.

The data modes are divided into 5 groups: Min, Nrm, Har, Exm and Special.

5.3.1 The minimum modes.

The duration of the Minimum mode data formats is 16 minutes.

Mode	Index	Masses	Azimuth angles	Energies	Polar angles	Max sets
Idle *	0					
Void	1					
Mspo	2	2	1	32	1	15
Void	3					
Msis	4	6	1	96	1	5
Mexm	5	32	1	96	1	5
Void	6					
Void	7					

*) The Idle mode produces no scientific data and is described under the Special modes.

5.3.1.1 Minimum spectra only (Mspo).

The energy deflection is stepped through 32 levels starting at the solar wind start index.

For each scan all data for the two masses protons and alpha (table look up) are integrated over the sunward facing sectors. This produces a maximum of 15 sets of 2 masses * 32 E-levels spectra. As many as can be fitted (on the average to stay within the TM capacity) in the current SID block size are transmitted.

Layout: 1 header
n 2*32 spectra (Compressed F8)

5.3.1.2 Minimum selected ion species (Msis).

The energy deflection is stepped through all 96 levels for each of the 16 entrance steps.

For each scan all data for 6 selected ion species (table look up) are integrated over all angles (azimuth and polar). This produces a maximum of 5 sets of 6 masses * 96 E-levels spectra. As many as can be fitted (on the average to stay within the TM capacity) in the current SID block size are transmitted.

Layout: 1 header
n 6*96 spectra (Compressed F8)

5.3.1.3 Minimum energy-mass matrix (Mexm).

The energy deflection is stepped through all 96 levels for each of the 16 entrance steps.

For each scan all data for 32 mass bins are integrated over all angles (azimuth and polar). This produces a maximum of 5 sets of 32 mass-bins * 96 E-levels spectra. As many as can be fitted (on the average to stay within the TM capacity) in the current SID block size are transmitted.

Layout: 1 header
n 32*96 spectra (Compressed F8)

5.3.2 The normal modes (Nrm).

The duration of the Normal mode format is 192 seconds.

The energy deflection is stepped through all 96 steps for each of the 16 entrance steps.

The normal mode (group) is subjected to an automatic change of the data reduction scheme (if enabled) in order to adapt to the current TM capacity (SID).

The order of the reduced data matrix is always Mass-Azimuth-Energy-Polar with Mass being the fastest varying index. The masses are integrated by means of energy dependent lookup tables.

The reduction scheme.

Mode	Index	Masses	Azimuth angles	Energies	Polar angles
Nrm-0	8	6	16	96	16
Nrm-1	9	6	16	96	8
Nrm-2	10	6	16	96	4
Nrm-3	11	6	16	96	2
Nrm-4	12	6	8	96	2
Nrm-5	13	6	4	96	2
Nrm-6	14	3	4	96	2
Nrm-7	15	3	4	96	1

Layout: 1 header
1 data set (Compressed F8)

5.3.3 The burst high angular resolution modes (Har).

The duration of the burst high angular resolution mode format is 192 seconds.

The energy deflection is stepped through all 96 steps for each of the 16 entrance steps.

The burst high angular resolution mode (group) is subjected to an automatic change of the data reduction scheme (if enabled) in order to adapt to the current TM capacity (SID).

The order of the reduced data matrix is always Mass-Azimuth-Energy-Polar with Mass being the fastest varying index.

The reduction scheme.

Mode	Index	Masses	Azimuth angles	Energies	Polar angles
Har-0	16	16	16	96	16
Har-1	17	16	16	96	8
Har-2	18	16	16	96	4
Har-3	19	8	16	96	4
Har-4	20	4	16	96	4
Har-5	21	2	16	96	4
Har-6	22	2	8	96	4
Har-7	23	2	8	96	2

Layout: 1 header
 1 data set (Compressed F8)

5.3.4 The burst energy-mass matrix modes (Exm).

The duration of the burst energy-mass matrix mode format is 192 seconds.
 The energy deflection is stepped through all 96 steps for each of the 16 entrance steps.

The burst energy-mass matrix mode (group) is subjected to an automatic change of the data reduction scheme (if enabled) in order to adapt to the current TM capacity (SID).

The order of the reduced data matrix is always Mass-Azimuth-Energy-Polar with Mass being the fastest varying index.

The reduction scheme.

Mode	Index	Masses	Azimuth angles	Energies	Polar angles
Exm-0	24	32	16	96	16
Exm-1	25	32	16	96	8
Exm-2	26	32	16	96	4
Exm-3	27	32	16	96	2
Exm-4	28	32	8	96	2
Exm-5	29	32	4	96	2
Exm-6	30	32	2	96	2
Exm-7	31	32	2	96	1

Layout: 1 header
 1 data set (Compressed F8)

5.4 The special modes.

The special modes are mainly aimed for ground testing and calibration, but may well be used also when in orbit. Typically "Test" for commissioning.

As opposed to the science modes, the special modes do not allow any Tm FIFO backlogging.

The Test and the Cal1 mode will be synchronized to the ESA packets provided they run in combination with the Telemetry modes Tst and Cal respectively. The Fake mode is always synchronized to the ESA packets.

The order of the imager data transmitted are of type imager dump (snap shot), i.e. in the order as seen from the imager memory.

For Test and Cal1 modes that is mass*azimuth and for Cal2 mass*azimuth*energy.

Mode	Index	Content
Test	32	H/W close information and an Imager snapshot
Cal1	33	HV information and one Imager in 16-bit uncompressed words
Cal2	34	HV information and 96 Imagers (one per Energy level) in compressed F8
Fake	35	An incremental (by one) 16-bit counter in 16-bit uncompressed words
Void	36	
Void	37	
Void	38	
Void	39	

5.4.1 The test mode (Test).

The test mode delivers “hard ware close” information and do not contain any compressed data. It is 600 bytes long and will be synchronized to the ESA TM packets if SID=Tst (ICA-IMA nr 5) is used.

It contains the following data:

Byte offset	Length in bytes	Bits	Content
0	16		Standard header. See §5.5
16	2		Command word 0 return
18	2		Command word 1 return
20	20		10 16-bit AD monitor values. See &5.4.6
40	1		Void
41	1		Nos. 1355-link forced resets
42	1		Nos. 1355-link resets seen
43	1		Nos. 1355-link credit failures
44	2	15-10 9-8 7-4 3-0	EEPROM programming result Reprogramming counter Failure bits Destination EEP section Source EEP section
46	1		Nos. Watch dog resets
47	1		Nos. machine error resets
48	1		Void
49	3		48-bits S/W switch status. See §5.4.7
52	1		Noise reduction level
53	1		The gas pressure as seen from ROSINA. ICA only
54	2	15 14-12 11-0	Copy from HK format Direct command switch Pacc. low reference level Energy deflection HV reference
56	2	15 14-12 11-0	Copy from HK format Tm overflow flag Pacc. high reference level Energy deflection LV reference
58	2	15 14-12 11-0	Copy from HK format Pacc. current level (high=1 or low=0). Grid LV reference Entrance HV reference
60	2		CPU fault register
62	2		CPU fault address
64	1		Gas pressure low level. ICA only
65	1		Gas pressure high level. ICA only
66	2		CPU BIT result
68	2		Current program version running
70	1		Nos. sample overruns
71	1		Nos. sweep overruns
72	1		Nos. post overruns
73	1		Void
74	2		+28V monitor.
76	2		Fifo low water mark (Fmin)
78	2		Fifo high water mark (Fmax)
80	2		Fifo force limit (Ffrc)
82	2		Fifo clear limit (Fclr)
84	2		IMA Tm scaling factor. IMA-VIA only
86	1	7-6 5-3 2-0	Image memory test result Test counter. Memory half 1 test result Memory half 0 test result
87	1		E-level for Image snapshot
88	512		Imager snapshot in F8 code

5.4.2 The calibration-1 mode (Cal1).

The calibration-1 mode is specially designed for Imager calibration. It is 1074 bytes long and will be synchronized to the ESA TM packets if SID=Cal (ICA-IMA nr 3) is used.

Byte offset	Length in bytes	Bits	Content
0	16		Standard header. See §5.5
16	2		The digital deflection HV reference
18	2		The digital deflection LV reference
20	2		The digital entrance HV reference
22	1	7-4 3-0	The Opto. HV digital reference The Mcp. HV digital reference
23	1	7-4 3-0	The digital Post acc. HV reference The Grid LV digital reference
24	20		10 16-bit AD monitors. See §5.4.6
44	2		+28V monitor
46	1		Entrance angle index
47	1		Energy level index
48	2		Void
50	1024		Full Imager in 16-bit words

5.4.3 The calibration-2 mode (Cal2).

The calibration-2 mode is specially designed for Imager calibration. It delivers Imagers for a full 96 E-level sweep. The data is in compressed F8 code.

Byte offset	Length in bytes	Bits	Content
0	16		Standard header. See §5.5
16	2		The digital deflection HV reference
18	2		The digital deflection LV reference
20	2		The digital entrance HV reference
22	1	7-4 3-0	The Opto. HV digital reference The Mcp. HV digital reference
23	1	7-4 3-0	The digital Post acc. HV reference The Grid LV digital reference
24	20		10 16-bit AD monitors. See §5.4.6
44	2		+28V monitor
46	1		Entrance angle index
47	1		Energy level index
48	2		Void
50	nn		96 energy levels of full Imager in compressed F8

5.4.4 The faked data mode (Fake).

The Fake mode is specially designed to test the 1355-link for transmissions from the experiment to the PIU/MAIN-unit. It simply delivers a header followed by a word sequential counter as uncompressed data. It automatically adjusts the data size to match the current SID and will therefore always be synchronized to the ESA TM packets. Except for the header missing data can easily be detected.

Layout: 1 header.

An incremental counter to fill the current Sid packet.

5.4.5 The Idle mode.

The mode index refers it to the Minimum group, but may as well be regarded as a special mode. This mode does not produce any science data.

The Idle mode may be entered in two ways.

1) By command.

If entered by command the Opto and Mcp HV are regulated down to 0 reference, but the +28V Main switch stays ON. Also all science tm output are inhibited. Data in the tm FIFO are kept for later transmission. Commanding the experiment into the idle mode opens up for memory management activities (patch, dump or check).

2) Automatic (**ICA only**).

The experiment will enter Idle mode if the gas pressure as delivered by ROSINA exceeds a predefined upper limit or the experiment receives a thruster fire warning. When entered this way the +28V main switch to the HV supplies is switched off. Data in the tm FIFO, however, will continue to be transmitted.

5.4.6 The 16-bit AD monitors.

The AD monitors are stored in the following order.

Byte offset	Length in bytes	Content
0	2	Opto. HV
2	2	Mcp. HV
4	2	Upper entrance HV
6	2	Lower entrance HV
8	2	Post acceleration HV
10	2	Energy deflection HV
12	2	Energy deflection LV
14	2	Sensor unit temperature
16	2	Grid LV
18	2	DPU temperature

Actual calibration constants will be specified in the ICMA_ADC_CAL document.

5.4.7 The switch status bits.

The switch bits are coded as 0=Off and 1=On.

Bit	Content	Type
0	Mcp. +28V	H/W
1	Opto. +28V	H/W
2	Main +28V	H/W
3	Post acceleration HV	S/W
4	Grid LV	S/W
5	Entrance HV	S/W
6	Energy deflection LV	S/W
7	Energy deflection HV	S/W
8	Direct command	S/W
9	Watchdog	H/W
10	Gas HV control	S/W ICA only
11	Thruster firing HV control	S/W ICA only
12	Void	
13	Compression	S/W
14	Alternating post acceleration	S/W
15	Post acceleration level	S/W. Not really a switch
16	Auto reduction changes	S/W
17	Shadow masking	S/W
18	Bad HV masking	S/W
19	Void	
20	Void	
21	Void	
22	Test flag	S/W
23	Internal. Not commandable	

5.5 The standard header.

Each data format starts with a standard header containing the following information

Byte offset	Length in bytes	Bits	Content
0	3		Sync. Pattern. 0xE3 0x31 0xCA
3	1	7-6 5-0	Unit (1=ICA 2=IMA 3=VIA) Mode (index)
4	1		Experiment data format counter (Edf)
5	1	7 6 5 4 3-0	HV ramping in progress Tm Fifo emptied Checksum 0 failure Checksum 1 failure Number of sets in Minimum modes
6	1	7 6 5 4 3-0	Compression switch Auto reduction change switch Alternating post acceleration switch Post acceleration level Test pattern
7	1		Fifo filling. Number of 3-wrd packets in F8
8	1	7 6 5 4-0	Post processing overrun Sweep processing overrun Sample processing overrun PROM(0)/EEPROM section(1-16) loaded
9	1	7 6-0	Reset due to Watchdog or Machine error. Solar wind energy start index
10	3		Format start time in units of 31.25 msec. *
13	1	7 6 5-4	Bad HV masking switch Shadow masking switch The mass lookup table nr. VIA only
13	3	19-0	Format length in words

*) As the Format start time only consists of 24 bits, the MSB part should be taken from the ESA packet time. The 24 bits covers about 6 days.

5.5.1 Header parameters description.

Sync. Pattern.

The 3 bytes 0xE3 0x31 0xCA marks the start of a new EDF (Experiment Data Format). A search for this is required as the EDF's floats in the tm data stream.

Unit.

This parameter (2 bits) defines the experiment unit as follows:

- 0 Undefined
- 1 ICA
- 2 IMA
- 3 VIA

Mode.

This is the data reduction mode index used for the data in this EDF. The corresponding mode acronyms are given in §5.3 and §5.4.

Experiment data format counter.

This is an 8-bit running counter incremented by 1 for each released EDF. It swaps over to 0 after 255.

HV ramping in progress.

This bit will set if HV ramping has been performed during the data taking for this EDF.

Tm Fifo emptied.

This bit will set if the tm fifo is emptied before the start of this EDF. Always forced to and from special EDF's

Checksum 0,1 failures.

These bits will set if the corresponding checksum (0 or 1) fails during RAM booting. Sets from both PROM and EEPROM booting.

Number of sets in Minimum modes.

This parameter (4 bits) gives the number of data sets in this EDF for the minimum modes.

Compression switch.

This bit indicates whether data compression is enabled or not. 0=Disabled 1=Enabled.

Auto reduction change switch.

This bit indicates whether automatic data reduction change is enabled or not. 0=Disabled 1=Enabled.

Alternating post acceleration switch.

This bit indicates the post acceleration mode. If set (1) it is alternating else it is fixed.

Post acceleration level.

This bit gives the post acceleration level used for this format. 0=Low 1=High.

Test pattern.

For testing purposes a number of imager test patterns can be commanded. This parameter (4 bits) gives the actual test pattern number used. Ensure it is 0 for real scientific data.

Fifo filling

This gives the approximate number of 1355 link packets in the tm fifo. To convert to words, unpack the F8 code and multiply by 3.

Post,Sweep,Sample processing overrun.

These bits are set if a process overruns, i.e. the current data processing is not finished when a new is requested.

PROM(0)/EEPROM(1-16) loaded.

This parameter (5 bits) gives the program code currently loaded and running in RAM. It is coded as:
0=PROM 1-16=EEPROM section 0-15.

Reset due to Watchdog or Machine error.

This bit will set if the experiment has rebooted due to a watchdog or machine error reset.

Solar wind energy start index.

This parameter (7 bits) gives the energy start index when in the 32 level energy mode.

Format start time in units of 31.25 msec.

These 3 bytes is the starting time of this EDF. Note that more significant bits must be taken from the ESA packet time. Some attention should be paid close in time when this 3 bytes counter swaps around. That happens at about once per 6 days.

Bad HV masking switch.

This bit indicates if imager data is masked (set to zero) or not for angles/energies that can not be reached due to insufficient or too inaccurate HV. 0=Disabled 1=Enabled.

Shadow masking switch.

This bit indicates if imager data is masked (set to zero) or not for angles that are regarded as obscured by other S/C items. 0=Disabled 1=Enabled.

Mass lookup table nr.

This nr (0-2) indicates the actual mass lookup table used for this format.

Format length in words.

This parameter (20 bits) gives the total length of the format (EDF) in words.

5.6 Telemetry/Data reduction mode combinations.

In principle any Data reduction mode can be combined with any Telemetry mode. All combinations will, however, not optimize the use of the telemetry capacity. There are no precautions or restrictions built into the S/W to refuse some combinations. In the worst case (like a burst mode in the Minimum Sid) no science data at all will be delivered due to Tm FIFO clearing, provided the Auto reduction change is enabled.

The table below gives the anticipated combinations. Other combinations may, however, be used as a result of experiences from in orbit operation. Likewise the Fifo controlling limits may be trimmed.

Telemetry mode	Data reduction modes
Minimum (0)	Minimum modes
Normal (1)	Normal modes
Burst (2)	Burst modes (Har, Exm)
Calibration (3)	Calibration 1. Tailored
Special (4)	Calibration 2
Test (5)	Test. Tailored
Ima (6). IMA only	Burst modes (Har, Exm)

The Fake and Idle modes are applicable in all Telemetry modes.

6.0 The Housekeeping format.

The housekeeping format consists of 24 bytes delivered once per acquisition period. This rate is independent of the current Telemetry mode (Sid) in effect.

The ICA-IMA housekeeping format contains the following parameters:

Byte offset	Length in bytes	Bits	Content
0	1	7-2 1-0	Current data reduction mode. For index see §5.3 & 5.4 Last command status where: 0=Ok 1=Parameter out of range 2=Invalid 3=Erroneous opcode
1	1		HV switch status. The first 8 switches. See §5.4.7
2	1	7 6-4 3 2 1 0	The new command received toggle bit The current Sid number Post acceleration mode (Fixed/Alternating). +28V Main HV present * +28V Opto HV present * +28V Mcp HV present *
3	1		Fifo filling in terms of internal packets (words/3) in F8
4	2		The first word command return.
6	1		The Opto. HV monitor
7	1		The Mcp. HV monitor
8	1		The Energy deflection HV monitor
9	1		The Energy deflection LV monitor
10	1		The Post acceleration HV monitor
11	1		The Grid LV monitor
12	1		The Sensor unit temperature
13	1		The DPU Temperature
14	2	15 14-12 11-0	The direct command switch Post acceleration low level reference Energy deflection HV reference
16	2	15 14-12 11-0	Tm Fifo overflow Post acceleration high level reference Energy deflection LV reference
18	2	15 14-12 13	Post acceleration level (high or low) Grid LV reference. ICA-IMA only. The Dfl. HV range bit. VIA only.

		12 11-0	The Ent. HV range bit. VIA only. Entrance HV reference
20	2	15-13 12-9 8-0	Opto. HV default reference Mcp. HV default reference Entrance upper HV monitor
22	2	15-13 12-9 8-0	Opto. HV current reference Mcp. HV current reference Entrance lower HV monitor

*) For an explanation of the present status, See ICA/IMA Command Description Issue 1.4.

The monitor calibration constants will be specified in the ICMA_ADC_CAL document.

Important NOTE. Byte 2, bit 3 was intended to be the HV safety plug status (HV enabled/disabled). This status had to be taken out for technical reasons. The bit is now used to indicate the post acceleration mode of operation (Fixed or Alternating).

6.1 HK parameters description.

Current data reduction mode.

This gives the data reduction mode index (6 bits) currently running. The corresponding mode acronyms are given in §5.3 and 5.4.

Last command status.

This parameter (2 bits) gives the status of the last received command. The coding is

0=Ok	1=Parameter out of range
2=Invalid in current context	3=Erroneous opcode

HV switch status.

This gives the status of the HV switches (the first 8 from the switch register), where 0=Off and 1=On. The bit and switch relations are given in §5.4.7

New command received toggle bit.

This bit will toggle 0/1 each time a new command is received and the command status and the command return is fed to the HK transmit buffer.

The current Sid number.

This parameter (3 bits) gives the currently used Sid (tm mode). The acronyms and average bit rates are given in §5.1

Post acceleration mode.

By default, the post acceleration runs on a fixed HV setting. It can, however, be commanded to alternate between the preset high and low level HV. This bit is encoded as 0=Fixed, 1=Alternating.

+28V Main, Opto, Mcp HV present.

These 3 bits indicate the actual presence of the +28V after respective switch. 0=No and 1=Yes. See §6.0 for the bit switch-relations.

Fifo filling in terms of internal packets.

This gives the approximate number of 1355 link packets in the tm fifo. To convert to words, unpack the F8 code and multiply by 3. For F8 code, see § 7.0.

The first word command return.

This holds the first word (16 bits) of the last command received.

The HV, LV and temperature monitors at offsets 6-13.

These are 8-bit unsigned ADC readings for HV, LV and temperature monitors. Calibration factors will determine the sign. See §6.0 for the relation between offset and corresponding monitor.

The direct command switch.

ICA/IMA commands are of two types, direct or synchronized. The synchronized ones are executed at the end of format only. Setting the direct command switch ON (1) will turn synchronized commands to be direct.

Post acceleration low level reference.

This is the default digital low level post acceleration reference (3 bits).

Energy deflection HV reference.

This is the digital HV reference value associated with the monitor reading in this format (12 bits).

Tm Fifo overflow.

This bit is set to one if a tm fifo overflow has occurred. That is 0=No overflow 1=Overflow.

Post acceleration level.

This bit indicates the current post acceleration level. 0=Low 1=High.

Energy deflection LV reference.

This is the digital LV reference value associated with the monitor reading in this format (12 bits).

Grid LV reference (ICA-IMA only).

This is the digital grid LV reference value associated with the monitor reading in this format (3 bits).

The Dfl. And Ent. Range bits (VIA only).

This gives the HV range bit settings at the time of the monitor sampling.

Entrance HV reference.

This is the digital HV reference value associated with the monitor reading in this format (12 bits).

Opto. HV default reference.

This is the default digital Opto. HV reference value. That is the target value for ramping (3 bits).

Mcp. HV default reference.

This is the default digital Mcp. HV reference value. That is the target value for ramping (3 bits).

Entrance upper HV monitor.

This is a 9-bit unsigned ADC reading for the upper entrance HV monitor. Calibration factors will determine the sign.

Opto. HV current reference.

This is the current digital Opto. HV reference value associated with the monitor reading in this format (3 bits).

Mcp. HV current reference.

This is the current digital Mcp. HV reference value associated with the monitor reading in this format (3 bits).

Entrance lower HV monitor.

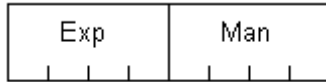
This is an 9-bit unsigned ADC reading for the lower entrance HV monitor. Calibration factors will determine the sign.

7.0 Special data characteristics.

The experiment uses some special tools to handle data. They are briefly described below.

7.1 The F8 code.

In order to reduce the number of bits to transmit, the S/W normally converts 32/16 bit items into a hybrid 8-bit floating code. The maximum capacity is numbers up to 507903. If greater (32-bits only) the number is set to the maximum. It is regarded as a hybrid due to the fact that numbers less or equal to 32 are transmitted as integers. The layout is:



where Exp is the Exponent and Man the Mantissa. Numbers less or equal to 32 are used as is, that is they will be coded as 0x00 – 0x20. If greater the real mantissa part will be used with the MSB stripped of (always a one, not transmitted) and the next four MSB bits set into “Man”. The Exp part will be the real exponent adjusted for the new bias (32) and set into Exp.

This is a simple C routine to unpack the F8 coded data:

```
int unpack_f8(int acc)
{  int exp;

   exp=(acc >> 4) & 0x0F;
   if(exp > 1)
   { acc=(acc & 0x0F) | 0x10;
     acc=acc << (exp-1);
   }

   return acc;
}
```

7.2 Data compression.

The ICA-IMA compression consists of two functional parts: a preprocessor and an adaptive entropy coder.

The preprocessor first converts a 16 or 32 bit word to a hybrid floating 8-bit byte (F8-code). It then uses the delayed predictor technique (to calculate δ 's) for the mapping process.

The bit compression uses Rice's adaptive coding (CCSDS 121.0-B-1). From above (F8-code) the implemented compression software works with 8 bit length data only (Types=0-7).

7.2.1 Compressed data layout.

The compressed data layout consists of records subdivided into blocks. With exception for type 0, sub 1 each record holds compressed data for 128 bytes. The layout is a variant of the CCSDS 121.0-B-1 recommendation.

The differences are:

- 1) A Record always starts with a record length in bytes and if required a bit padding field at the end to ensure whole bytes. This way the next record may be located (except for some special situations) if the decompression fails in a record.
- 2) The order of Fundamental sequences (Fs) and Split bits (Sb) are Fs+Sb,Fs+Sb..... instead of Fs,Fs.... ,Sb,Sb... Again if a decompression fails in a block, the already decompressed bytes may be correct. This also allows for short blocks, short records at the end of a fully compressed data area.
- 3) The number of zero run blocks is given as a fixed binary 3 bit field instead of a Fs code.
- 4) The type 0 second extension (sub=1) do not use the CCDS one. Instead a special zero run record is introduced for the ICA-IMA experiments. The reason is that both experiment have large areas in shadow. When in shadow all data are zeroed out giving rise to long sequences of records with zero run blocks. Instead of counting zero run blocks, zero run records are counted. Example record: 0x03,0x00,0x17 would decompress to $128 \cdot 8 = 1024$ bytes of 0x00.

For details see CCSDS-121.0-B-1.

Record.

Length	Reference	Block 0	Block 1	Block N	Pad
--------	-----------	---------	---------	-------	---------	-----

Block (Type 0.0).

Type = 0	Sub=0	Block count-1
----------	-------	---------------

Block (Type 0.1).

Type = 0	Sub=1	Record count-1
----------	-------	----------------

Block (Type 1-6).

Type=1-6	Fs0+Sb0	Fs1+Sb1	FsN+SbN
----------	---------	---------	-------	---------

Block (Type 7).

Type = 7	Byte 0	Byte 1	Byte N
----------	--------	--------	-------	--------

Fields

Name	Bits	Short description
Length	8	The total length in bytes of the record
Reference	8	The uncompressed reference value for the record
Block	Variable	A block of bits holding compressed data for 16 bytes *)
Pad	Variable	Bit padding to ensure whole bytes for a record
Type	3	The compression type (0-7)
Sub	1	The type 0 subtype extension (0-1)
Block count-1	3	Number of zero run blocks – 1
Record count-1	4	Number of zero run records – 1
FsN+SbN	Variable	The Fundamental sequence + the Split bits for byte N
Byte	8	Un uncompressed byte

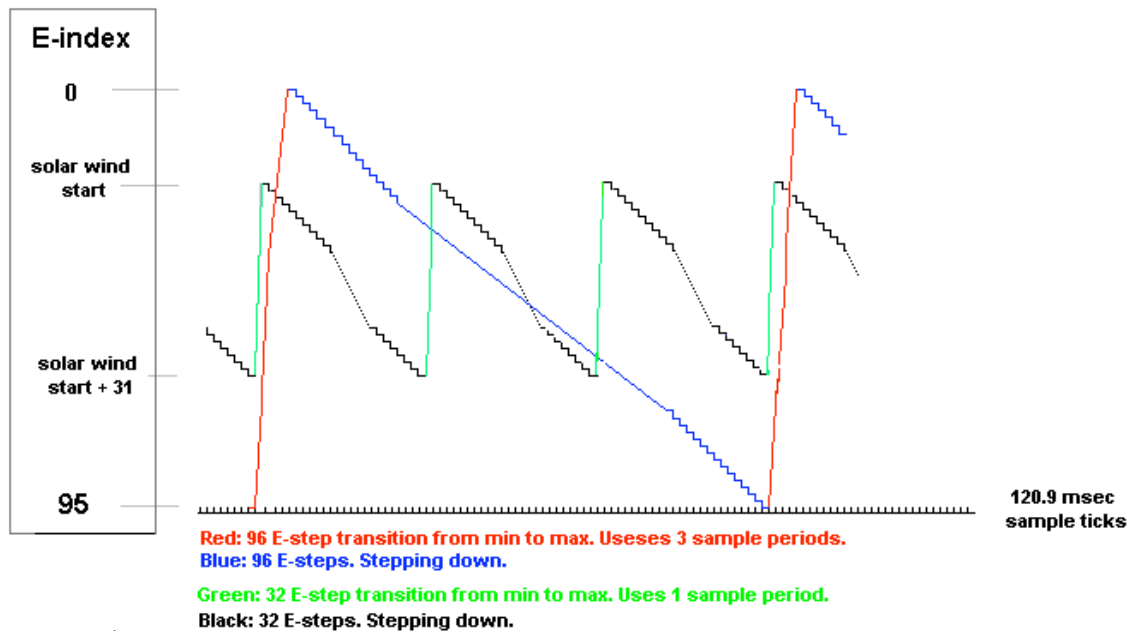
*) Block 0 only holds data for 15 bytes. The Reference gives the 16:th byte.

8.0 Timing and time tagging.

8.1 General.

Disregarding any clocks like DPU master, the experiment operation (measurement) is governed by the imager sampling time (120.9 msec). The imager supplies a mass * azimuth matrix for a given energy and elevation (polar angle) per sample. The energy and elevation is controlled by changing electrostatic HV deflection systems. The energy cycle always starts at the maximum energy and is then stepped down to the minimum level. The cycle is then repeated by forcing the HV to its maximum. The change from low to high is allocated one sample period to ensure proper HV relaxing. The maximum number of energy levels are 96. There are, however, modes that use 32 consecutive levels only out of the 96. They also require a sample period for HV relaxation. Thus for a proper coherent operation, the 32 level mode requires 33 sampling periods leading to 99 sampling periods for the 96 level energy modes. The "dead" HV transition period is always placed in front of each energy scan (1 sample for 32 energy levels and 3 for 96 energy levels). The figure below shows the principles.

Symbolic sketch of the ICA/IMA energy stepping for 96 and 32 E-levels. They are organized to always be in synchronism.



8.2 Time tagging.

The term time tagging here refers to the Iscience format (EDF=Experiment Data Format) time transmitted in the header of each EDF. This time always refer to the start of the first sample in the data collection scheme for the current format. That is, any HV relaxing period is NOT included, but may have to be taking into account for subsequent cycles (energy and/or elevations). The EDF time is composed of the time delivered by S/C and an internal timer. What ever, the accuracy of the S/C timer the is scaled down to 31.5 msec accuracy. Also note that the EDF time is 3 bytes wide only. More significant bits must be taken from tm packet times. All times are with respect to S/C time. Any correlation/correction to UTC should be done after the 3 byte time has been complemented with more significant bits from the ESA packet time. Bee observant that when the 3 byte ICA/IMA timer swaps around, the packet MSB may already have been updated by one prior to be applicable for the time. This is due to the tm fifo saving of tm data. This will not happen very often and can always be corrected for. The reason for only 3 bytes time tagging is to reduce the overhead by the header in the low rate tm modes. The timer will swap around about once per 6 days.

9.0 Data reduction considerations.

The experipents utilizes an automatic way of adjusting the data reduction in order not to produce too much data for tm down load. This is accomplished by integrating "adjacent" samples together. There is no attempt onboard to divide down the counts by number of samples integrated Mostly not advisable for "Poission" counting statistics. The number of samples can, however, be obtained on ground by the knowledge of the onboard steering tables. This is not a subject of this manual.



ASPERA-4

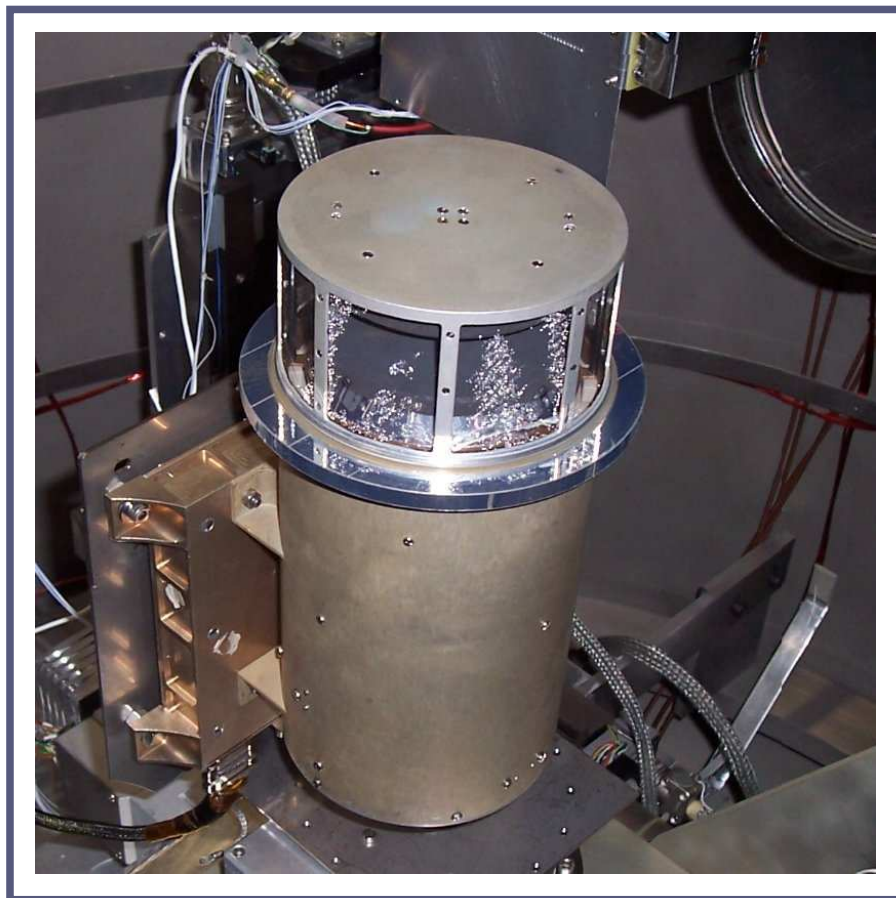


**Venus
Express**

Reference : **VE-ASP-TN-060402**
Issue : **1** Rev. : **1**
Date : **2006-06-17**
Volume : **-** Page: **13**

APPENDIX 10.
IMA: CONVERSION TO PHYSICS UNITS

Venus Express ASPERA-4
IMA BIBLE
V.1.0 January 26, 2006



Andrei Fedorov

Centre d'Etude Spatiale Rayonnement, Toulouse, France

With kind help of [Hans Borg](#) (IRF) and [Nicolas Penne](#) (CESR)

1 IMPORTANT NOTE

This text is supplied with a number of files that are the generic parts of "The Bible".

2 Internal IMA data array and associated physical terms.

Internal representation of IMA data is an array ($32 \times 16 \times 96 \times 16$) or ($AzIndex, RmIndex, EnIndex, ElIndex$). Each value of this array is a count of the corresponding cell. The first index of array varies faster. Here:

$RmIndex = 0 \div 31$ - radial position of the cell along one sector of the detector. It codes M/Q of the particle. (M is the mass of the ion and Q is the ion charge).

$AzIndex = 0 \div 15$ - number of azimuthal sector that this cell belongs. It codes the azimuthal angle Φ of the incident particle.

$EnIndex = 0 \div 95$ - corresponding number of the energy step. It codes E/Q of the incident ion. Here E is the particle energy.

$ElIndex = 0 \div 95$ - this index codes elevation angle Θ of the incident particle.

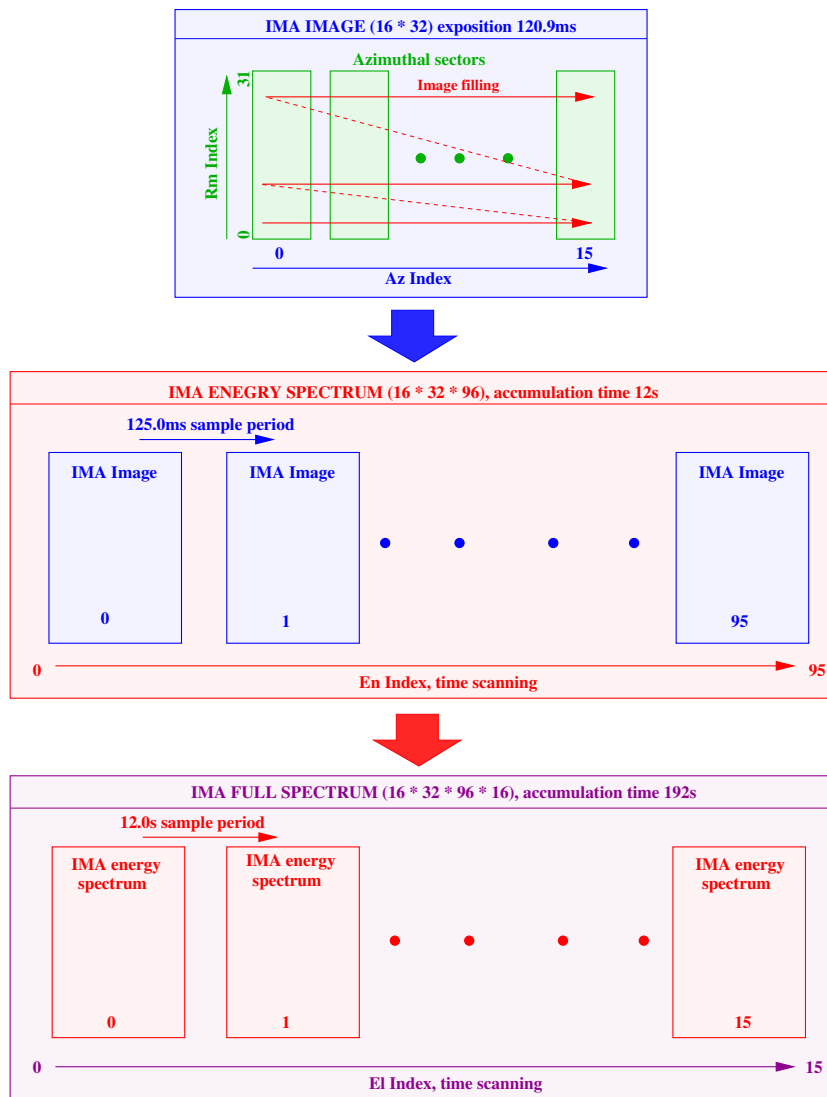


Figure 1: IMA data accumulation diagram. Red arrows in the top panel show the order of filling of the **IMA_Image**.

Data accumulation process is shown in Figure 1. **IMA_Image** consisting of an array ($AzIndex, RmIndex$)

is accumulated for each energy step and each polar angle. It is real exposition of $16 * 32 = 512$ independent counters (cells) working in parallel. Exposition time is $120.9ms$. 96 consequence **IMA_Image**(EnIndex) creates one **IMA_Energy_Spectrum**. One image follows the previous image with period = $125.0ms$. Thus one **IMA_Energy_Spectrum** is accumulated in $12.0s$. Sequence of 16 of **IMA_Energy_Spectrum**(ElIndex) taken with different polar angles creates a **IMA_Full_Spectrum**. **IMA_Full_Spectrum** is generated each $192.0s$.

3 Telemetry modes

This section describes conversion a **IMA_Full_Spectrum** to an array transmitted to the telemetry. Section introduces *TRmIndex*, *TAzIndex*, *TEnIndex*, and *TElIndex* values.

Not implemented yet. TBD

4 Energy table.

Energy table establish relation between E/Q of the ion and *EnIndex* value. This table is in "EnTable.txt" file. The format of this file is described in the file header. The resume of IMA energy steps is given in Table 1.

Table 1: VEX IMA Energy table, V.1.0, Apr 20 2004

EnI	E/Q														
0	29999.9	1	27629.1	2	25444.8	3	23431.6	4	21581.6	5	19871.5	6	18301.3	7	16855.5
8	15526.2	9	14298.1	10	13163.2	11	12121.6	12	11165.5	13	10287.1	14	9470.9	15	8724.7
16	8032.9	17	7395.5	18	6812.5	19	6276.1	20	5778.7	21	5320.0	22	4900.3	23	4511.6
24	4155.7	25	3828.1	26	3524.6	27	3246.5	28	2989.7	29	2753.1	30	2535.1	31	2334.6
32	2150.0	33	1980.2	34	1823.8	35	1679.4	36	1547.0	37	1424.0	38	1311.7	39	1208.7
40	1112.5	41	1024.2	42	944.0	43	869.1	44	800.9	45	736.7	46	679.2	47	625.8
48	576.3	49	530.8	50	488.0	51	449.3	52	414.5	53	381.1	54	351.7	55	323.6
56	298.2	57	274.1	58	252.7	59	232.7	60	213.9	61	197.9	62	181.9	63	167.1
64	153.8	65	141.7	66	131.0	67	120.3	68	111.0	69	101.6	70	93.6	71	86.6
72	79.8	73	73.5	74	67.6	75	62.3	76	57.4	77	52.8	78	48.7	79	44.8
80	41.3	81	38.0	82	35.0	83	32.2	84	29.7	85	27.4	86	25.2	87	23.2
88	21.4	89	19.7	90	18.1	91	16.7	92	15.4	93	14.1	94	13.0	95	12.0

5 Elevation table.

Elevation table gives correspondence between Θ and *EnIndex* and *ElIndex*. Appropriate file is "ElTable.txt". The format of the file is described in its header. The summary of IMA elevation table is shown in Table 2. Value less than -50.0 means that given **IMA_Energy_Spectrum**absents in the telemetry data flow (BUT not in the **IMA_Full_Spectrum** !).

Table 2: VEX IMA Elevation table, V.2.0, 11 Oct 2005

ElIndex	0	1	2	3	4	5	6	7	8	9	10	11	12	13	14	15
EnIndex																
0	-100.0	-100.0	-100.0	-100.0	-100.0	-14.0	-8.4	-2.8	2.8	8.4	14.0	-100.0	-100.0	-100.0	-100.0	-100.0
1	-100.0	-100.0	-100.0	-100.0	-19.6	-14.0	-8.4	-2.8	2.8	8.4	14.0	19.6	-100.0	-100.0	-100.0	-100.0
2	-100.0	-100.0	-100.0	-100.0	-19.6	-14.0	-8.4	-2.8	2.8	8.4	14.0	19.6	-100.0	-100.0	-100.0	-100.0
3	-100.0	-100.0	-100.0	-100.0	-19.6	-14.0	-8.4	-2.8	2.8	8.4	14.0	19.6	-100.0	-100.0	-100.0	-100.0
4	-100.0	-100.0	-100.0	-25.2	-19.6	-14.0	-8.4	-2.8	2.8	8.4	14.0	19.6	25.2	-100.0	-100.0	-100.0
5	-100.0	-100.0	-100.0	-25.2	-19.6	-14.0	-8.4	-2.8	2.8	8.4	14.0	19.6	25.2	-100.0	-100.0	-100.0
6	-100.0	-100.0	-30.8	-25.2	-19.6	-14.0	-8.4	-2.8	2.8	8.4	14.0	19.6	25.2	30.8	-100.0	-100.0
7	-100.0	-100.0	-30.8	-25.2	-19.6	-14.0	-8.4	-2.8	2.8	8.4	14.0	19.6	25.2	30.8	-100.0	-100.0
8	-100.0	-36.4	-30.8	-25.2	-19.6	-14.0	-8.4	-2.8	2.8	8.4	14.0	19.6	25.2	30.8	36.4	-100.0
9	-100.0	-36.4	-30.8	-25.2	-19.6	-14.0	-8.4	-2.8	2.8	8.4	14.0	19.6	25.2	30.8	36.4	-100.0
10	-42.0	-36.4	-30.8	-25.2	-19.6	-14.0	-8.4	-2.8	2.8	8.4	14.0	19.6	25.2	30.8	36.4	42.0
11	-42.0	-36.4	-30.8	-25.2	-19.6	-14.0	-8.4	-2.8	2.8	8.4	14.0	19.6	25.2	30.8	36.4	42.0
12	-42.0	-36.4	-30.8	-25.2	-19.6	-14.0	-8.4	-2.8	2.8	8.4	14.0	19.6	25.2	30.8	36.4	42.0
13	-42.0	-36.4	-30.8	-25.2	-19.6	-14.0	-8.4	-2.8	2.8	8.4	14.0	19.6	25.2	30.8	36.4	42.0

Table 2: continued

14	-42.0	-36.4	-30.8	-25.2	-19.6	-14.0	-8.4	-2.8	2.8	8.4	14.0	19.6	25.2	30.8	36.4	42.0
15	-42.0	-36.4	-30.8	-25.2	-19.6	-14.0	-8.4	-2.8	2.8	8.4	14.0	19.6	25.2	30.8	36.4	42.0
16	-42.0	-36.4	-30.8	-25.2	-19.6	-14.0	-8.4	-2.8	2.8	8.4	14.0	19.6	25.2	30.8	36.4	42.0
17	-42.0	-36.4	-30.8	-25.2	-19.6	-14.0	-8.4	-2.8	2.8	8.4	14.0	19.6	25.2	30.8	36.4	42.0
18	-42.0	-36.4	-30.8	-25.2	-19.6	-14.0	-8.4	-2.8	2.8	8.4	14.0	19.6	25.2	30.8	36.4	42.0
19	-41.9	-36.4	-30.8	-25.2	-19.6	-14.0	-8.4	-2.8	2.8	8.4	14.0	19.6	25.2	30.8	36.4	42.0
20	-42.0	-36.4	-30.8	-25.2	-19.6	-14.0	-8.4	-2.8	2.8	8.4	14.0	19.6	25.2	30.8	36.4	42.0
21	-42.0	-36.3	-30.8	-25.2	-19.6	-14.0	-8.4	-2.8	2.8	8.4	14.0	19.6	25.2	30.8	36.4	42.0
22	-42.0	-36.3	-30.8	-25.2	-19.6	-14.0	-8.4	-2.8	2.8	8.4	14.0	19.6	25.2	30.8	36.4	42.0
23	-41.9	-36.4	-30.8	-25.2	-19.6	-14.0	-8.4	-2.8	2.8	8.4	14.0	19.6	25.2	30.8	36.4	42.0
24	-41.9	-36.3	-30.7	-25.2	-19.6	-14.0	-8.4	-2.8	2.8	8.4	14.0	19.6	25.2	30.8	36.4	42.0
25	-42.0	-36.4	-30.8	-25.1	-19.6	-14.0	-8.4	-2.8	2.8	8.4	14.0	19.6	25.2	30.8	36.4	42.0
26	-41.9	-36.3	-30.7	-25.2	-19.6	-14.0	-8.4	-2.8	2.8	8.4	14.0	19.6	25.2	30.8	36.4	42.0
27	-42.0	-36.4	-30.8	-25.1	-19.5	-13.9	-8.4	-2.8	2.8	8.4	14.0	19.6	25.2	30.8	36.4	42.0
28	-42.0	-36.4	-30.8	-25.2	-19.6	-14.0	-8.4	-2.8	2.8	8.4	14.0	19.5	25.2	30.7	36.4	41.9
29	-42.0	-36.3	-30.8	-25.2	-19.6	-14.0	-8.3	-2.8	2.8	8.4	13.9	19.6	25.2	30.8	36.4	41.9
30	-42.0	-36.3	-30.8	-25.1	-19.6	-14.0	-8.4	-2.8	2.8	8.3	14.0	19.5	25.2	30.8	36.4	42.0
31	-42.0	-36.4	-30.7	-25.1	-19.5	-13.9	-8.3	-2.7	2.8	8.4	14.0	19.6	25.2	30.8	36.4	41.9
32	-42.0	-36.4	-30.8	-25.2	-19.6	-14.0	-8.4	-2.8	2.8	8.4	14.0	19.6	25.2	30.8	36.4	42.0
33	-42.0	-36.4	-30.8	-25.2	-19.6	-14.0	-8.4	-2.8	2.8	8.4	14.0	19.6	25.2	30.8	36.4	42.0
34	-42.0	-36.4	-30.8	-25.2	-19.6	-14.0	-8.4	-2.8	2.8	8.4	14.0	19.6	25.2	30.8	36.4	42.0
35	-42.0	-36.4	-30.8	-25.2	-19.6	-14.0	-8.4	-2.8	2.8	8.4	14.0	19.6	25.2	30.8	36.4	42.0
36	-42.0	-36.4	-30.8	-25.2	-19.6	-14.0	-8.4	-2.8	2.8	8.4	14.0	19.6	25.2	30.8	36.4	42.0
37	-42.0	-36.4	-30.8	-25.2	-19.6	-14.0	-8.4	-2.8	2.8	8.4	14.0	19.6	25.2	30.8	36.4	42.0
38	-42.0	-36.4	-30.8	-25.2	-19.6	-14.0	-8.4	-2.8	2.8	8.4	14.0	19.6	25.2	30.8	36.4	42.0
39	-42.0	-36.4	-30.8	-25.2	-19.6	-14.0	-8.4	-2.8	2.8	8.4	14.0	19.6	25.2	30.8	36.4	42.0
40	-42.0	-36.4	-30.8	-25.2	-19.6	-14.0	-8.4	-2.8	2.8	8.4	14.0	19.6	25.2	30.8	36.4	42.0
41	-42.0	-36.4	-30.8	-25.2	-19.6	-14.0	-8.4	-2.8	2.8	8.4	14.0	19.6	25.2	30.8	36.4	42.0
42	-41.9	-36.4	-30.8	-25.2	-19.6	-14.0	-8.4	-2.8	2.8	8.4	14.0	19.6	25.2	30.8	36.4	42.0
43	-42.0	-36.4	-30.8	-25.2	-19.6	-14.0	-8.4	-2.8	2.8	8.4	14.0	19.6	25.2	30.8	36.4	42.0
44	-42.0	-36.4	-30.8	-25.2	-19.6	-14.0	-8.4	-2.8	2.8	8.4	14.0	19.6	25.2	30.8	36.4	41.9
45	-42.0	-36.4	-30.8	-25.2	-19.6	-14.0	-8.4	-2.8	2.8	8.4	14.0	19.6	25.2	30.8	36.4	42.0
46	-42.0	-36.4	-30.8	-25.2	-19.5	-14.0	-8.4	-2.8	2.8	8.4	14.0	19.6	25.2	30.7	36.4	42.0
47	-42.0	-36.4	-30.8	-25.2	-19.6	-14.0	-8.4	-2.8	2.8	8.4	14.0	19.6	25.2	30.8	36.4	42.0
48	-41.9	-36.4	-30.8	-25.2	-19.6	-14.0	-8.4	-2.9	2.8	8.4	14.0	19.6	25.2	30.8	36.4	42.0
49	-42.0	-36.3	-30.8	-25.1	-19.6	-13.9	-8.4	-2.7	2.8	8.3	14.0	19.6	25.2	30.8	36.4	42.0
50	-42.0	-36.4	-30.8	-25.1	-19.6	-14.0	-8.4	-2.9	2.8	8.4	13.9	19.6	25.2	30.8	36.3	42.0
51	-42.0	-36.3	-30.8	-25.2	-19.6	-13.9	-8.4	-2.8	2.7	8.4	14.0	19.6	25.1	30.8	36.4	42.0
52	-42.0	-36.4	-30.8	-25.2	-19.7	-13.9	-8.3	-2.8	2.8	8.4	14.0	19.6	25.2	30.8	36.4	41.9
53	-42.0	-36.4	-30.9	-25.1	-19.5	-14.0	-8.4	-2.8	2.7	8.3	14.1	19.6	25.2	30.8	36.4	41.9
54	-42.0	-36.4	-30.8	-25.1	-19.6	-13.9	-8.4	-2.7	2.8	8.3	14.0	19.5	25.2	30.8	36.5	42.0
55	-42.0	-36.4	-30.8	-25.2	-19.6	-14.0	-8.4	-2.8	2.8	8.5	14.1	19.7	25.3	30.7	36.3	41.9
56	-42.0	-36.4	-30.7	-25.2	-19.6	-13.9	-8.4	-2.8	2.9	8.3	14.0	19.7	25.1	30.8	36.5	41.9
57	-42.0	-36.3	-30.8	-25.1	-19.7	-14.0	-8.5	-2.8	2.9	8.4	14.1	19.5	25.2	30.7	36.4	41.9
58	-41.9	-36.4	-30.7	-25.3	-19.6	-13.9	-8.5	-3.0	2.9	8.4	14.0	19.5	25.2	30.9	36.3	42.0
59	-42.0	-36.3	-30.7	-25.1	-19.7	-14.0	-8.4	-2.8	2.9	8.3	13.9	19.6	25.2	30.8	36.5	41.9
60	-42.1	-36.2	-30.7	-25.2	-19.6	-14.1	-8.5	-2.7	2.8	8.4	13.9	19.5	25.3	30.9	36.4	42.0
61	-41.9	-36.5	-30.8	-25.1	-19.7	-14.0	-8.3	-2.9	2.8	8.5	13.9	19.6	25.3	30.7	36.4	42.1
62	-42.1	-36.5	-30.7	-25.2	-19.7	-13.8	-8.3	-2.8	2.7	8.5	14.0	19.5	25.0	30.9	36.4	41.9
63	-41.9	-36.3	-30.7	-25.1	-19.5	-13.9	-8.3	-2.7	2.9	8.5	14.1	19.7	25.3	30.9	36.5	42.1
64	-41.9	-36.2	-30.9	-25.2	-19.6	-13.9	-8.2	-2.9	2.7	8.4	14.1	19.8	25.0	30.7	36.4	42.1
65	-41.9	-36.2	-30.9	-25.2	-19.5	-14.2	-8.5	-2.8	3.0	8.3	14.0	19.7	25.0	30.7	36.5	42.2
66	-42.2	-36.5	-30.7	-25.0	-19.7	-14.0	-8.3	-3.0	2.7	8.5	14.2	19.5	25.2	31.0	36.2	42.0
67	-42.2	-36.5	-30.8	-25.1	-19.3	-14.2	-8.4	-2.7	3.0	8.2	13.9	19.6	25.3	31.0	36.2	41.9
68	-41.9	-36.2	-30.6	-25.0	-19.3	-14.2	-8.6	-3.0	2.7	8.3	14.0	19.6	25.2	30.9	36.5	42.2
69	-41.8	-36.3	-30.8	-25.3	-19.8	-14.2	-8.1	-2.6	2.9	8.4	13.9	19.4	25.0	31.1	36.6	42.1
70	-42.1	-36.1	-30.8	-25.4	-19.5	-14.1	-8.2	-2.8	2.5	8.5	13.8	19.8	25.1	31.1	36.4	41.7
71	-42.1	-36.3	-30.5	-25.5	-19.7	-13.9	-8.9	-3.1	2.7	8.5	14.3	19.3	25.1	30.9	36.6	41.7
72	-41.7	-36.3	-30.8	-25.3	-19.8	-14.3	-8.0	-2.6	2.9	8.4	13.9	19.4	24.9	31.2	36.6	42.1
73	-41.9	-36.0	-30.9	-24.9	-19.8	-13.8	-8.7	-2.8	3.2	8.3	14.3	19.4	25.3	30.4	36.4	42.3
74	-41.8	-36.3	-30.7	-25.2	-19.7	-14.1	-8.6	-3.0	2.5	8.1	13.6	19.2	25.6	31.2	36.7	42.3
75	-42.4	-36.4	-30.4	-25.4	-19.3	-14.3	-8.3	-3.3	2.7	8.8	13.8	19.8	24.8	30.9	35.9	41.9
76	-41.7	-36.2	-30.8	-25.3	-19.9	-14.5	-7.9	-2.5	3.0	8.4	13.9	19.3	24.8	30.2	36.8	42.2
77	-41.7	-35.8	-31.1	-25.2	-19.2	-14.5	-8.6	-2.7	3.2	8.0	13.9	19.8	25.7	30.5	36.4	42.3
78	-41.4	-36.3	-31.2	-24.8	-19.6	-15.8	-8.0	-2.9	2.2	8.7	13.8	20.2	25.4	30.5	36.9	42.1
79	-42.2	-36.6	-31.1	-25.5	-19.9	-14.3	-8.7	-3.2	2.4	8.0	13.6	19.2	24.8	30.3	35.9	41.5
80	-41.3	-36.8	-30.7	-24.6	-20.1	-14.0	-8.0	-3.4	2.6	8.7	13.2	19.3	25.4	31.4	36.0	42.0
81	-41.6	-36.6	-30.0	-25.1	-20.2	-13.6	-8.7	-2.1	2.9	7.8	14.4	19.3	25.9	30.8	35.8	42.4
82	-41.6	-36.2	-30.8	-25.5	-21.9	-14.8	-7.6	-2.3	3.1	8.5	13.8	19.2	24.5	29.9	37.1	42.4
83	-41.2	-35.4	-31.5	-25.7	-19.9	-14.1	-8.3	-2.4	3.4	9.2	13.1	18.9	24.7	30.5	36.4	42.2
84	-42.7	-36.4	-30.0	-25.8	-19.5	-13.2	-9.0	-2.7	3.7	7.9	14.2	20.5	24.7	31.1	37.4	41.6
85	-41.8	-37.2	-30.3	-28.0	-18.9	-14.3	-7.5	-2.9	1.7	8.6	13.1	20.0	24.6	31.4	36.0	42.9

Table 2: continued

86	-42.9	-35.4	-30.5	-25.5	-20.5	-13.1	-8.1	-3.1	1.8	9.3	14.3	19.2	24.2	31.6	36.6	41.6
87	-41.2	-35.8	-33.1	-25.0	-19.6	-14.2	-8.8	-3.4	2.0	7.4	12.8	20.9	26.3	31.7	37.1	42.5
88	-41.8	-35.9	-30.1	-24.2	-18.3	-15.4	-9.6	-3.7	2.2	8.0	13.9	19.7	25.6	31.5	37.3	43.2
89	-42.2	-39.0	-29.5	-26.3	-19.9	-13.6	-7.2	-4.0	2.4	8.7	15.1	18.3	24.6	31.0	37.3	40.5
90	-42.3	-35.4	-32.0	-25.1	-18.2	-14.7	-7.8	-4.4	2.6	9.5	12.9	19.8	26.7	30.2	37.1	40.5
91	-46.0	-34.7	-31.0	-23.5	-19.7	-12.2	-8.5	-1.0	2.8	6.5	14.0	17.8	25.3	29.0	36.5	40.3
92	-41.8	-37.7	-29.6	-25.5	-21.4	-13.3	-9.2	-1.1	3.0	7.1	15.2	19.3	23.4	31.5	35.6	43.7
93	-40.9	-36.5	-32.1	-23.3	-18.8	-14.4	-10.0	-1.2	3.3	7.7	12.1	21.0	25.4	29.8	34.2	43.1
94	-39.7	-34.9	-30.1	-25.3	-20.5	-15.7	-6.1	-1.3	3.5	8.3	13.1	17.9	27.5	32.3	37.2	42.0
95	-43.1	-37.8	-32.6	-27.4	-17.0	-11.8	-6.6	-1.4	3.9	9.1	14.3	19.5	24.7	29.9	35.1	40.3

6 Azimuth table.

Azimuth table (file "AzimTable.txt") shows central directions of each azimuthal sector $\Phi(AzIndex)$. This table also shown in Table 3. Angles in degrees are counted from X_{SC} to Z_{SC} . here XYZ_{SC} are Venus Express spacecraft axis.

Table 3: VEX IMA Azimuthal table, V.1.0, 20 Jan 2006

0	1	2	3	4	5	6	7	8	9	10	11	12	13	14	15
78.8	56.3	33.8	11.3	348.8	326.3	303.8	281.3	258.8	236.3	213.8	191.3	168.8	146.3	123.8	101.3

Thus the unit vector corresponding to the central direction of the azimuthal sector if $\Theta = 0$ $XY_{sect}(AzIndex)$ is:

$$X_{sect} = \cos(\Phi(AzIndex))$$

$$Z_{sect} = \sin(\Phi(AzIndex))$$

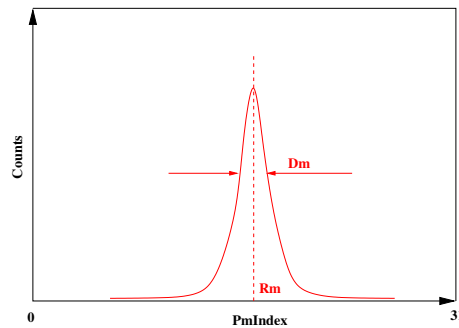
And the unit vector corresponding to the **real** direction of the corresponding sector $XYZ(AzIndex, EnIndex, ElIndex)$ is:

$$X = \cos(\Phi(AzIndex)) \cdot \cos(\Theta(EnIndex, ElIndex))$$

$$Y = \sin(\Theta(EnIndex, ElIndex))$$

$$Z = \sin(\Phi(AzIndex)) \cdot \cos(\Theta(EnIndex, ElIndex))$$

7 Mass table.

Figure 2: Definition of Rm and Dm values.

Ions of the given mass and the given energy creates a Gaussian peak distributed along the radius of the azimuthal sector of the instrument. Figure 2 clarifies this statement and defines the properties

of the mass peak. The figure shows one column of **IMA_Image** corresponding to fixed *AzIndex*. Counts are distributed around central position *Rm* as follows:

$$Counts(RmIndex) = Cmax \cdot e^{-0.5 \frac{(RmIndex-Rm)^2}{Dm^2}}$$

Here *Cmax* is the counts at the *Rm* point, and *Dm* represents a width of the distribution.

Table 4: VEX IMA Mass table, V.1.0, 20 Jan 2006

<i>PaccIndex</i>	<i>Pacc,V</i>	#	GfitP	GfitD	Kpacc	Kmass
0	39.	0	-2.95160	-0.02483	1.00000	-0.59430
0	39.	1	2.17791	0.32915	-0.00000	1.42718
0	39.	2	-0.00941	-0.01229	0.00000	-0.01472
3	1902.	0	-4.51042	0.85391	0.96520	0.00000
3	1902.	1	2.50365	0.29801	0.12167	1.00000
3	1902.	2	-0.02667	-0.01468	-0.08778	-0.00000
6	3615.	0	-7.25836	0.86668	0.77036	-0.11609
6	3615.	1	2.88211	0.27801	0.51016	1.09303
6	3615.	2	-0.04061	-0.01184	-0.28072	-0.01449

Table 4 and corresponding file "MassTable.txt" provide information of about *Rm* and *Dm* as functions of *PaccIndex* and *EnIndex*. *PaccIndex* is an internal IMA constant defined by telecommand. (See section **IMA Telemetry Format**). *PaccIndex* can be 0, 1,... 7. But calibration information exists for *PaccIndex* = 0, 3, 6 only. *Rm* and *Dm* are calculated as follows (*PI* = *PaccIndex*):

$$M_{eff} = Kmass_0(PI) + Kmass_1(PI) \cdot M/Q + Kmass_2(PI) \cdot (M/Q)^2$$

$$Pacc_{eff} = Pacc(PI) \cdot (Kpacc_0(PI) + Kpacc_1(PI)/M_{eff} + Kpacc_2(PI)/M_{eff}^2)$$

$$G_{eff} = 10^3 / \sqrt{(E/Q(EnIndex) + Pacc_{eff}) \cdot M_{eff}}$$

$$Rm = GfitP_0(PI) + GfitP_1(PI) \cdot G_{eff} + GfitP_2(PI) \cdot G_{eff}^2$$

$$Dm = GfitD_0(PI) + GfitD_1(PI) \cdot G_{eff} + GfitD_2(PI) \cdot G_{eff}^2$$

Here *M/Q* is Mass per a Charge of the ion (1 for H^+ , and 44 for $C0_2^+$ for instance), and *E/Q(EnIndex)* is an Energy per Charge of the ion (see **Energy table** section).

8 Common NetCDF file.

You can find all information described above in the common file **ima_info.nc**. This file is written in NetCDF standard. Format of this file is the same for IMA MEX and IMA VEX. One can found NetCDF standard in <http://www.unidata.ucar.edu/software/netcdf/>. IDL provides a set of functions to manipulate with NetCDF files. The header of **ima_info.nc** is as follows:

```
netcdf ima_info {
dimensions:
    ImaModeDim = 40 ;
    ImaParDim = 4 ;
    ImaEnerDim = 96 ;
    ImaElevDim = 16 ;
    ImaAzimDim = 16 ;
    ImaAzimSize = 2 ;
    ImaPacDim = 8 ;
```

```

    ImaKFSize = 4 ;
    ImaKFN = 4 ;
variables:
    short ImaModes (ImaModeDim, ImaParDim) ;
    float ImaEner (ImaEnerDim) ;
    float ImaElev (ImaEnerDim, ImaElevDim) ;
    float ImaAzim (ImaAzimDim, ImaAzimSize) ;
    float ImaMassKF (ImaPacDim, ImaKFN, ImaKFSize) ;

// global attributes:
    :DateOfCreation = "Fri.Jan.20.2006" ;
    :Mission = "VEX" ;
    :Experiment = "ASPERA-4" ;
    :Instrument = "IMA" ;
    :EnVersion = "1.0" ;
    :ElVersion = "2.0" ;
    :AzVersion = "1.0" ;
    :MassVersion = "1.0" ;
    :ProgVersion = "6.1" ;
    :Program = "ima_info.pro" ;
    :Author = "Fedorov" ;

```

Names of arrays in this file are self described. Contents of each array is as follows:

1. Each line of **ImaModes**, corresponding to fixed telemetry mode (see **Operational Modes** section) is: $TRmIndex$ size, $TAzIndex$ size, $TEnIndex$ size, $TElIndex$ size.
2. Format of **ImaEner** array is obvious.
3. **ImaElev** gives the $Y = \sin(\Theta(EnIndex, ElIndex))$ values. Value "-1000.0" means that this point is skipped in the telemetry array.
4. **ImaElev** contains X_{sect} and Z_{sect} .
5. Each line of **ImaMassKF** corresponding to fixed $PaccIndex = ImaPacDim$ and fixed $ImaKFN$ is $Pacc$, A_0 , A_1 , A_2 . For $ImaKFN = 0$, $A = GfitP$, for $ImaKFN = 1$, $A = GfitD$, for $ImaKFN = 2$, $A = Kpacc$, and for $ImaKFN = 3$, $A = Kmass$.